UNIVERSIDAD COMPLUTENSE DE MADRID

FACULTAD DE CIENCIAS QUÍMICAS

TESIS DOCTORAL

Estudio de la dinámica molecular de nanocompuestos de caucho natural

Study of the molecular dynamics of natural rubber nanocomposites

MEMORIA PARA OPTAR AL GRADO DE DOCTOR

PRESENTADA POR

Marianella Hernández Santana

Directores

Miguel Ángel López-Manchado
Tiberio A. Ezquerra

Madrid, 2013

UNIVERSIDAD COMPLUTENSE DE MADRID

FACULTAD DE CIENCIAS QUÍMICAS

CONSEJO SUPERIOR DE INVESTIGACIONES CIENTÍFICAS

INSTITUTO DE CIENCIA Y TECNOLOGÍA DE POLÍMEROS

INSTITUTO DE ESTRUCTURA DE LA MATERIA

ESTUDIO DE LA DINÁMICA MOLECULAR DE NANOCOMPUESTOS DE CAUCHO NATURAL

MARIANELLA HERNÁNDEZ SANTANA

TESIS DOCTORAL

Madrid, 2012

ESTUDIO DE LA DINÁMICA MOLECULAR DE NANOCOMPUESTOS DE CAUCHO NATURAL

STUDY OF THE MOLECULAR DYNAMICS OF NATURAL RUBBER NANOCOMPOSITES

MARIANELLA HERNÁNDEZ SANTANA

TESIS DOCTORAL

DIRECTORES:

Dr. MIGUEL ANGEL LÓPEZ-MANCHADO

Dr. TIBERIO A. EZQUERRA

A mi familia

PREFACE

Nanotechnology is recognized as one of the most promising fields of research of 21st century. The beginning of nanotechnology and nanoscience research can be traced back over 40 years. However, it was in the past decade that the world witnessed bigger strides of this technology from both academic and industrial points of view. The growth of nanoscience and nanotechnology has been possible because of the success in the synthesis of nanomaterials in conjunction with the advent of tools for characterization and manipulation.

The term "nanocomposite" refers to every type of composite material having fillers in the nanometer size range, at least in one dimension. For such nanocomposites the total interfacial phase becomes the critical parameter, rather than the volume fraction of the filler. Due to the dispersion of nanofillers, nanocomposites exhibit markedly improved properties when compared to pure materials or their traditional composites.

In the field of nanotechnology, polymer matrix based nanocomposites have generated a significant amount of attention. It is widely recognized that introducing nanoparticles with different shapes like spheres, rods or plates into polymer matrices, greatly enhances the mechanical properties such as stiffness, impact and tensile strength; besides, physical properties like barrier against gases, erosion resistance and reduced flammability can be achieved. Thus, the prospect of a new materials technology that can function as a low-cost alternative to high-performance composites for applications ranging from automotive to food packaging to tissue engineering has become irresistible to researchers around the world.

In particular, rubber nanocomposites have attracted the attention of many researchers due to their unique properties. In rubbers, fillers are used to achieve products with improved properties for end use applications. It is well known that rubber reinforcement is a very important issue in rubber science and engineering. The research on rubber reinforcement is a traditional but vitally essential topic.

However, many issues in this aspect are presently still not well understood and explained. Moreover, when rubber reinforcement is obtained by using nanoparticles, it is even more difficult to clearly understand the relationship between the microstructure and properties. The special character of rubber, being a multi-component system (for example, rubber, vulcanizing agent, accelerants, reinforcements, etc.), complicates the analysis of the parameters affecting the rubber/nanoparticle composite formation.

Within this context, this Doctoral Thesis will attempt to answer the following questions: i) is molecular dynamics related to the reinforcing efficiency of nanosized fillers?; ii) what characterization technique could be used for studying molecular dynamics of elastomer nanocomposites?; iii) do layered silicate nanofillers and carbon based nanofillers behave equally in rubber matrices? and iv) do additives present in a rubber compound affect the molecular dynamics of the rubber matrix?

This research, then, has been a challenge to address, first, the effect of the presence of the filler on the local and global motions of polymer chains in Natural Rubber/layered silicate nanocomposites, studied by means of broad-band dielectric spectroscopy. It has also been examined how the vulcanization and vulcanization additives affect the dynamics of the nanocomposites.

In addition, this investigation has dealt with the effect of carbon nanostructures (carbon nanotubes and functionalized graphene sheets) on the molecular dynamics of Natural Rubber. These carbon nanostructures have acquired great interest in the scientific community due to their excellent intrinsic properties. It is important to highlight that, the graphene sheets started, at the end of this thesis period, to be commercially available. Accordingly, this part of this work is among the first ones in the polymers field.

Finally, the “strain-induced crystallization” phenomenon present in Natural Rubber has been investigated, since it is known that the crystal structures formed may act like reinforcing fillers and are responsible for the exceptionally good

strength and fatigue properties of this material in relation to their synthetic homologous elastomer. Thus, it is of outmost importance, to study the effect of the strain-induced crystallization on the segmental dynamics of vulcanized Natural Rubber.

This Doctoral Thesis has been divided into seven chapters. As a broader introduction to the subject, Chapter I provides a historical background on polymer nanocomposites, Natural Rubber nanocomposites and on the study of the molecular dynamics of elastomeric nanocomposites. Chapter II gives a detailed account of the measurement techniques used and of the procedures followed during the course of this study.

Rubbers are complex systems consisting of a wide variety of ingredients such as accelerators, activators, and vulcanizing agents. Thus, the aim of Chapter III is to provide a detailed view on how these constituents may affect the molecular dynamics of Natural Rubber. Chapter IV considers the dynamics of Natural Rubber/layered silicate nanocomposites, and the analysis of the results in terms of how the type and content of filler can affect the segmental and chain dynamics of the rubber. Also, the influence of the vulcanization process on the dynamics is addressed in this chapter. In an analogous manner, the results obtained for Natural Rubber/carbon based fillers nanocomposites are discussed in Chapter V. In Chapter VI, the effect of strain induced orientation on the segmental dynamics of vulcanized Natural Rubber and its nanocomposites is examined. The study is focused on the effect of network structure and the strain-induced crystallization, as investigated by synchrotron X-ray scattering, on the segmental dynamics of Natural Rubber. Finally, the conclusions of the thesis and future perspectives are given in Chapter VII.

Due to the rapid progress of this field of research in relation to the concepts presented, it seemed necessary over the past three years to submit parts of this work for publication to scientific journals. The publications are as follows:

- Hernández Marianella, Ezquerra Tiberio A., Lopez-Manchado Miguel A., Effects of Orientation on the Segmental Dynamics of Natural Rubber, *Materials Science Forum* **2012**, 714, 57-61.
- Marianella Hernández, Tiberio A. Ezquerra, Raquel Verdejo, Miguel A. López-Manchado, Role of Vulcanizing Additives on the Segmental Dynamics of Natural Rubber, *Macromolecules* **2012**, 45(2), 1070-1075.
- Raquel Verdejo, Marianella Hernández, Natacha Bitinis, Jose M. Kenny, Miguel A. López Manchado, Vulcanization Characteristics and Curing Kinetics of Rubber-Organoclay Nanocomposites, Chapter 9 in "Rubber-Clay Nanocomposites", ed. Maurizio Galimberti, John Wiley & Sons, **2011**, ISBN: 978-0-470-56210-9.
- Natacha Bitinis, Marianella Hernández, Raquel Verdejo, José M. Kenny, Miguel A. López-Manchado, Recent Advances in Clay/Polymer Nanocomposites, *Advanced Materials* **2011**, 23(44), 5229–5236.
- Marianella Hernández, Miguel A. López-Manchado, Alejandro Sanz, Aurora Nogales, Tiberio A. Ezquerra, Effects of Strain Induced Crystallization on the Segmental Dynamics of Vulcanized Natural Rubber, *Macromolecules* **2011**, 44(16), 6574–6580.
- Marianella Hernández, Javier Carretero-González, Raquel Verdejo, Tiberio A. Ezquerra, Miguel A. López-Manchado, Molecular Dynamics of Natural Rubber/Layered Silicate Nanocomposites as Studied by Dielectric Relaxation Spectroscopy, *Macromolecules* **2010**, 43(2),643-651.
- Javier Carretero-González, Haris Retsos, Emmanuel P. Giannelis, Tiberio A. Ezquerra, Marianella Hernández, Miguel A. López-Manchado, Miscibility-Dispersion, Interfacial Strength and Nanoclay Mobility Relationships in Polymer Nanocomposites, *Soft Matter* **2009**, 5(18), 3481-3486.

Even though this Doctoral Thesis has been developed almost completely in Spain, it is written in English in order to facilitate and promote its scientific impact. Nonetheless, an extensive resume in Spanish is attached at the end of the manuscript.

AGRADECIMIENTOS

Deseo expresar mi agradecimiento:

Al Ministerio de Ciencia y Tecnología de Venezuela por la beca otorgada para la realización de esta Tesis Doctoral.

A mis Directores de Tesis, Dr. Miguel Angel López-Manchado y Dr. Tiberio A. Ezquerra. A Miguel Angel por haber confiado en mí desde el primer momento y abrirme las puertas de su grupo de investigación sin conocerme. Disculpa por todos los "dolores de cabeza" que esta estudiante venezolana te dio, pero al final creo que valió la pena ¿verdad? A Tiberio, gracias por iniciarme en el mundo de las propiedades dieléctricas. Tu actitud siempre "positiva" me contagiaba hasta cuando te mostraba los peores resultados. Gracias por muchos gratos momentos conversando de cosas distintas a las dieléctricas!

A todos los integrantes del grupo de Nanocompuestos del Instituto de Ciencia y Tecnología de Polímeros. A los chicos "Lean Lean", "Mario Chico Guapo", La Peponi, Iván y Nico, por hacerme sentir joven! A Raquel, por sus críticas siempre constructivas y por sus ayudas informáticas. A José María por sus charlas tan divertidas y variadas. Y por supuesto a mis compañeras de despacho, Mar, Lauris y Nat, por su amistad, por horas compartidas hablando de cualquier cosa. Un especial agradecimiento a Mar, mi nueva compañera de congresos y viajes gastronómicos, por compartir juntas estos últimos meses de escritura de tesis. No puedo dejar de agradecer también a Miguel Arroyo, por sus paellas, por su gran sentido del humor y su eterna sonrisa…

A Alex y Aurora del Instituto de Estructura de la Materia, por sus buenos consejos, disposición a ayudarme en todo momento, sobre todo en temas tan desconocidos para mí como WAXS, SAXS, NEUTRONES, y todo aquello relacionado con "*The Big Bang Theory*". Gracias chicos! Gracias también por los agradables ratos en Grenoble y en Oxford. Al Dr. Daniel Rueda por su ayuda con el uso del FIT2D©.

A los madrileños, quienes me han acogido durante estos 4 años de aventura y me han permitido adoptar su ciudad como mía.

No puedo dejar de mencionar a mis recordados estudiantes y a mis queridos compañeros de la Universidad Simón Bolívar de Venezuela, Jeanette, Carmen R., Rosestela, Vicente, María Virginia y Carmen A., por ayudarme desde lejos y motivarme a seguir avanzando. En especial a Mirenchu, amiga incondicional, compañera eterna de congresos y de clases de elastómeros. Un día me dijiste: "Escríbele a López-Manchado, a lo mejor puedes hacer la tesis con él". Y así fue……

A mis papás, gracias a quienes soy lo que soy hoy. Gracias por su amor incondicional. Su constancia y sus deseos de superación son valores que me llevaron a realizar esta tesis. A mis queridos hermanos, parte importante de mi vida, gracias por su apoyo "a distancia".

Y finalmente, a mi querido Alf, mi amor eterno. Gracias por emprender esta aventura juntos y por confiar en mí. Y a mis hijos, Tata y Pulgui, un mejor futuro para Ustedes fue el motor que motivó la realización de este Doctorado.

MUCHAS GRACIAS

TABLE OF CONTENTS

LIST OF TABLES

LIST OF FIGURES

LIST OF SYMBOLS AND ABBREVIATIONS

A_c	Area below the crystalline peaks
A_a	Area below the amorphous halo
b	Shape parameter which describes the symmetric broadening of the equivalent relaxation time distribution function
B	Empirical Vogel-Fülcher-Tamman parameter
c	Shape parameter which describes the asymmetric broadening of the equivalent relaxation time distribution function
C_0	Capacitance of the empty sample holder
d	Basal spacing
D	Fragility strength
$\vec{D}$	Dielectric displacement
$\overrightarrow{D_0}$	Amplitude of the dielectric displacement
E	Young's modulus
$\vec{E}$	Electric field
$\overrightarrow{E_0}$	Amplitude of the electric field
F	Frequency of the applied electric field
g	Correlation factor
$G´$	Elastic modulus
$G´´$	Storage modulus
$I*$	Current circulating through the sample
k	Boltzmann constant, $1.381*10^{-23}$ $kg.m^2/s^2.K$
L	Long spacing
m	Fragility index
M	Molecular weight of the repeating unit
M_w	Weight-average molecular weight
$M*$	Complex dielectric modulus
$M´$	Real part of complex dielectric modulus
$M´´$	Imaginary part of complex dielectric modulus, loss modulus
N_A	Avogadro´s number, $6.023*10^{23}$ $1/mol$
q	Scattering vector

S_{min}	Minimum torque
S_{max}	Maximum torque
t	Time
t_{s2}	Scorch time, induction period
t_{90}	Optimum cure time, time needed to achieve 90% of the maximum torque
T	Temperature
T_0	Ideal glass transition or Vogel temperature
T_0^{NM}	Vogel temperature for the normal mode
T_g	Glass transition temperature
T_m	Melting temperature
U^*	Voltage circulating through the sample
X_c	Mass fraction crystallinity index
Z^*	Complex impedance

$\Delta\varepsilon$	Dielectric strength
ΔS	Delta torque
δ	Phase lag in the dielectric displacement
ε^*	Complex dielectric permittivity
ε'	Real part of complex dielectric permittivity, dielectric permittivity
ε''	Imaginary part of complex dielectric permittivity, dielectric loss
ε_0	Vacuum permittivity, 8.854×10^{-12} F/m
ε_s	Static dielectric constant
ε_∞	Instantaneous dielectric constant
ε_r	Elongation at break
λ	Strain ratio
λ^0	Onset strain of crystallization
λ_w	Wave length
μ	Dipole moment
μ_{eff}	Effective dipole moment
θ	X-ray scattering angle

π	3.1416
ρ	Density
σ_{dc}	direct current (d.c.) conductivity
σ_r	Tensile strength
σ_{100}	Stress at 100% elongation
σ_{300}	Stress at 300% elongation
σ_{500}	Stress at 500% elongation
τ	Characteristic relaxation time
τ_{HN}	Characteristic relaxation time according to Havriliak-Negami equation
τ_{max}	Relaxation time for the α-relaxation
τ_{New}	Average relaxation time for the new mode
τ_{Normal}	Average relaxation time for the normal mode
$\tau_{Segmental}$	Average relaxation time for the segmental mode
υ	Volume fraction of the conducting inclusion
ω	Angular frequency

AC	Alternating current
BDS	Broad-band dielectric spectroscopy
CB	Carbon black
CEC	Cation exchange capacity
CNa+	Cloisite® Na^+
CNT	Carbon nanotubes
CRI	Cure rate index
CVD	Chemical vapor deposition
C15A	Cloisite® 15A
C25A	Cloisite® 25A
C30B	Cloisite® 30B
DMA	Dynamic mechanical analysis
DSC	Differential scanning calorimetry
DRS	Dielectric relaxation spectroscopy
ENR	Epoxidized natural rubber
FGS	Functionalized graphene sheets

f-MWCNT	Functionalized multi-walled carbon nanotubes
FTIR	Fourier-transform infrared spectroscopy
GO	Graphite oxide
LDH	Double layered hydroxide
LDPE	Low density polyethylene
mEq/100g	one thousandth of a chemical equivalent per 100g
MBTS	Mercapto benzothiazyl disulfide
MMT	Montmorillonite
MWCNT	Multi-walled carbon nanotubes
MWS	Maxwell-Wagner-Sillars interfacial polarization
NBR	Nitrile rubber
NMR	Nuclear magnetic resonance
NR	Natural rubber
phr	Parts per hundred parts of rubber
PI	Poly(isoprene)
PLG	Poly(lactide-co-glycolide)
POMA	Poly(n-octyl methacrylate)
PRI	Plasticity retention index
PTFE	Polytetrafluorethylene
PUR	Polyurethane
SA	Stearic acid
SAXS	Small angle X-ray scattering
SBR	Styrene-butadiene rubber
SEM	Scanning electron microscopy
SIC	Strain-induced crystallization
SWCNT	Single-walled carbon nanotubes
TEM	Transmission electron microscopy
TGA	Thermal gravimetric analysis
TPU	Thermoplastic polyurethane
TSDC	Thermally stimulated depolarization currents
ULMR	Ultrasonically-assisted latex mixing and *in situ* reduction
VFT	Vogel-Fülcher-Tamman dependence
WAXS	Wide angle X-ray scattering

XPS	X-ray photoelectron spectroscopy
XRD	X-ray diffraction
XSBR	Carboxylated styrene-butadiene rubber
ZnO	Zinc oxide

ABSTRACT

This Doctoral Thesis presents the results of the study of the molecular dynamics of Natural Rubber (NR) nanocomposites with layered silicate (montmorillonite) and carbon based nanofillers (carbon nanotubes and functionalized graphene sheets), by means of broad-band dielectric spectroscopy, in order to understand the physical relations between the different phases and interfaces present in the nanocomposite and its implication on the improvement of the final properties of the material.

The effects of nanofiller type and content, as well as the presence of vulcanizing additives, on the dynamics of the elastomeric matrix, were evaluated. In addition, the effect of strain-induced crystallization on the segmental dynamics of NR nanocomposites was assessed by correlating dielectric spectroscopy results with X-ray scattering.

Results show that non-vulcanized NR exhibits two relaxations: at low temperatures, a segmental mode associated to the motions of chain segments, corresponding to the glass transition temperature, and at high temperatures, a normal mode associated to global motions of the polymeric chains. With regard to the segmental mode, neither the content nor the nature of the filler has a significant effect. While the presence of vulcanizing additives, slows down the segmental dynamics of the NR matrix, especially the ZnO clusters which can act as cross-link precursors. In addition, a "new mode" associated to a restricted segmental relaxation due to the polymeric chains in the interfacial polymer/nanofiller regions appears in the spectra of NR/organoclay nanocomposites. This new relaxation is detectable in non-vulcanized and in vulcanized NR matrices, and it is related to fillers with high degree of intercalation. The results of strain-induced crystallization corroborate the segmental nature of this "new mode" and give evidence of an amorphous/semi-crystalline transition at low deformations. This fact can explain the improvement in physical and mechanical properties observed for these systems.

SUMARIO

La presente Tesis Doctoral refleja los resultados del estudio de la dinámica molecular de nanocompuestos de Caucho Natural (NR) reforzados con silicatos laminares (montmorillonita) y con cargas derivadas de carbono (nanotubos de carbono y láminas de grafeno funcionalizadas), empleando la técnica de espectroscopia dieléctrica, con el fin de entender las relaciones físicas entre las diferentes fases e interfases presentes en el nanocompuesto y su implicación en la mejora de las propiedades finales del material. Se evaluó la influencia del contenido y naturaleza de las nanocargas sobre la dinámica de la matriz elastomérica, sin vulcanizar y vulcanizada, así como el efecto de los aditivos de vulcanización. De igual manera, se estudió el efecto de la cristalización inducida por deformación sobre la dinámica segmental de nanocompuestos de NR, correlacionando los resultados de la espectroscopia dieléctrica con los de la difracción de rayos X. Los resultados obtenidos muestran que el NR sin vulcanizar exhibe dos relajaciones: a bajas temperaturas, un modo segmental asociado con el movimiento de segmentos de cadena, correspondiente a la temperatura de transición vítrea; y a altas temperaturas, un modo normal ligado a los movimientos globales de la cadena polimérica. Con respecto al modo segmental, se mostró que ni el incremento en el contenido de nanocarga ni la naturaleza de la misma tienen un efecto significativo. Mientras que los aditivos de vulcanización, ralentizan los movimientos segmentales de cadena, especialmente los agregados de ZnO que actúan como precursores de entrecruzamiento. Adicionalmente, en los espectros de los nanocompuestos de NR y arcilla orgánicamente modificada aparece un "nuevo modo" asociado a una relajación segmental restringida debido a las cadenas poliméricas en las regiones interfaciales polímero/nanocarga. Esta nueva relajación se detecta en matrices de NR vulcanizadas y no vulcanizadas, y está asociada a cargas con alto grado de intercalación. Los resultados de la cristalización inducida por deformación corroboran la naturaleza segmental de este "nuevo modo" y evidencian una transición de estado amorfo/semi-cristalino a bajas deformaciones. Este hecho puede explicar la significativa mejora de propiedades físicas y mecánicas observadas en estos sistemas.

CHAPTER I. INTRODUCTION

I.1. Natural Rubber

I.1.1. *General Aspects*

Rubbers are polymeric materials endowed with the properties of flexibility and elastic extensibility. By the application of force, the molecules straighten out in the direction in which they are being pulled and on release from being extended, they spontaneously recover their normal, random arrangements. Rubbery materials are, however, not simply of academic interest. In everyday life, rubber is a vital material, particularly in engineering applications, of which the pneumatic tire is the best known example.

Rubbery behavior is exhibited by many polymeric materials. Among them Natural Rubber (NR) was the first to be industrially exploited. Natural Rubber is nowadays complemented by a range of synthetic materials which have found niches in the market because of such characteristics as tensile strength, heat resistance, oil resistance, resistance to burning and low air permeability.

Natural Rubber is one of nature's unique materials. The native Americans of tropical South America's Amazon basin knew of rubber and its uses long before Christopher Columbus's explorations brought it to the attention of Europeans. Natural Rubber is obtained from the sap ("latex") of several rubber-yielding plants by coagulation. The commercial market, however, is totally dominated by one plant, *Hevea Brasiliensis.* Nowadays, Far East producers (Malaysia, Indonesia, Thailand and Sri Lanka) account for about 80% of the NR market.

The rubber latex occurs in tiny vessels embedded in the inner cortex of the bark of the tree. Incisions into the bark cause the latex to exude as a result of osmotic pressure. The exudate is collected in cups and then subsequently coagulated to obtain a dry rubber. Figure I.1 shows a picture sequence representing the steps for obtaining dry coagulated NR.

Figure I.1. Picture sequence for obtaining dry coagulated Natural Rubber.

NR molecules consist mainly of *cis*-1,4-polyisoprene:[1]

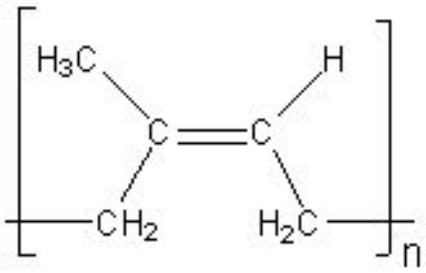

with practically no evidence for any *trans* materials, in the natural product, in contrast to the synthetic polyisoprene. The molecular weight of the natural polymer is very high but varies between lattices from different tree clones. Nonetheless, typical values of weight-average molecular weight (M_w) can range from 3.4 x 10^6 to 10.2 x 10^6 g/mol.[1-3] Due to this high molecular weight, it is often difficult to blend the additives unless NR is subjected to intensive working, the process known as *mastication*, by which the polymer becomes progressively more plastic rather than elastic, capable of flowing and may therefore be shaped. The mastication involves the rupture of molecules by shearing forces imposed during bulk deformation of the rubber, and thus, decreases the molecular weight.[1]

The very flexible backbone of NR leads to a very low glass transition temperature (T_g) of about -64 °C. Besides, due to its highly regular structure, NR is capable of crystallizing.[4] Crystallization may also be induced by stretching samples such as in a tensile test. As a result of this stress-induced crystallization, the tiny crystal

structures formed act like reinforcing particles, and enable NR to exhibit high strengths. Moreover, when the rubber is stretched, the internal shearing action tends to align the long molecules preferentially in the stretching direction, being this orientation easily detectable by optical methods.

Commercial raw Natural Rubber has also a small, but highly important number of non-rubber constituents. These may compromise as much as 5-8% of the total composition. Most important are the natural-occurring proteins, phospholipids, sugars, and fatty acids. These non-rubber constituents can influence the methods of coagulation, the vulcanization and ageing characteristics of rubber compounds, and so the physical properties of NR.[1-3]

I.1.2. *Vulcanization*

Vulcanization is the chemical reaction which brings about the formation of cross-links between the long chains of rubber molecules (see Figure I.2). This reaction transforms the soft plastic-like material into a strong elastic one.

The three dimensional structure produced by cross-linking restricts the mobility of the molecules and reduces the ability to crystallize. Simultaneously, it improves elasticity, elastic modulus and hardness over a wide temperature range.

The process of cross-linking or curing of NR was first discovered some 170 years ago by Charles Goodyear.[1] The vulcanizing agent used at that time was sulfur and it remains as the basis of nearly all commercial vulcanizing procedures. Today, however, sulfur is used in conjunction with a number of other agents and the vulcanization mechanism has become more and more complex from the chemical point of view. Basically, inorganic metal oxides and organic chemicals are added in order to accelerate the cross-linking reaction, to facilitate material processing and to improve some properties of the end product.

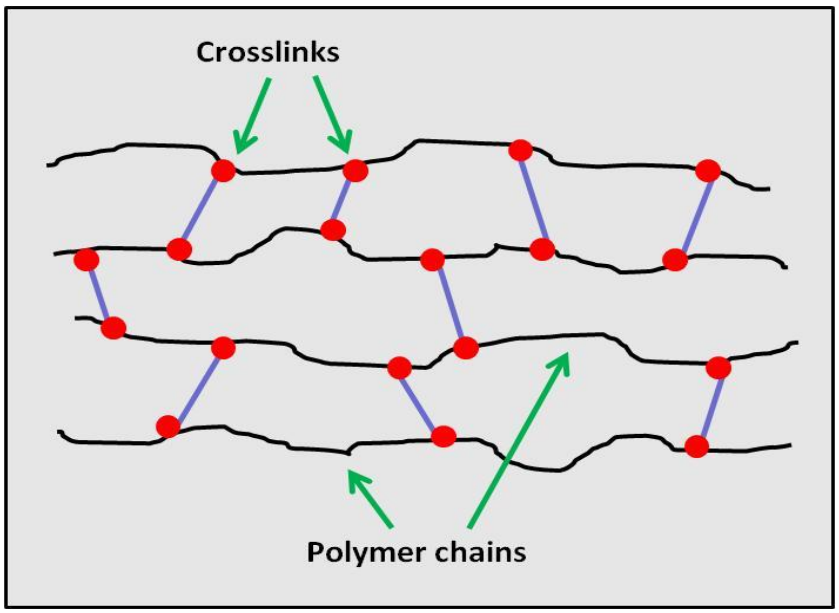

Figure I.2. Structural diagram of a vulcanized rubber.

Typical accelerated sulfur vulcanization of NR involves three components: sulfur, accelerator, and activators, which in a conventional system are used in the quantities indicated in column A of Table I.1.

Table I.1. Typical conventional (A) and efficient vulcanization (B) systems for use in Natural Rubber expressed as parts per hundred parts of rubber (phr).

	A Conventional system (phr)	**B Efficient vulcanization system (phr)**
Natural Rubber	100	100
Sulfur	2.0 – 3.5	0.4 – 0.8
Accelerator	1.2 – 0.4	5.0 – 2.0
Activator (ZnO)	3.0 – 5.0	3.0 – 5.0
Fatty acid (Stearic acid)	1.0 – 1.5	1.0 – 1-5

Accelerators vary in their chemical structure being normally inorganic substances which can be grouped by their acidic or basic nature. Typical commercial accelerators used in NR compounds fall into one of the following chemical groups:

guanidines, thiazoles, thiurams, and/or sulphenamides. The main reason for using accelerators is to aid in controlling the time required for vulcanization and thus to improve the properties of the vulcanized material. The activators, on the other hand, are used to increase the vulcanization rate by activating the accelerator so that it performs more effectively. Activators normally form an activator complex constituted by an inorganic compound (mainly metal oxides) and an organic acid. Zinc oxide is the most commonly employed oxide and it is generally used in combination with stearic acid to form a rubber-soluble soap in the rubber matrix.[3] It is believed that they react in some manner to form intermediate complexes with the accelerators. The complex thus formed is more effective in activating the sulfur present in the mixture, and so increasing the curing rate.

Sulfur vulcanization requires the presence of double bonds on the elastomer backbone. Sulfur is combined in the cross-linking network in a number of ways as schematically illustrated in Figure I.3.

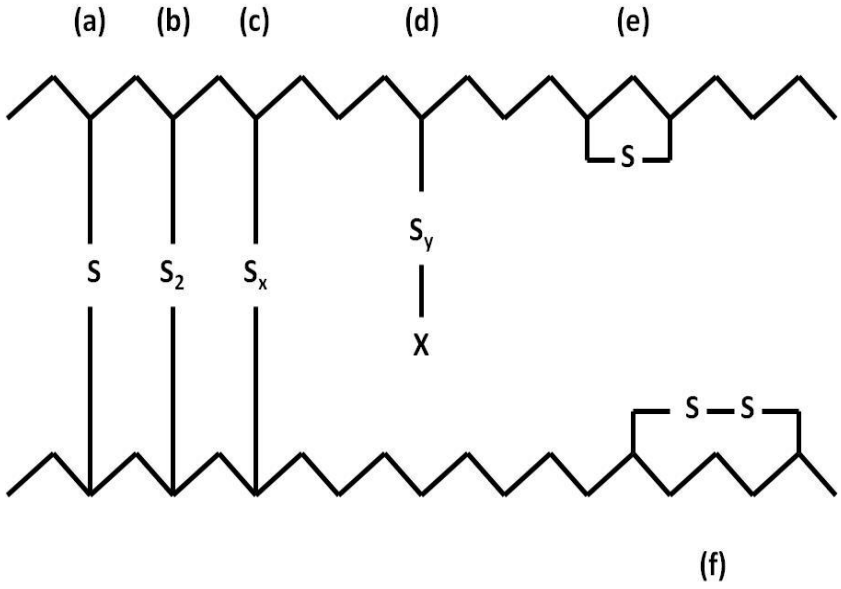

Figure I.3. Typical chemical groups present in a sulfur-vulcanized Natural Rubber network: (a) monosulphide cross-link; (b) disulphide cross-link; (c) polysulphide cross-link (x=3-6); (d) pendant sulphide; (e) cyclic monosulphide; (f) cyclic disulphide.

The ratio of monosulphidic to disulphidic and polysulphidic bonds has been shown to have an important effect on the properties of the vulcanized material. The proportion of monosulphidic is higher for efficient vulcanization systems (see column B of Table I.1). In general terms, the efficient vulcanization systems (high accelerator/sulfur ratio) confer improved thermal and oxidative ageing and reversion resistance with low compression set at 70 °C. On the other hand, they tend to have lower tensile strength, fatigue resistance and resilience but higher physical creep rates than conventional vulcanized NR.[1]

The use of organic peroxides is also an alternative way for vulcanizing rubbers.[1,3] Although not very popular with NR, it is widely used in saturated rubbers such as ethylene-propylene rubber (EPR) and silicones, which cannot be cross-linked by sulfur. When the peroxides decompose, free radicals are formed on the rubber chains, and these chains can then combine to form cross-links. These links only involve carbon-to-carbon bonds and are quite stable (see Figure I.4).

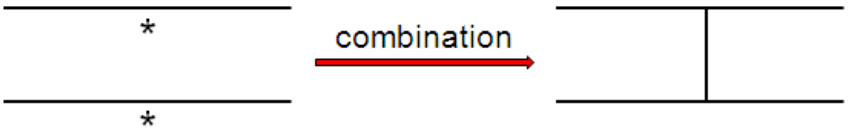

Figure I.4. Schematic representation of cross-links formed in a peroxide vulcanization reaction.

The vulcanization curves of a rubber compound are currently obtained by monitoring the increase of the torque required to maintain a given amplitude of oscillation at a temperature in an oscillating-disk rheometer. This apparatus continuously measures the dynamic shear modulus of a heated test specimen as a function of vulcanization time. It has been assumed that the increase in torque during vulcanization is proportional to the number of cross-links formed per unit of volume of rubber. The torque is automatically plotted versus time to give a so-called curing curve. A typical curing curve of a rubber is shown in Figure I.5. From this curve, most of the vulcanization characteristics of the test compound can be

directly determined. The registered parameters deduced from the curing curves are detailed below:[5]

Scorch Time (t_{s2}): It is the time required for the torque value to increase by 2 units over the minimum. It indicates the time available before onset of vulcanization and, it provides a good assessment of the scorch safety of a rubber compound. Lower scorch values correlate with an increased likelihood of premature cross-linking (precocity).

Optimum Cure Time (t_{90}): It is the time in which 90 % of the delta torque is reached. This is a useful estimate of the overall cure rate at a given temperature. As overheating of the material could lead to reversion processes.

Cure Rate Index (*CRI):* It is a direct measure of the fast curing nature of rubber compounds and can be calculated using the following expression:

$$CRI = 100 \,/\, (t_{90} - t_{s2}) \qquad \text{I.1}$$

Minimum torque value (S_{min}): It represents an index of material viscosity and can be related to the dispersion of the filler and the filler-polymer interaction. In general, it indicates the extent of mastication.

Maximum torque value (S_{max}): It represents the highest level of cross-linking possible at a given vulcanization temperature.

Delta torque ($\Delta S = S_{max} - S_{min}$): It is the difference between the maximum and the minimum torque, and it is related to the cross-linking density of a vulcanizate. So, it is an efficient means of measuring the effects of additives on the cure efficiency.

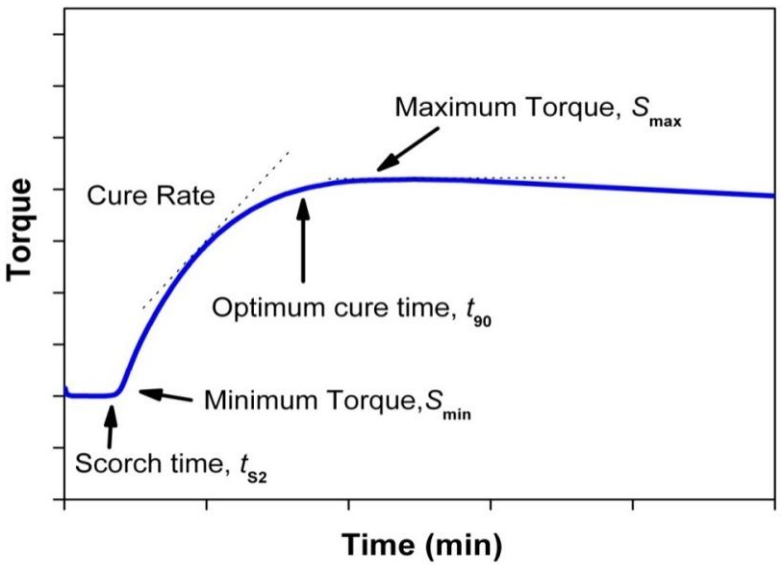

Figure I.5. Schematic representation of a curing curve, with its corresponding parameters.

I.2. Polymer Nanocomposites

I.2.1. *Basic Aspects*

Polymer nanocomposites are a new class of materials in which the dimension of one of its phases, at least, is of the order of few nanometers. Thus, a nanocomposite is a nanostructured material consisting of a dispersion of nanosized reinforcing particles inside a polymer matrix. Because of their nanometer size, nanocomposites show unique properties typically not shared by more conventional macroscopically filled polymers and therefore offer new technology and business opportunities. The main feature of a nanoparticle is that it has at least one dimension in the nanometric range.[6-8]

Nanofillers are necessarily nanoscopic and have a high specific surface area. The uniform dispersion of nanoscopically sized particles can lead to an ultra large interfacial area between the constituents per volume of material, approaching 700 m^2/cm^3 in dispersions of layered silicates in polymers. Thus, in polymer nanocomposites with only a low volume percent of dispersed nanoelements (< 10

wt.%), the entire polymer matrix may be considered to be a nanoscopically confined interfacial polymer. In the case of nanocomposites, the properties of the material are more related to the nanoparticle-matrix interface. Thus the total interfacial phase becomes the critical parameter, rather than the volume fraction of the filler.[9-13]

Three types of nanocomposites can be distinguished depending on how many dimensions of the dispersed particles are found in the nanometric range. When the nanometric scale involves the three dimensions (Figure I.6a) they are referred to as isodimensional nanoparticles. Typical examples of this class are spherical nanoparticles of silica obtained by *in situ* methods such as sol-gel,[14,15] as well as semiconducting nanoclusters, among others. When the nanometric scale affects two dimensions being the third larger (Figure I.6b), the particle is in a "stretched" state. Typical examples of this class are carbon nanotubes[16] or cellulose whiskers[17] which are extensively studied as reinforcing nanofillers yielding materials with exceptional properties. The third type of nanocomposite is characterized by having dispersed particles with only one dimension in the nanometric range (Figure I.6c). This class involves platelet like particles such as layered silicates[10] or graphene sheets. In this case, the filler is present in the form of sheets of one to a few nanometer thick and of hundreds to thousands nanometers long.

In this study nanocomposites based on a Natural Rubber matrix filled with layered silicates, carbon nanotubes and functionalized graphene sheets have been analyzed. The structural characteristics of the three types of nanoparticles used in this Thesis are described below.

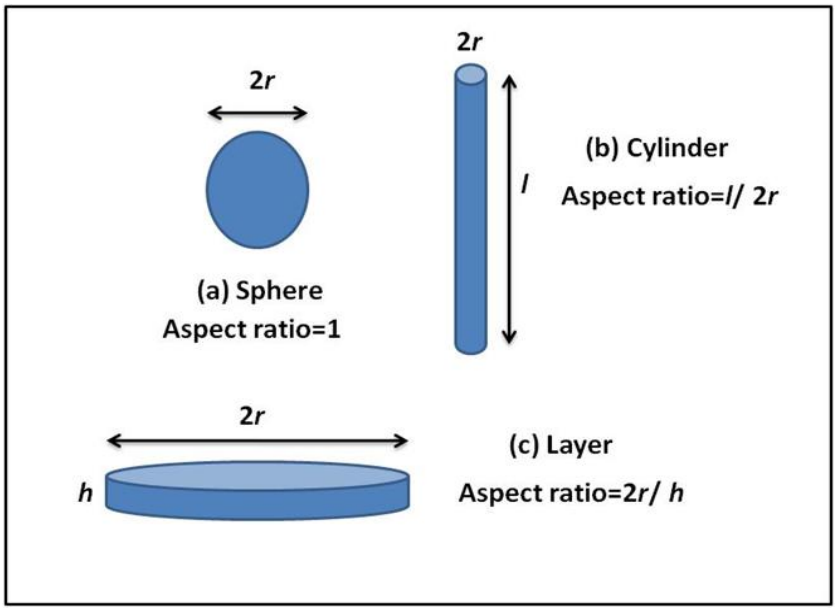

Figure I.6. Schematic representation of nanoparticles as a function of their dimensions in the nanometric range.

I.2.2. *Layered Silicates*

The layered silicates commonly used in nanocomposites belong to the structural family known as the 2:1 phyllosilicates. Their crystal lattice consists of two-dimensional layers where a central octahedral sheet of alumina or magnesia is fused to two external silica tetrahedron by the tip (Figure I.7) so that the oxygen ions of the octahedral sheet do also belong to the tetrahedral sheets. These layers organize themselves to form stacks with a regular Van der Waals gap in between them called the *interlayer* or the *gallery*. Isomorphic substitution within the layers (for example, Al^{3+} replaced by Mg^{2+} or by Fe^{2+}, or Mg^{2+} replaced by Li^{+}) generates negative charges that are counterbalanced by alkali or alkaline earth cations situated in the interlayer.[6,10,13] As the forces that hold the stacks together are relatively weak, the intercalation of small molecules between the layers is possible.

Montmorillonite, Hectorite and Saponite are the most commonly used layered silicates. Their chemical formulae are as follows:

Montmorillonite: $M_x(Al_{4-x}Mg_x)Si_8O_{20}(OH)_4$

Hectorite: $M_x(Mg_{6-x}Li_x)Si_8O_{20}(OH)_4$

Saponite: $M_xMg_6(Si_{8-x}Al_x)O_{20}(OH)_4$

where M corresponds to the monovalent cation and x the degree of isomorphous substitution (between 0.5 and 1.3). Their typical structure is given in Figure I.7.

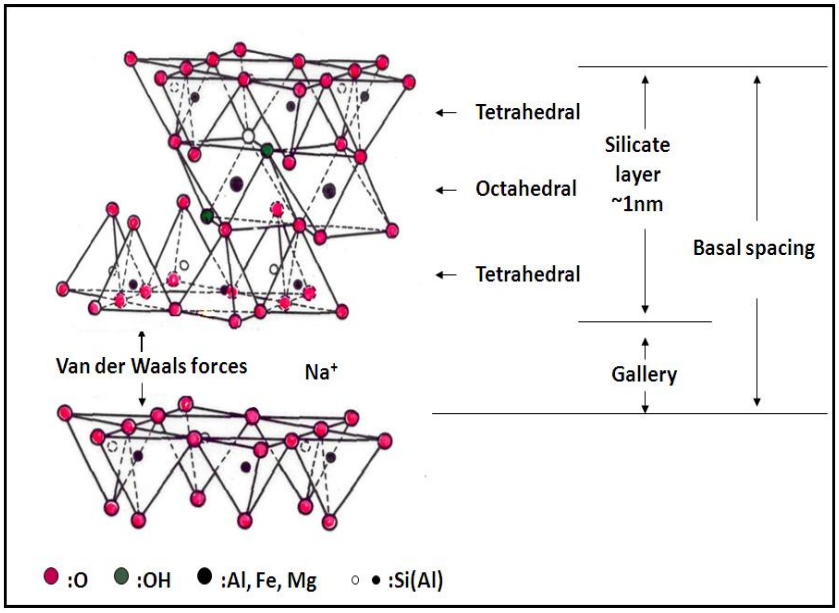

Figure I.7. Ideal structure of 2:1 phyllosilicates.[6,13]

This type of clay is characterized by a moderate negative surface charge (known as the cation exchange capacity, CEC and expressed in mEq/100g). The charge of the layer is not locally constant as it varies from layer to layer and must rather be considered as an average value over the whole crystal. Proportionally, even if a small part of the charge balancing cations is located on the external crystallite surface, the majority of these exchangeable cations are located inside the galleries. When the hydrated cations are ion-exchanged with organic cations such as more bulky alkyl ammoniums, it usually results in a larger interlayer spacing.

Pristine layered silicates usually contain hydrated Na^+ or K^+ ions. Ion-exchange reactions with cationic surfactants, including primary, tertiary and quaternary ammonium ions, render the normally hydrophilic silicate surface into an organophilic one named as organosilicate. This effect makes possible the intercalation within the galleries of given species like, for example, polymers. The

role of the alkyl ammonium cations in the organosilicates is to lower the surface energy of the inorganic component and to improve the wetting characteristics with the polymer. This organo-modification increases the distance between silicate layers and the compatibility with the polymer matrix, thus facilitating the insertion of polymer chains within the interlayer spacing.[6,10,18] A schematic representation of the modification of a silicate layer is displayed in Figure I.8.

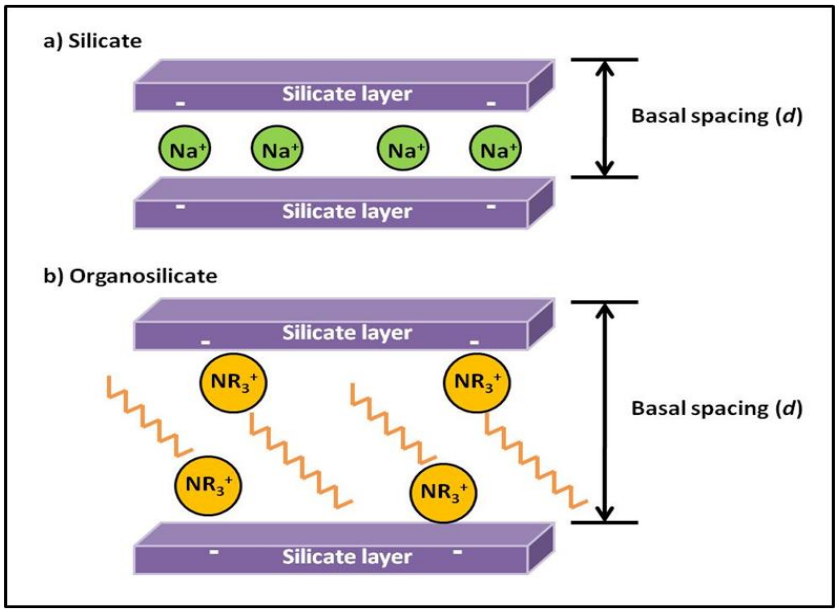

Figure I.8. Schematic representation of: a) silicate and b) organosilicate. R can be replaced by any chemical unit.

In general, layered silicates have layer thickness in the order of 1 nm and a very high aspect ratio (*i.e.* 10-1000). The addition of only a small percentage of nanofiller in a polymer matrix, when properly dispersed, gives rise to a high interfacial area as compared with that of a conventional polymer composite. An intimate relation between the dispersion, rubber–filler interactions, and morphology of the nanocomposites exists which is responsible for the final behavior of the materials.

When a layered silicate is mixed with a polymer different types of composites with different morphologies can be obtained, depending on the nature of the

components and on the method of preparation, as represented in Figure I.9 and briefly described next.[6,10,19]

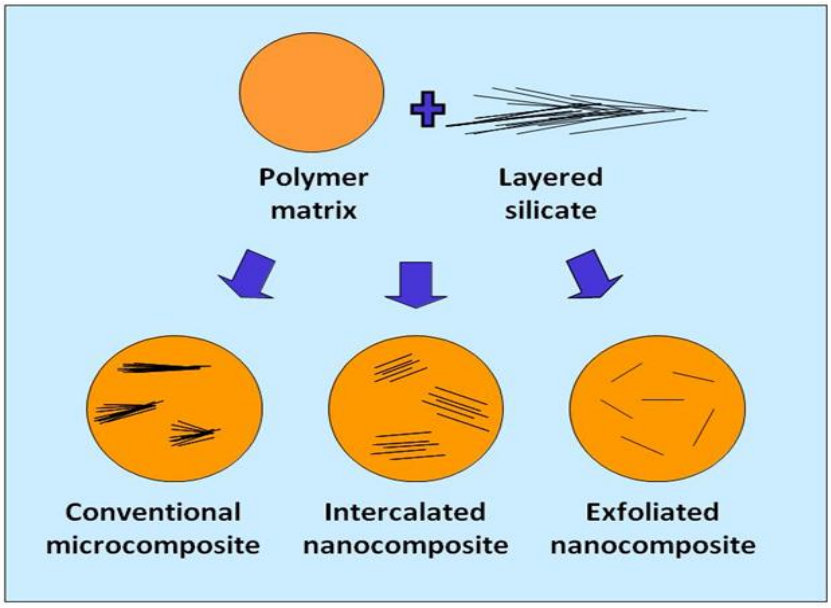

Figure I.9. Schematic representation of the different types of polymer/layered silicate composites.

- Conventional Composites

Generally, microcomposites are where the filler, with particle size in the range of microns (*i.e.*, carbon black clusters or other inorganic filler), and the polymer matrix form two well separated phases. In this case, the polymer is unable to intercalate between the silicate sheets.

- Intercalated Nanocomposites

This morphology is obtained when polymer chains intercalate between the silicate layers giving rise to a well-ordered multilayer morphology consisting in alternating polymer phase and inorganic layers. The intercalation of the polymer chains usually increases the interlayer spacing of the clay, leading to a shift of the diffraction maximum characterizing the interlayer spacing towards lower-angle values. The angle and basal spacing (d) values are related through the Bragg's law:

$$\lambda_w = 2d \sin\theta \qquad \text{I.2}$$

- Exfoliated Nanocomposites

When the silicate layers are completely and individually dispersed in the polymer matrix, an exfoliated or delaminated morphology is obtained. In this case, the ordered structure of the layered silicate is lost and the average distance between exfoliated layers depends on clay loading and on the method of processing. Here, no diffraction maxima are detected in the X-ray diffraction (XRD) diffractograms either because the interlayer spacing is too large to be detected or because the nanoparticle has lost its ordered structure.

I.2.3. *Carbon Based Nanofillers*

Over recent years, carbon nanotubes (CNT) have inspired scientists for a range of potential applications.[20-23] Carbon nanotubes (CNT) are one of the recently discovered allotropic forms of carbon with a unique atomic structure consisting in covalently bonded carbon atoms arranged in long cylinders with typical diameters in the range 1–50 nm and a wide variety of lengths. Individual carbon nanotubes are characterized by a high aspect ratio (typically 300–1000), high flexibility[24] and unique combination of mechanical, electrical and thermal properties.[25,26] The combination of these properties with a very low mass density[27] makes them potentially useful as ideal reinforcing fibers for high-performance polymer composites. However, the incorporation of nanotubes is not a trivial task if a good dispersion is required. Researchers have employed different techniques to attain optimum dispersion of nanotubes in the polymer matrix. Chemical modification of CNT seems to be the best technique in order to obtain more homogeneous dispersion through covalent and non-covalent attachments of some functional groups of CNT with the matrix.[28]

CNT are usually produced by three techniques: arc discharge, laser ablation and chemical vapor deposition. The quality and yield of CNT strongly depend on the synthesis and purification techniques and on the specific growth conditions used.[29] There are two basic types of CNT: single-walled carbon nanotubes

(SWCNT) and multi-walled carbon nanotubes (MWCNT). The structure of a SWCNT can be generated by wrapping a one-atom thick layer of graphite into a seamless cylinder. The carbon atoms in the cylinder have partial sp^3 character that increases as the radius of curvature of the cylinder decreases. MWCNT, on the other hand, consist of multiple layers of graphite arranged in concentric cylinders with an interlayer distance close to the distance between graphene layers in graphite (circa 0.34 nm). A schematic representation of SWCNT and MWCNT is displayed in Figure I.10.

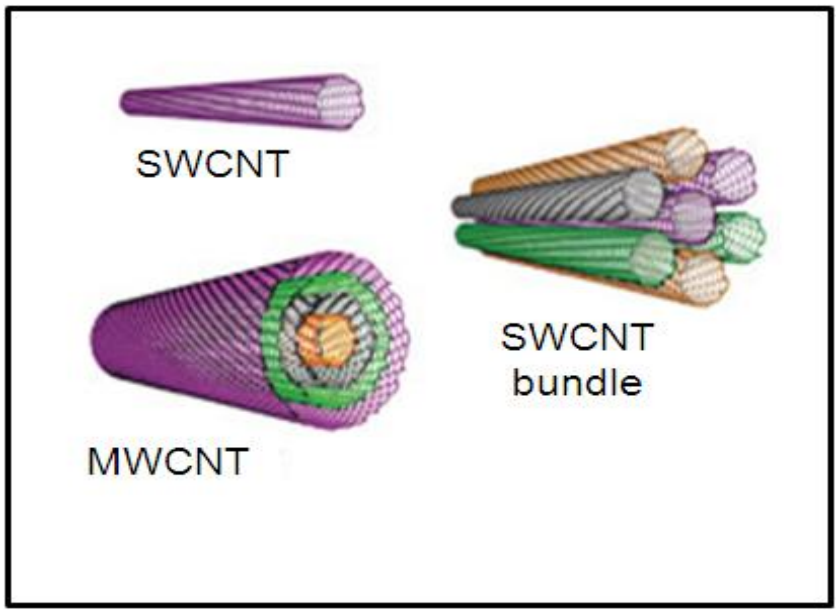

Figure I.10. Schematic representation of SWCNT and MWCNT. *Adapted from [30] Copyright 2008.*

The different preparations of CNT give mixtures of diameters, length, and nanotube chiralities along with different amounts and type of impurities. This heterogeneity clearly influences the purification and properties of CNT. In any case, CNT possess unique electrical and mechanical properties. SWCNT can be metallic or semi-conducting depending on the chirality of the tubular arranged graphitic layer and on the diameter of the nanotube, properties that are not shared by the MWCNT. Reported overall mechanical properties correspond to a Young's modulus of an average of 1.8 TPa and tensile strength of 50-200 GPa.[31,32]. On the other hand, thermal conductivity lies between 1000-2000 W/m.K,[22,33] while

electrical conductivity is in the order of 10^2-10^6 S/cm.[34,35] These properties among others render CNT potential nanomaterials in applications such as energy storage, structural materials, conductive materials, biological applications and so on.

Recently, graphene has attracted a tremendous amount of attention and has emerged to be an exciting material with potential applications as a reinforcing material for polymer nanocomposites.[36,37] Graphene is also an allotrope of carbon consisting on a single carbon layer of graphite (sp^2-bonded carbon atoms), as shown in Figure I.11.

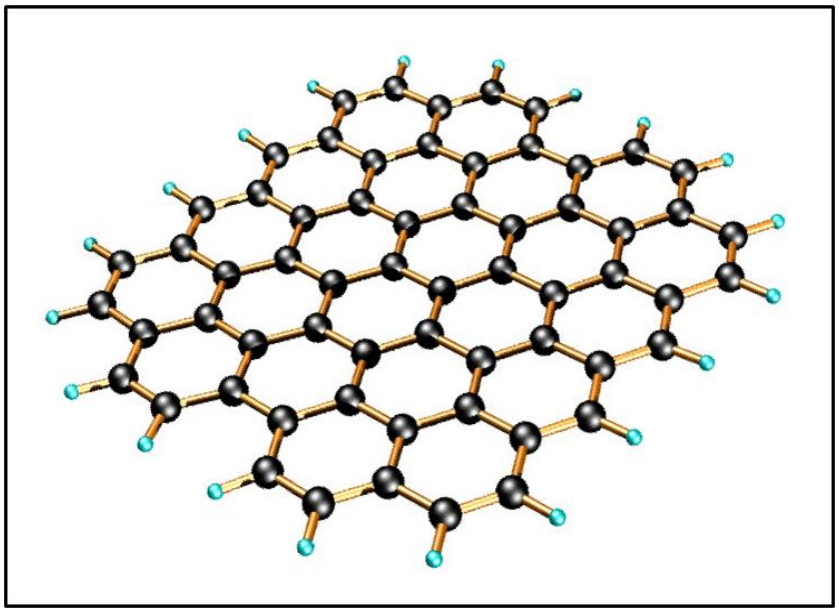

Figure I.11. Idealized structure of a single graphene sheet.

Defect-free graphene presents outstanding physical properties, such as high thermal conductivity (5000 W/m.K), Young's modulus (1 TPa) and ultimate strength of 130 GPa. Furthermore, graphene possesses a large specific area (theoretical limit: 2630 m^2/g), gas permeability and high electron mobility.[36,38,39] Thus, it can be a good candidate of nanofiller to enhance the mechanical, thermal, and electrical properties of composite materials.

To produce graphene, various approaches have been used including chemical vapor deposition (CVD) of methane gas,[40-42] graphite oxide thermal reduction,[43,44] and one-step graphite exfoliation.[45] Among these, the process of obtaining graphite oxide (GO) from natural graphite powder and its further reduction to graphene has been extensively studied due to its elaboration simplicity and to its economic feasibility. This method consists on the oxidation of graphite powder in the presence of concentrated mineral acids and oxidizing agents which yields a large variety of GO and subsequent adiabatic thermal expansion to render functionalized graphene sheets (FGS).[37]

It is important to highlight that both graphite and GO have a layered structure qualitatively similar to certain silicates referenced in this study. Indeed, by dispersion into a polymer matrix, both nanoclays and functionalized graphene sheets exhibit similar states of dispersion depending upon factors such as the processing technique and the affinity between the phases. Moreover, nanoclay fillers often exhibit comparable aspect ratios to graphene-based fillers (up to 1000). Thus, the three morphological states suggested for polymer/layered silicate nanocomposites (see Figure I.9) are also possible with graphene-based nanocomposites.[46]

I.2.4. *General Methods of Preparation of Polymer Nanocomposites*

Effectively incorporating nanofillers to a polymer matrix may present a number of special challenges. The primary difficulties involve dispersing the filler homogeneously throughout the matrix, and achieving good bonding between the filler and the polymer. The procedures mainly used to prepare polymer nanocomposites can be included into the following groups: i) solution mixing, ii) *in situ* polymerization, and iii) melt processing.[6,10,12,22,33,47,48] Each method has individual requirements depending on the nature of the filler involved (layered silicate or carbon based nanofillers); nonetheless, the basic aspects of how to prepare the nanocomposite are common to all the systems.

- Solution Mixing

This method uses a solvent system in which the soluble polymer or pre-polymer is first mixed with the filler, and then the solvent is evaporated in a controlled way. In the particular case of polymer-clay nanocomposites, the layered silicate is swollen by the solvent. Upon solvent removal, the clay layers reassemble around the polymer, resulting in a polymer–clay nanocomposite.[10,49] While the preparation of polymer-carbon based filler nanocomposites involves mixing a carbon based nanofiller dispersion with a polymer solution and controlled evaporation of the solvent with or without vacuum conditions. In general, the most efficient dispersion of carbon based nanofillers is achieved by bath or tip sonication. In order to facilitate solubilization and mixing, the carbon nanofillers are often functionalized prior to adding to the polymer solution.[33,48] The solution mixing approach is limited to polymers that freely dissolve in common solvents.

- *In situ* polymerization

In the *in situ* polymerization method, the filler is first swollen (clay) or dispersed (carbon based nanofillers) within the monomer solution (or liquid monomer), followed by the polymerization step. Polymerization can be initiated either by heat or radiation, or by an initiator or catalyst.

- Melt processing

Due to the fact that many polymers soften when heated above their glass transition temperature (amorphous polymers) or their melting temperature (semi-crystalline polymers), melt processing has been a very valuable technique for the fabrication of nanocomposites. This is the most promising method and it has great advantages over both previously described methods, being both compatible with current industrial processes and environmentally friendly, owing to the absence of solvents.

In this method, the polymer and filler are mixed by application of intense shear forces. In particular cases, polymer chains can reptate from the molten mass into the silicate galleries to form either intercalated or exfoliated nanocomposites.[50]

On the other hand, achieving homogeneous dispersions of carbon based nanofillers in melts is generally more difficult than with solutions, and high concentrations of filler are hard to achieve, due to the high viscosities of the mixtures.[33,48]

Also, depending on the final morphology/shape of the nanocomposite, the bulk samples can then be processed by several techniques such as extrusion and injection molding.

I.2.5. *Properties and Applications of Polymer Nanocomposites*

Over the past decade, many academic and industrial researchers have incorporated nanocomposites technology to enhance properties of thermoplastics, thermosets, rubbers and biodegradable polymers. By doing so, they have virtually increased the versatility of these materials since the property enhancements have allowed them to commercially compete with traditional materials. The properties conferred by the nanoparticle added to the polymer matrix are remarkable. Some of the property improvements that can be mentioned are:[7]

- Efficient reinforcement with minimal loss in ductility and impact strength with as little as 2-5 % of these particles,
- Thermal endurance,
- Flame retardance,
- Improved liquid and gas barrier properties,
- Improved abrasion resistance,
- Reduced shrinkage and residual loss, and
- Altered electrical, electronic and optical properties.

Although the potential for the commercial application of nanocomposites is enormous, the actual application has been occurring at a very slow pace. However, it is clear that commercial applications of nanocomposites are still in their infancy, but if the market forecasts are right, nanocomposites could turn out to have a significant impact. Dispersions of nano-scale reinforcements in polymers are

already entering the marketplace in automotive and packaging applications, albeit in a low-profile manner and slower than had been anticipated. But that pace is expected to speed up dramatically. According to a report published in 2006 by BCC Research,[51] global consumption of nanocomposites is expected to reach 214,081 metric tons, or $1.4 billion in value, by 2014, with an annual growth rate of 27.1%, as shown in Figure I.12.

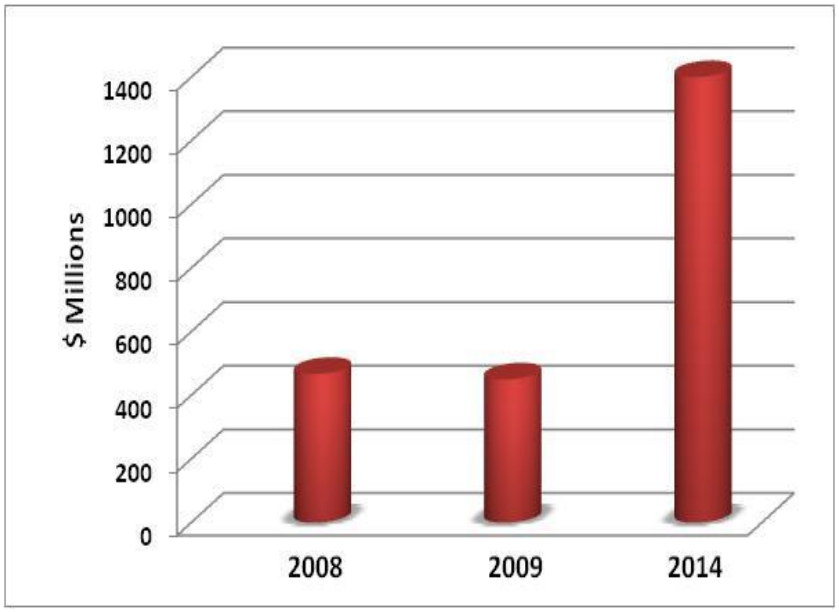

Figure I.12. Global consumption of nanocomposites, 2008-2014.[51]

According to this report, clay nanocomposites accounted for nearly one-quarter (24%) of total nanocomposite consumption by value in 2005, followed by metal and metal oxide nanocomposites (19%) and carbon nanotube composites (15%). By the end of 2011, clay nanocomposites were projected to increase their market share to 44%. Between 2005 and 2011, carbon nanotube nanocomposites, however, lost market share, down to 7.5%. With respect to the market share by application, packaging was expected to become the leading nanocomposite application, with over 28% of the market as displayed in Figure I.13. A detailed list of current nanocomposite applications and commercial products is also provided in Table I.2.

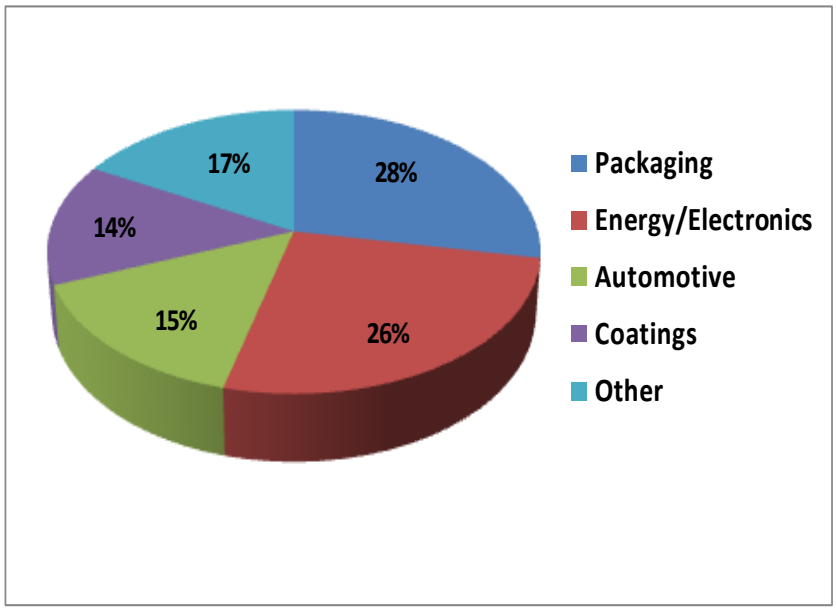

Figure I.13. Expected market share of nanocomposites by application for 2011.[51]

Finally, it is important to mention that performance not yet meeting expectations may not be due to any inherent flaws in the concept of nanocomposite technology. It is rather due to the fact that the production of nanocomposites is very system-specific. The understanding of the chemistry of filler modification, the physics and thermodynamics of filler dispersion, and the interplay of filler-polymer at the interface is crucial to the development of customized nanocomposites.

Table I.2. Summary of polymer nanocomposite applications and commercial products.[7]

Application	Characteristics	Nanocomposite	Commercial product
Packaging	Improved : ✓ Modulus ✓ Strength ✓ Heat distortion temperature ✓ Barrier properties	Nylon nanocomposites, polyolefin nanocomposites	Juice or beer bottles, multi-layer films, containers, packaging
Automotive	✓ Stiffer, stronger, less brittle, lighter ✓ More easily recycled ✓ Improved flame retardance and temperature resistance ✓ Very good impact properties	Nylon nanocomposites, polyolefin nanocomposites, rubber nanocomposites, and biodegradable poly lactide	Timing belt, cover, engine cover, barrier, fuel line, tire side-wall, electrical enclosure
Energy/Electronics	✓ Conductivity ✓ Environmental stability	Polyurethane nanocomposites, silicone nanocomposites	Thin-film capacitors in integrated circuits, solid polymer electrolytes for batteries, dielectric elastomer actuators

I.3. Natural Rubber Nanocomposites

Elastomers are usually reinforced with mineral fillers in order to get substantial improvements in strength and stiffness. Without the filler, rubber formulations would yield resilient products having elastic properties but very little strength. So, strength properties are introduced by the addition of rigid entities, and the inclusion of these fillers to rubber formulations results in the optimization of properties, especially to meet given application or sets of performance parameters.

The extent of property improvement depends on several parameters including the size of particles, their aspect ratio, their degree of dispersion and orientation in the matrix and the degree of adhesion with the rubber chains.[52] Traditionally, carbon black has been the primary filler used by the rubber industry. However, since the 1950´s non-black fillers such as precipitated silica have been increasingly used. At present, nanometer-scale reinforcing particles have attracted considerable attention from rubber scientists because of their small size and the corresponding increase in the surface area achieving the required mechanical properties at low filler loadings.

Over the past few years rubber nanocomposites based on Natural Rubber (NR) have received increasing attention and have been widely discussed by scientists by considering the number of potential nanofillers such as layered silicates, talc, silica and carbon based fillers. The next two sections provide information about the recent developments in NR nanocomposites focusing on layered silicates and carbon based nanofillers.

I.3.1. *Natural Rubber/Layered Silicate Nanocomposites*

Rubber nanocomposites based on NR with layered silicates has been a focus of research in recent years. Exfoliated and partially intercalated structures were successfully prepared by the different processing techniques exposed above (see section I.2.2). First findings were published by Bala *et al.*[53] and Joly *et al.*[54]. They presented the effect of alkyl ammonium salt of dodecylamine intercalated

montmorillonite (MMT) as filler on NR, reporting a good dispersion of the organoclay particles within the polymer matrix as deduced from scanning electron microscopy (SEM) and transmission electron microscopy (TEM), which finally enhanced the mechanical properties of NR.

Later on, a NR–organoclay nanocomposite with a fully exfoliated structure was firstly reported by López-Manchado *et al.*[55,56] They reported that the cure characteristics of pristine NR were affected by the organoclay, shortening the optimum vulcanization time. This effect was mainly attributed to the amine groups coming from the organic modification of the clay. The addition of the organosilicate also resulted in a sensible increase in the torque value as compared to the pristine NR, as an indication of higher number of cross-links formed. Also, Arroyo *et al.*[57] studied the possibility of substituting carbon black with white fillers, in particular by an organically modified montmorillonite as a reinforcement of NR. So, the physical and mechanical characteristics of NR filled with 10 phr of organoclay and 10 and 40 phr of carbon black were compared. The organoclay gave rise to a higher degree of cross-linking than the counterpart with carbon black, which was reflected in an increase on the mechanical properties.

One important aspect to take into account when dealing with elastomer/silicate nanocomposites is the compatibility between the nanosilicates and the rubber matrix. It is well known that the organoclay can be more easily dispersed in polar polymers than in non-polar ones, such as NR. For this reason, epoxidized natural rubber (ENR) has been used as a compatibilizer for NR–organoclay nanocomposites.[58-60] An interesting and innovative morphology was checked by Arroyo *et al.*[60] Most of the exfoliated nanoclay layers were selectively located at the NR–ENR interface. In addition, the organoclay gave rise to a finer and more homogenous dispersion of ENR phase. In fact, a clear decrease in the size of the dispersed ENR droplets was observed, which suggested that the organoclays might behave as compatibilizer agents reducing the interfacial tension between both polymer phases.

From these findings, different research groups focused their efforts on the evaluation of the industrial performance of NR nanocomposites[61] and on the understanding of the reinforcement of rubber matrices by the addition of nanoclays. López-Manchado *et al.*[62] studied the influence of inorganic nanoparticles on the cross-linking mechanism of NR by applying the tube model[63], since a deeper knowledge of this issue is of crucial importance to explain the improved properties of these nanocomposites and the mechanism of reinforcement by highly anisotropic fillers. Molecular network parameters derived from this model point out a different filler/elastomer reinforcement mechanism as a function of filler. It is well known that the inorganic particles are characterized by a high aspect ratio, so the optimum dispersion of even a small amount of nanoparticles (exfoliated nanocomposites) is enough to interact with the total rubber mass. Furthermore, these nanoparticles mainly exhibit physical adsorptions with the elastomer due to its inorganic nature. This leads to the formation of a highly ordered and entangled structure in which the mobility of rubber chains is hindered for lateral fluctuations by the presence of neighboring chains.

More recently, the phenomenon of strain-induced crystallization on NR/silicate nanocomposites has attracted the attention of many researchers. Carretero *et al.* [64,65] found that the presence of interfacial interactions between nanoparticles and polymer matrix and the enhanced mobility of the polymer on the clay surface are crucial in promoting strain-induced crystallization in NR nanocomposites. Moreover, they concluded that nanoclay introduces a dual crystallization mechanism due to the alignment of nanoparticles during stretching. Qu *et al.*[66] also reported similar findings on NR/silicate nanocomposites. They found that the nanomorphology of the clay dispersed in the NR matrix plays a decisive role in the crystallization behavior of NR during deformation, and that an increase in the exfoliation of the organosilicate leads to an increase in the promotion of strain-induced crystallization of NR.

I.3.2. *Natural Rubber/Carbon Based Filler Nanocomposites*

Carbon nanotubes (CNT) have shown to be attractive fillers in various applications due to their unique combination of outstanding mechanical properties, high electrical conductivity and reinforcement quality. Due to these excellent properties, an increasingly enthusiasm to explore their potential as nanofillers has been observed in the last decade. In this sense, many research groups have made comparisons on the reinforcement effects of conventional fillers such as carbon black (CB) and CNT to a NR matrix. As an example, López-Manchado *et al.*[67] characterized the effects of the incorporation of SWCNT on the physical and mechanical properties of NR. SWCNT behaved as effective accelerators, decreasing the time of the cross-linking reaction. The authors observed a strong filler-matrix interaction, which was reflected in a marked increase of the storage modulus as well as a noticeable shift of the glass transition temperature towards higher temperatures.

Bokobza *et al.*[68,69] prepared MWCNT/NR nanocomposites at several filler concentrations (in the range 1.0–9.1 wt%) by solution mixing. The results were also compared with those obtained with conventional CB. The authors observed that at a given strain level, a noticeable increase in the stress was achieved with a filler content of 2.4 wt.%. They demonstrated that the reinforcement provided by MWCNT was much higher than that by CB at the same filler loading. Furthermore, the authors studied the influence of CNT on the electrical properties of these systems. At an equivalent filler loading, samples filled with MWCNT displayed higher conductivity than those containing CB.

It is known that the dispersion of CNT into rubber materials is problematic due to the high aspect ratio of the CNT and high viscosity of the rubber. In addition, the interaction between the CNT and the rubber matrix is poor. So, in order to improve the adhesion between CNT and NR at the interface, several researchers have reported studies based on CNT that have been superficially modified. Sui *et al.*[70,71] observed that after being treated with acid and ball-milling, CNT dispersed well in the rubber matrix and interfacial interaction between them was

improved. The vulcanization times, scorch and optimum cure time decreased and the maximum torque increased after adding acid treated and ball milled CNT into NR. Also, Shanmugharaj *et al.*[72] found that 3-aminopropyltriethoxisilane functionalized CNT increased the scorch time and optimum cure time in the sulfur vulcanization of NR. NR/silane functionalized CNT composites exhibited higher modulus, tensile strength and elongation at break compared to NR vulcanizates due to the higher polymer-filler interaction between the silanized CNT and NR vulcanizates. Other type of treatment of CNT has been reported by Bhattacharyya *et al.*[73] They have reinforced NR using carboxylated multiwalled carbon nanotubes (c-MWCNT) dispersed with sodium dodecyl sulfate. The tensile and dynamic-mechanical tests demonstrated a strong enhancement in modulus (10-fold) and tensile strength (2-fold) at low strain in the rubbery state with up to 8.3 wt% of c-MWCNT. Dielectric measurements at room temperature revealed a low percolation threshold (< 1 wt.%) associated with the formation of an interconnected nanotube network.

In the last few years, research on NR nanocomposites has been addressed to the use of hybrid filler systems based on CNT and other conventional fillers (silica and CB). That is the case of the study reported by Cataldo *et al.*[74], in which MWCNTs were added to a CB-filled NR compound. The results show that the effects of the addition of MWCNT are dramatic and cause a strong increase in the viscosity and in the hardness and modulus with a neat reduction on elongation at break due to the stiffening effect of the MWCNT. Drawbacks of the NR nanocomposites prepared with MWCNT appear under dynamic testing. The cyclic deformation of the nanocomposite specimens, both under compression or under extension, revealed a strong hysteresis and heat generation due to internal friction between the surface of the nanotubes and the rubber matrix. This fact confirmed the poor surface interaction between MWCNT and the NR matrix. Also, Klüppel *et al.*[75,76] investigated the modification of technologically relevant properties due to the incorporation of CNT in silica-filled NR compounds. They demonstrated that the incorporation of CNT results in promising synergetic effects. The final materials show an enhanced mechanical stiffness and tensile strength, an increased modulus, and a high electrical conductivity with quite low amounts of CNT, though

the tear resistance under dynamical loading is slightly reduced. By means of dynamic mechanical analysis and dielectric broad-band spectroscopy, a better understanding of the conduction mechanism, the polymer/tube interaction, and the filler networking in CNT nanocomposites was achieved.

Concerning rubber/graphene nanocomposites, due to the recent development of graphene, the literature on this subject is still in its early stages but developing rapidly. Few interesting studies have already been reported illustrating the potential of these new nanocomposites based on rubber matrices such as nitrile rubber (NBR),[77,78] styrene-butadiene rubber (SBR),[79] silicone foam[80], thermoplastic polyurethane (TPU),[81] and butyl rubber.[82] To our best knowledge, only a patent[83] and a recently published work made by Yuan *et al.*[84] have been reported using a NR matrix. Yuan *et al.*[84] have proposed a new method, *i.e.*, ultrasonically-assisted latex mixing and *in situ* reduction (ULMR) process to prepare NR/graphene composites. GO was dispersed into NR latex using an ultrasonic field and was then reduced *in situ*, followed by latex coagulation to obtain the NR/graphene masterbatch. The results show that this method produces a much better dispersion and exfoliation of graphene in the matrix and contributes to an increase in the tensile strength compared to conventional direct mixing. Also, with increasing graphene content, the maximum torque, cross-link density, elastic modulus, and thermal conductivity of NR/graphene composites were found to increase.

I.4. Molecular Dynamics of Polymer Nanocomposites

One important objective in polymer science is the interrelation between molecular dynamics and structure which can be directly related to the physical properties of the system. In particular, studies of segmental dynamics and the related glass transition are of fundamental interest for understanding, and thus tailoring, properties improvement at the molecular level. Nonetheless, the study of the dynamics of polymeric materials is not a simple task since it deals with molecular chains of very large length which exhibit a great variety of movements ranging

from simple local motions like vibrations and rotations of atoms and/or groups of atoms, to cooperative motions of short and long range involving chain segments or even the molecular chain as a whole. Moreover, upon dealing with polymer nanocomposites, factors such as polymer–filler interactions, filler size, roughness and morphology (degree of dispersion), may affect polymer dynamics and need to be critically considered.

Relaxation techniques appear as a basic tool to investigate molecular dynamics of polymers. Such techniques are based on the response of the material to an external source (electric field, strain, pressure, temperature, etc.) which displaces it away from its equilibrium state in the absence of the exiting field. The return to its original state, after removal of the exiting field, is known as a relaxation process. Relaxations can be experimentally assessed by measuring a characteristic magnitude sensitive to the disturbance (polarization, stress, volume change, enthalpy, etc.). Relaxation properties can be very important in polymer processing. Some processes require polymers being elastic while others need the polymer to be viscoelastic. Thus, relaxation processes may play an important role through a complex pattern of temperature and frequency-dependent properties. In particular, relaxation properties can be studied by dynamic mechanical analysis (DMA), broad-band dielectric spectroscopy (BDS), or nuclear magnetic resonance (NMR) spectroscopy among others. In this chapter, the attention has been focused on the broad-band dielectric spectroscopy technique, since it has been extensively used throughout the present work.

I.4.1. *Broad-band Dielectric Spectroscopy (BDS)*

Dielectric spectroscopy is a useful tool for studying the molecular dynamics of polymers. This is due to the fact that a broad dynamical range between 10^{-2} up to 10^{9} Hz can be covered by this method. Therefore, motional processes which take place for polymeric systems on extremely different time scales can be investigated in a broad frequency and temperature range. Moreover, the motional processes depend on the morphology and microstructure of the system under investigation. Thus, information on the structural state of the material can be directly extracted by taking the molecular mobility as a probe for the structure. This method is sensitive to molecular fluctuation of dipoles within the system. These fluctuations are related to the molecular mobility of groups, segments or whole polymer chains which show up as different relaxation processes.

In dielectric spectroscopy, the external source is an electric field, $\vec{E}$, which originates the polarization of the material giving different types of responses: i) atomic polarization due to slight displacements of atoms or groups of atoms of the macromolecule; ii) electronic polarization that causes induced dipoles due to the distortion of the electron cloud of each atom with respect to the positive nucleus; and iii) the orientational polarization, which corresponds to the reorientation of the permanent dipoles in the direction of the applied electric field. Atomic and electronic polarizations are characterized by an instant response (lower than 10^{-13} s) regardless of the temperature. Thus, in the frequency window employed by this technique, the orientational polarization is expected to be responsible for the observed relaxation behavior.[85]

As previously mentioned, the response of a polymer to an applied electric field is strongly affected by the type of dipoles associated to the chain bonds. For long chain molecules there are different possibilities for the orientation of a molecular dipole vector with respect to the polymer backbone (Figure I.14).[85] Macromolecules with molecular dipoles fixed parallel to the backbone are called Type A polymers, while for Type B polymers, the dipole moment is rigidly attached

perpendicular to the chain skeleton. Chain molecules having the dipoles in a more or less flexible side chain are called Type C.

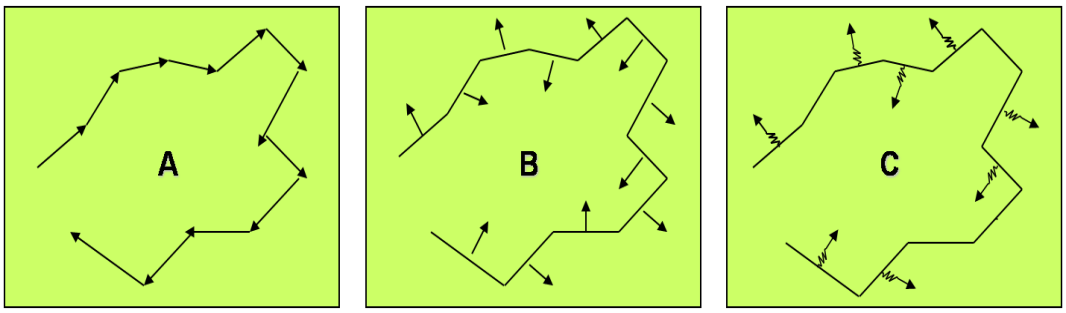

Figure I.14. Schematic representation of the different types of dipoles associated to the polymer chain.[85]

Due to the fact that molecular motions of polymer systems are controlled by very different time and length scales, different parts of the net dipole moment can be reoriented by diverse motional processes. Such motional processes can be localized to some bonds or to short side chain giving rise to local relaxations. On a larger spatial and longer time scale and for temperatures above the glass transition the so called segmental mode or α-relaxation becomes relevant and involves the relaxation of segments of the polymer chain. At even longer times and more extended length scale, for A-type polymers with a component of the dipole moment parallel to the chain, an additional process can be observed referred to as normal-mode relaxation. In this case, the translational motion of the whole chain can be characterized by the relaxation of the end-to-end dipole. This is possible because the molecular dipole vectors, that are parallel to the repeating unit, sum up over the chain. Therefore, this process referred to as normal mode relaxation, can be related to the overall chain dynamics.[85-87] An overview of such relaxation processes is given in Figure I.15.

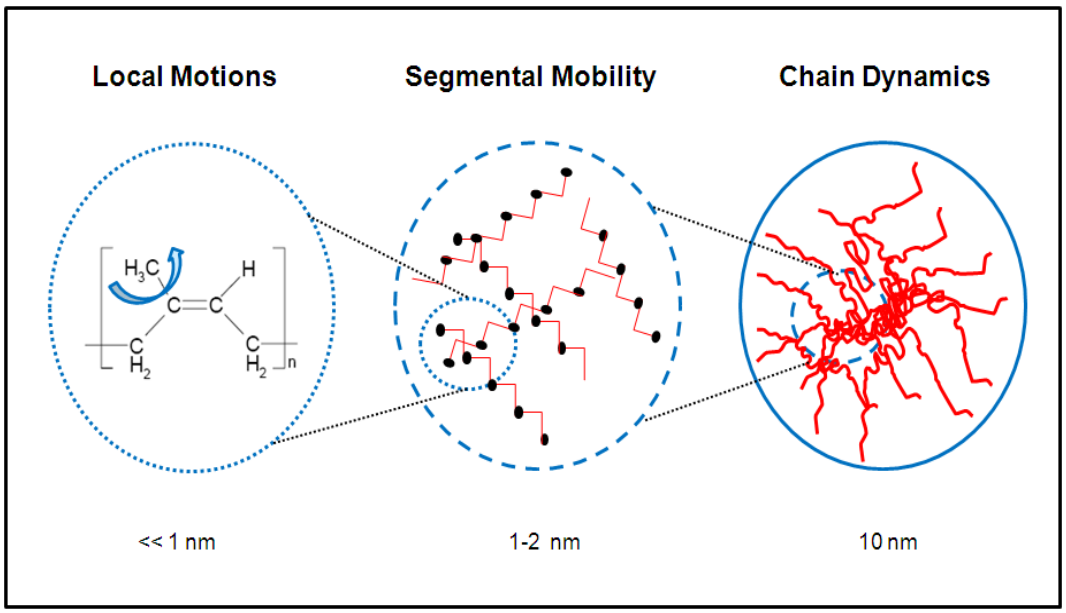

Figure I.15. Schematic representation of length scales and motional processes in polymeric systems.

It can be considered that permanent dipoles associated to the chain bonds act like "markers" that help to evaluate the movement of the chains as a function of the frequency of the electric field and temperature. When an electric field is applied, the orientational distribution changes and becomes anisotropic. In order to reach the new equilibrium state, a finite time is required since intermolecular forces hinder free rotation of the units that contribute to dipoles. For independent units, this movement can be described as a rotational diffusion resulting in a complete reorientation in a characteristic relaxation time, τ. While for interacting dipoles, the movement to equilibrium is characterized by a distribution of relaxation times. Only when sufficient time is allowed after the application of an electric field for the orientation to attain equilibrium, the maximum polarization (highest observable dielectric constant) will be realized in a material. If ample time is allowed, then the observed dielectric constant is called the static dielectric constant, ε_s. On the other hand, if the polarization is measured immediately after the field is applied, allowing no time for dipole orientation to take place, then the observed instantaneous dielectric constant, denoted ε_∞ will be low and due to deformational effects alone. Somewhere in between these extremes of timescale there must therefore be dispersion from a high (ε_s) to a low dielectric constant (ε_∞).

In order to obtain this dispersion, let us consider the application of an alternating electric field $\vec{E}$, amplitude $\vec{E}_0$ and angular frequency $\omega\,(\omega = 2\pi F)$, across a dielectric material:

$$\vec{E} = \vec{E}_0 \cos \omega t \qquad \text{I.3}$$

This will produce polarization which alternates in direction, and, if the frequency is high enough, the orientation of any dipoles which are present will inevitably lag behind the applied field. Mathematically, we can express this as a phase lag δ in the electric displacement:

$$\vec{D} = \vec{D}_0 \cos(\omega t - \delta) \qquad \text{I.4}$$

which may be written as

$$\vec{D} = \vec{D}_1 \cos \omega t + \vec{D}_2 \sin \omega t \qquad \text{I.5}$$

where

$$\vec{D}_1 = \vec{D}_0 \cos \delta \quad \text{and} \quad \vec{D}_2 = \vec{D}_0 \sin \delta \qquad \text{I.6}$$

This leads us to define two dielectric constants:

$$\varepsilon' = \frac{\vec{D}_1}{\varepsilon_0 \vec{E}_0} \quad \text{and} \quad \varepsilon'' = \frac{\vec{D}_2}{\varepsilon_0 \vec{E}_0} \qquad \text{I.7}$$

It is convenient to combine these two quantities into a complex dielectric constant of relative permittivity:

$$\varepsilon^* = \varepsilon' - i\varepsilon'' \qquad \text{I.8}$$

ε' and ε'' are experimentally observable quantities which may be used to characterize the dielectric dispersion over a range of frequencies. In order to be able to interpret any such dispersion behavior, it is first necessary to forge a link between these macroscopic observable quantities and molecular properties, by postulation of a reasonable model which describes the way the molecules respond to the applied field.

The theory of Debye[88] was pioneer in the treatment of dielectric relaxations. Based on this theory, for the particular case of an alternating field represented by the real part of equation I.2, which produces an alternating displacement as expressed in equation I.3, the complex dielectric constant or dielectric permittivity may be written as:

$$\varepsilon^* = \frac{\vec{D}(t)}{\varepsilon_0 \vec{E}(t)} = \varepsilon_\infty + \frac{\varepsilon_S - \varepsilon_\infty}{1 + i\omega\tau} \qquad \text{I.9}$$

which is called the Debye dispersion equation. Equating real and imaginary parts of the two sides,

$$\varepsilon'(\omega) = \varepsilon_\infty + \frac{\varepsilon_S - \varepsilon_\infty}{1 + \omega^2\tau^2} \qquad \text{I.10}$$

$$\varepsilon''(\omega) = \frac{\varepsilon_S - \varepsilon_\infty}{1 + \omega^2\tau^2}\omega\tau \qquad \text{I.11}$$

The dependency of these components with frequency is represented in Figure I.16. The dielectric loss peak has a half-height width of 1.14 decades. The maximum loss value occurs when $\omega\tau$=1, corresponding to a critical frequency ω_{max}=$1/\tau$, and location of this peak provides the easiest way of obtaining the relaxation time from experimental results. The difference in the dielectric constant measured at low and high frequencies is called the *dielectric strength* ($\Delta\varepsilon$) of the relaxation and it is related to the area under the absorption curve:

$$\Delta\varepsilon = \varepsilon_s - \varepsilon_\infty = \frac{2}{\pi}\int_{-\infty}^{+\infty} \varepsilon''(\omega)\, d(ln\omega) \qquad \text{I.12}$$

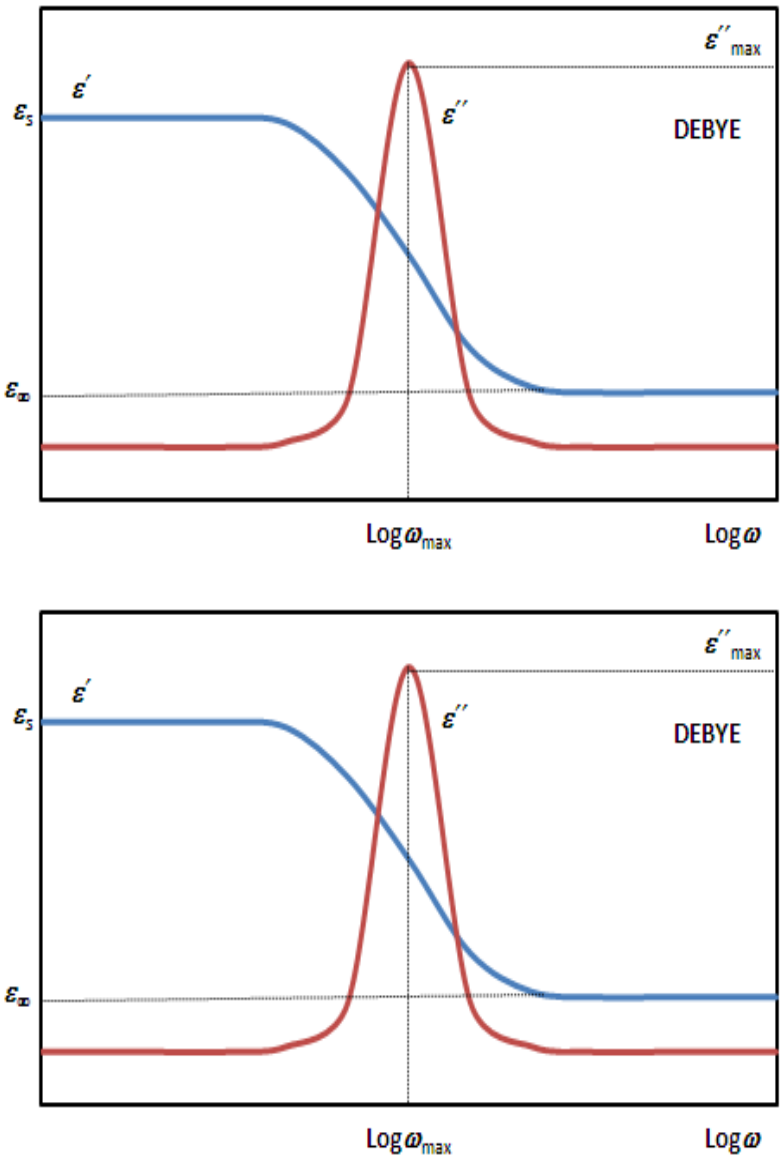

Figure I.16. Dielectric dispersion curves corresponding to a Debye process (TOP) and a Havriliak-Negami process (BOTTOM).

Relaxations observed in polymers, however, show broader dispersion curves and lower maxima than those predicted by the Debye model (see Figure I.16). The most general form for describing the experimental results comes from the Havriliak-Negami (HN) equation[89] which generalizes the Debye equation by including two new parameters that model the shape of the relaxation:

$$\varepsilon^*_{HN}(\omega) = \varepsilon_\infty + \frac{\varepsilon_S - \varepsilon_\infty}{[1+(i\omega\tau_{HN})^b]^c} \qquad \text{I.13}$$

where τ_{HN} represents the characteristic Havriliak-Negami relaxation time, which corresponds to the most probable relaxation time of the relaxation time distribution function[90] and b and c are the so-called shape parameters ($0 < b, c \leq 1$) which describe the symmetric and the asymmetric broadening of the equivalent relaxation time distribution function, respectively. τ_{HN} is related to the frequency of maximum loss, $F_{max} = 1/(2\pi\tau_{max})$ by the following equation:[91]

$$\tau_{max} = \frac{1}{2\pi F_{max}} = \tau_{HN}\left[\sin\frac{b\pi}{2+2c}\right]^{-1/b}\left[\sin\frac{bc\pi}{2+2c}\right]^{1/b} \qquad \text{I.14}$$

Both characteristic relaxation times coincide when the relaxation spectrum is symmetric, $c = 1$.

Usually different relaxation processes and often also a conductivity contribution add up. If the latter is of pure electronic origin it has no contribution to ε', while ε'' can be rewritten as:[85]

$$\varepsilon''_\sigma = \left(\frac{\sigma_{dc}}{\varepsilon_0\omega}\right)^s \qquad \text{I.14}$$

where σ_{dc} is the d.c. conductivity of the sample, ε_0 denotes the dielectric permittivity of vacuum ($\varepsilon_0 = 8.854 \times 10^{-12}$ F/m), ω the angular frequency and s an exponent ($0 < s < 1$) which depends on the nature of the conduction mechanism. Hence, the dielectric function

$$\varepsilon^*(\omega) = -i\left(\frac{\sigma_{dc}}{\varepsilon_0\omega}\right)^s + \varepsilon^*_{HN}(\omega) \qquad \text{I.15}$$

can be fitted to the data.[89]

I.4.2. *Dielectric Spectroscopy of Polymer Nanocomposites*

Dielectric spectroscopy has been employed to investigate molecular dynamics in relation to structure and morphology in polymer nanocomposites. To date, a wide range of polymer matrices have been analyzed, as well as different nanoparticles. For instance, Pissis *et al.*[92] studied three systems based on an epoxy resin matrix and different inclusions (modified smectite clay, conducting carbon nanoparticles and diamond nanoparticles), and two others with silica nanofiller (styrene-butadiene rubber/silica and polyimide/silica nanocomposites). Two opposite effects seem to be common to the nanocomposites studied and dominate their behavior: (1) immobilization/reduction of mobility of a fraction of the chains at the interface due to chemical or physical bonds with the nanoparticles, and (2) loosened molecular packing of the chains due to geometrical confinement, resulting in an increase of free volume and of molecular mobility.

On the other hand, Kalganokar *et al.*[93] have investigated the molecular dynamics of poly(ethylene glycol-*co*-cyclohexane-1,4-dimethanol terephthalate) nanocomposites based on an organically modified layered silicate. They found that the presence of the silicate accelerated the α-relaxation dynamics in the nanocomposites accompanied by a depression in T_g which was attributed to the reduced intermolecular cooperativity between intercalated polymer chains.

Biodegradable matrices have also been examined. As an example, Giannelis *et al.*[94] used dielectric relaxation spectroscopy to study the toughening mechanism of poly(lactide-co-glycolide) (PLG) when adding small amounts of surface modified clay nanoparticles. The clay nanocomposites showed a slow relaxation mode, most likely due to interfacial adsorption of PLG chains on the surface of the clay nanoparticles. They attributed the dramatic increase in toughness to physical cross-links introduced by the clay nanoparticles. The physical cross-links increase the brittle fracture strength of the polymer and, consequently, trigger a toughening mechanism via multiple crazing and shear yielding.

Furthermore, in order to estimate the role of surface effects at nanoparticle-polymer interface in polymer nanocomposites, Lopez *et al.*[95] used two types of fumed silica (Aerosil) nanosized particles: hydrophilic and hydrophobic; and a poly(n-octyl methacrylate) (POMA) matrix. Their findings revealed that the characteristic frequency of the α-process of the nanocomposites was shifted to higher values in comparison with the pure bulk polymer at the same temperature. This suggests that filling the polymer with nanoparticles resulted in the shift of its glass transition temperature, T_g to lower temperatures. The reduction in T_g was slightly bigger in the case of hydrophobic particles than in samples filled with hydrophilic particles with the same concentration. They attributed this change in T_g to the existence of a developed solid particle-polymer interface and to the difference in the dynamic behavior of the polymer in the surface layers at this interface compared to the bulk behavior.

Cheng *et al.*[96] also studied the influence of particle surface chemistry on the dielectric behavior of silica/epoxy nanocomposites. Silica nanoparticles, both unmodified and modified with the coupling agent KH-550 (g-aminopropyl-triethoxysilane) were used. Dielectric measurements showed that for all of the nanocomposite samples, the dielectric loss maxima shifted towards lower temperatures with respect to the control sample. Epoxy nanocomposites containing modified silica particles had also a broader distribution of relaxation time, indicating that the coupling agent enabled the nanoparticles to act corporately with the epoxy molecules by comparably prolonging the epoxy molecules. Therefore, the mobility of polymer molecules was enhanced. In addition, the extra free volume at the interface could assist the polymer mobility and therefore, the transition temperature was lowered.

More recently, Schönhals *et al.*[97] prepared fully exfoliated nanocomposites of organically modified doubled layered hydroxide (LDH) and low density polyethylene (LDPE). The prepared materials were investigated by differential scanning calorimetry (DSC) and in detail by dielectric spectroscopy. The DSC experiments showed that the degree of crystallinity decreased linearly with increasing content of the LDH. The dielectric response of pure LDPE showed

different weak relaxation processes, a γ-process at low temperatures which corresponds to localized fluctuations in the amorphous parts of LDPE and a β-relaxation which corresponds to the dynamic glass transition due to cooperative segmental fluctuations. The intensity of the β-relaxation increased with the concentration of LDH. The analysis of the β-relaxation region revealed the existence of two processes: a relaxation process at lower frequency assigned to LDPE segments with a reduced molecular mobility close to LDH layers, while the process at higher frequencies could be related to LDPE segments in a farther distance from the surface of the nanofiller. In the nanocomposite materials, an additional process due to Maxwell-Wagner-Sillars (MWS) polarization was observed.

The study of the dynamics of rubber nanocomposites by means of broad-band dielectric spectroscopy has also been of interest for several research groups such as Pissis *et al.*[98-100] and Klüppel *et al.*[101-103] Pissis *et al.* studied a series of poly(dimethylsiloxane) networks filled with silica nanoparticles synthesized *in situ*[98,99] and by sol-gel techniques.[100] In addition to the α-relaxation associated with the glass transition of the polymer matrix, they observed a slower α-relaxation assigned to polymer chains close to the polymer/filler interface whose mobility is restricted due to interactions with the filler surface.

Klüppel *et al.*[101,102] evaluated the effects of nanostructured fillers like organoclay and silica on carboxylated nitrile rubber. Three relaxation processes were detected. The relaxation processes at low and medium temperatures, assigned to the β-process and the glass transition, respectively. While the relaxation process at high temperatures was due to the formation of zinc-carboxyl-clusters. They also studied SBR-silica nanocomposites.[103] They found that the position of the glass transition of the investigated samples was not influenced by the addition of filler. In addition, they reported a low temperature process for the silica filled samples with significant different dynamics compared to the β-process, and ascribable to the silica itself and not based on the silica elastomer interaction.

They concluded that the “silica process” reflects the mobility of hydration water at the silica surface.

The dynamics of Natural Rubber nanocomposites has also been a matter of interest for several researchers. The following section gives a detailed review focused on common features and differences in the effects of nanoparticles on NR matrix dynamics, as revealed by dielectric techniques. Effects on the overall dielectric behavior, on local relaxations and, in particular, on segmental dynamics, are discussed.

I.4.3. *Dielectric Spectroscopy of Natural Rubber Nanocomposites*

The dynamics of synthetic polyisoprene (PI) by using dielectric spectroscopy was originally studied by Adachi and Kotaka[104-106] over 20 years ago. Since these studies, PI has been the subject of extensive experimental research.[107-111] More recently, the dynamics of its natural counterpart (NR) has also been studied,[112-115] but only in the last decade nanocomposites have been subject of interest for different research groups. As an example, Page *et al.*[116] studied the dielectric relaxation behavior in blends of sodium montmorillonite with low molecular weight synthetic PI. These authors report three relaxation processes: the normal mode, the segmental mode and an additional relaxation process at a temperature region below the glass transition temperature, T_g, of the pure polymer component. They assigned this relaxation process to the segmental motion of the chains intercalated in the interlayers of the clay.

Mijovic *et al.*[117] reported on the molecular dynamics of nanocomposites of low molecular weight synthetic PI and two organically modified clays (C25A and C30B), comparing results obtained by means of dielectric relaxation spectroscopy (DRS) and by dynamic mechanical analysis (DMA). Dielectric spectra of nanocomposites reveal no effect of clay loading or type on the average relaxation time for segmental mode relaxation, while the normal mode becomes faster with increasing clay content. A direct comparison of DRS and DMA results, made by deconvolution of dielectric and viscoelastic spectra, showed excellent agreement

between the average relaxation time for both segmental and normal mode relaxations. An observed increase in the elastic modulus G' and in the storage modulus G'' is indicative of the interactions between the dispersed layered silicates and the PI matrix.

Stephen *et al.*[118] also reported comparative results on the viscoelastic and dielectric properties of nanostructured layered silicates (sodium bentonite clay and sodium fluorohectorite clay) and NR, carboxylated styrene butadiene rubber (XSBR) and their blends. Upon the addition of filler, the storage modulus of nanocomposites was found to increase due to the enhanced contact surface area between polymer and filler. However, at higher concentration the modulus was found to decrease owing to the agglomeration of filler. With regard to dielectric properties they reported an increase on the permittivity value of the nanocomposites due to the high conductivity of the filler and the presence of polar groups in the silicates.

Psarras *et al.*[119,120] continued with the study of dielectric properties of nanocomposites based on NR and polyurethane (PUR) lattices filled with sodium fluorohectorite clay. Among their results, it can be mentioned a relaxation process in the low frequency range and relatively high temperatures, attributed to pronounced interfacial relaxation phenomena. This effect is observed in heterogeneous systems because of the accumulation of mobile charges at the constituents interface. They also found that the layered silicate appeared to be more compatible and thus better intercalated by the PUR than by the NR.

The study of the effects of the nanoclay on the different network components (topological constraints and defects) of NR by means of dielectric spectroscopy was initiated by Carretero *et al.*[65] He found that the inclusion of highly anisotropic nanoparticles led to microscale segmental variations, giving rise to the formation of a relative homogeneous network structure in rubber.

On the other hand, the relaxation dynamics of single-walled carbon nanotube (SWCNT)/polyisoprene (PI) nanocomposites were examined by Lee *et al.*[121]

Both functionalized and pristine nanotubes were used and their effect on dynamics compared. Functionalized nanocomposites were characterized by an increase in the time scale of the normal mode process as a consequence of the strong surface interactions between the polymer matrix and the nanotubes. The exact opposite behavior was seen in pristine nanocomposites where a decrease in the time scale of the normal mode relaxation was observed and attributed to weaker surface interactions and the effect of confinement on dynamics. The segmental process in of both types of nanocomposites was not affected by the presence of nanotubes.

More recently, Diaz-Calleja *et al.*[122] studied the molecular dynamics of nanocomposite materials obtained from NR reinforced with different amounts of cellulose II nanoparticles (in the range of 0 to 30 phr) by dielectric spectroscopy. The dielectric spectra of the nanocomposites exhibit: (a) two overlapped α-relaxations associated respectively with the dynamic glass transitions of NR and of the lipid present in NR; (b) a β-relaxation associated with local chain dynamics of cellulose and (c) a relaxation process associated to the presence of traces of water in cellulose. The spectra exhibit conductivity phenomena at low frequencies and high temperatures. The samples were also studied in the dry state.

Finally, Fragiadakis *et al.*[123] studied the effect of *in situ* synthesized 10 nm silica nanoparticles on the glass transition and dynamics of NR networks using BDS, DSC and thermally stimulated depolarization currents (TSDC). They found that even in the absence of specific polymer filler interactions, polymer segments within a few nanometers of the filler particles exhibit relaxation times up to 2-3 orders of magnitude slower and reduced heat capacity increment at the glass transition compared to bulk NR. These effects are only observed when the nanoparticles are uniformly distributed in the polymer matrix.

I.5. Main Objectives

Most of the studies up to date highlight that obtaining homogeneously dispersed nanofillers on an elastomer matrix is a must in order to improve the performance of the matrix. However, this fact is not enough for explaining the markedly difference with respect to elastomer compounds filled with conventional fillers. Moreover, although a large amount of research work has been devoted to characterizing the relationship between structure and properties of polymer nanocomposites, little attention has been paid to elucidate the mechanism of its mechanical reinforcement.

Thus, the main objective of this Doctoral Thesis was the study of the molecular dynamics of Natural Rubber nanocomposites in order to understand the physical relations between the different phases and interfaces present in the nanocomposite and its implication on the improvement of the final properties of the material.

To fulfill this main objective, this research has focused on three specific aspects:

- The first one is related to the effect on the dynamics of Natural Rubber of the additives required for the vulcanizing process. A detailed explanation on how these constituents affect the molecular dynamics and some related properties of Natural Rubber has not been reported up-to-date. The understanding of both the network structure and molecular mobility is expected to be useful in order to control the vulcanizing process system and to improve the properties of the final material.

- Secondly, a detailed evaluation of the dynamics of Natural Rubber nanocomposites has been accomplished by means of dielectric spectroscopy. By examining both the segmental and normal modes of NR, the precise effect on the polymer dynamics and on the vulcanization process of nanoparticle concentration and type has been assessed. Different types of nanofillers

including layered silicates, carbon nanotubes and functionalized graphene sheets have been analyzed.

- Finally, in an attempt to better understand the effect of strain induced orientation on the segmental dynamics of vulcanized Natural Rubber and its Natural Rubber nanocomposites, a series of X-ray scattering and broad-band dielectric spectroscopy experiments have been performed.

CHAPTER II. MATERIALS AND METHODS

II.1. Materials

II.1.1. *Natural Rubber (NR)*

Natural Rubber supplied by *Malaysian Rubber* (Berhad, Malaysia), under the trade name SMR CV60 was the polymer employed in this study as matrix of the prepared nanocomposites. It will be referred to as NR for simplification throughout this study. Some of the commercial characteristics of the polymer are shown in Table II.1.

Table II.1. Characteristics of SMR CV60.[1]

Parameter	Value
Dirt retained on 44-μm aperture (max. % weight)	0.03
Ash content (max. % weight)	0.50
Nitrogen content (max. % weight)	0.60
Volatile matter content (max. % weight)	0.80
Plasticity retention index PRI (min. %, 140 °C)	60
Mooney viscosity (ML,1+4,100 °C)	60

NR was characterized by several techniques, differential scanning calorimetry (DSC), thermal gravimetric analysis (TGA) and ^{13}C nuclear magnetic resonance spectroscopy (^{13}C NMR). The results are presented as supplementary information in Appendix A.

II.1.2. *Additives*

The ingredients employed as vulcanizing additives in the preparation of NR compounds are listed in Table II.2 mentioning their chemical structure, main function within the compound and the supplier.

Table II.2. Characteristics of the vulcanizing additives employed in NR compounds.

Name	Chemical structure	Function	Supplier
Zinc oxide	ZnO	Activator	*Bayer*
Stearic acid	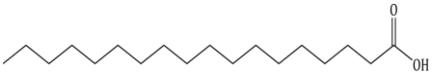	Activator	*Aldrich*
Mercapto benzothiazyl disulfide (MBTS)	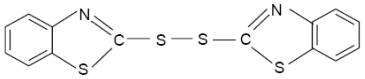	Accelerator	*Flexys*
Sulfur	S_8	Vulcanization agent	*Repsol*

II.1.3. *Fillers*

- Layered Silicates

Two layered silicates were employed in this study, a natural sodium-montmorillonite named Cloisite®Na^+ and its variant organically modified with a quaternary ammonium salt, Cloisite®15A. Both samples were provided by *Southern Clay Products Inc*. (Gonzales, USA). For the purpose of this research they will be denoted as CNa+ and C15A, respectively. The structural characteristics of the silicates are reported in Table II.3.

Table II.3. Technical characteristics of the layered silicates employed in this research.

Clay	Organic modifier	Modifier concentration (mEq/100g clay)	Basal spacing, *d* (nm)
Cloisite® Na^+ (CNa+)	none	---	1.17
Cloisite® 15A (C15A)	2M2HT[a]	125	3.15

[a] 2M2HT: dimethyl, dehydrogenated tallow, quaternary ammonium. The tallow consists in ~65% of C_{18}, ~30% of C_{16}, and ~5% of C_{14}, and a chloride anion.[124]

The basal spacing of the clays was experimentally determined by X-ray diffraction by applying the Bragg equation. The spectra are shown in Chapter IV.

- Multi-walled Carbon Nanotubes (MWCNT)

Aligned multi-walled carbon nanotubes (MWCNT) were grown by the chemical vapour deposition (CVD) injection method in a tubular quartz reactor contained within a heating furnace.[125,126] This method is based on the injection of a ferrocene (*Aldrich* 98%)/toluene solution (20 mL of 3 wt% of ferrocene in toluene) at a constant rate of 5 mL/h, under an inert argon atmosphere (325 mL/min) and at a temperature of 760 °C at atmospheric pressure. The reaction time was calculated taking into account the injection rate of the solution and adding 1.5 h. Once the reaction finished and the furnace reached room temperature, MWCNT were removed from the quartz tube and stored in a sealed container prior to use. Figure II.1 illustrates the equipment employed for the synthesis of the MWCNT.

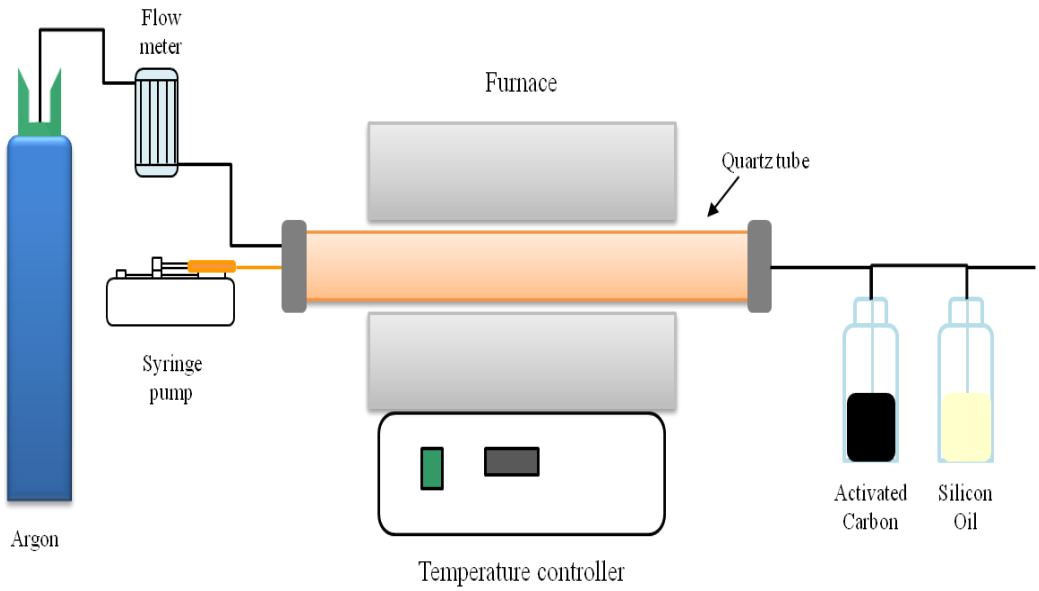

Figure II.1. Schematic representation of the furnace employed for the synthesis of MWCNT.

- Functionalized Multi-walled Carbon Nanotubes (f-MWCNT)

As-synthesized MWCNT, prepared as outlined above, were chemically treated with a 3:1 concentrated sulphuric/nitric acid mixture and refluxed at 120 °C for 30 min. Then, the mixture was filtered through a glass filter funnel using a PTFE membrane (0.2 μm pore size, *Millipore*) and washed with distilled water several times until neutral pH. The f-MWCNT were then dried at 120 °C and stored in a sealed container under vacuum prior to use to avoid possible effects of chemisorbed water due to their hydrophilic nature.[127,128] A schematic representation of the reaction is given in Figure II.2.

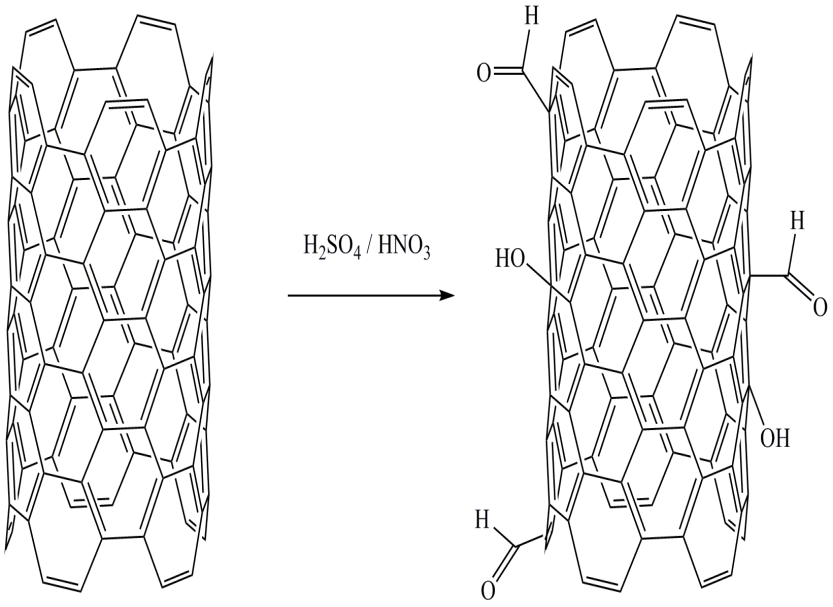

Figure II.2. Schematic representation of the functionalization of MWCNT.

- Functionalized Graphene Sheets (FGS)

The synthesis of functionalized graphene sheets was carried out following the steps schematically illustrated in Figure II.3. First, graphite oxide (GO) was produced using natural graphite powder (universal grade, 200 mesh, 99.9995%, *Fluka*) according to the Brödie method.[129,130] In a typical preparation procedure, a reaction flask with 20 mL fuming nitric acid was cooled to 0 °C in a

cryostat bath for 20 min. Then, the graphite powder (1 g) was carefully dispersed to avoid agglomeration. After that, $KClO_3$ (8 g) was gradually added over 1 h, in order to avoid sudden increases in temperature due to the exothermic nature of the reaction. The mixture was stirred for 21 h maintaining the reaction temperature at 0 °C. Then, it was diluted in distilled water and filtered using a PTFE membrane until the filtrate reached a neutral pH. The GO obtained was dried and stored in a vacuum oven at 50 °C until use. The GO was thermally exfoliated at 1000 °C under an inert argon atmosphere for a short time, usually less than 1 min, to produce the functionalized graphene sheets (FGS).

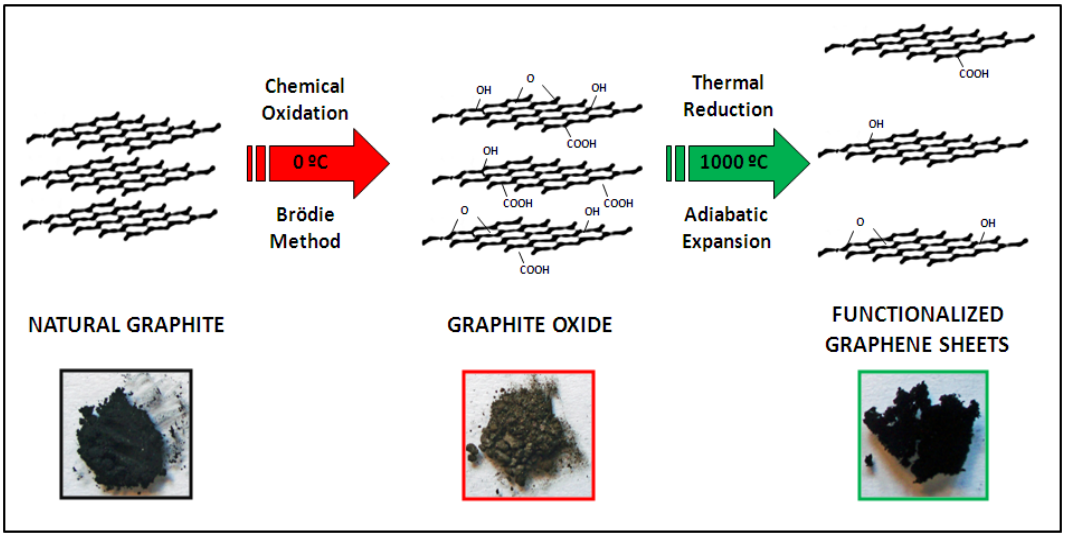

Figure II.3. Schematic representation of the steps followed for the synthesis of functionalized graphene sheets.

II.2. Preparation of NR Nanocomposites

All the compounds were prepared in an open two-roll laboratory mill (*Comerio Ercole MGN-300S*) at room temperature. The rotors operated at a speed ratio of 1:1.4. First, the mastication of the rubber took place. Afterwards, all the vulcanizing additives except sulfur were added to the rubber prior to the incorporation of the filler and, finally, sulfur was added. The mixing time was kept constant in all cases. The general formulation of NR compounds is detailed in Table II.4.

Table II.4. Formulation of NR nanocomposites.

Ingredient	Content (phr)[a]
NR	100
Zinc oxide (ZnO)	5.0
Stearic acid (SA)	1.0
Mercapto benzothiazyl disulfide (MBTS)	1.0
Sulfur (S)	2.5
Filler	variable

[a]phr: parts per hundred parts of rubber

NR compounds were vulcanized in an electrically heated hydraulic press (*Gumix TP300/450/1*) at 150 °C and 200 MPa. The optimum cure time, t_{90} was derived from the curing curves previously determined by means of a Rubber Process Analyzer (*Alpha Technologies RPA2000*).

The morphology, physical and mechanical properties and molecular dynamics of non-vulcanized and vulcanized NR compounds reinforced with several nanoparticles (layered silicates, multi-walled carbon nanotubes, functionalized multi-walled carbon nanotubes and functionalized graphene sheets) were examined. The filler content used in each case varied according to the particular objectives of this research. Complementary information on specific procedures and compound formulation is presented in the experimental section of each chapter of results and discussion.

II.3. Experimental Methods

II.3.1. *Characterization of Fillers*

- X-ray Diffraction (XRD)

The nature and morphology of the clay nanoparticles (CNa+ and C15A) was analyzed by means of X-ray diffraction. A diffractometer (*Bruker D8 Advance*) was employed with a radiation source of CuKα and wave length λ_w= 0.154 nm operated at 40 kV and 40 mA. The incidence angle (2θ) was fixed between 1° and 30° and the scan rate was 0.02°/s.

The basal spacing (d) was evaluated by applying Bragg´s law, defined as

$$\lambda_w = 2d \sin\theta \qquad \text{II.1}$$

XRD was also used for analyzing the exfoliation process of graphite in order to obtain FGS.

- Transmission Electron Microscopy (TEM)

The morphology of the carbon based nanofillers (MWCNT, f-MWCNT and FGS) was determined through transmission electron microscopy (*Philips Tecnai 20*), operated at an accelerating voltage of 120 kV. The samples were prepared by drop-casting a dilute suspension in THF onto a carbon grid and allowing the solvent to evaporate.

- X-ray Photoelectron Spectroscopy (XPS)

XPS was used to determine the surface chemical composition and bonding of MWCNT, f-MWCNT and FGS. XPS studies were performed on a *VG Escalab 200R* spectrometer equipped with a hemispherical electron analyzer operated on a

constant pass energy mode and non-monochromatized Mg X-ray radiation ($h\upsilon$=1253.36 eV) at 10 mA and 12 kV. The samples were first placed in a copper holder mounted on a sample rod in the pre-treatment chamber of the spectrometer and then degassed at room temperature for 1h before being transferred to the analysis chamber. Data analysis was performed with the XPS peak program. The spectra were decomposed by the least-squares fitting routine using a Gauss Lorentz product information after subtracting a Shirley background. The binding energies (BE) were normalized by using the C_{1s} peak (284.8 eV) of carbon as an internal standard.

- Raman Spectroscopy

Raman spectroscopy is a straight forward characterization technique to analyze the structural quality of graphitic materials such as graphite, diamond and carbon nanotubes. The amount of ordering and degree of sp^2 and sp^3 bonding provides a unique Raman "fingerprint" for each carbon nanostructure.

Raman spectroscopy was performed on a *Renishaw Invia* raman microscope. The analyses were done using an argon laser at 514.5 nm excitation wavelength. The carbon nanofillers were placed on a glass slide and air-dried before the measurements were taken.

II.3.2. *Characterization of Nanocomposites*

- X-ray Diffraction (XRD)

The intercalation degree of the NR chains into the silicate gallery was analyzed by means of X-ray diffraction. The equipment and conditions employed were the same as the ones used in the characterization of the filler.

- Transmission Electron Microscopy (TEM)

The dispersion and morphology of the nanoclays (CNa+ and C15A) in the rubber matrix were determined through transmission electron microscopy was determined through transmission electron microscopy (*Philips Tecnai 20*), operated at an accelerating voltage of 120 kV. TEM samples with ~40 nm thickness were prepared by sectioning at -140 °C using a cryoultramicrotome (*Leica Ultracut UCT)* with a diamond knife.

- Rheometry

The evaluation of the rheometric properties of the prepared NR and NR nanocomposites was performed from the curing curves obtained in a Rubber Process Analyzer (*Alpha Technologies RPA2000*), at a temperature of 150 °C, with a disk oscillating amplitude of 1° and a maximum time for all the curing process of 40 min. The resultant t_{90} from each curve was the time employed for the vulcanization of each of the systems analyzed in this work.

- Differential Scanning Calorimetry (DSC)

Differential scanning calorimetry (*Perkin-Elmer DSC7*) was performed in order to investigate the thermal transitions present in NR and its layered silicate nanocomposites. The scan rate was 10 °C/min in the temperature range from -75 to 75 °C, following a heating/cooling/heating cycle in nitrogen atmosphere in order to eliminate the thermal history of the material.

- Tensile Experiments

Tensile stress–strain properties of vulcanized NR and its nanocomposites were measured in a dynamometer (*Instron 3366*) at 25 °C and at a cross-head speed of 500 mm/min. Rectangular-shaped specimens were mechanically cut out from the vulcanized film samples. At least five specimens of each sample were tested.

II.3.3. *Broad-band Dielectric Spectroscopy (BDS)*

BDS measurements were performed on a BDS-40 high resolution dielectric analyzer (*Novocontrol Technologies GmbH*). This equipment is composed of an ALPHA type dielectric interface and a QUATRO type temperature controller. The experiments were carried out over a frequency window of $10^{-1} < F/\text{Hz} < 10^{7}$ (being $F = \omega/2\pi$ the frequency of the applied electric field and ω the corresponding angular frequency) in the temperature range from -150 to 150 °C in 5 °C steps. The temperature of the experiments was controlled by liquid nitrogen flow, with an error for each range of frequency of ± 0.1 °C.

NR and NR nanocomposites film samples were used for the BDS measurements. Films were mounted in the dielectric cell between two parallel gold-plated electrodes. In some cases Kapton spacers were used to keep the thickness constant during the experiment.[131]

The complex permittivity ε^* of each given sample was calculated from the measurement of the complex impedance Z^* given by

$$Z^*(\omega) = \frac{U^*(\omega)}{I^*(\omega)} \qquad \text{II.2}$$

where U^* and I^* are the voltage and current circulating through the sample at a certain angular frequency ω. Once the impedance has been measured, ε^* can be calculated by means of

$$\varepsilon^*(\omega) = \varepsilon' - i\varepsilon'' = \frac{1}{i\omega Z^*(\omega) C_0} \qquad \text{II.3}$$

where ε' and ε'' are the real and imaginary part of the complex dielectric permittivity, respectively and C_0 corresponds to the capacity of the empty sample holder.

The corresponding mathematical analysis of the relaxation curves obtained was performed by the phenomenological Havriliak-Negami (HN) function[85,89] described in Section I.4.1.

II.3.4. *Wide Angle X-ray Scattering (WAXS) and Small Angle X-ray Scattering (SAXS) with Synchrotron Radiation*

WAXS and SAXS measurements were performed in order to evaluate the crystallization behavior under uniaxial deformation of NR and NR/layered silicate nanocomposites. Experiments were carried out at the BM16 beam line[132] (*European Synchrotron Radiation Facility-ESRF*, Grenoble, France). The measurements were performed in transmission. Each stretched sample-frame assembly was placed in the beam path. The wavelength of the X-rays used was 0.09795 nm. The two-dimensional WAXS/SAXS patterns were recorded using a MarCCD camera (*X-Ray Research GmbH*). The image acquisition time for each frame was 3 s for WAXS and 1 s for SAXS. The diffraction angle was calibrated by a standard sample of alumina. All measured images were corrected for background, beam fluctuations and sample absorption. The data analysis software FIT2D© was used to analyze the WAXS/SAXS images.

CHAPTER III. ROLE OF VULCANIZING ADDITIVES ON THE DYNAMICS OF NATURAL RUBBER[#]

[#]Part of the work described in this chapter has been published in *Macromolecules* **2012**, 45(2), 1070-1075. *Reprinted by permission from [133] Copyright 2012.*

III.1. Introduction

Sulfur vulcanization is the traditional method for curing polydiene rubbers including NR. However, although sulfur vulcanization is a relatively old large-scale industrial process, and considerable research in studying this process has been performed over the last several decades, a complete fundamental understanding of this complex chemical process remains as a significant scientific challenge. A rigorous research effort continues today aiming to unravel the mechanisms of the individual steps in the sulfur vulcanization process.[134,135] The difficulties encountered in this research field must be accredited by a combination of diversity and complexity. As mentioned in Chapter I the vulcanization reaction usually involves the use of several chemical ingredients such as a vulcanizing agent (sulfur (S)), an accelerator, and an activator complex formed by a fatty acid (stearic acid (SA)) and zinc oxide (ZnO). The situation is further complicated by two factors: (a) the interaction of the accelerators and activators, each component influencing the reactivity of the other and (b) by the way in which these interactions affect the vulcanization mechanism.

Plenty of literature[1,113,136-140] reveals that the addition of these chemicals in small quantities with respect to raw rubber affects the processability and the final properties of the vulcanized compounds. In general, the use of accelerators in combination with zinc activators has a pronounced effect on the rate of vulcanization and on the distribution of cross-links formed. In addition, the durability of rubber articles as well as the physical properties, in particular the tensile strength, are very much improved by organic accelerators.

Nonetheless, it is streaking that despite the enormous practical knowledge developed so far, a detailed description on how these constituents affect the molecular dynamics and the related properties of non-vulcanized NR is unknown. Moreover, most vulcanization systems have been developed by skillful and elaborated techniques based on the trial-and-error method.[141] Thus, a detailed discussion on the relationship between molecular dynamics and the effect of each one of the additives in the vulcanization system, prior to vulcanization, is of great

interest not only for technological developments but also for a better understanding to the NR properties. In this chapter, experimental evidence, by using broad-band dielectric spectroscopy (BDS), about the changes on the segmental and chain dynamics of non-vulcanized NR when every vulcanizing additive has been added is presented. It will be shown how description of the interactions between the vulcanizing additives and the NR chains can help to elucidate the reactions involved in the sulfur vulcanization mechanism.

III.2. Experimental

A typical sulfur rubber formulation was used in order to analyze the effect of each one of the ingredients on the NR molecular dynamics, as expressed in Table III.1. The samples prepared are referred to as NR/*x*/*y*/*z*, where *"x"*, *"y"*, and *"z"*, correspond to each of the additives present in the compound. It should be emphasized that this chapter is restricted to non-vulcanized samples. This means that, even though the vulcanization additives have been added, the vulcanization reaction has not taken place.

Table III.1. Formulation and ingredients used in the preparation of NR/additives compounds.

Ingredient	Content (phr)
NR	100
Zinc oxide (ZnO)	5.0
Stearic acid (SA)	1.0
Mercapto benzothiazyl disulfide (MBTS)	1.0
Sulfur (S)	2.5

In order to perform BDS measurements, samples of neat NR and NR/additives compounds as disk-shaped films were prepared by compression molding at room temperature. The disk samples were then mounted in the dielectric cell between

two parallel gold-plated electrodes. Kapton© spacers of 74 μm of thickness were used to prevent short circuits.[131] Because of the use of spacers the measured values have to be considered as relative ones.

III.3. Dynamics of NR

Similar to synthetic 1,4-*cis*-poly(isoprene) (PI),[107,108,116,117] two distinct regions of dielectric dispersion are present in NR. Figure III.1 shows the temperature and frequency dependence of the dielectric loss ε'' for NR. The two relaxation processes are well separated on frequency and temperature. Starting from lower temperatures, the faster process, referred to as segmental mode, occurs above the glass transition temperature (T_g = -64 °C) while the slower, referred to as normal mode, appears as a broader relaxation at temperatures above T= 50 °C.

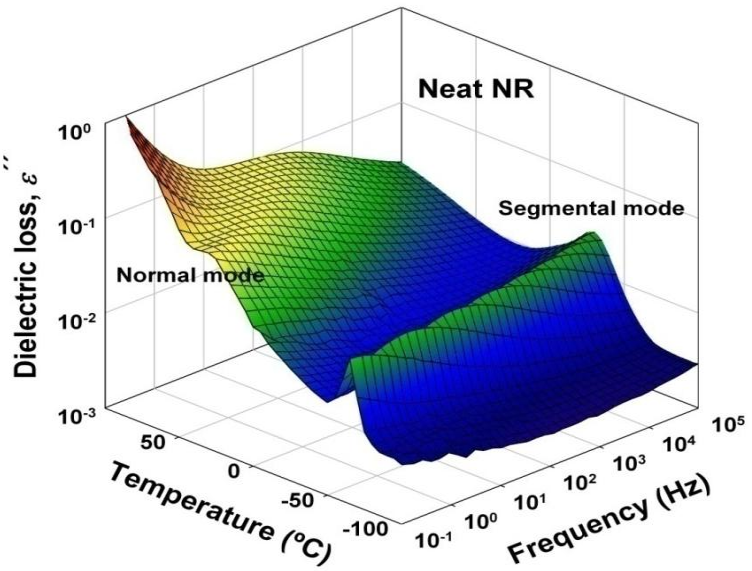

Figure III.1. 3D representation of the frequency and temperature dependence of the dielectric loss ε'' for neat NR.

The segmental mode is related to the segmental motions of the polymer chain and it originates from local motions of the perpendicular dipole moment. The normal

mode corresponds to motions of the entire chain caused by net chain dipole originated by the different dipole components parallel to the chain backbone. In the following sections, the influence of the vulcanization ingredients on the segmental and chain dynamics of non-vulcanized NR will be addressed.

III.4. Segmental Dynamics of NR/Additives Compounds

The values of the dielectric loss ε'' for the segmental mode of NR samples measured in the available frequency range are shown in Figure III.2. For the sake of comparison and in order to avoid the effect of the non-absolute character of the measured ε'', the data have been normalized to the corresponding ε''_{max} of every curve. As expected, the segmental mode manifests itself for all systems by a maximum in ε''. It is evidenced that the presence of additives shifts the maximum of the loss peak to slightly lower frequencies, suggesting a slower dynamics for the NR/additives compounds. In addition, a clear asymmetric broadening towards the low-frequency side of the dielectric loss curves is clearly detected.

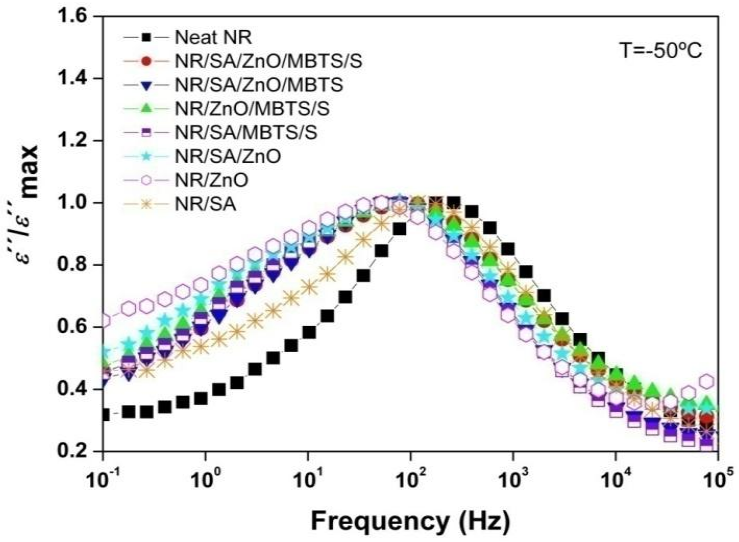

Figure III.2. Normalized dielectric loss ε'' versus frequency of NR and NR/additives compounds in the region of the segmental mode.

Such a behavior suggests the existence of a second dynamic process slower but close to the segmental mode of NR appearing when additives are present. In one hand, it is worth to notice that the relaxation behavior of the NR/SA compound is the closest to the neat NR. On the other hand, the rest of the NR/additives compounds present a more pronounced broadening at the low frequency side of the dielectric loss curves.

In order to estimate separately the contribution of each additive on both relaxation processes, the dielectric loss spectra of NR compounds are grouped in Figure III.3 as three different series. In Series 1 it is intended to study the effect of sulfur (S) and accelerator (MBTS), while results from Series 2 and Series 3 serve to elucidate the effect of the activator complex (SA/ZnO) in the presence or absence of other additives. Some of the figures shown in the series are duplicated for the sake of clarity and better understanding of the systematic removal of the different vulcanizing additives.

Every dielectric spectrum is analyzed and the experimental data of ε'' versus frequency is fitted in terms of the phenomenological Havriliak-Negami (HN) function[85,89] described in Section I.4.1. A superposition of two HN relaxation processes (named α' and α in order of increasing frequency) corresponding to each one of the experimentally determined relaxations, plus a conductivity contribution, are considered to fit the dielectric data (see Figure III.3).

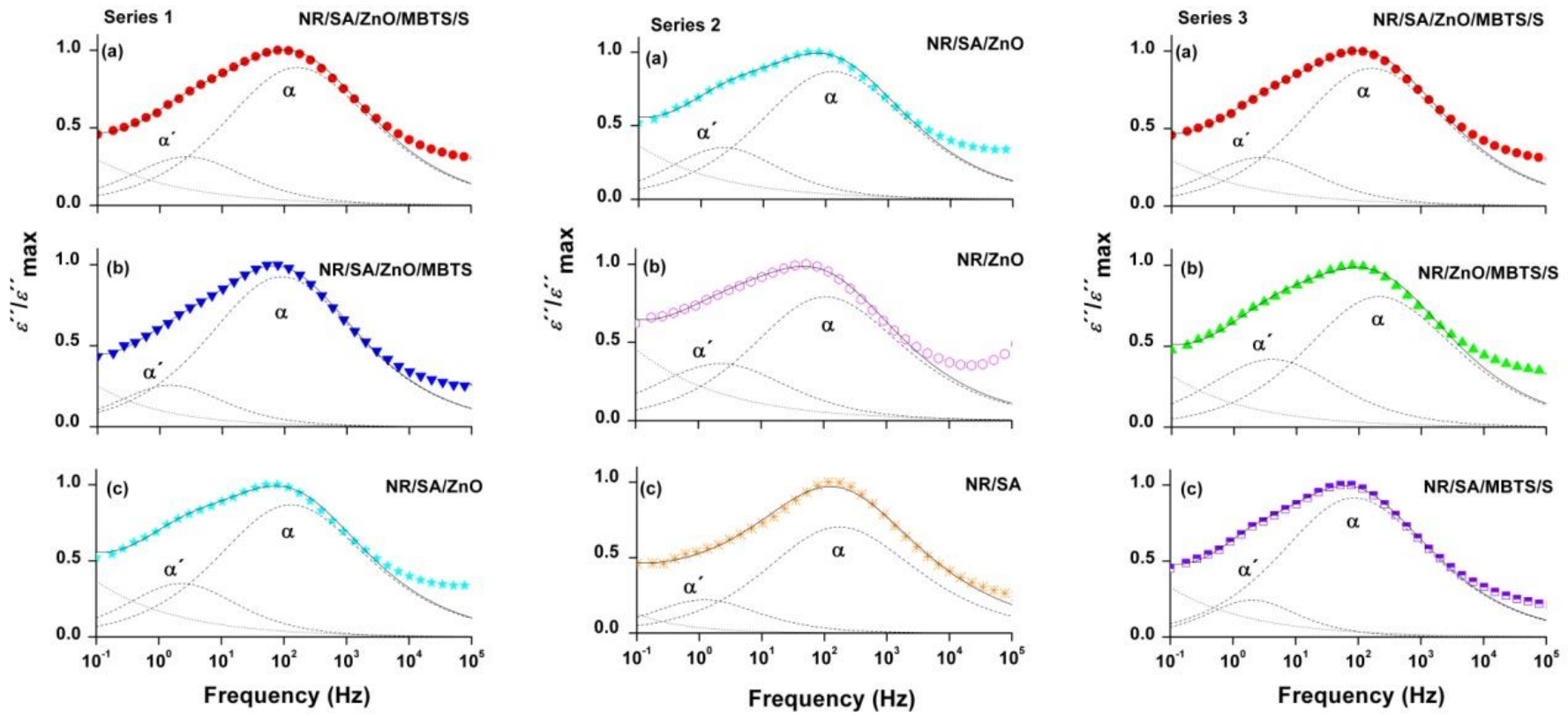

Figure III.3. Deconvolution results for the normalized dielectric loss ε'' of NR/additives compounds at T=-50 °C. Solid lines represent the HN fitting curve, dashed lines the individual processes, and dotted lines the conductivity contribution.

The relaxation parameters ($\Delta\varepsilon$, b, c and τ_{HN}) representative of each fitting are calculated (see Table III.2). It should be noted that several fitting procedures are examined, and the selected fitting protocol was chosen since it was considered as the method that ensured more physical coherence. In a first approach, it is assumed that the main relaxation process (α) is not significantly affected by the additives. Accordingly, a similar shape than that of the α-relaxation of neat NR is considered. Thus, the shape parameters b and c are kept constant and similar to those obtained for neat NR (b=0.527; c=0.833). While for the α'-relaxation, the parameter c is set to a value of 1 in order to force a symmetric shape and thus, a narrower distribution of relaxation times. Considering asymmetric shape for the α' process renders no reasonable fitting for the overall process. As expected, the strength relaxation intensity ($\Delta\varepsilon$) is higher for the α-relaxation than for the α'-relaxation for all compounds.

Table III.2. Representative values of the fitting parameters of the HN function for neat NR and NR/additives compounds at T=-50 °C.

Compound	$\Delta\varepsilon_{\alpha}$	$\Delta\varepsilon_{\alpha'}$	$\tau_{HN\alpha}$	$\tau_{HN\alpha'}$
Neat NR	1.431×10^{-01}	---	1.045×10^{-03}	---
NR/SA/ZnO/MBTS/S	1.169×10^{-01}	3.211×10^{-02}	1.370×10^{-03}	5.799×10^{-02}
NR/SA/ZnO/MBTS	3.119×10^{-02}	8.782×10^{-03}	2.403×10^{-03}	1.115×10^{-01}
NR/ZnO/MBTS/S	6.355×10^{-02}	2.865×10^{-02}	1.048×10^{-03}	3.900×10^{-02}
NR/SA/MBTS/S	7.785×10^{-02}	1.279×10^{-02}	2.556×10^{-03}	7.941×10^{-02}
NR/SA/ZnO	6.514×10^{-02}	2.232×10^{-02}	1.599×10^{-03}	6.463×10^{-02}
NR/ZnO	6.699×10^{-02}	2.763×10^{-02}	2.062×10^{-03}	7.112×10^{-02}
NR/SA	4.975×10^{-02}	7.061×10^{-03}	1.328×10^{-03}	1.341×10^{-01}

From Figure III.3 Series 1 results one can infer that sulfur (S) and accelerator (MBTS) are not likely to be responsible for the appearance of the slower process represented by α'. In this case, one can clearly see that after elimination of MBTS and S from the compound (Series 1c), the shoulder at low frequencies is still present.

Next, the effect of the activator complex (SA/ZnO) (Figure III.3 Series 2) is evaluated. Several authors[137,142-144] have studied the influence of the activator complex on the cross-linking reaction of NR. Recently, Ikeda *et al.*[136] have proposed that the combination of ZnO with the other reagents is crucial to control the quality of the vulcanization. Here it can be corroborated by BDS that ZnO is the element with stronger effect on the segmental dynamics of NR. In this sense, the low frequency shoulder characterized by α' appears when the complex SA/ZnO is present (Figure III.3 Series 2a). However, the elimination of SA from the formulation leaves α' almost unaffected (Figure III.3 Series 2b). The origin of this slow relaxation in NR has been recently discussed in the literature. In a previous study, Ortiz-Serna *et al.*[115] attributed this slower relaxation to the dynamics of SA linked to the polymer chains. The experimental measurements herein presented indicate that this slower relaxation is mainly attributed to the presence of ZnO. The influence of ZnO on the dielectric behavior of polymer matrices has previously been discussed. Psarras *et al.*[145,146] found an additional relaxation mode related to the presence of ZnO in epoxy resin-ZnO composites, in the same frequency and temperature range as the α-relaxation, leading to a mutual superposition. They attributed this behavior to polarization effects taking place in parts of the ZnO, which are relaxing under the influence of the AC electric field. Also, Smaoui *et al.*[147] found that the presence of ZnO in epoxy nanocomposites increased the interactions at the interface, so decreasing the orientation capabilities of dipoles under the effect of an AC electric field.

ZnO is known as the best activator for sulfur vulcanization. There is nowadays, however, an increasing concern regarding the potential environmental and health effects related to the release of zinc compounds into the environment from rubber

products or rubber production.[148] Thus, it is desirable to keep the ZnO content in rubber compounds as low as possible, not only for environmental but also for economical reasons. Nonetheless, the exact role of ZnO on the network structure has not been well understood. Several theories have been postulated, and the complexity of the vulcanization process has given rise to many uncertainties and contradictions in the literature about the influence of ZnO during the different stages of the process and its exact mechanisms.[134,135,149] One of the proposed mechanisms[134,138,150] suggests that ZnO plays the role of a catalyst and promotes the initial response by activating and bringing together reactants. It is assumed that ZnO is distributed in the form of crystal particles in the rubber compounds. Molecules of accelerators, sulfur, and fatty acid are adsorbed on the surface of the ZnO, forming intermediate complexes (benzothiazole-zinc complex). The reactant of the benzothiazole-zinc complex does not have appreciable solubility in rubber, but the solubility and reactivity can be enhanced by the presence of SA in that forming zinc stearate.[136,143] On the other hand, some authors[113] suggest that the ionic nature of zinc stearate is responsible for the appearance of a second relaxation process in vulcanized NR, which may be attributed to rubber chains of lower mobility which are tightly bounded to zinc stearate surface. It is known that in the case of ion-containing polymers, ion pairs segregate to form ion aggregates, which restrict the mobility of adjacent segments of the polymer chains and form a separate rigid phase.[151,152] These immobile segments of the rubber chains undergo relaxation at lower frequencies. This means that some restrictions on the segmental dynamics of NR chains due to the surrounding environment are expected. In this context, the BDS results provide strong evidence about the activation effect that ZnO has on the vulcanization process of NR. The α'-relaxation could be attributed to the ionic clusters of ZnO forming physical entanglements within the rubber chains. These clusters can act as cross-link precursors as schematically represented in Figure III.4. Results from Figure III.3 Series 3 confirm that the absence of ZnO in the formulation reduces significantly the intensity of the α'-relaxation.

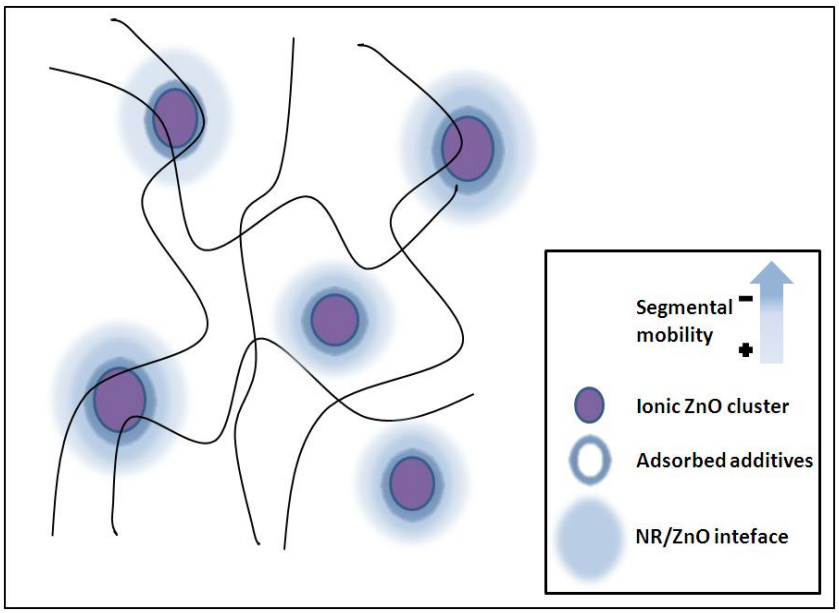

Figure III.4. Schematic representation of proposed morphological structure of NR/additives compound as derived from the BDS measurements.

Figure III.5 displays the dielectric strength values of both relaxation processes for NR with the different additives. The error bars have been estimated applying different fitting protocols in order to establish the merits of the previous fitting assumptions. Two interesting results can be extracted from the analysis of this chart. Firstly, the NR/SA compound has the lower intensity relation value, so it can be presumed a minor contribution of SA to the α'-relaxation. This fact is in agreement with the results shown in Figure III.2, where, as previously mentioned, there is certain similarity between the normalized loss curves of neat NR and NR/SA compound. The second interesting result extracted from Figure III.5 is the higher intensity relation value obtained for all compounds where ZnO is present. Thus, it becomes quite clear that the origin of the slower process present in the NR compounds can be directly associated with the presence of ZnO.

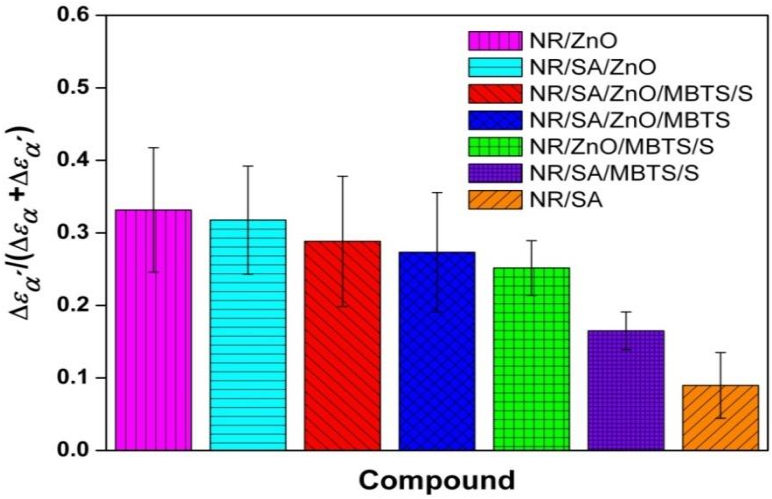

Figure III.5. Dielectric strength intensity relation of the α- and α'- relaxations of NR/additives compounds. Bars correspond to average values representative of different possible HN fittings.

III.4.1. *Temperature Dependence of the Segmental Dynamics of NR/Additives Compounds*

The calculation of the relaxation times allows one the determination of the temperature dependence of the relaxation processes. Figure III.6 illustrates the relaxation time τ_{max} for the α- and α'- relaxation, as a function of the reciprocal temperature. Both processes display a curvature characteristic of a Vogel-Fülcher-Tamman (VFT) dependence, characteristic of cooperative relaxations:[87]

$$\tau_{max} = \tau_0 exp\left(\frac{B}{T-T_0}\right) \qquad \text{III.1}$$

where τ_0 and B are empirical parameters, and T_0 is the so-called ideal glass transition or Vogel temperature, which is generally 30-70 K below T_g.[87] In recent times, the parameter B is represented as $B= DT_0$, being D another magnitude known as fragility strength which can be related to the nature of the glass transition temperature.[153] To reduce the effect of misleading parameters on data fitting to the VFT equation over a limited frequency range, a value of

Logτ_0≈14 was assumed for both relaxations according to theoretical considerations.[154] The VFT equation considers that the relaxation rate increases rapidly at lower temperatures because of the reduction of free volume. The calculated values of B and T_0 are listed in Table III.3 for all compounds.

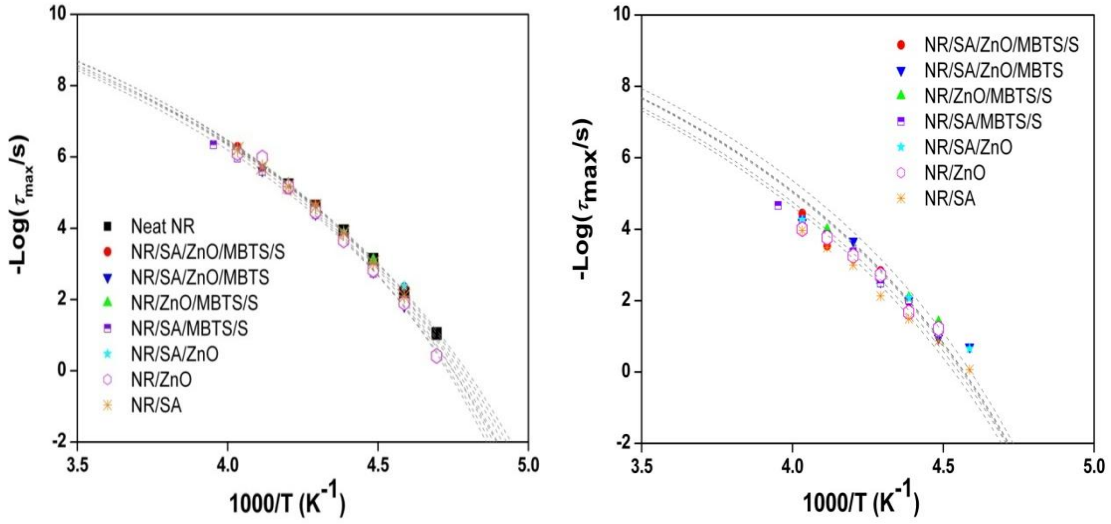

Figure III.6. Temperature dependence of the average relaxation time of NR and NR/additives compounds. Left: α-relaxation process. Right: α'-relaxation process.

As far as the α-relaxation time is concerned, there is a slight difference between the NR and NR/additives compounds curves shown in Figure III.6(Left), with a displacement to higher temperatures when additives are present. It can then be concluded that in the temperature range studied, the presence of additives tends to slow down the segmental mode process of the NR matrix, with an increment of up to 6 °C in the T_0 values for the NR/ZnO compound with respect to neat NR, as shown in Table III.3. On the other hand, the fitting protocol applied for the α'-relaxation considered values of $T_{0\alpha'} \geq T_{0\alpha}$; lower values of $T_{0\alpha'}$ do not seem physically meaningful, since the α'-relaxation is a restricted segmental relaxation and only one T_g is detectable for all compounds. Nonetheless, in Figure III.6(Right) it is shown that the VFT fit curves for this relaxation are not so well resolved within the temperature range studied.

Table III.3. VFT fitting parameters, fragility strength (*D*) and fragility index (*m*) of NR and NR/additives compounds, corresponding to the α- and α'- relaxation.

Compound	*B*	T_0 (K)	*D*	*m*
α-relaxation				
Neat NR	681.4	160	4.3	154.3
NR/SA/ZnO/MBTS/S	698.2	163	4.3	153.4
NR/SA/ZnO/MBTS	660.8	164	4.0	162.3
NR/ZnO/MBTS/S	650.9	164	4.0	164.2
NR/SA/MBTS/S	696.1	161	4.3	152.2
NR/SA/ZnO	645.5	164	3.9	166.2
NR/ZnO	634.7	166	3.8	170.3
NR/SA	676.4	161	4.2	156.6
α'-relaxation				
NR/SA/ZnO/MBTS/S	770.6	163	4.7	140.6
NR/SA/ZnO/MBTS	769.3	164	4.7	141.7
NR/ZnO/MBTS/S	772.3	164	4.7	140.9
NR/SA/MBTS/S	822.0	161	5.1	131.4
NR/SA/ZnO	767.6	164	4.7	142.4
NR/ZnO	725.6	166	4.4	151.0
NR/SA	833.3	161	5.2	130.1

Several schemes have been proposed to classify the degree of departure from the Arrhenius behavior of the α-relaxation time.[153,155,156] The strong-fragile scheme proposed by Angell[155] allows one to classify glass-forming systems on the basis of the temperature dependence exhibited by the relaxation time. A magnitude referred to as fragility[157] is related to the manner in which temperature affects in general the dynamics of liquids and in particular their viscosity and molecular mobility above T_g. Fragility can be quantified,[91,153,157-159] through the fragility strength *D* of the VFT equation (equation III.1). In this case, the fragility index *m*, defined as the apparent

activation energy of either shear viscosity or relaxation time of the α- and α'-relaxation,[153,159] can be estimated as follows:

$$m = \frac{\partial log(T)}{\partial\left(\frac{T_g}{T}\right)_{T=T_g}} = \frac{DT_0T_g}{\left(T_g - T_0\right)^2 \ln 10} = 16 + \frac{590}{D} \qquad \text{III.2}$$

For polymers, fragility has been associated with the cooperativity of the segmental relaxation.[153,156] Within this context, polymers whose segmental motions require high cooperativity would depart strongly from an Arrhenius behavior and would exhibit lower *D* (higher *m*) values than those requiring less cooperative motions. In this case both, the fragility strength and the fragility index (*m*) of all compounds were determined and the results included in Table III.3. As shown in Table III.3, the values obtained are $D \approx 4\text{-}5$ indicating that NR is a dynamically fragile material. This is somehow expected since segmental relaxation times of polymeric materials exhibit the largest deviations from the Arrhenius law.[114,153,160] Moreover, the observed increment on *m* lets us presume that as additives are incorporated into the NR matrix, more cooperativity is needed in order to accomplish segmental motions. It is worth mentioning that the *m* values corresponding to the NR/ZnO compound are the highest of all values, thus corroborating the previously proposed model where the ionic clusters of ZnO may form physical entanglements within the rubber chains, acting as cross-link precursors. In addition, it is noticeable that the α'-relaxation process presents higher *D* values; meaning a more Arrhenius-like behavior than the bulk α-relaxation.[123]

III.5. Chain Dynamics of NR/Additives Compounds

At higher temperatures and lower frequencies than the α-relaxation, a broader relaxation is observable and assigned to the normal mode process, as illustrated in Figure III.7. The normal mode process, detectable because of the dipole component parallel to the backbone, corresponds to motions of the entire chain. This general

relaxation is qualitatively similar for all the samples investigated, although in some cases it is largely masked by a conductivity contribution that affects the low frequency tail of the relaxation curves, according to:

$$\varepsilon''_{HN} = \varepsilon''_{\sigma} + \varepsilon''_{r} = \left(\frac{\sigma_{\mathrm{dc}}}{\varepsilon_0 \omega}\right)^{s} + \varepsilon''_{NM} \qquad \text{III.3}$$

where ε''_{σ} and $\varepsilon''_{r} = \varepsilon''_{NM}$ correspond to the conductivity and normal mode relaxation contributions, respectively; σ_{dc} is the d.c. conductivity of the sample , ε_0 denotes the dielectric permittivity of vacuum (ε_0=8.854 × 10^{-12} F/m), ω the angular frequency and s an exponent ($0 < s < 1$) depending on the nature of the conduction mechanism.

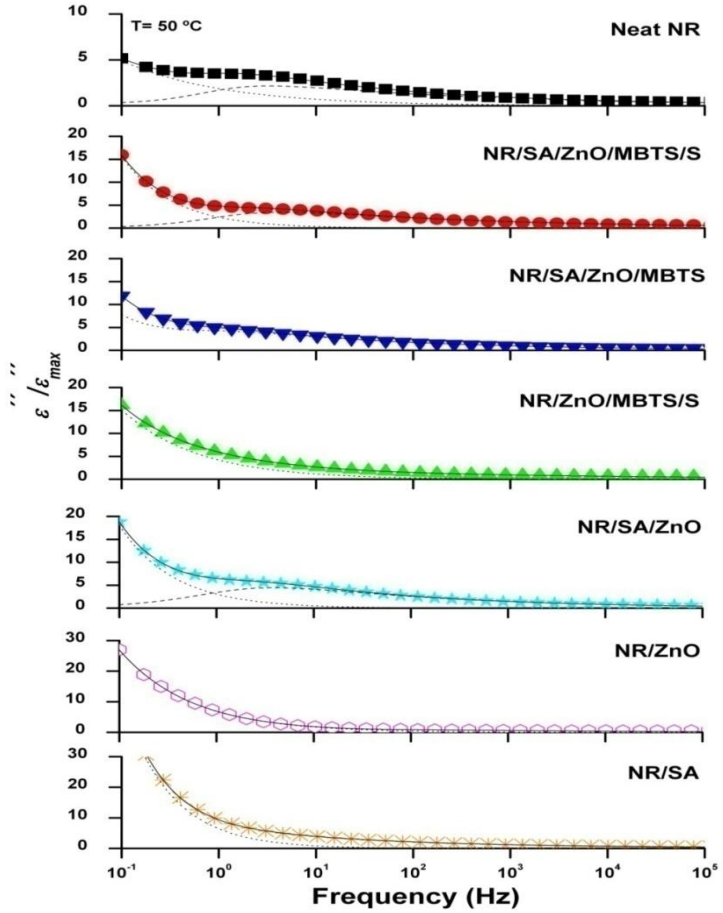

Figure III.7. Frequency dependence of normalized dielectric loss ε'' for neat NR and NR/additives compounds as indicated on each plot, in the region of the normal mode at T=50 °C. Solid lines represent the HN fitting ε''_{HN}, dashed lines the normal mode ε''_{NM}, and dotted lines the conductivity contribution ε''_{σ}.

Figure III.8 shows the normalized conductivity contribution at a frequency of 10^{-1} Hz. From the inspection of this chart it is notorious that all the NR/additives compounds display a higher conductivity contribution than neat NR. Moreover, NR compounds with only one additive, *i.e*. NR/ZnO and NR/SA, display the highest values, while all the other NR compounds present lower values due to their intrinsic heterogeneous nature consisting of more than one interface. This rise in conductivity can be associated to the phenomenon known as Maxwell-Wagner-Sillars (MWS) interfacial polarization, which will be deeply discussed in Chapter IV. Such phenomenon occurs in materials comprised of more than one phase with non-identical dielectric properties, as a result of accumulation of charges at the interfaces of two electrically different media. It depends essentially on the volume fraction, geometry and conductivity of the dispersed phase and the permittivity of the phases.[85,161] In this study, it is clear that NR/additives compounds comprise more than one phase and that interfacial polarization is present. Besides, it could be presumed that as the interface is more homogenous, a more intense conductivity contribution could be noticed.

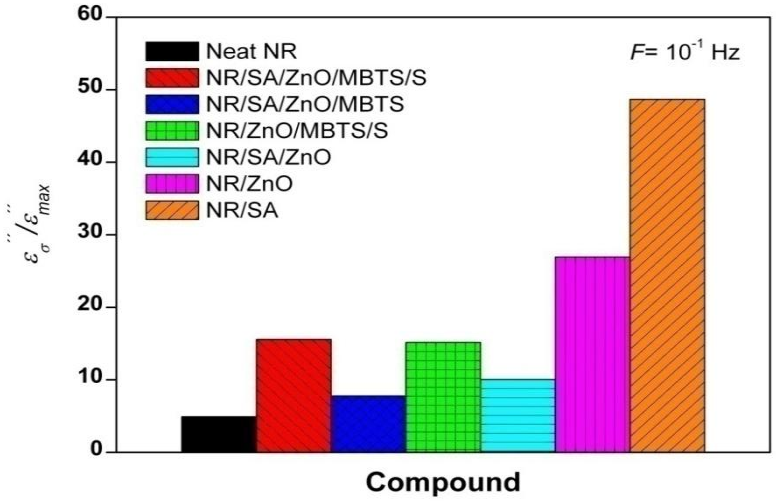

Figure III.8. Normalized conductivity contribution at a frequency F=10^{-1} Hz for neat NR and NR/additives compounds as indicated on the plot.

Despite the strong presence of conductivity, a physical deconvolution of the loss spectra of the normal mode is possible in some cases and thus, the obtained values of the average relaxation time for the normal mode as a function of the temperature can be visualized in Figure III.9. The temperature dependence of the relaxation time departures from the simple Arrhenius behavior; exhibiting a curvature at high temperatures. This characteristic temperature dependence can be described by the VFT equation previously mentioned. The dashed lines in Figure III.9 indicate the fittings of the VFT equation to the experimental data. The fitting parameters are reported in Table III.4. The main effect observed in the dynamics of the normal mode is the slight decrease in the time scale of the NR/additives compounds with respect to neat NR. Faster normal mode processes in *cis*-polyisoprene have previously been observed under confinement by Floudas *et al.*[110] and by Carretero *et al.*[114] These authors suggest a model of a NR star formed of multi arms with dangling ends. Based on these premises, in this research additive domains could be considered as the core of the star acting as connecting points between the rubber chains. Thus, a broad distribution in the relaxation spectrum, which becomes faster due to the shorter chain lengths as compared to the whole chain, is expected.

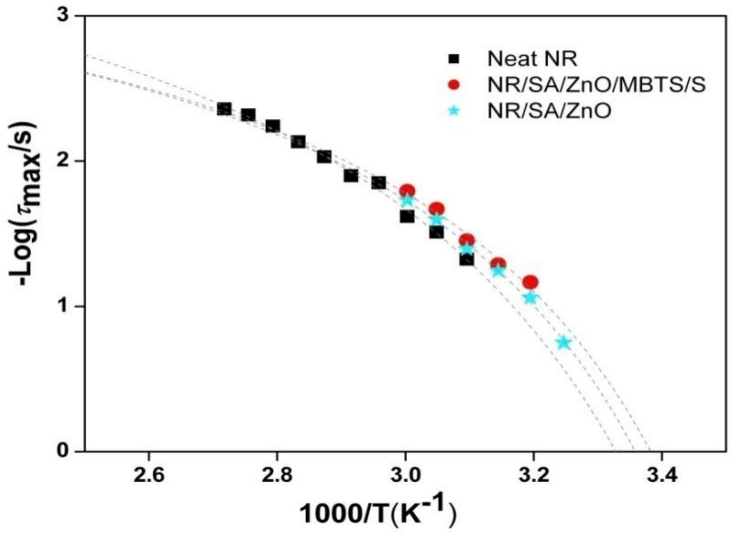

Figure III.9. Temperature dependence of the average relaxation time for the normal mode of NR and NR/additives compounds, as indicated on the plot.

Table III.4. VFT fitting parameters of NR and NR compounds, corresponding to the normal mode.

Compound	$\mathbf{Log}\,\tau_0$	B	T_0^{NM} (K)
Neat NR	3.97	179.8	255.0
NR/SA/ZnO/MBTS/S	3.82	169.7	250.0
NR/SA/ZnO	3.73	155.3	254.6

III.6. Summary

In this chapter, an experimental study has been accomplished on the influence of the vulcanizing components in the molecular dynamics of NR. The results reveal a slowing down of the segmental dynamics of NR restricting the motion of NR chains tightly bounded to additives surface. In general, when ZnO is present, a visible second dynamic process is detected. Systematic elimination of the different vulcanizing additives leads to ascribe this slow process to strong interfacial interactions formed at the interfaces between the ZnO ionic clusters and the NR polymer segments, forming initial physical entanglements between both components, which may act as cross-linking precursors. These results can help to understand basic issues related to the network structure and molecular mobility of NR, essentials for the optimization of the vulcanization process, the role of additives and their interactions with the NR matrix. Moreover, the better understanding of the role of ZnO in the vulcanization reaction is a key issue for the ongoing efforts to reduce zinc content in the rubber formulations without reducing the overall quality of the products.

On the other hand, the chain dynamics of NR is also affected by the presence of vulcanizing additives; with an effect contrary to the one found for the segmental process. Thus, the observed decrease in the time scale of the normal mode is envisioned as a consequence of the effect on dynamics of the NR chains that are confined within the additives domains.

CHAPTER IV. DYNAMICS OF NATURAL RUBBER/LAYERED SILICATE NANOCOMPOSITES[#]

[#]Part of the work described in this chapter has been published in *Soft Matter* **2009**, 5(18), 3481-3486; *Macromolecules* **2010**, 43(2), 643-651 and in *Advanced Materials*, **2011**, 23(44), 5229–5236. *Reprinted by permission from[162] Copyright 2010.*

IV.1. Introduction

The aim of this chapter is to study the dielectric properties of Natural Rubber (NR)/layered silicate nanocomposites, analyzing the relaxation spectra and correlating the local and global motions of polymer chains with its structure.

At first, results from the global characterization of the nanocomposites by means of X-ray diffraction, transmission electron microscopy, rheometry and mechanical properties are reported. Then, the dielectric spectroscopy results are detailed, examining how the segmental and normal modes of the NR chains are affected by the presence of silicate particles. The effects of the concentration of clay on the time and length scale of the relaxation processes, plus a comparison between nanosilicates are also shown. Finally, the influence of the vulcanization and how the cross-linking process affects the dielectric spectra of the nanocomposites are discussed.

IV.2. Experimental

Non-vulcanized nanocomposites were prepared consisting of the neat rubber and the filler. Throughout this chapter, the samples are referred to as NR/*xy*, where "*x*" and "*y*" correspond to the amount and type of filler respectively. The filler content used, expressed as parts per hundred parts of rubber (phr), is listed in Table IV.1.

Table IV.1. Layered silicate content used in non-vulcanized NR nanocomposites.

Layered silicates	Content (phr)
CNa+	5.0
C15A	1.0, 2.5, 5.0, 7.5 and 10.0

Vulcanized nanocomposites were also prepared according to the formulation compiled in Table IV.2. The samples are referred to as vulcNR/*xy*, following the same nomenclature as for the non-vulcanizates.

Table IV.2. Formulation and ingredients used in the preparation of vulcanized NR nanocomposites.

Ingredient	Content (phr)
NR	100
Zinc oxide (ZnO)	5.0
Stearic acid (SA)	1.0
MBTS	1.0
Sulfur (S)	2.5
Filler	CNa+ 5.0 C15A 5.0; 10.0

IV.3. Characterization of Natural Rubber/Layered Silicate Nanocomposites

IV.3.1. *Structural Characterization*

The structure of the neat clays (C15A and CNa+) and of the NR/clay nanocomposites was evaluated by means of XRD in order to analyze the possible interaction between the montmorillonite and the rubber. Figure IV.1 shows the respective diffractograms and the values of basal spacing corresponding to the diffraction maxima, calculated according to Bragg's law (see equation II.1).

The results obtained confirm previous studies presented by other researchers.[57,60,65,163] It is clear that a pronounced intercalation is achieved by the incorporation of the C15A clay to the NR matrix. In fact, the high intensity characteristic diffraction maxima at 2θ=3.2° and 2θ=7.1° of the C15A disappear, providing a strong evidence of the insertion of the elastomer into the silicate galleries, disrupting the regular stacked-layer structure of the organosilicate and giving rise to an exfoliated structure.[60] In the case of the CNa+ nanocomposite,

the characteristic peak at 2θ=7.8° also disappears. Nonetheless, this result might be a consequence of the low intensity of the diffraction peak of the CNa+ and low content of clay present in the composite, and not to the intercalation of NR chains.

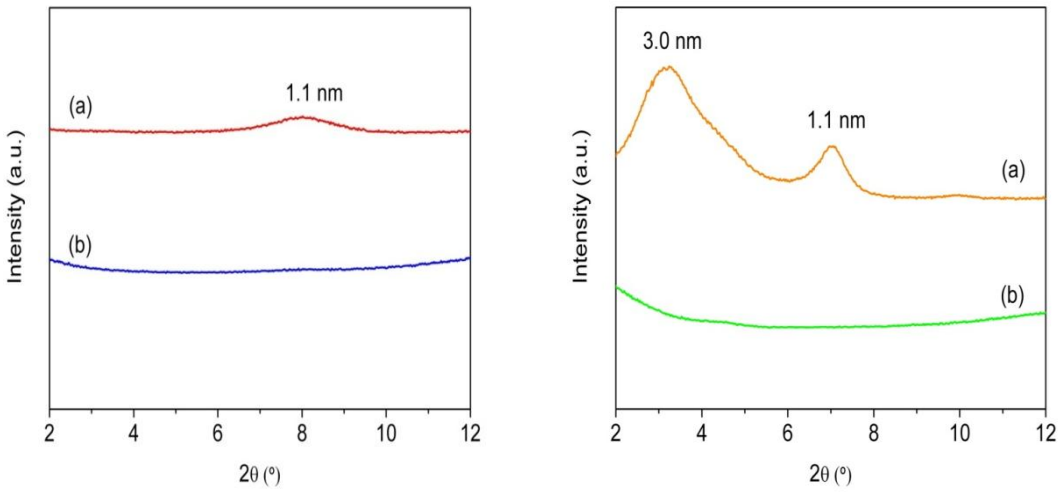

Figure IV.1. Left: XRD patterns of: (a) CNa+ and (b) NR/5CNa+. Right: XRD patterns of: (a) C15A and (b) NR/5C15A.

In order to complement the study on the structural variations of the NR nanocomposites, a surface morphology analysis was performed using TEM. Figure IV.2 shows the more representative images of the prepared nanocomposites. As it can be seen, the microphotographs confirm that the C15A silicate layers are better exfoliated and randomly dispersed throughout the elastomer matrix as monolayers, while the incorporation of the unmodified clay CNa+ only gives rise to a conventional composite at a microscopic scale.

It should be mentioned that the XRD patterns and the TEM images shown here correspond to vulcanized NR nanocomposites with 5 phr of clay. Nonetheless, equivalent results were obtained for the non-vulcanized samples, thus inferring that the vulcanization process does not have an important influence on the exfoliation process of the clay.

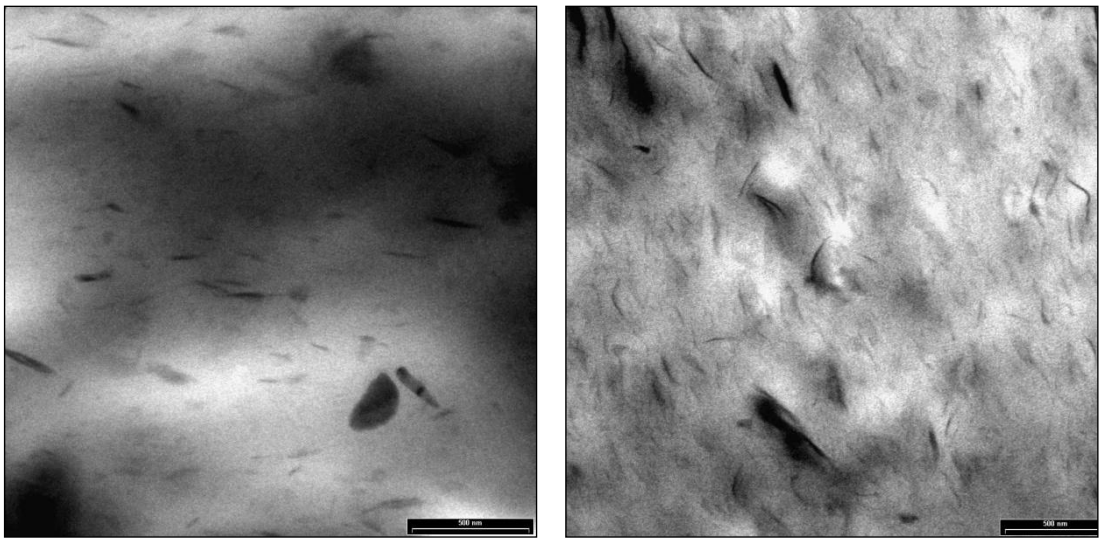

Figure IV.2. Left: TEM image of NR/5CNa+ nanocomposite. Right: TEM image of NR/5C15A nanocomposite. The scale bar corresponds to 500 nm.

IV.3.2. *Rheometry*

The vulcanization reaction is an irreversible process that gives rise to the formation of a three-dimensional network structure of polymer chains chemically bonde to one another, converting a plastic material into an elastic one. Moreover, the vulcanization curves give a rather complete picture of the overall kinetics of the compound. Thus, in the particular case of rubber nanocomposites, it is necessary to understand the effect of nanoparticles in the vulcanization reaction in order to achieve a material with desired properties. In this section, the rheometric properties of NR and its nanocomposites were analyzed at 150 °C. The vulcanization curves of the pristine NR and its clay nanocomposites are graphically represented in Figure IV.3. The registered parameters deduced from the curves are summarized in Table IV.3. As a reminder, the scorch time (t_{s2}) is the induction time before onset of vulcanization; optimum cure time (t_{90}) is the time in which 90% of the delta torque is reached, while the cure rate index (*CRI)* measures the fast curing nature of rubber compounds. The minimum (S_{min}) and maximum (S_{max}) torque value can be related to an index of material viscosity and, to the possible cross-linking degree at a given vulcanization temperature, respectively.

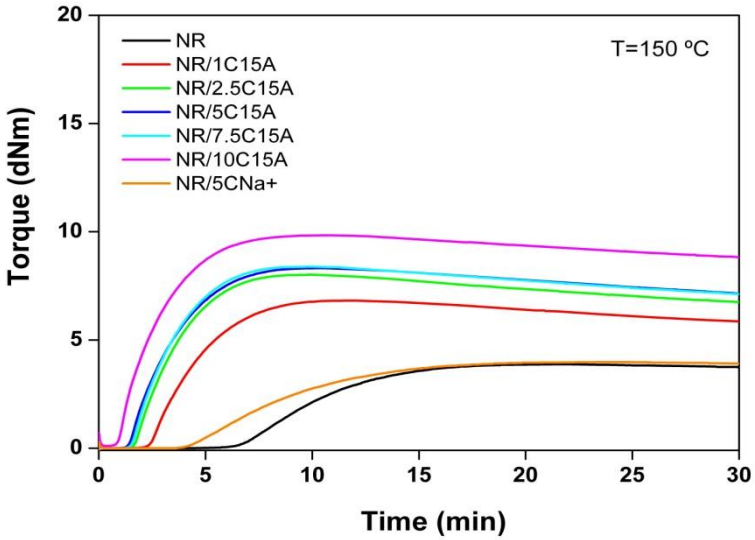

Figure IV.3. Curing curves of neat NR and its clay nanocomposites obtained at T=150 °C.

Table IV.3. Curing characteristics of NR and NR/clay nanocomposites at T=150 °C.

Compound	t_{s2} (min)	t_{90} (min)	S_{max} (dNm)	S_{min} (dNm)	ΔS (dNm)	CRI (min^{-1})
NR	9.8	14.5	3.88	0.06	3.82	21.3
NR/1C15A	3.3	7.2	6.82	0.03	6.79	25.7
NR/2.5C15A	2.9	6.8	8.02	0.03	7.99	25.7
NR/5C15A	2.1	5.9	8.32	0.03	8.29	26.3
NR/7.5C15A	2.0	5.8	8.39	0.03	8.36	26.3
NR/10C15A	1.3	5.3	9.84	0.03	9.81	25.0
NR/5CNa+	7.9	14.1	3.98	0.05	3.93	16.2

The analysis of these parameters reflects that the presence of CNa+ does not affect the cure characteristics of the rubber, probably due to a poor compatibility between the unmodified clay and the hydrophobic polymer. On the other hand, it is worth noting that both vulcanization times, t_{s2} and t_{90}, are sharply reduced by the incorporation of the organosilicate (C15A), showing accelerated vulcanization with respect to that of pure NR and of the unmodified silicate (CNa+) counterpart. Also,

it can be seen that both parameters decrease with increasing organosilicate loading. Thus, it can be inferred that the C15A behaves as an effective accelerant agent for NR vulcanization, acting as a catalyst.[5] These results are confirmed by the *CRI* values, which show an increase with the addition of the organosilicate, attributed to the amine functionalities in the nanosilicates structure. It is well known that amine groups facilitate the curing reaction of SBR and NR compounds[134,164-166], due to the formation of a transition metal complex in which sulfur and amine groups participate. Moreover, the synergetic combination of a benzothiazyl accelerant with an amine produces a particular accelerant effect on the rubber vulcanization reaction.

On the other hand, the S_{max} and ΔS increase significantly by the addition of the organosilicate, corroborating the strong reinforcing effect of this filler and the good interfacial adhesion occurred between the rubbery matrix and the organosilicate.[5] Furthermore, the increase on ΔS is related to the cross-linking density of the rubber phase.[167,168] Thus, these results suggest that NR becomes more cross-linked in the presence of the organoclay. It is worth mentioning the slight decrease S_{min}. It is assumed that the addition of inorganic nanoparticles decreases this parameter due to the amine functionality present in the organosilicate acting as a lubricant for rubber compounds.[5]

IV.3.3. *Mechanical Properties*

The conventional tensile test is one of the most important methods of polymer testing. Also for elastomers, it is one of the basic tests for determining the quantitative characterization of *strength* and *deformability*, which are often described as “ultimate properties”.[169] In this sense, the effects of clay content on the mechanical properties of the NR nanocomposites were studied. A characteristic stress-strain curve is presented in Figure IV.4 for NR, NR/5C15A and NR/5CNa+ nanocomposites. Results obtained from tensile measurements are compiled in Table IV.4, where σ_{xxx} corresponds to the tensile stress at “xxx”% of elongation, σ_r

to the tensile strength (tensile stress at maximum) and ε_r to the elongation (tensile strain) at break.

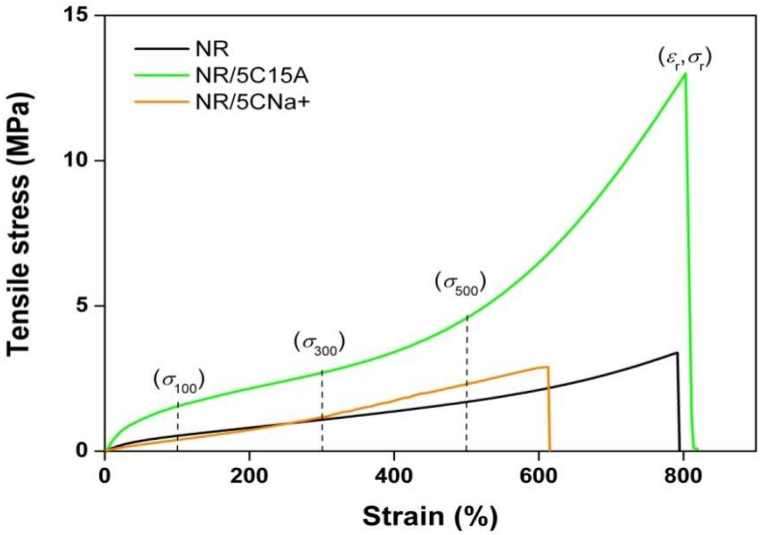

Figure IV.4. Representative stress-strain curves of NR and NR/5C15A and NR/5CNa+ nanocomposites.

Table IV.4. Mechanical properties of NR/layered silicate nanocomposites.

Compound	σ_{100} (MPa)	σ_{300} (MPa)	σ_{500} (MPa)	σ_r (MPa)	ε_r (%)
NR	0.55±0.05	1.10±0.04	1.83±0.08	3.17±0.25	831±45
NR/1C15A	0.88±0.06	1.92±0.09	3.47±0.22	9.69±0.98	869±97
NR/2.5C15A	1.07±0.06	2.33±0.08	4.23±0.13	13.30±1.18	827±51
NR/5C15A	1.30±0.06	2.59±0.16	4.56±0.31	13.86±0.91	823±22
NR/7.5C15A	1.43±0.11	2.70±0.17	4.60±0.33	15.18±3.79	812±36
NR/10C15A	1.44±0.14	2.63±0.10	4.60±0.03	17.88±1.66	789±31
NR/5CNa+	0.49±0.21	1.17±0.51	2.48±0.91	2.95±0.68	631±48

From the analysis of the data compiled in Table IV.4, it can be seen that the incorporation of the CNa+ has little effect on the composite mechanical properties, suggesting that a standard composite at the microscale level has been formed with the filler showing no reinforcing effect for the composition herein considered.

However, a sensible increase in the mechanical properties is obtained by adding the C15A. These results prove the strong reinforcing effect of this filler even at low percentages. The anisotropy and high surface-to-volume ratio of the organoclay contribute to the excellent reinforcing capability of this filler. That is, it acts as short reinforcing fiber with nanoscale architecture, increasing the interfacial area between both phases. The optimum dispersion of even a small quantity of nanoparticles is enough to interact with the total rubber mass, *i.e.*, a few rubber chains remain free of interaction with the nanoparticle. Thus, a significant amount of the rubber phase is forming a highly entangled structure due to the formation of intense elastomer/nanoclay interactions. This structure is responsible of the high performance of these materials.

With respect to the values of the elongation at break (ε_r) of the nanocomposites it initially remain unaffected with the incorporation of the organoclay. However, further increment on filler content results in a gradual reduction in elongation at break, as expected.

These results can be correlated with the structural and morphological characteristics of the fillers in the nanocomposites (Figure IV.1 and Figure IV.2) since the exfoliation of the clay in the rubber matrix and the favorable interaction between the modified filler and rubber, enhance the mechanical properties of the NR. Moreover, rheometry results are also corroborated, since the improved stiffness in presence of the organoclay can be related to a higher cross-linking degree.

Finally, it can be said that the general characterization (morphology, rheometry and mechanical properties) of the NR/layered silicate nanocomposites exposed so far is intimately related to the filler structure and has contributed to a better knowledge of the physical properties of the materials herein studied. Nonetheless, in order to understand the structure/property correlations between the different phases and interfaces present in the nanocomposite and its implication on the variation of the final properties of the material, a further insight at a molecular level is required. Thus, the following sections will deal with a detailed study on the

dynamics of the NR/layered silicate nanocomposites by means of broad-band dielectric spectroscopy.

IV.4. Dynamics of Non Vulcanized NR/Layered Silicate Nanocomposites

In order to visualize the different dynamic processes present in the non-vulcanized samples herein studied, representative 3D plots of neat NR, NR/5C15A and NR/5CNa+ nanocomposites are shown in Figure IV.5, Figure IV.6 and Figure IV.7, respectively.

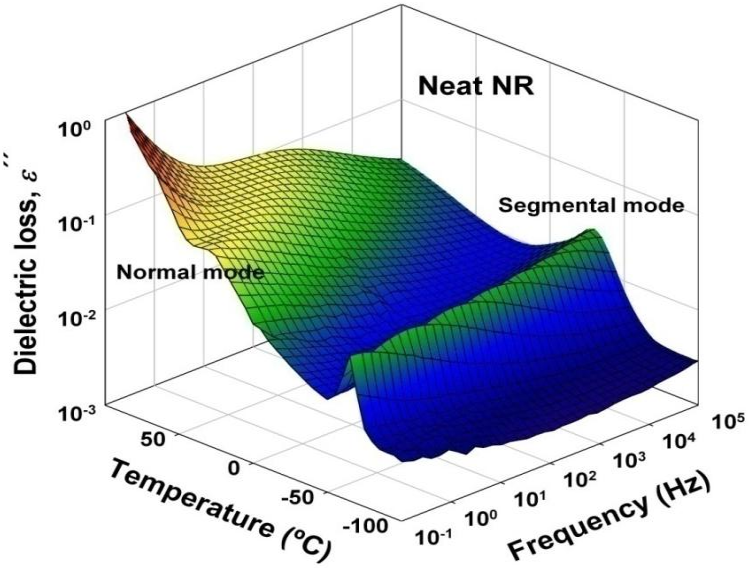

Figure IV.5. 3D representation of the frequency and temperature dependence of the dielectric loss ε'' for neat NR.

As previously mentioned (Chapter III) two relaxation modes are present in NR, as it can be observed in Figure IV.5. For temperatures above the glass transition temperature (T_g = -64 ºC) the segmental mode related to the segmental motions of the polymer chain is observed. While at higher temperatures, a more intense process which can be assigned to the normal mode is clearly detected.

In the case of both nanocomposites (Figure IV.6 and Figure IV.7) the segmental mode, or α-relaxation, is still detectable and appears located in the same temperature range as for neat NR. A second process appears at higher temperatures in the NR/5C15A nanocomposite (Figure IV.6) which apparently differs from the normal mode of neat NR. This process will be hereafter referred to as "new mode" and will be further discussed. This new mode seems to be absent in the NR/5CNa+ nanocomposite (Figure IV.7) which only exhibits the segmental mode and an additional process at low temperatures most likely due to the electric dipole rotations of the absorbed water in the silicate gallery.[65,170] Moreover, at high temperatures conductivity dominates the low frequency tail of the spectra of the NR/5C15A and NR/5CNa+ nanocomposites, thus no defined relaxation process can be appreciated in that temperature range.

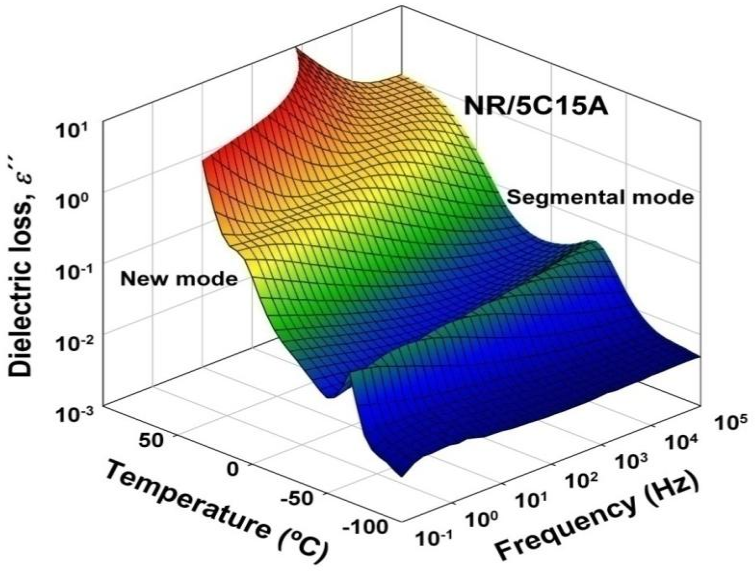

Figure IV.6. 3D representation of the frequency and temperature dependence of the dielectric loss ε'' for non-vulcanized NR/5C15A nanocomposite.

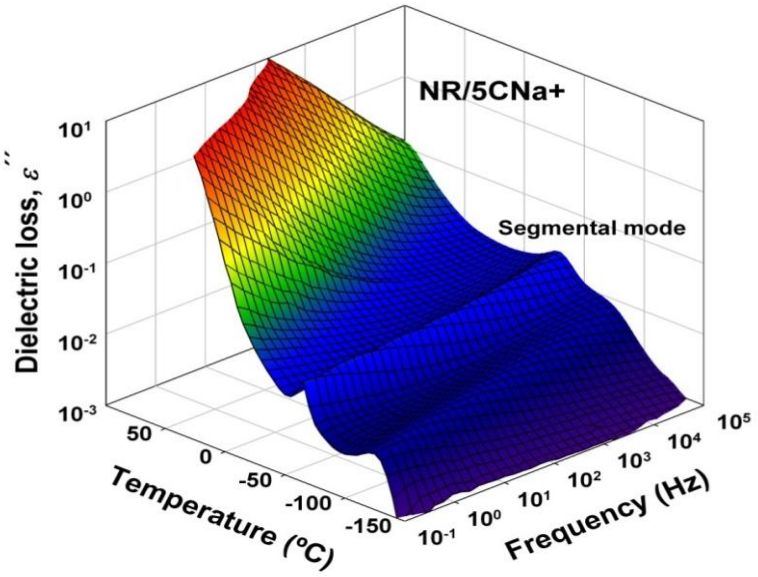

Figure IV.7. 3D representation of the frequency and temperature dependence of the dielectric loss ε'' for non-vulcanized NR/5CNa+ nanocomposite.

Figure IV.8, Figure IV.9 and Figure IV.10 describe the dielectric loss spectra (ε'' versus frequency) for neat NR and its nanocomposites over a wide range of frequency at different temperatures. In all the spectra, the dielectric loss maxima are shifting to higher frequencies with increasing temperature. This shift in the frequency of the maximum loss is characteristic of thermally activated processes.

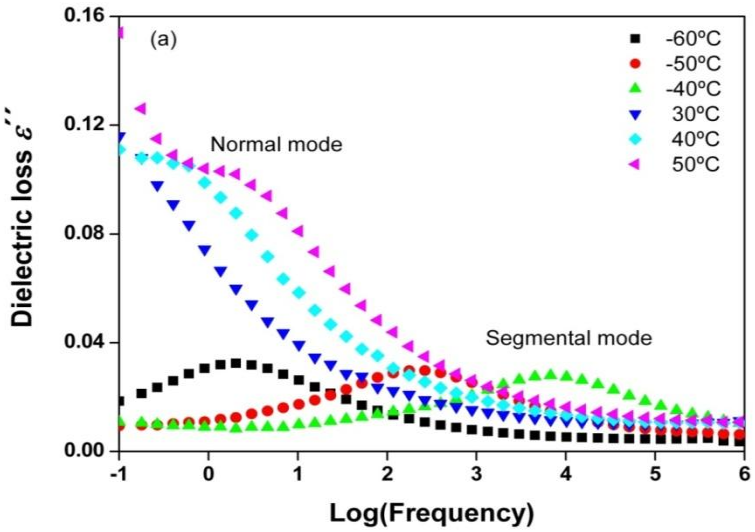

Figure IV.8. Dielectric loss ε'' vs. frequency for neat NR.

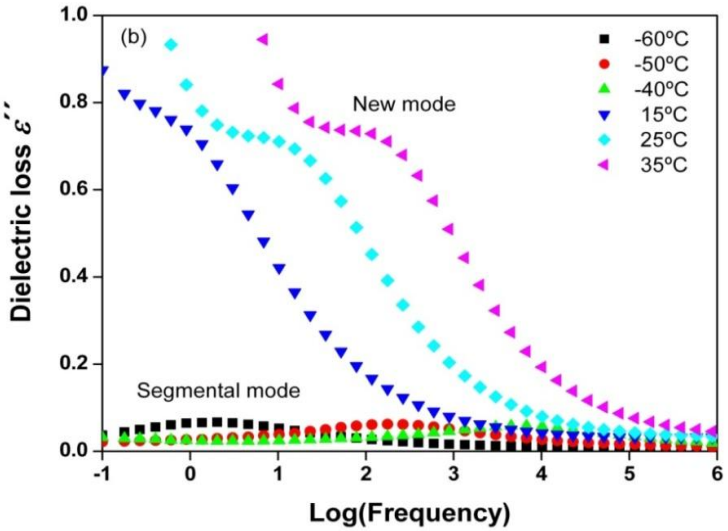

Figure IV.9. Dielectric loss ε'' vs. frequency for non-vulcanized NR/5C15A nanocomposite.

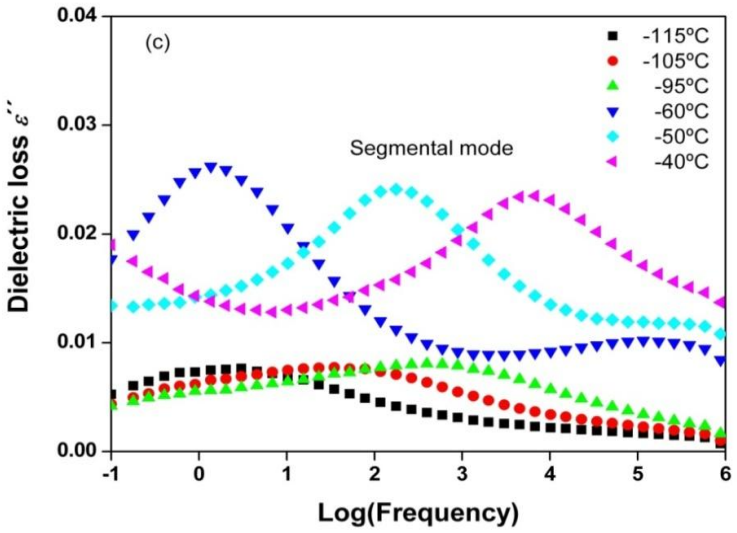

Figure IV.10. Dielectric loss ε'' vs. frequency for non-vulcanized NR/5CNa+ nanocomposite.

In order to better examine the different relaxations present in all composites, the discussion of the results has been divided into low temperature and high temperature processes.

IV.4.1. *Low Temperature Process: Segmental Relaxation*

Figure IV.11 shows selected normalized dielectric loss spectra at T = -50 ºC for neat NR and the non-vulcanized NR/5C15A and NR/5CNa+ nanocomposites. From the spectra hereby presented, one can notice that the segmental mode process (α-relaxation) is well resolved in the frequency domain and shows a relatively broad and asymmetric peak regardless the type of filler incorporated in the nanocomposite if compared to the spectrum of neat NR.

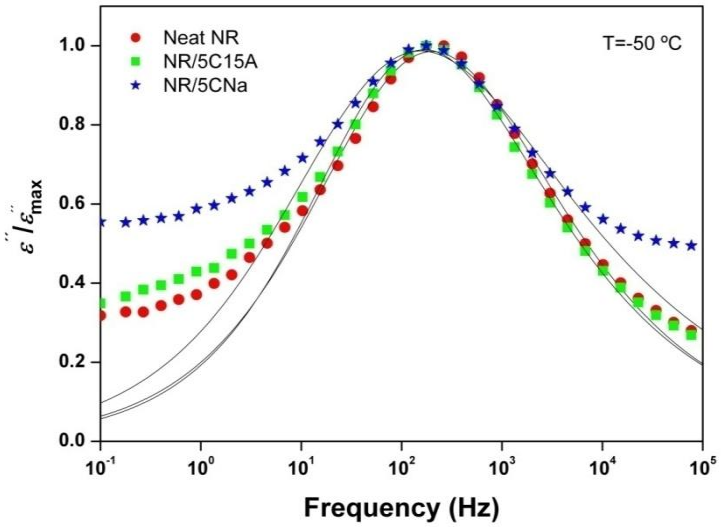

Figure IV.11. Frequency dependence of normalized dielectric loss ε'' of the NR nanocomposites indicated on the plot in the region of the segmental mode. Solid lines correspond to HN fittings.

These results suggest the independence of the glass transition process with the silicate incorporated. As a matter of fact, the invariance of the glass transition has been verified when the silicate type and content varies from 1 to 10 phr by calorimetric measurements, as it can be seen in Figure IV.12. A single glass transition around -70 ºC is observed for all samples. This evidences that the thermodynamic glass transition of NR/C15A nanocomposites corresponds to the NR matrix, in agreement with the dielectric data shown in Figure IV.11 for the

segmental mode. Thus, no significant changes on the segmental molecular dynamics of the NR come into sight by the addition of layered nanosilicates to the rubber matrix.

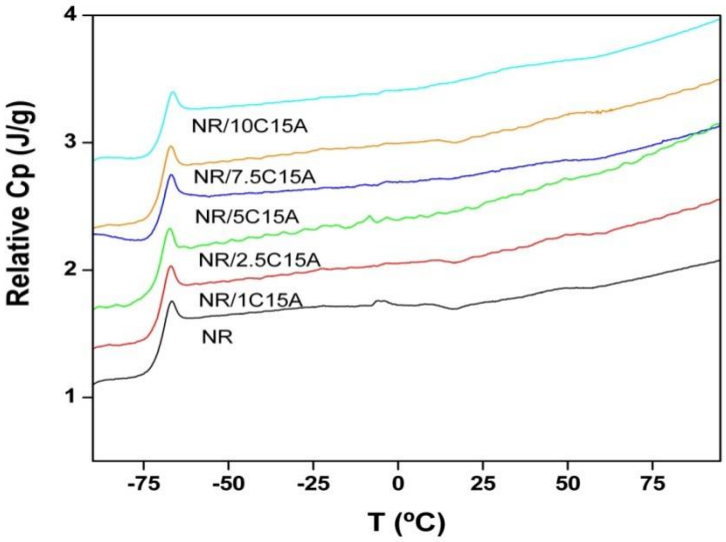

Figure IV.12. DSC heating thermograms (second runs, displaced vertically for clarity) obtained for NR and the NR/C15A nanocomposites with the clay content indicated on the plot.

One can also see that all three spectra presented in Figure IV.11 can be well described by the HN function. The characteristic parameters of this function such as $\Delta\varepsilon$, b, c and τ_{HN} are obtained. Table IV.5 shows these parameters for temperatures in the region of the segmental mode.

This analysis corroborates that the dynamics of the segmental mode is independent of both silicate type and content. The corresponding values for τ_{max}, shown in Figure IV.13, reveal a Vogel-Fülcher-Tamman (VFT) dependence of τ_{max} with the reciprocal temperature.

Table IV.5. HN parameters for the segmental mode of NR and its nanocomposites.

Compound	T (°C)	$\Delta\varepsilon$	b	c	τ_{HN} (s)
Neat NR	-55	1.497×10^{-01}	0.492	1	6.093×10^{-3}
	-50	1.445×10^{-01}	0.527	0.833	1.045×10^{-3}
	-45	1.402×10^{-01}	0.557	0.683	2.383×10^{-4}
NR/5C15A	-55	3.144×10^{-01}	0.522	0.832	1.031×10^{-2}
	-50	3.079×10^{-01}	0.497	0.924	1.032×10^{-3}
	-45	2.920×10^{-01}	0.505	0.938	1.537×10^{-4}
NR/5CNa+	-55	1.399×10^{-01}	0.439	0.937	1.001×10^{-2}
	-50	1.431×10^{-01}	0.448	0.749	1.863×10^{-3}
	-45	1.416×10^{-01}	0.433	0.811	2.261×10^{-4}

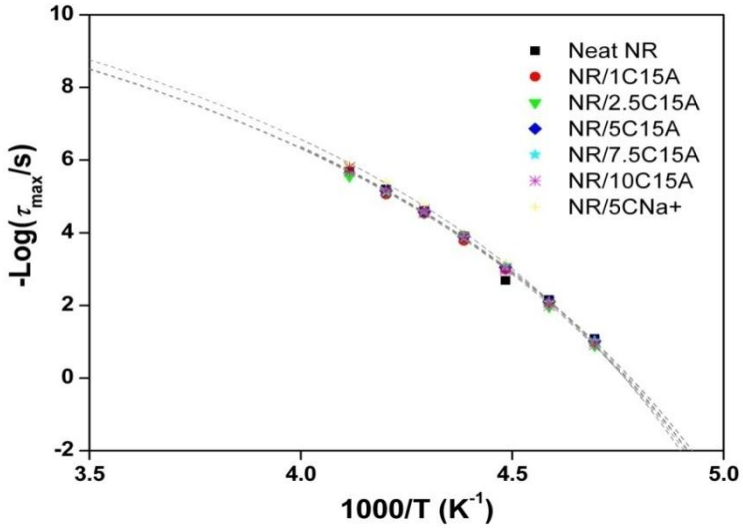

Figure IV.13. Temperature dependence of the average relaxation time for the segmental mode of NR and its nanocomposites with clay loading as a parameter.

One can clearly see that neither an increase in nanosilicate loading nor the type of filler added has an effect on the time scale of the segmental mode process of the NR matrix, as also presented in Table IV.6.

Table IV.6. VFT fitting parameters, fragility strength and fragility index of non-vulcanized NR and NR nanocomposites.

Compound	B	T_0 (K)	D	m
Neat NR	681.4	159.7	4.3	154.3
NR/1C15A	678.2	161.0	4.2	156.1
NR/2.5C15A	687.6	160.5	4.3	153.7
NR/5C15A	686.5	160.9	4.3	154.3
NR/7.5C15A	680.4	160.8	4.2	155.4
NR/10C15A	673.6	161.6	4.2	157.6
NR/5CNa	695.7	159.4	4.4	151.2

IV.4.2. *High Temperature Processes: New and Normal Modes*

- New Mode

Figure IV.14a shows selected dielectric loss spectra at T = 40 ºC for NR and the NR/5C15A and NR/5CNa+ nanocomposites in the temperature region where the new mode is observed for the NR/5C15A. From the spectra presented in this figure, one can observe that neither NR nor NR/5CNa+ exhibit this new mode, being only detectable for the nanocomposite with the filler C15A. As mentioned before, the nanosilicate C15A is a montmorillonite modified with a quaternary ammonium salt. This modification results in a more pronounced intercalation of the NR chains, as corroborated by previous authors[57,65,163] and in this study (see section IV.3.1). Therefore, due to an enhanced interaction of the NR chains with the clay surface one could expect a rubber phase fraction with restricted mobility located close to the polymer/filler interface. These interactions should be absent in the unfilled NR matrix or conventional NR composites with poorer intercalation as in those based on unmodified clay (CNa+).

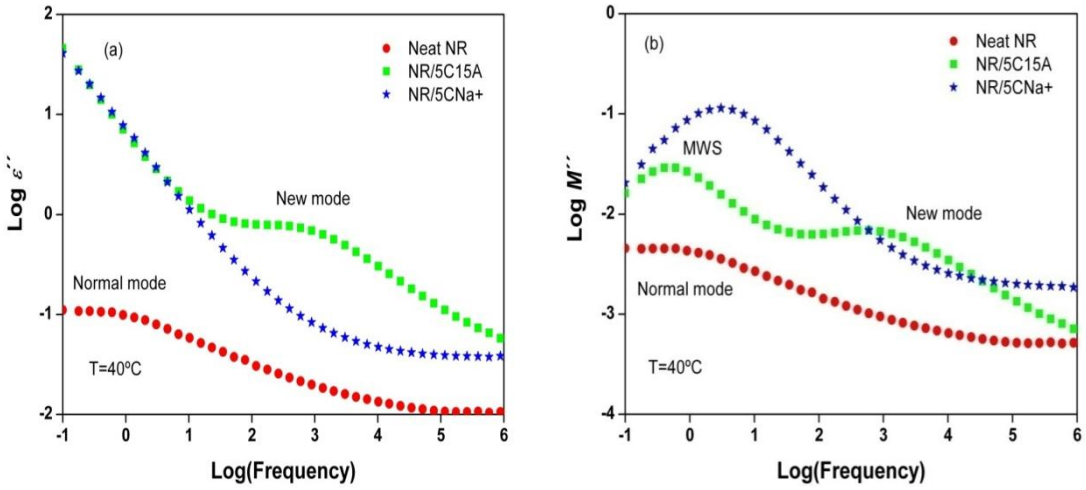

Figure IV.14. (a) Dielectric loss ε'', and (b) Dielectric loss modulus M'', in the frequency domain for neat NR and its nanocomposites.

In order to better understand the physical nature of the new mode, the dielectric modulus formalism was employed (see Figure IV.14b). The permittivity and modulus formalisms describe the same electrical relaxation phenomena. However, under different conditions a specific form could allow to extract more information with respect to the occurring physical processes. In this case, the experimental dielectric data are initially expressed in terms of real and imaginary part of permittivity and then transformed, via equation IV.1, to the complex dielectric modulus:

$$M^* = \frac{1}{\varepsilon^*} = \frac{1}{\varepsilon' - i\varepsilon''} = \frac{\varepsilon'}{\varepsilon'^2 + \varepsilon''^2} + i\frac{\varepsilon''}{\varepsilon'^2 + \varepsilon''^2} = M' + iM'' \qquad \text{IV.1}$$

where M' is the real and M'' the imaginary part of the dielectric modulus, respectively. The interpretation of relaxation phenomena via the dielectric modulus offers some advantages upon other treatments, since large variations in the permittivity and loss at low frequencies and high temperatures are minimized. Further, difficulties occurring from the electrode nature, the electrode-specimen contact and the injection of space charges and absorbed impurities can be neglected. Arguments and examples for the resulting benefits of the dielectric modulus form have been presented elsewhere.[120,171]

For the purpose of this research, the modulus spectra of nanocomposites offer an added insight into their dynamics because high conductivity makes identification of relaxation processes in the permittivity spectra difficult, though not impossible.[121] Figure IV.14b shows the dielectric modulus spectra of the pure NR and its nanocomposites (NR/5C15A and NR/5CNa+).

In the low frequency region, a relaxation process can be observed in the nanocomposites regardless the type of clay added, while this process is absent in the pure NR. The incorporation of nanoclay caused additional relaxation dispersion due to an interfacial polarization at the nanoclay/polymer interface, the so-called Maxwell-Wagner-Sillars (MWS) effect. The MWS relaxation refers to the frequency dependence of interfacial polarization (ion accumulation) that occurs at the interface between materials with differing dielectric constants, such as polymer and layered silicate. The MWS transition is expected at the low frequency range and involves rather high ε' and ε'' values.[161] Interfacial polarization is always present in materials comprised of more than one phase. This kind of polarization arising at the interfaces is due to the migration of charge carriers through different phases of the composite material resulting in differential charge accumulation at the interfaces. When these charges are forced to move by the application of an external electric field, the motion will be hindered at various points of the composite material differently, causing space charge to appear. The appearance of such space charge can distort the macroscopic field and appears as polarization to an external observer.[93]

Figure IV.14b also reveals for the NR/5C15A nanocomposite the presence of the new mode reflected in Figure IV.14a accompanied at lower frequencies by the MWS interfacial polarization. Some interesting features can be noted regarding the influence of clay content on the new mode by representing the dielectric strength as a function of the filler content (Figure IV.15) for the NR/C15A nanocomposites. Here one can notice a slight increasing tendency in dielectric strength ($\Delta\varepsilon$) with clay loading. This behavior supports the assignment of the new mode to a phase of the polymer close to the polymer/filler interface.

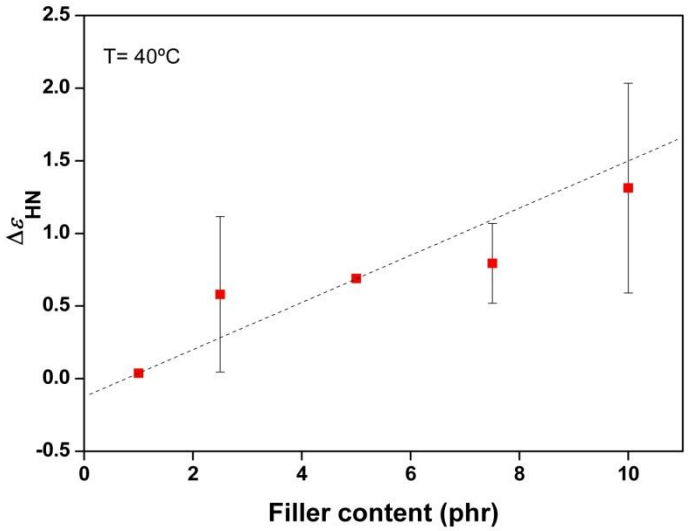

Figure IV.15. Relaxation strength of the new mode as a function of clay loading for the NR/C15A nanocomposites.

In similar way to the segmental mode, the average relaxation times of the new mode observed for the NR/C15A nanocomposites have been represented in Figure IV.16 as a function of the reciprocal temperature at several filler content. The data reveal that this new relaxation becomes faster as increasing filler content. Other aspect that should be highlighted from this figure is the fact that the new mode has a weaker temperature dependence than the segmental relaxation and does not present the curvature characteristic of a Vogel-Fülcher-Tamman (VFT) behavior, having an almost Arrhenius dependence.

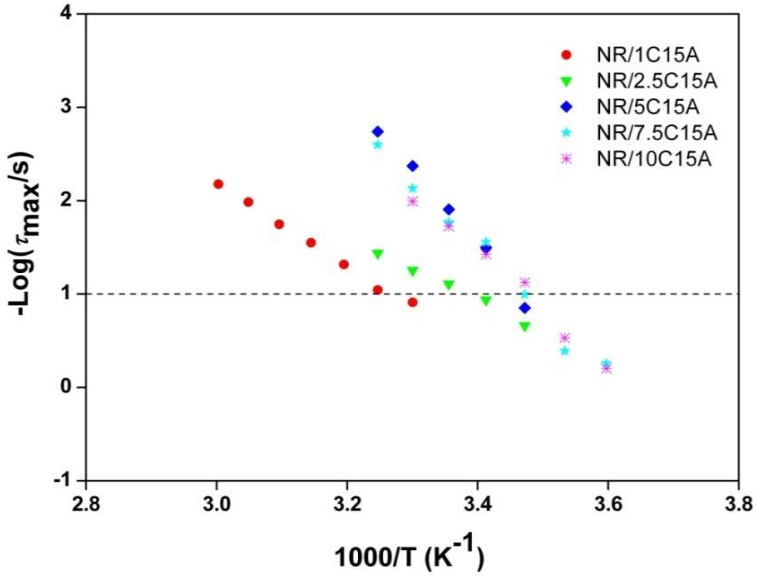

Figure IV.16. Temperature dependence of the average relaxation time for the new mode of NR/C15A nanocomposites with clay loading as a parameter.

In order to illustrate this effect, Figure IV.17 shows the temperatures at which the average relaxation time of the new mode reaches a value of 0.1 s. It becomes evident that the new mode speeds up with filler content and levels off for loadings higher than 5 phr. In principle one would expect confinement effects to be increasingly important as filler content increases. In general, segmental dynamics may become faster by confinement when the confinement volume becomes comparable to that of the cooperative rearranging regions.[172] In this case, the fastening of the new mode dynamics with increasing filler content can be understood as due to a reduction of volume available for the polymer chains intercalated within the galleries formed by the silicate layers. This would imply that an increasing number of layered silicates accommodate NR chains in the central area of the intergallery without expanding the basal spacing, thus resulting in increased relaxation rate.[117,119,120] Interestingly, however, when higher content of clay is added (up to 10 phr) one could presume that a percolated network of nanoparticles that can influence relaxation could be formed resulting in additional restriction effects that compensate the confinement.

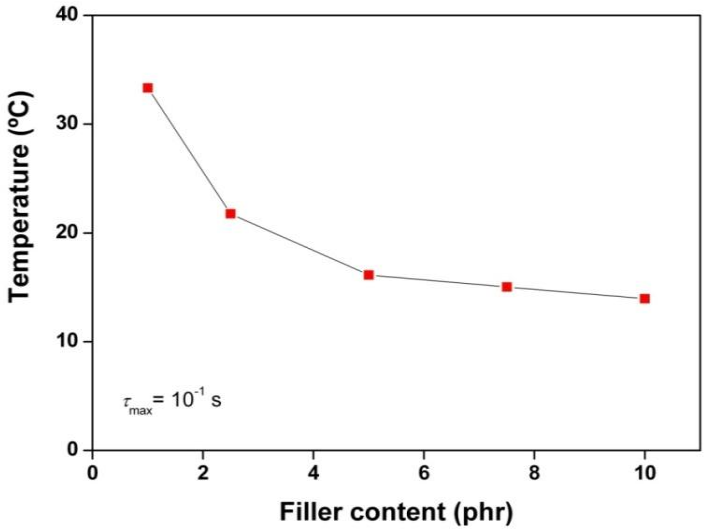

Figure IV.17. Temperature dependence of the new mode at $\tau_{max}=10^{-1}$ s for NR/C15A nanocomposites with clay loading.

- Normal Mode

If the spectrum of neat NR (Figure IV.5) is analyzed one can clearly see that the normal mode process is present at high temperatures at frequencies below the α-process and overlapped with the electrical conductivity contribution. The overall chain dynamics is reflected by this process. Figure IV.18 illustrates the deconvolution results of the normal mode of NR. On the other hand, as mentioned before, at high temperatures conductivity dominates the low frequency tail of the spectra of the NR/5C15A and NR/5CNa+ nanocomposites, thus no defined normal mode process can be appreciated in that temperature range with the required accuracy.

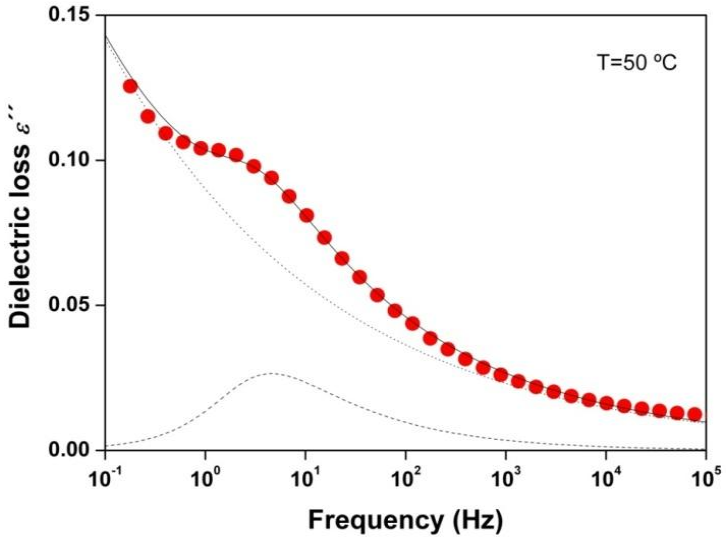

Figure IV.18. Deconvolution results for the dielectric loss ε'' of neat NR at T=50 ºC. Solid lines represent the HN fitting curve, dashed lines the individual process and dotted lines the conductivity contribution.

A careful analysis of the temperature dependence of the different processes (Figure IV.19) evidences that the global chain dynamics (normal mode) of NR is slower than the segmental mode and exhibits weaker temperature dependence than that of the α-relaxation. This can be understood by considering that the segmental motion proves smaller length scales than those proven by the normal mode process.[85] In between the normal and the segmental modes of the NR matrix, lays the new mode of the NR/C15A nanocomposites. For the sake of clarity in Figure IV.19 only data for the NR/5C15A nanocomposite have been shown. The new mode is clearly slower than the segmental mode, but faster than the normal mode process of NR.

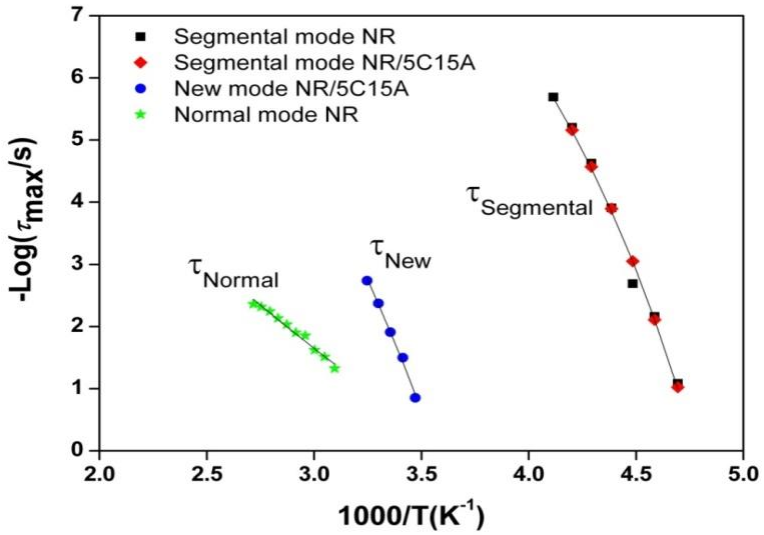

Figure IV.19. Temperature dependence of the average relaxation time for normal, new and segmental mode of neat NR and its nanocomposites.

Petychakis *et al.*[110] have investigated the effect of confinement on the global chain dynamics of polyisoprene in controlled porous glass media. They found that for high molecular weights (7 K and 10 K), the normal mode speeds up due to the effective shorter chains which flow out from the pores. In a similar way, Serghei *et al*.[109] studied the dynamics in thin films of *cis*-1,4-polyisoprene. They found that if the thickness of the polymer layer becomes comparable to the radius of gyration of the chain, a confinement-induced mode is detected being assigned to fluctuations of terminal sub-chains, which develop due to immobilization of polymer segments in interaction with a confining interface. This confinement-induced mode becomes faster with decreasing film thickness. These two interpretations could lead us to think that the new mode present in the NR/C15A nanocomposite could be a faster normal mode, in which the inclusion of nanofiller particles divides the bulk in smaller domains, reducing intermolecular cooperativity and thus accelerating the global chain dynamics of the NR matrix. Nonetheless, in order to complement the analysis about the nature of the new mode observed in the NR/C15A nanocomposites and to confirm whether or not the above interpretations are a possible explanation to the findings herein

presented, the molecular dynamics of the vulcanized NR/silicate nanocomposite is evaluated.

IV.5. Dynamics of Vulcanized NR/Layered Silicate Nanocomposites

The dielectric measurements have been proven to be useful for studying the rubber vulcanization reaction. The most common method of vulcanizing rubber is to mix it with sulfur and heat it up. This procedure results in cross-linking of the polymer chains by mono- or polysulphide bridges (see Figure I.3). A side reaction is also known to proceed along cross-linking, leading to formation of heterocyclic groups in the polymer chains. In sulfur vulcanizates correspondingly, the following polar groups are found: (a) the carbonyl groups present in the non-vulcanized rubber and those formed during vulcanization; (b) mono- or polysulphide cross-links; (c) S-C bonds in the heterocyclic groups in the main chains, as shown in Figure I.3.[161] In particular, in vulcanized NR, the change in the segmental mobility is generally observed as a shift of the glass-rubber transition to higher temperatures and an increase in the dispersion amplitudes.[161] Additionally the normal mode vanishes due to the cross-linking and the concurrent loss of significant dynamics.

In the following sections, the relaxation phenomena present in sulfur vulcanized NR and NR/layered silicate nanocomposites are discussed.

IV.5.1. *Effect of Vulcanization on the Segmental Dynamics*

For the sake of comparison, Figure IV.20 shows the normalized dielectric loss data for the vulcanized samples of NR, NR/5C15A and NR/5CNa+ in the temperature region of the segmental dynamics. The corresponding spectrum for non-vulcanized NR is also shown. The results indicate that vulcanizing by sulfur induces a slowing down of the segmental dynamics (shift to lower frequencies) and an increase of the dispersion amplitudes. The latter effect indicates that the side reaction resulting in heterocyclic groups is effective because they would hinder the segmental motion

and they would increase the total number of polar groups involved, with a subsequent increase of the dispersion amplitude or the loss maximum.[161]

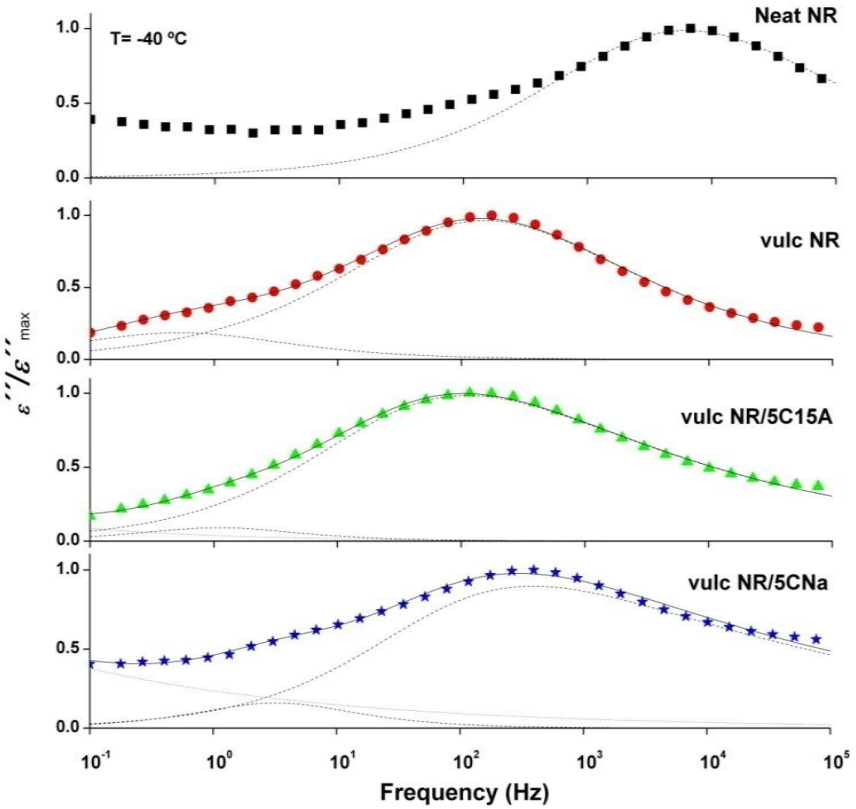

Figure IV.20. Frequency dependence of normalized dielectric loss ε'' for vulcanized samples of NR and NR/5C15A and NR/5CNa+ nanocomposites in the temperature region of the segmental dynamics. The corresponding spectrum for neat NR is also shown. Solid lines represent the HN fitting curve, dashed lines the individual processes, and dotted lines the conductivity contribution.

Another important aspect that should be highlighted from Figure IV.20 is the contribution of a low frequency process. The systematic dielectric study presented in Chapter III indicates that ZnO has influence on this excess of dielectric loss.

Figure IV.21 shows the relaxation times of the segmental mode corresponding to vulcanized samples of NR, NR/5C15A, NR/10C15A and NR/5CNa+. The relaxation times for non-vulcanized NR have been also included. The observed increase in the average relaxation time due to the vulcanization reaction can be interpreted straightforward considering the network formation. It is evident that the

formation of polysulphide cross-links and cyclic sulphide structures cause restrictions on the segmental motions of the polymer chains. Moreover, this high frequency process exhibits almost no dependence on the degree of filling (5 and 10 phr of C15A). On the other hand, the slightly faster segmental dynamics of the NR/5CNa+ sample could in a first approach be associated to the hydroxyl groups present in the surface of the silicate, which interact with the accelerant, thus restricting the vulcanization reaction.

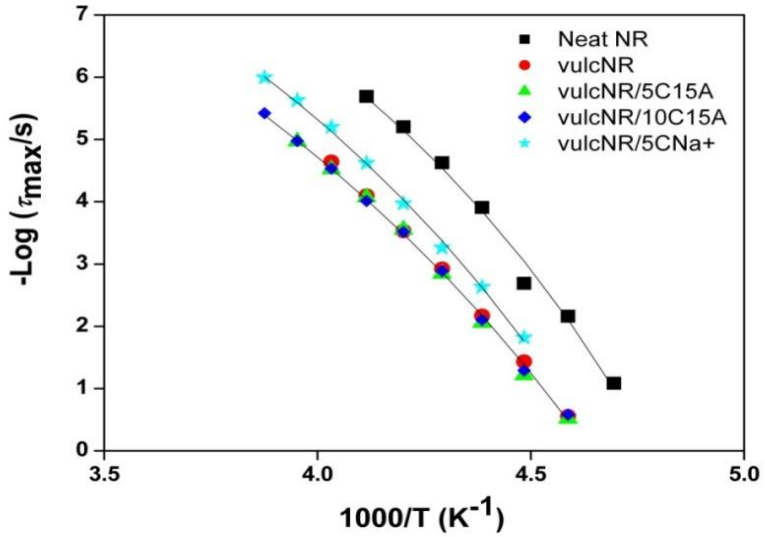

Figure IV.21. Temperature dependence of the average relaxation time of the segmental mode corresponding to vulcanized samples of NR and NR/C15A and NR/CNa+ nanocomposites.

IV.5.2. *Effect of Vulcanization on the New and Normal Mode Dynamics*

As previously mentioned in Chapter III (section III.3) NR exhibits above the glass transition temperature, T_g, two relaxation processes related to the segmental and chain dynamics in order of increasing temperature.[114] However, in vulcanized NR the process associated to chain dynamics, referred to as normal mode,[173] is suppressed as a consequence of the cross-linking. Therefore, vulcanized NR only exhibits above T_g=-64 °C one relaxation process, α-relaxation or segmental mode, which manifests itself by a maximum in ε''(F) (see Figure IV.22).

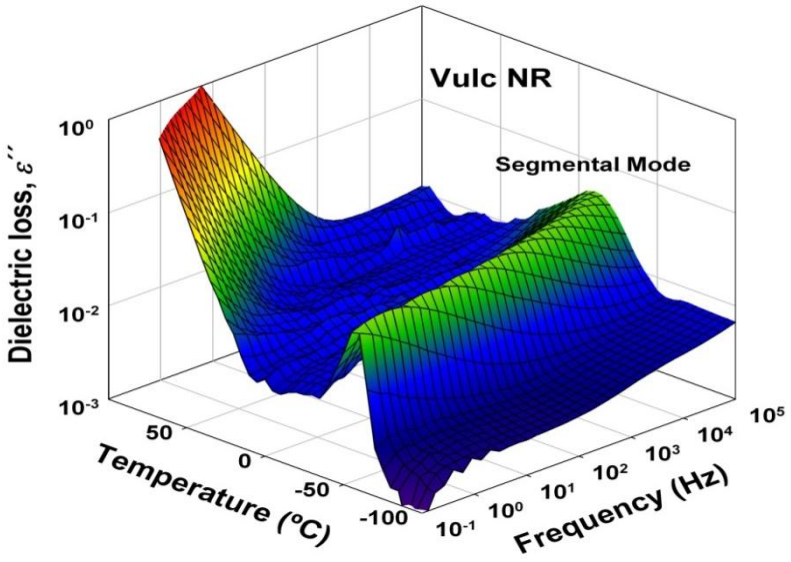

Figure IV.22. 3D representation of the frequency and temperature dependence of the dielectric loss ε'' for the investigated vulcanized NR sample.

Figure IV.23a shows the dielectric loss data for the vulcanized samples of NR, NR/5C15A and NR/5CNa+ nanocomposites. The selection of the spectra at T=90 ºC is made with the intention of studying the temperature region where the normal mode of non-vulcanized NR and the new mode of non-vulcanized NR/5C15A nanocomposite were previously detected and are clearly resolved. It is clear the absence of a normal mode in the vulcanized samples. It is known that the normal mode of vulcanized NR becomes broader and decreases in amplitude upon vulcanization due to suppression of large-scale motions of the dipole oriented parallel to the polymer backbone.[85] However, the process corresponding to the new mode is present for the vulcanized NR/5C15A nanocomposite. Once again, the modulus formalism was used to further analyze this relaxation.

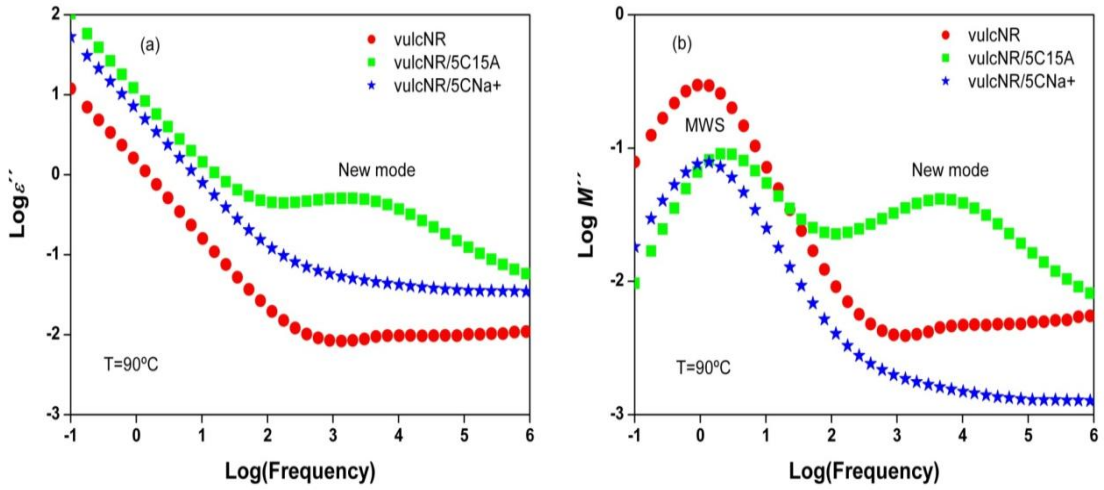

Figure IV.23. (a) Dielectric loss ε'', and (b) Dielectric loss modulus M'', in the frequency domain for vulcanized samples of NR and NR/5C15A and NR/5CNa+ nanocomposites.

Figure IV.23b illustrates the dielectric modulus spectra of vulcanized NR and its nanocomposites. The maximum at low frequencies corresponds to the MWS relaxation. In particular, in the vulcanized NR compound, this process can be a consequence of the vulcanizing additives (sulfur, accelerators, activation complex, etc.) added to the rubber matrix in order to ensure that the cross-linking reaction takes place. The addition of these components makes the polymeric material to be a heterogeneous media consisting of different phases with different dielectric permittivities and conductivities.[101,174,175] Accordingly, for the vulcanized nanocomposites, the presence of the MWS process has a similar explanation as for the non-vulcanized nanocomposites: the interfacial polarization (ion accumulation) that occurs at the interface between materials with differing dielectric constants, such as rubber and layered silicates.

At high frequencies the dielectric spectrum of the vulcanized NR/5C15A nanocomposite has similarities with that of the non-vulcanized NR/5C15A nanocomposite, since the presence of a second process associated with the new mode is noted.

The relaxation times of the segmental mode and new mode for the vulcanized samples are shown in Figure IV.24 as a function of the reciprocal temperature. One can clearly see that the new mode is also slower than the segmental one for the vulcanized samples. Similarly as previously discussed for the non-vulcanized samples, this effect can be understood by assigning the new mode as being caused by a restricted segmental dynamics. Accordingly, the new mode can be associated to cooperative movements of polymer chains in the interface layer around the clay particles.

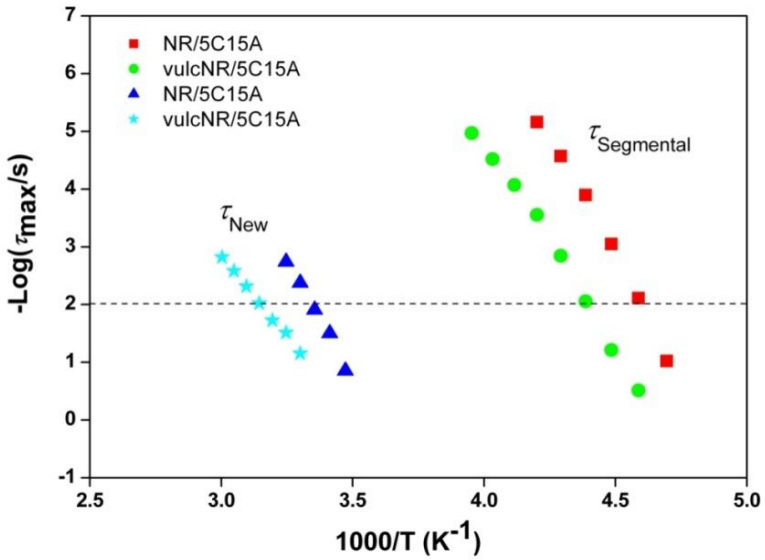

Figure IV.24. Temperature dependence of the average relaxation time for the segmental and new mode of non-vulcanized and vulcanized samples of NR/5C15A nanocomposites.

The new mode is present independently of whether or not the rubber matrix has been vulcanized. One can notice that both segmental and new mode exhibit equivalent shifts in temperature with vulcanization. Thus, this fact further supports the assumption drawn from the non-vulcanized nanocomposites study suggesting that the new mode present in the NR/C15A nanocomposites corresponds effectively to a restricted segmental relaxation. Here, it is proposed that part of the polymer chains are partially immobilized as an interface layer around the clay particles and so the interfacial effects dominate the bulk properties of the material, as shown in Figure IV.25.

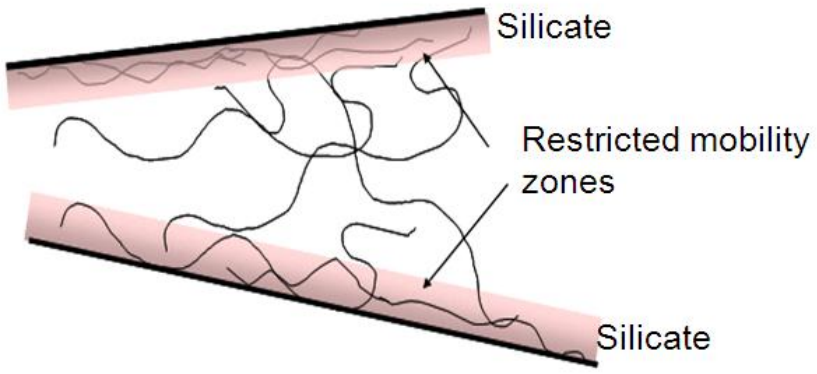

Figure IV.25. Schematic representation of the restricted segmental mobility between silicate layers.

IV.6. Summary

Dielectric relaxation spectroscopy has been proven to be a powerful technique for investigating molecular dynamics in a series of nanocomposites consisting of NR and C15A and CNa+ layered silicates. The measurements show that neither an increase in nanosilicate loading nor the type of filler added has an effect on the segmental mode process of the NR matrix. Besides, the Maxwell-Wagner-Sillars effect is present in all nanocomposites and is attributable to the interfacial polarization at the nanoclay/polymer interface.

A new mode ascribed to a restricted segmental relaxation appears in the NR/C15A nanocomposites regardless of the vulcanization of the NR matrix. This new mode can been attributed to the segmental dynamics of polymer chains at the interfacial polymer-particle regions. Part of the polymer chains are partially immobilized as an interface layer around the clay particles, and thus, the interfacial effects dominate the bulk properties of the material.

CHAPTER V. DYNAMICS OF NATURAL RUBBER/CARBON BASED FILLER NANOCOMPOSITES

V.1. Introduction

The present chapter is focused on the dynamics of NR nanocomposites prepared containing different carbon based nanoparticles including, multi-walled carbon nanotubes (MWCNT), functionalized multi-walled carbon nanotubes (f-MWCNT) and functionalized graphene sheets (FGS). Results of this comprehensive study are provided in the following sections, mainly characterizing the dielectric behavior, but also analyzing the cure behavior, mechanical properties and structural characteristics of the prepared nanocomposites. The relationships between these properties and nanoparticle nature are presented in this chapter. The main focus here is the influence of both nanofillers and vulcanizing additives on the molecular dynamics of NR nanocomposites.

V.2. Experimental

V.2.1. *Non-vulcanized Nanocomposites*

Non-vulcanized nanocomposites were prepared consisting of the pure rubber and the nanofiller. The samples are referred to as NR/*xy*, where "*x*" and "*y*" correspond to the amount and type of filler (MWCNT, f-MWCNT, FGS), respectively.

Additionally, non-vulcanized nanocomposites of the pure rubber, nanofiller and vulcanizing additives were also prepared. The system containing all the vulcanizing chemicals (SA, ZnO, MBTS, and S) was chosen, according to the formulation expressed in Table V.1. In this case the samples are referred to as NR/additives/*xy*, where "additives" stands for all the vulcanizing additives, "*x*" for the filler content and "*y*" for the type of carbon based nanofiller.

Table V.1. Formulation and additives used in the preparation of non-vulcanized NR nanocomposites.

Additives	Content (phr)
NR	100
Zinc oxide (ZnO)	5.0
Stearic acid (SA)	1.0
Mercapto benzothiazyl disulfide (MBTS)	1.0
Sulfur (S)	2.5
Carbon based nanofiller	MWCNT (0.1 and 0.5) f-MWCNT (0.1) FGS (0.1, 0.5 and 1.0)

V.2.2. *Vulcanized Nanocomposites*

Vulcanized NR/carbon based filler nanocomposites were also prepared according to Table V.1. The samples are referred to as vulcNR/*xy*, following the same nomenclature as for the non-vulcanizates.

V.3. Characterization of Natural Rubber/Carbon Based Filler Nanocomposites

V.3.1. *Structural Characterization of Carbon Based Nanofillers*

- X-ray Diffraction (XRD)

XRD data are obtained for natural graphite, graphite oxide (GO) and functionalized graphene sheets (FGS). The interlayer distance changes are calculated from the XRD data and hence the exfoliation of the FGS is assessed. X-ray diffraction patterns of natural graphite, GO and FGS are shown in Figure V.1. Natural graphite presents a diffraction maximum at 2θ = 26º corresponding to a basal spacing

d=0.34 nm calculated according to the Bragg's law, (see equation II.1). During the oxidation process, graphite flakes break down into smaller GO flakes. The value of the diffraction maximum diminishes to 17º (*d*=0.52 nm) due to the intercalation by oxygen groups.[176] On the other hand, FGS presents a broad and weak maximum around 2θ = 24º indicating that most of the FGS material consists on exfoliated graphite, *i.e.* graphene sheets.[80]

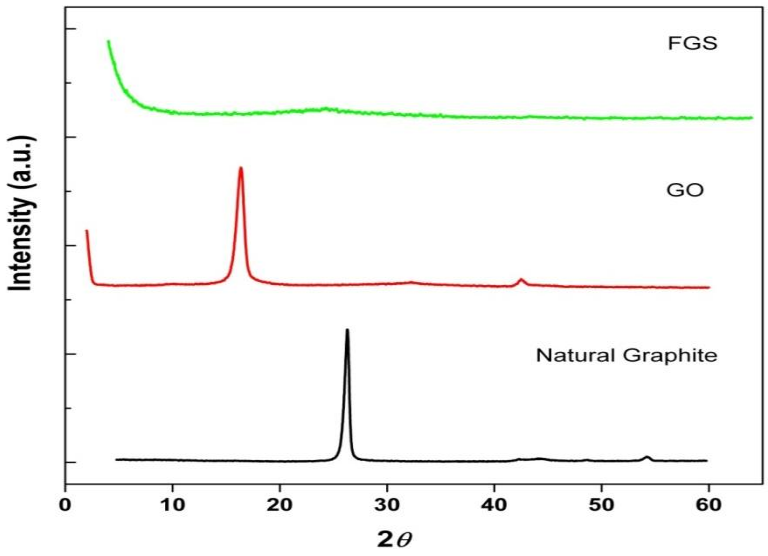

Figure V.1. X-ray diffraction patterns of natural graphite, graphite oxide and functionalized graphene sheets.

- Transmission Electron Microscopy (TEM)

The morphology of carbon based fillers was observed by transmission electron microscopy. The images of MWCNT and f-MWCNT are shown in Figure V.2 and Figure V.3. Pristine MWCNT present the characteristic tube-like structure with well-graphitized concentric layers. The diameter of the as-synthesized MWCNT is 41 ± 14 nm and the interlayer distance is 0.34 nm. As it can be observed in Figure V.2b, some amorphous carbon remains on the sidewalls of the carbon nanotubes, while at lower resolutions (Figure V.2a) some catalyst particles can be detected.

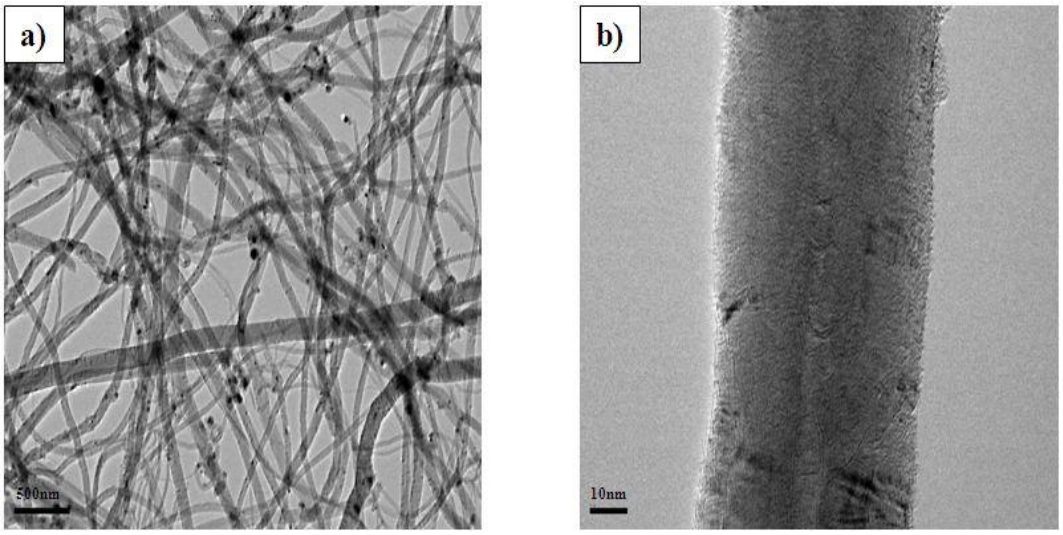

Figure V.2. TEM image of MWCNT at a resolution of: a) 500nm and b) 10 nm.

The effect of the oxidation of MWCNT can be clearly observed in Figure V.3. The acid treatment of MWCNT causes severe etching of the graphitic surface and hence the size of the nanofillers is affected. The diameter of f-MWCNT is 32 ± 11, which is 10 nm smaller than MWCNT. Furthermore, an alteration of the structural integrity and the length of the nanotubes can be observed.

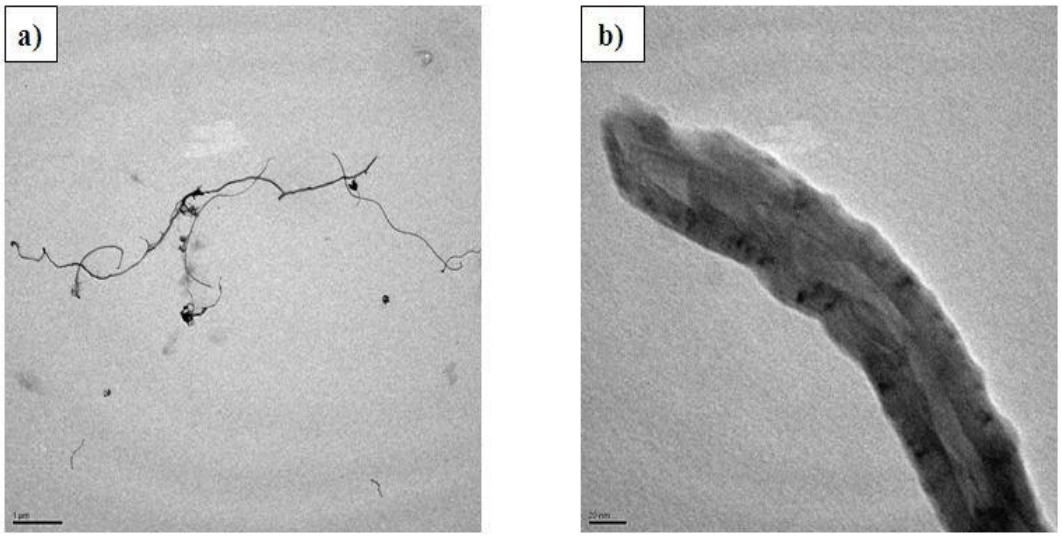

Figure V.3. TEM image of f-MWCNT at a resolution of: a) 1 μm and b) 20 nm.

High resolution TEM images of FGS (Figure V.4a) show the characteristic wrinkled structure of the particle due to the thermal shock to which it has been subjected. Figure V.4b shows the presence of stacks of a small number of graphene sheets, of

up to 7 layers, with inter-graphene spacing of 0.6 nm. The selected area electron diffraction (SAED) pattern of those stacks presents only weak and diffuse rings, confirming the loss of long range ordering. This result is in agreement with a recent study where the exfoliation of FGS particles on single sheets was found to be roughly 80 % of the material.[176]

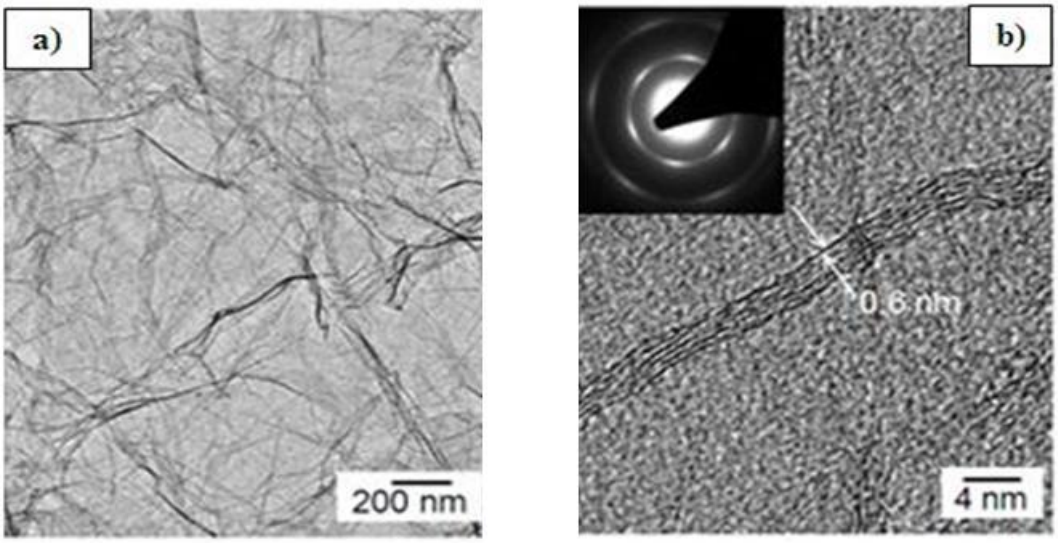

Figure V.4.TEM image of FGS at a resolution of: a) 200 nm and b) 4 nm.

- Raman Spectroscopy

Raman spectroscopy was used to determine the functional groups present in the carbon based nanofillers employed in this study. Raman spectra of MWCNT, f-MWCNT and FGS are shown in Figure V.5. The most distinctive observed bands of carbon nanofillers are the *G* band (in-plane tangential stretching of the carbon-carbon bonds in graphene sheets) at ~ 1570 cm^{-1}, the *D* band (attributed to the presence of disorder or amorphous carbon in graphitic materials) at ~ 1350 cm^{-1} and the *D'* band at ~ 1610 cm^{-1} (overtone resonance feature induced by disorder and defects).[125,177-180] The I_D/I_G ratio is widely used as a measure of the defects quantity in graphitic materials and it can be calculated from the Lorentzian deconvolution of the *D* and *G* band.

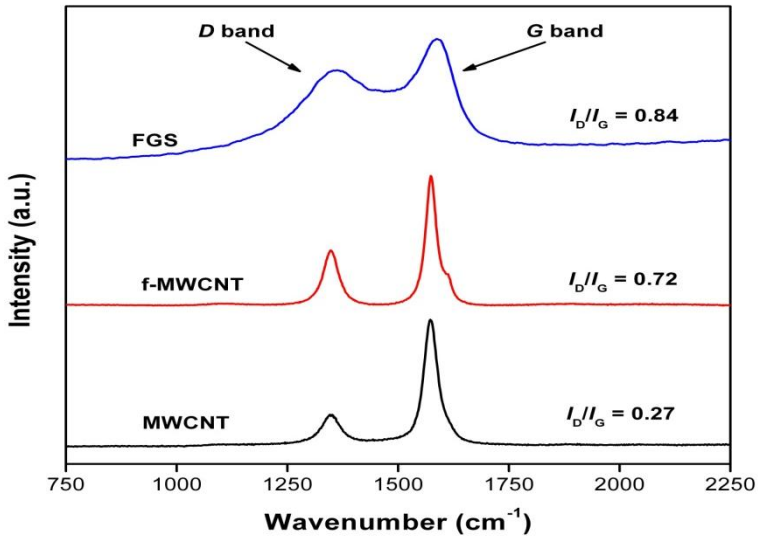

Figure V.5. Raman spectra of MWCNT, f-MWCNT and FGS.

It can be observed in Figure V.5 that the main difference between MWCNT and f-MWCNTs is an increase on the relative intensity of the *D* band. Thus, it can be assumed that there is an increase on the defect sites on the sidewalls of the nanotubes due to the functionalization. Furthermore, it can be noted that a weak shoulder appears at around 1610 cm^{-1} corresponding to the *D'* band, which confirms the inclusion of defects.

In contrast, FGS exhibits a broader *G* and *D* band attributed to higher disorder in graphite. The broadening of the *G* band results from the formation of epoxy, hydroxyl and carbonyl groups during the preparation of the FGS.[181] The thermal expansion of the GO to obtain FGS leaves topological defects on graphene with the subsequent broadening of the *D* band.

- X-ray Photoelectron Spectroscopy (XPS)

XPS was used to determine the surface chemical composition and bonding of MWCNT, f-MWCNT and FGS. The C_{1s} and O_{1s} spectra of carbon nanofillers are shown in Figure V.6 and the relative amounts are reported in Table V.2. The C_{1s} spectra (left side figures) were dominated by a single peak at 284.8 eV assigned to the sp^2 C-C bonds of graphitic carbon. The deconvolution of the C_{1s} peak into

different fitting curves has been assigned to a high intensity peak between 285-286 eV of sp^3 C-atoms, while the peaks in the region 286.3-290.5 eV have been assigned to carbon attached to different oxygen groups. It can be observed that the C_{1s} spectra show a broad weak component at around 291.5 eV which corresponds to $\pi \rightarrow \pi^*$ transition of carbon atoms in graphene structures.[43,182-184]

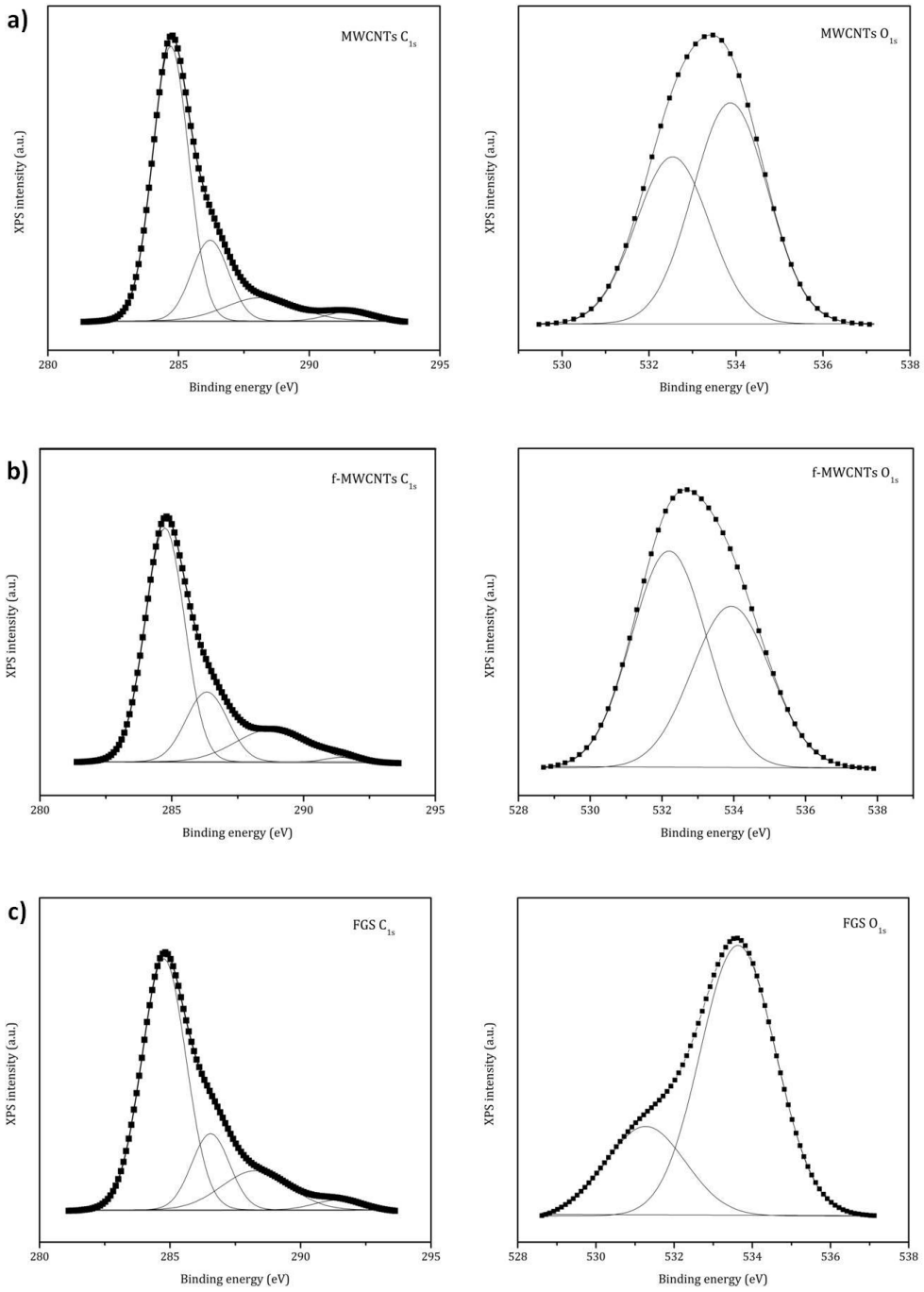

Figure V.6. High resolution C_{1s}(left) and O_{1s} (right) XPS spectra of a) MWCNT, b) f-MWCNT and c) FGS. Deconvoluted fitting curves of the spectra are also shown.

As it can be observed in Table V.2, the functionalization of MWCNT introduces new oxygen groups on the surface of the nanofillers and a decrease on the carbon graphitic layer.

The information provided by the C_{1s} spectra was complemented analyzing the O_{1s} spectra since they are more surface specific than the C_{1s}.[185] The O_{1s} spectra (right side figures) show a broad peak indicating that different oxygen-containing groups are present in the surface of the carbon nanofillers (Figure V.6). The deconvoluted peaks are centered at 532.2 eV and 533.6 eV, which correspond to O=C surface groups and O-C bonds,[184] respectively.

The surface atomic ratios of oxygen to carbon are calculated from the area of the O_{1s} peak divided by the area of the C_{1s} peak normalized by the atomic sensitivity factors.[186] Hence, the atomic amount of oxygen atoms estimated for MWCNT, f-MWCNT and FGS are 2.5%, 17.9% and 9.2%, respectively. These values confirm the successful functionalization of MWCNT and the presence of functional groups on FGS derived from the GO.

Table V.2. Binding energy (BE) peaks, peak assignment and atomic percentage for MWCNT, f-MWCNT and FGS.

Peak	BE (eV)	Assignment	Atomic percentage (%)		
			MWCNT	f-MWCNT	FGS
C_{1s}	284.6-285.8	C-C sp^2 C-C sp^3	86	63	65
	286.3-286.5	C-O-C	-	20	17
	288.0-289.0	-O-C=O	11	16	16
	291.0-291.5	π-π^*	3	1	3
O_{1s}	531.5	-O-C=O			26
	532.0-532.5	C=O	43	56	
	533.5-533.9	C-O-C	57	44	74

V.3.2. *Rheometry*

The effect of carbon based fillers on the rheometric properties of NR nanocomposites has been analyzed. The vulcanization curves of neat NR and its nanocomposites are graphically represented in Figure V.7. The curing characteristics of the studied materials deduced from the curves at T=150 ºC, and expressed in terms of the scorch time, t_{s2}, optimum cure time, t_{90}, the minimum and maximum values of the torque, S_{min} and S_{max}, respectively, torque difference ($\Delta S = S_{max} - S_{min}$) and cure rate index, *CRI*, are compiled in Table V.3.

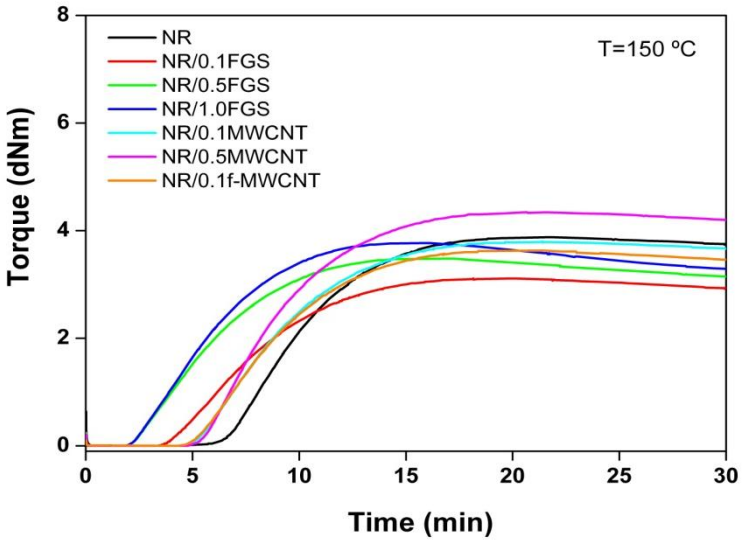

Figure V.7. Vulcanization curves of neat NR and its carbon based filler nanocomposites at T=150 ºC.

Table V.3. Curing characteristics of neat NR and its carbon based filler nanocomposites at T=150 ºC.

Compound	t_{s2} (min)	t_{90} (min)	S_{max} (dNm)	S_{min} (dNm)	ΔS (dNm)	*CRI* (min^{-1})
NR	9.8	14.5	3.88	0.06	3.82	21.3
NR/0.1FGS	8.2	12.8	3.11	0.03	3.08	21.7
NR/0.5FGS	6.1	10.2	3.48	0.03	3.45	24.4
NR/1.0FGS	5.7	10.0	3.77	0.03	3.74	23.3
NR/0.1MWCNT	8.8	13.9	3.80	0.02	3.78	19.6
NR/0.5MWCNT	8.8	13.8	4.34	0.02	4.32	20.0
NR/0.1f-MWCNT	8.6	13.5	3.63	0.02	3.61	20.4

From the data here presented, it can be seen that the scorch time (t_{s2}), which is, as previously mentioned, the measurement of incipient vulcanization of rubber, shows a reduction after the addition of any carbon based nanofiller, being this effect more evident when FGS is used as nanofiller. Some studies[72] indicate that the addition of these types of filler could delay the onset of vulcanization, due to the presence of functional groups such as carboxylic acid groups and oxygen groups on the surface of the nanofillers that absorb the basic accelerator additives. However, in this case the high thermal conductivity of the nanofillers[125] can explain the observed accelerating effects on the curing kinetics, thus promoting the fulfillment of the vulcanization reaction.[67,74] With respect to the time for reaching 90% of the maximum torque (t_{90}), it can be noticed that the trend with the filler addition is as with t_{s2}. In addition, at equivalent nanofiller content (0.1 phr), the higher thermal conductivity (5000 W/m.K)[36,46] and the higher specific surface (2630 m^2/g)[43,46,130] of FGS in contrast with MWCNT (1000-2000 W/m K; 100 to 300 m^2/g)[22,125,187] are features that play a vital role on accelerating the cross-linking reaction. This fact is corroborated by the *CRI* values presented in Table V.3.

It is also interesting to observe the difference between the minimum and maximum torque (ΔS). After an initial decrease upon adding the nanofiller, ΔS

increases on loading as compared with NR vulcanizates. This effect may be attributed to interfacial interactions of the nanofiller with the NR matrix. At higher loading, there is more filler-matrix interaction as corroborated by the mechanical properties described below.[188]

V.3.3. *Mechanical Properties*

Representative stress-strain curves for the neat polymer (NR) and for the NR nanocomposites filled with carbon based nanofillers are depicted in Figure V.8. The ultimate tensile properties reflect the expected tendency considering the presence of the nanophase fillers in the NR matrix. The incorporation of reinforcing particles in an elastomeric matrix leads to an enhancement of the elastic modulus (expressed as the stress at several deformations) and the rupture properties of the material (improved tensile strength, σ_r with no detriment on the elongation at break, ε_r).

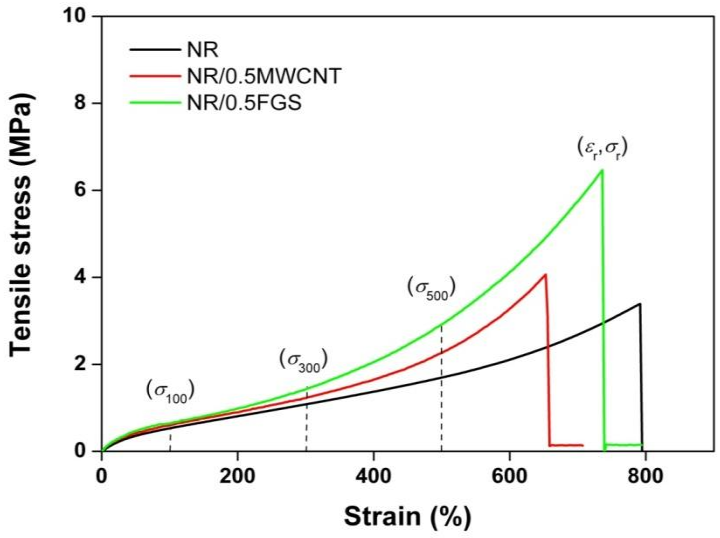

Figure V.8. Representative stress-strain curves of NR and NR/carbon based filler nanocomposites as indicated on the plot.

Significant improvements in mechanical properties of elastomeric matrices by CNT addition have been reported.[23,67,68,71,73,188] In this research there is a complex reinforcement as evidenced by improvement in tensile strength of the

nanocomposites with the filler loading (see Table V.4). There is an initial reduction of tensile strength as the nanofiller is present in small amounts. This could be attributed to a distortion of the cross-linking density of the natural network of NR. As further nanofiller is added the tensile strength increases, being this effect more notorious for the FGS. On the other hand, the elongation at break is scarcely reduced when the nanofiller is present.

Table V.4. Mechanical properties of vulcanized NR/carbon based filler nanocomposites.

Compound	σ_{100} (MPa)	σ_{300} (MPa)	σ_{500} (MPa)	σ_r (MPa)	ε_r (%)
NR	0.55±0.05	1.10±0.04	1.83±0.08	3.17±0.25	831±45
NR/0.1FGS	0.36±0.01	0.70±0.17	1.21±0.07	2.39±0.21	728±31
NR/0.5FGS	0.66±0.02	1.42±0.01	2.91±0.01	5.75±0.60	736±16
NR/1.0FGS	0.69±0.04	1.89±0.12	4.31±0.30	6.71±0.34	622±29
NR/0.1MWCNT	0.48±0.05	0.92±0.08	1.50±0.18	2.45±0.32	685±71
NR/0.5MWCNT	0.57±0.03	1.12±0.06	1.92±0.22	4.24±0.95	643±98
NR/0.1f-MWCNT	0.48±0.03	0.90±0.03	1.46±0.06	2.10±0.39	629±59

As it can be seen in Figure V.9 the enhancement of all the tensile parameters (σ_{100}, σ_{300}, σ_{500}, and σ_r) is exceptionally high for MWCNT and FGS nanocomposites with a minimum filler content of 0.5 phr, obtaining an increment of up to 135% in σ_{500} for the NR/1.0FGS nanocomposite. To the author´s knowledge, none of the studies reported up to date[68,70,73,83,84,188] attain those improvements with such small amount of nanofiller. It is worth noticing the more efficient reinforcing effect of FGS as compared to that of MWCNT, which can be attributed to the about one order of magnitude higher specific surface of FGS with respect to that of MWCNT. Besides, as previously discussed the FGS surface is rich of defects, free radicals and other irregularities which ensure a strong rubber-to-filler interaction both of physical and chemical nature and thus, a more immobilized rubber shell compared with large particles.[74]

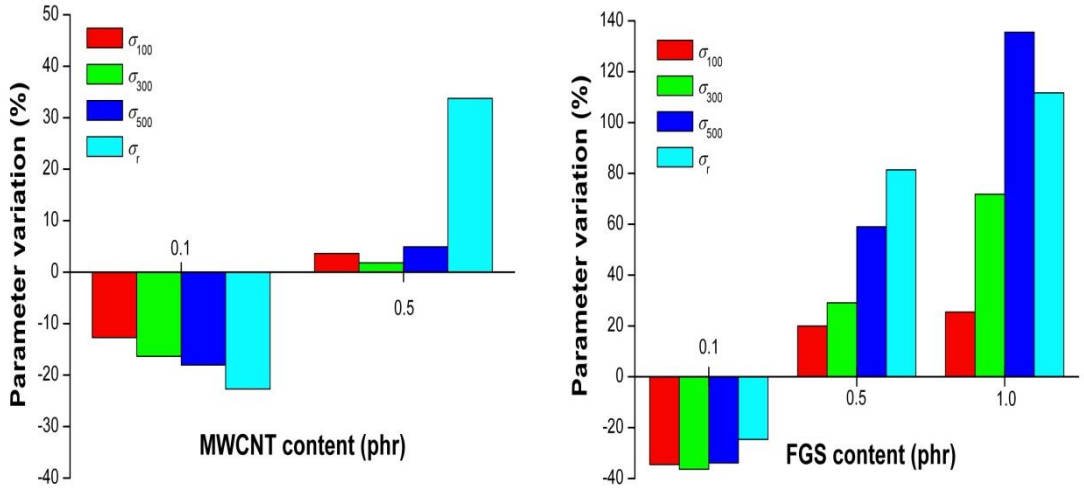

Figure V.9. Tensile parameters variation as a function of filler content.
Left: MWCNT; Right: FGS.

Finally, from the analysis of this preliminary characterization, it can be partially concluded that FGS is a suitable nanofiller for a NR matrix, in the sense that curing kinetics are accelerated and mechanical properties are highly improved. The strong rubber-filler interactions seem to be the origin of such enhancement. Nonetheless, in order to further analyze those interactions, a study of the dynamics of NR/carbon based filler nanocomposites is necessary.

V.4. Segmental Dynamics of Non-vulcanized NR/Carbon Based Filler Nanocomposites

In this section, the effect of the carbon based nanofillers on the segmental dynamics of non-vulcanized NR is discussed. Figure V.10 shows the dielectric relaxation spectra of NR and its nanocomposites in the temperature region where the segmental process is active. A careful examination of the dielectric spectra reveals that the frequency of maximum loss of segmental relaxation does not vary, when a fixed content (0.1 phr) of the carbon based fillers (MWCNT, f-MWCNT and FGS) is present. Similar behavior is reported by Mijovic *et al.* with PI/SWCNT

nanocomposites.[121] Also, this tendency is identical to the one found for the silicate nanocomposites (see Chapter IV), where the segmental process of the NR matrix is essentially unaffected by the addition of layered silicates.

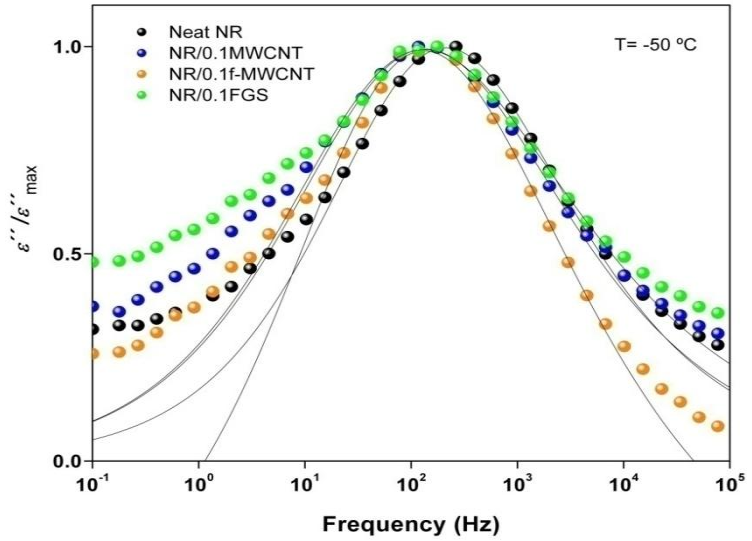

Figure V.10. Frequency dependence of normalized dielectric loss ε'' of the non-vulcanized nanocomposites indicated on the plot in the region of the segmental mode. Solid lines correspond to HN fittings.

The influence of vulcanizing additives on the segmental dynamics of non-vulcanized NR/carbon based fillers nanocomposites is also analyzed, following the approach described in Chapter III. As expected, Figure V.11 shows a clear broadening of the dielectric loss spectra at low frequencies corroborating the existence of a slower dynamic process (α') close to the segmental mode (α) of all nanocomposites when the vulcanizing additives are present, regardless of the nature of the carbon based nanofiller added (MWCNT, f-MWCNT and FGS).

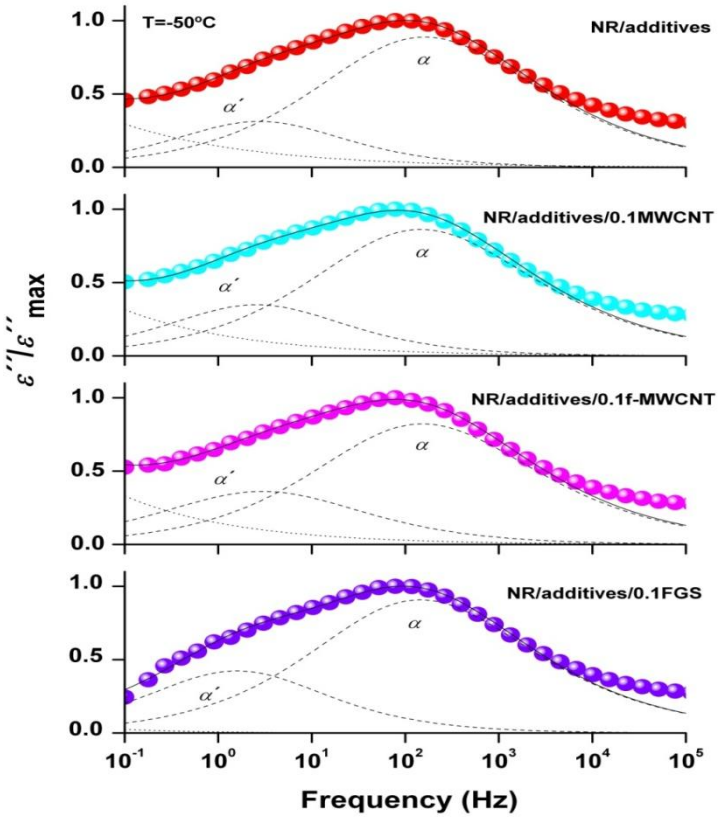

Figure V.11. Deconvolution results of the normalized dielectric loss ε'' of the non-vulcanized nanocomposites indicated on the plot in the region of the segmental mode. Solid lines correspond to HN fitting curves, dashed lines to individual processes and dotted lines to conductivity contribution.

The fitting procedure followed, in terms of the Havriliak-Negami (HN) function previously described, corresponds to the protocol expressed in Chapter III. In that sense, two HN relaxation processes (α' and α in order of increasing frequency) and a conductivity contribution were taken into consideration. The shape parameters b and c were kept constant and similar to those obtained for neat NR (b=0.527; c=0.833). While for the α'-relaxation, the parameter c was set to a value of 1 in order to force a symmetric shape and thus, a narrower distribution of relaxation times. Table V.5 shows the relaxation parameters representative of each fitting.

Table V.5. Representative values of the fitting parameters of the HN function for all tested compounds at T=-50 ºC.

Compound	$\Delta\varepsilon_{\alpha}$	$\Delta\varepsilon_{\alpha'}$	$\tau_{HN\alpha}$	$\tau_{HN\alpha'}$
NR/additives	$1.169x10^{-01}$	$3.211x10^{-02}$	$1.370x10^{-03}$	$5.799x10^{-02}$
NR/additives/0.1MWCNT	$6.756x10^{-02}$	$2.206x10^{-02}$	$1.511x10^{-03}$	$6.215x10^{-02}$
NR/additives/0.1f-MWCNT	$4.980x10^{-02}$	$1.987x10^{-02}$	$1.441x10^{-03}$	$5.353x10^{-02}$
NR/additives/0.1FGS	$6.942x10^{-02}$	$2.611x10^{-02}$	$1.532x10^{-03}$	$1.006x10^{-01}$

Figure V.12 presents the normalized dielectric loss spectra of NR/additives, NR/additives/MWCNT and NR/additives/FGS nanocomposites with different filler content. There is clear evidence of the asymmetric broadening towards the low-frequency side of the dielectric loss curves despite the filler content added, if compared to the spectrum of neat NR. Further, from the inspection of this figure the independence of the glass transition process with the amount of filler incorporated can be corroborated, since all of the spectra tend to superpose; and also, the shift to lower frequencies confirms the assumption drawn from the results presented in Chapter III, showing that the presence of vulcanizing additives slows down the segmental dynamics of the rubber matrix. Thus, no significant changes on the segmental dynamics of non-vulcanized NR come into sight by the addition of carbon based nanofillers.

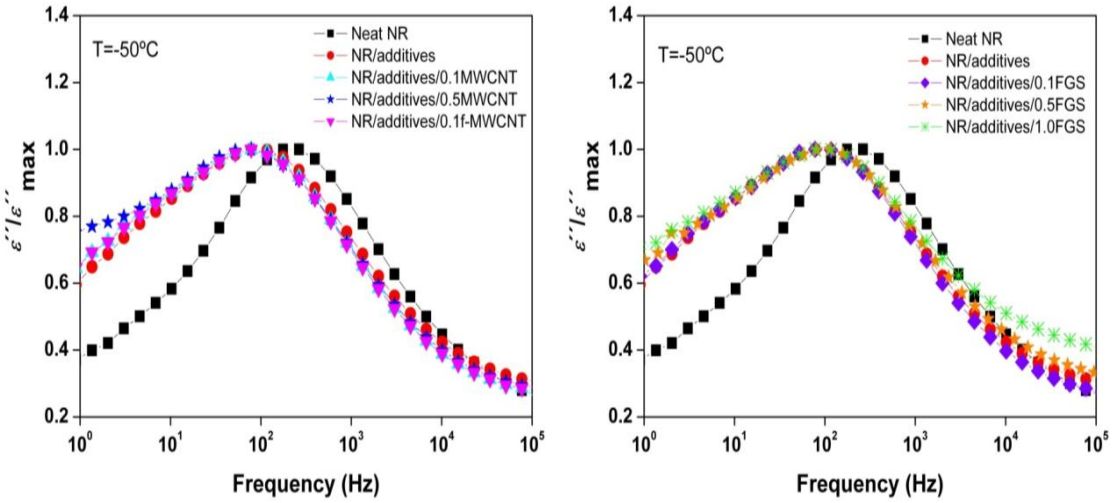

Figure V.12. Normalized dielectric loss ε'' versus frequency of non-vulcanized NR and NR nanocomposites as indicated on the plot in the region of the segmental mode at T=-50 ºC. Left: NR/additives/MWCNT nanocomposites; Right: NR/additives/FGS nanocomposites.

V.4.1. *Temperature Dependence of the Dynamics of Non-vulcanized NR/Carbon Based Filler Nanocomposites*

The independence of the segmental dynamics of NR with the addition of carbon based nanofillers, with or without vulcanizing additives, can be verified by the analysis of the temperature dependence of the relaxation time (τ_{max}) obtained from the HN fitting parameters.[91] The corresponding values for τ_{max}, shown in Figure V.13, reveal the Vogel-Fülcher-Tamman (VFT) dependence of τ_{max} with the reciprocal temperature as previously described in Section III.4.1. The calculated values of B and T_0 are compiled in Table V.6 for all compounds, where one can see that there is no variation on T_0 when the carbon based nanofillers are added to the rubber matrix. Nonetheless, there is a slight increase in T_0 when the vulcanizing additives are present, as expected.

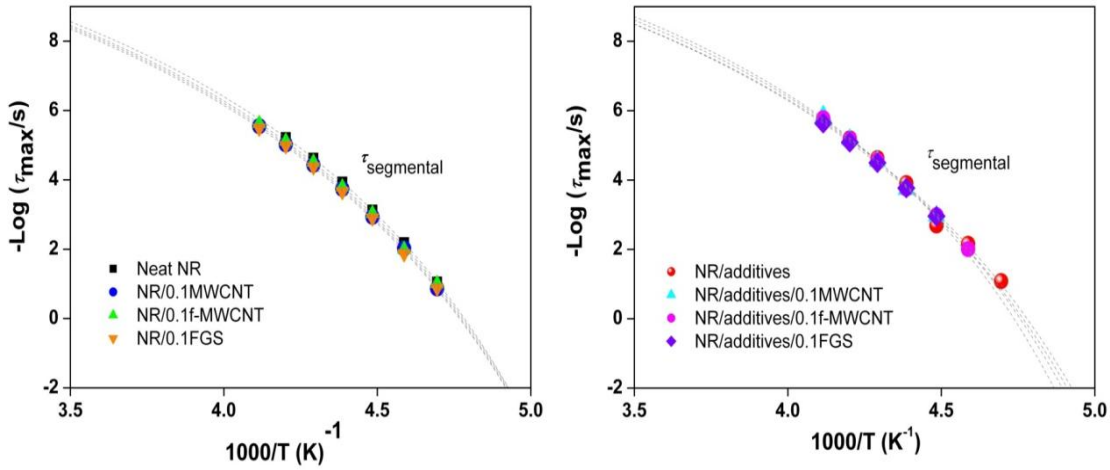

Figure V.13. Temperature dependence of the average relaxation time of non-vulcanized NR and NR nanocomposites. Left: without additives; Right: with additives.

Table V.6. VFT fitting parameters of non-vulcanized NR and NR nanocomposites, corresponding to the α-relaxation.

Compound	B	T_0 (K)
Neat NR	681.4	160.3
NR/0.1MWCNT	710.3	158.8
NR/0.1f-MWCNT	701.6	159.1
NR/0.1FGS	719.5	158.3
NR/additives	698.2	162.7
NR/additives/0.1MWCNT	634.1	163.7
NR/additives/0.1f-MWCNT	661.5	162.9
NR/additives/0.1FGS	690.1	160.5

As far as the relaxation time is concerned it can then be concluded that in the temperature range studied, the presence of carbon based nanofillers has no effect on the time scale of the segmental mode process of the non-vulcanized NR matrix, while the vulcanizing additives do exert a slowdown of the segmental motions of the NR chains.

V.5. Chain Dynamics of Non-vulcanized NR/Carbon Based Filler Nanocomposites

The normal mode relaxation dielectric curves are shown in Figure V.14 and Figure V.15 for the different investigated samples. Figure V.14 shows the effect of the nature of the filler on the normal mode. At first glance, there is a shift towards higher frequencies provoked by the nanofiller for MWCNT and FGS while no effect is observed for f-MWCNT (Figure V.14 left). This effect is somehow more evident for the system with the additives (Figure V.14 right). The effect on nanofiller concentration is not clear as the normal mode is masked by the conductivity contribution (Figure V.15). Anyhow, comparing the measurements for NR/additives/MWCNT (Figure V.15 left) and NR/additives/FGS (Figure V.15 right) systems, it becomes apparent a progressive shift towards higher frequencies of the maximum of the process as the nanofiller concentration increases.

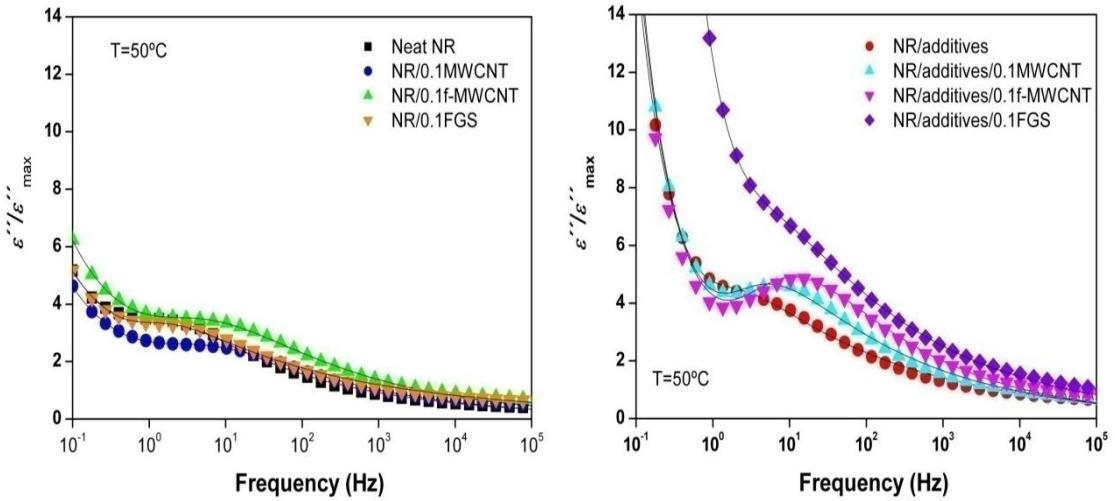

Figure V.14. Frequency dependence of normalized dielectric loss ε'' of the non-vulcanized NR nanocomposites indicated on the plot in the region of the normal mode. Solid lines correspond to HN fittings. Left: without additives; Right: with additives.

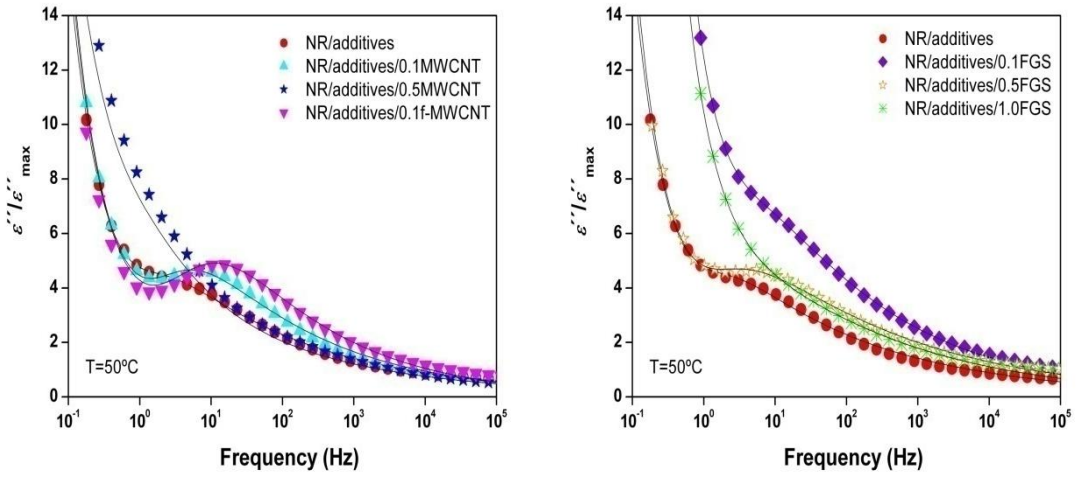

Figure V.15. Frequency dependence of normalized dielectric loss ε'' of non-vulcanized NR nanocomposites indicated on the plot in the region of the normal mode. Solid lines correspond to HN fittings. Left: NR/additives/MWCNT nanocomposites; Right: NR/additives/FGS nanocomposites.

In order to better visualize such behavior, Figure V.16 represents the relaxation maps for the normal mode of the investigated samples. As mentioned before (see Chapter I) NR is a complex biomaterial mainly composed of a linear chain formed by *cis*-1,4 isoprene units and by a small amount of natural components, including proteins and phospholipids. The presence of such natural components induces a multi-scaled microstructure characterized by natural cross-linking among the terminal groups of linear polyisoprene chains, which leads to formations of branch, star and network structures, termed as the "naturally occurring network".[189,190] The normal mode is assigned to the chain dynamics and, consequently, is strongly dependent on the molecular weight and on the mobility of the chain-end cross-links in the naturally occurring network of the NR. The present experiment allows one to speculate with the possibility that additives in general, both vulcanizing additives (as reported in Chapter III) and carbon based nanofillers, may disturb the end chain cross-linking system of NR producing dead ends which could render to faster normal mode.

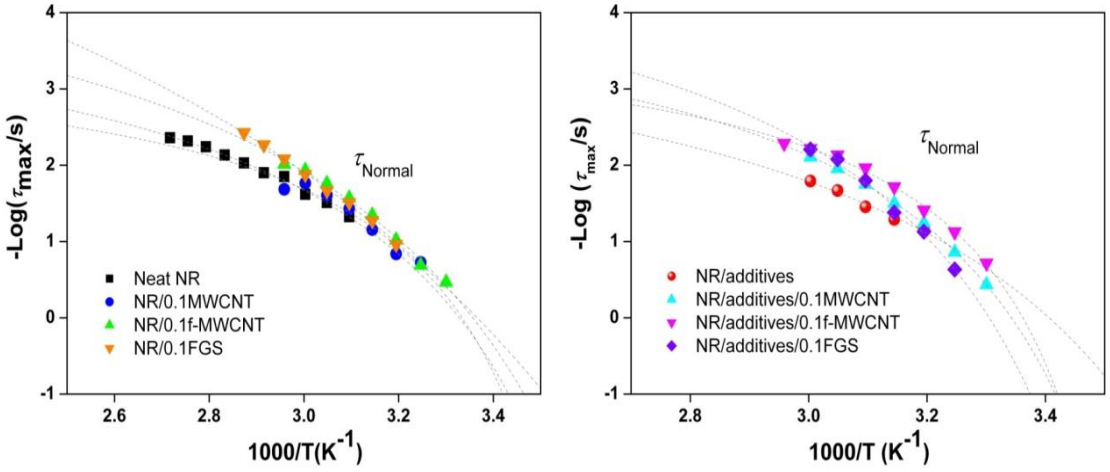

Figure V.16. Temperature dependence of the average relaxation time of non-vulcanized NR and NR nanocomposites. Left: without additives; Right: with additives.

V.6. Conductivity of Non-vulcanized NR/Carbon Based Filler Nanocomposites

Figure V.17 illustrates the variation of electrical conductivity in the frequency domain with increasing filler content at T= 50 ºC. At any given frequency, a slight increase in conductivity with increasing filler concentration can be observed. It is widely believed that electrical properties of nanocomposites depend primarily on the way the filler particles are distributed through the polymer matrix. At low levels of filler loading, the conductivity of the nanocomposite is slightly higher than that of the base polymer, because filler particles are isolated from each other by the insulating rubber matrix. As the concentration of nanofiller in the composite is increased, the filler particles begin to contact each other and a continuous path is formed through the volume of the sample for electrons to travel.[191] The formation of this conductive network is based on the principles of percolation theory.[192,193] Beyond a critical concentration of the filler, known as percolation threshold, an increase of the nanocomposite conductivity of several orders of magnitude is normally observed.[125] In a conducting composite, the conductivity is composed of two terms:

$$\sigma(F) = \sigma_{\mathrm{dc}} + AF^{x} \qquad \text{V.1}$$

Where σ_{dc} is the direct current conductivity, A is a constant and x is an exponent which describes the frequency (F) dependence of $\sigma(F)$. The term σ_{dc} appears as a plateau at low frequencies in the experiments. $\sigma(F)$ for neat NR presents the lack of a σ_{dc} and is characterized by a linear dependence of $\sigma(F)$ with an exponent x=1. This is the characteristic behavior of an insulator. As either additives or additives/MWCNT nanofillers are added to NR an incipient plateau appears at lower frequencies indicating a very modest effect on the overall conductivity of the nanocomposite (Figure V.17 top). A more significant appearance of a σ_{dc} contribution is detected for the nanocomposites of the FGS family where a clear plateau at low frequencies develops for the higher nanofiller concentrations (Figure V.17 bottom).

Numerous studies show that the percolation threshold and conductivity of nanocomposites depend strongly on the polymer matrix type and synthesis method, aspect ratio of filler, disentanglements of filler agglomerates, uniform spatial distribution of individual nanotubes or nanosheets, and degree of alignment.[22,23] In this study, the small amount of nanofiller introduced to the NR matrix could also be considered an important factor affecting the low values and modest increase in conductivity. This fact reduces the possibility of forming a network structure through direct interaction between the nanoparticles, or through chain bridging between them, which results in a reduction in electrical conductivity and a higher percolation threshold as compared to those in a composite with higher content of randomly oriented nanofillers.[46,194]

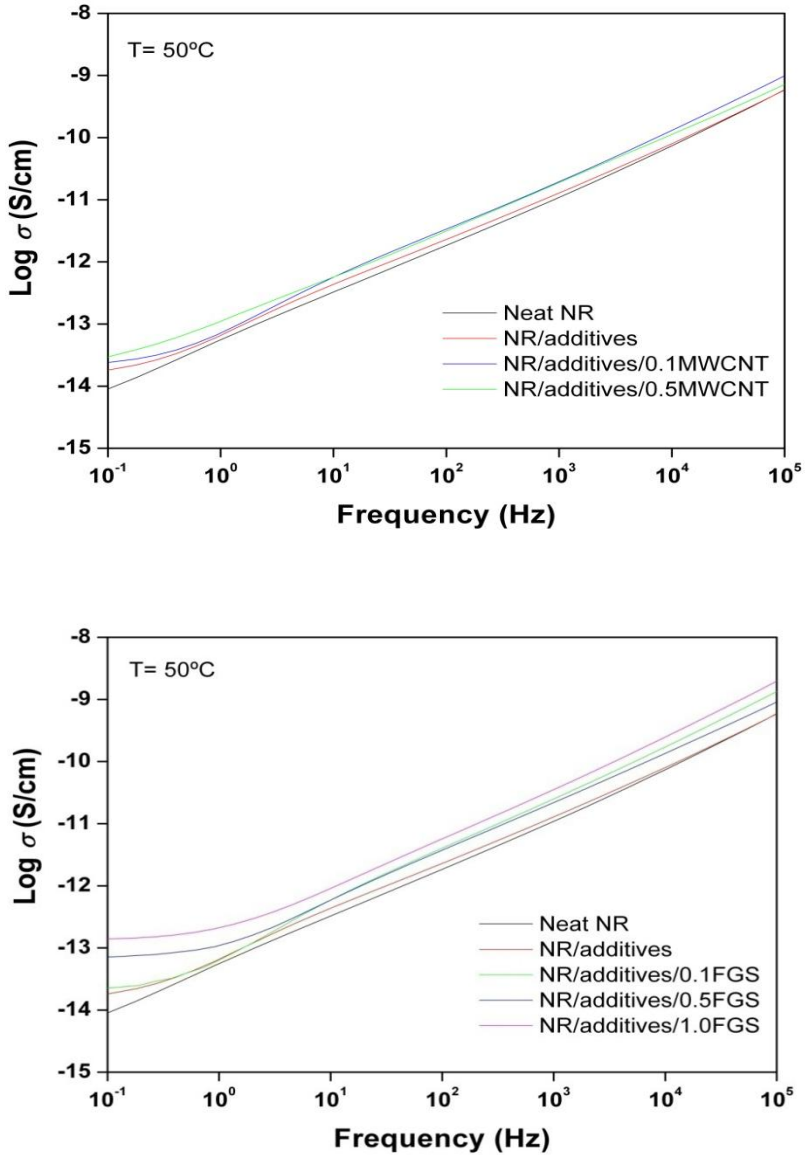

Figure V.17. Electrical conductivity of non-vulcanized NR and NR nanocomposites measured as a function of frequency with carbon based filler content (phr) as a parameter for: Top: MWCNT; Bottom: FGS.

V.7. Segmental Dynamics of Vulcanized NR/Carbon Based Filler Nanocomposites

As expected, the results presented in Figure V.18 and Figure V.19 clearly indicate that vulcanizing by sulfur induces a restricted rubber relaxation in the nanocomposites. The cooperative motions of the NR chains decrease because of the formation of a cross-linked network. The observed increase in the average relaxation time, as shown in Figure V.19, due to the vulcanization reaction can be interpreted straightforward considering the network formation. It is evident that the formation of polysulphide cross-links and cyclic sulphide structures cause restrictions on the segmental motions of the polymer chains. Moreover, this high frequency process exhibits almost no dependence on the type of nanofiller added to the rubber matrix.

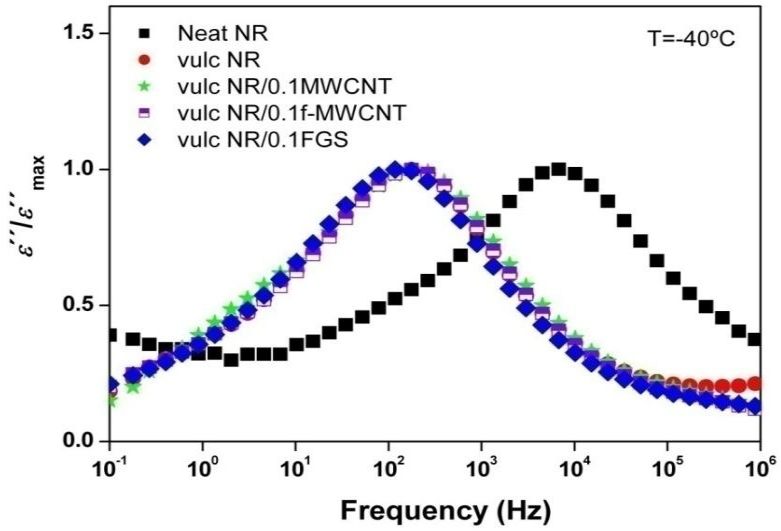

Figure V.18. Normalized dielectric loss ε'' versus frequency of vulcanized NR and NR nanocomposites as indicated on the plot in the region of the segmental mode at T=-40 ºC.

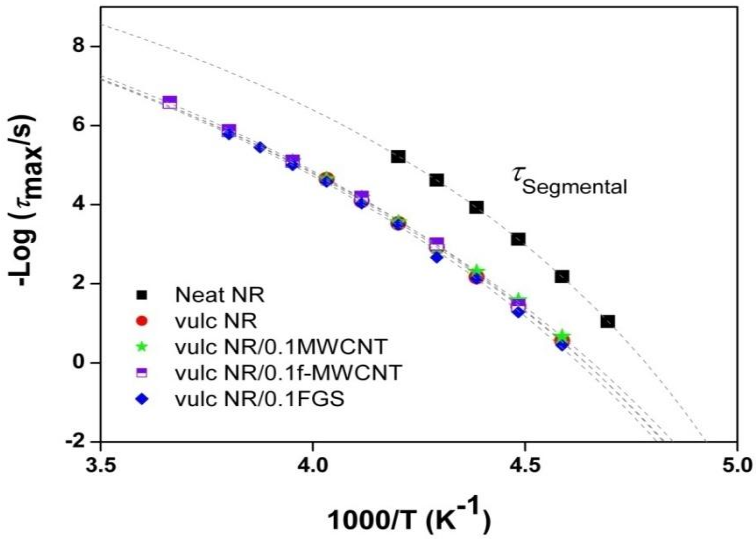

Figure V.19. Temperature dependence of the average relaxation time of vulcanized NR and NR nanocomposites.

V.8. Summary

The molecular dynamics of carbon based nanofiller reinforced NR composites has been studied as function of type of filler, filler loading and presence of vulcanizing additives. This study illustrates that irrespective of the type and amount of nanofiller in the NR composite, the segmental mode relaxation does not change.

The presence of vulcanizing additives, on the other hand, is important to dynamics as evidenced by the slowdown of the segmental mode and by the slight decrease in the time scale of the normal mode relaxation in NR/carbon based filler nanocomposites. The first effect is attributed to strong interfacial interactions formed at the interfaces between the additives clusters and the NR polymer segments, forming initial physical entanglements. While the second effect is envisioned as a consequence of the shorter length of chains within additive domains which accelerate the overall chain dynamics of the NR matrix.

Moreover, the strong interfacial interactions between FGS and the rubber matrix accelerate the cross-linking reaction and cause an important enhancement on the mechanical behavior of the NR nanocomposites.

CHAPTER VI. DYNAMICS OF NATURAL RUBBER NANOCOMPOSITES UNDER UNIAXIAL STRAIN#

#Part of the work described in this chapter has been published in *Macromolecules* **2011**, 44(16), 6574–6580, and in *Materials Science Forum* **2012**, 714, 57-61.

VI.1. Introduction

In many elastomeric applications, network chain dynamics under external stress/strain are critical for determining ultimate performance. Thus, a study on how the strain-induced crystallization affects the dynamics of a rubbery material is of outmost importance. To our best knowledge, no in-depth study on the effects of strain-induced crystallization on the molecular dynamics of vulcanized NR has been undertaken. In particular, it remains unknown the interrelationship between molecular dynamics and deformation in vulcanized NR. Broad-band dielectric spectroscopy (BDS) has been proven to be a powerful technique to investigate both segmental and chain dynamics of natural and synthetic rubbers.[114,173] In addition, the combination of BDS with X-ray scattering techniques has revealed as an efficient approach to deal with order-dynamics relationships.[196,197]

On the other hand, significant improvements in mechanical performance of NR/layered silicate nanocomposites can be accomplished, as previously reported in Chapter IV. However, in order to gain further insight into the mechanism of reinforcement by layered silicates, the strain-induced crystallization behavior and morphology of NR/layered silicate nanocomposites should also be investigated. Thus, the main objective of the present chapter is to understand the effect of strain induced orientation on the segmental dynamics of vulcanized NR and NR/layered silicate nanocomposites. The study is focused on the effect of network structure and the strain-induced crystallization, as investigated by synchrotron X-ray scattering, in the segmental dynamics of NR assessed by BDS.

VI.2. Experimental

In order to study the strain-induced crystallization behavior in vulcanized NR and NR/layered silicate nanocomposites, samples with strain ratios (λ) from 0 to 7.5 were prepared. The strain ratio was defined as $\lambda = l/l_0$, in which l_0 is the initial length of the sample and l is the length of the elongated one. It is worth mentioning that for the NR nanocomposites the highest strain ratio evaluated was λ =7.0. For

the purpose of this section, the nanocomposite samples were prepared with the organoclay C15A and with a fixed amount of 5 phr.

Tensile stress–strain properties of vulcanized NR and its nanocomposites were measured. All specimens were stretched by the movable clamp until the desired strain was achieved. Subsequently, each sample was held at the selected elongation, and glued either to a gold-plated electrode for BDS measurements, as shown in Figure VI.1, or to a metallic frame for the X-ray scattering experiments. The strained sample-electrode (frame) assembly was then separated from the dynamometer clamps.

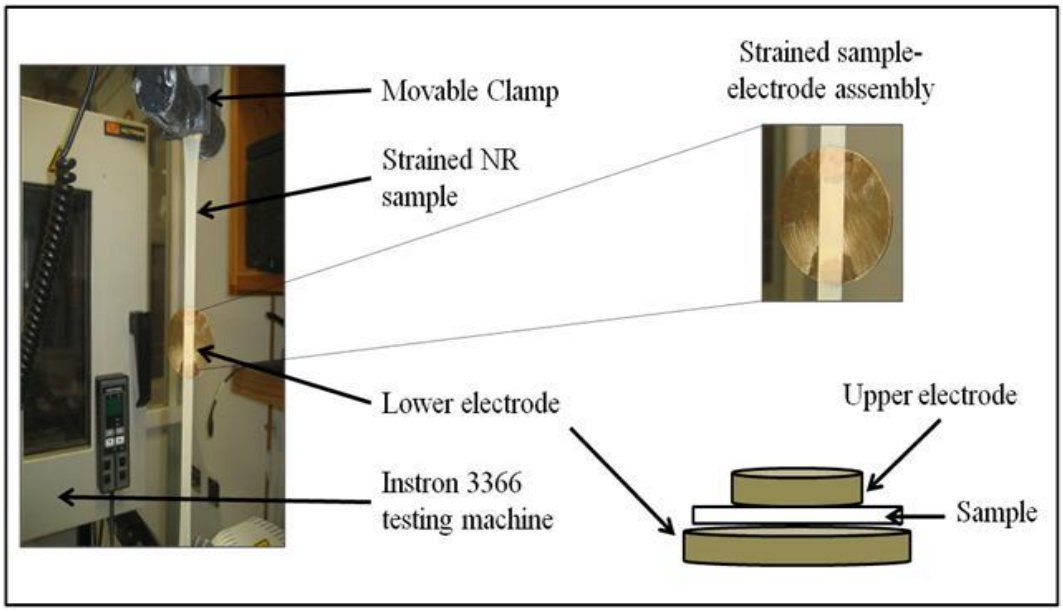

Figure VI.1. Schematic picture of strained sample-electrode assembly corresponding to a strain ratio λ =7.5.

For this particular study of the strain-induced crystallization phenomenon, the BDS experiments were carried out placing the stretched sample-electrode assembly in the dielectric cell between two parallel gold-plated electrodes. The experimental measurements of the stretched samples were done over a frequency window of $10^{-1} < F/Hz < 10^{7}$ in the temperature range from -100 to 100 °C in 5 °C steps.

VI.3. Natural Rubber

VI.3.1. *Strain-Induced Crystallization*

The tensile stress-strain curve of the vulcanized NR investigated here is shown in Figure VI.2. As expected, the mechanical behavior corresponds to an elastomer exhibiting rubber-like elasticity. In this case, the application of stress is considered to cause molecules to change from a coiled to an extended configuration instantaneously. The behavior is Hookean, with a linear relationship between stress and strain only at low strains.[198] A noticeable upturn in stress is observed as stretching proceeds, specifically after λ =3.0, characterized by a change in the slope of the stress-strain curve. This behavior is believed to be due to a crystallization process induced by stretching causing molecular alignment in the stretching direction. This peculiar effect, referred to as strain-induced crystallization,[4] provides vulcanized NR a self-reinforcement character which has been recognized as the main factor responsible for the toughness of the material. It is thought that strain-induced crystallites form an additional physical cross-linking network, bearing most of the applied load.

In order to quantitatively evaluate the strain-induced crystallization in the investigated vulcanized NR under uniaxial stretching, wide-angle X-ray (WAXS) diffraction patterns are measured for samples stretched at different strain ratios (from 0 to 7.5), as shown in Figure VI.2. For the initial undeformed sample (inset (a)), the pattern exhibits a halo characteristic of an amorphous isotropic material. A similar situation is observed even at λ =2.5 (inset (b)). However, at λ =3.0 (inset (c)) the presence of crystalline diffraction maxima can be already detected. Thus, it can be assumed that below λ =3.0 mainly orientation of polymer chains occurs. For strains higher than λ =3.0 (insets (d-g)), the WAXS patterns clearly show the diffraction maxima characteristic of an oriented crystalline phase revealing the occurrence of strain-induced crystallization. Moreover, the peak intensities of these reflections increase with increasing strain. This effect can be better

visualized by the 360º azimuthal integration of the WAXS patterns represented in Figure VI.3a. Here the 360º azimuthally integrated intensity has been represented as a function of the scattering vector $q = 4\pi/\lambda_w(\sin\theta)$ being λ_w the X-ray wavelength and 2θ the scattering angle. It is noteworthy that an amorphous halo remains during the stretching process suggesting the presence of a significant amorphous phase all along the process.

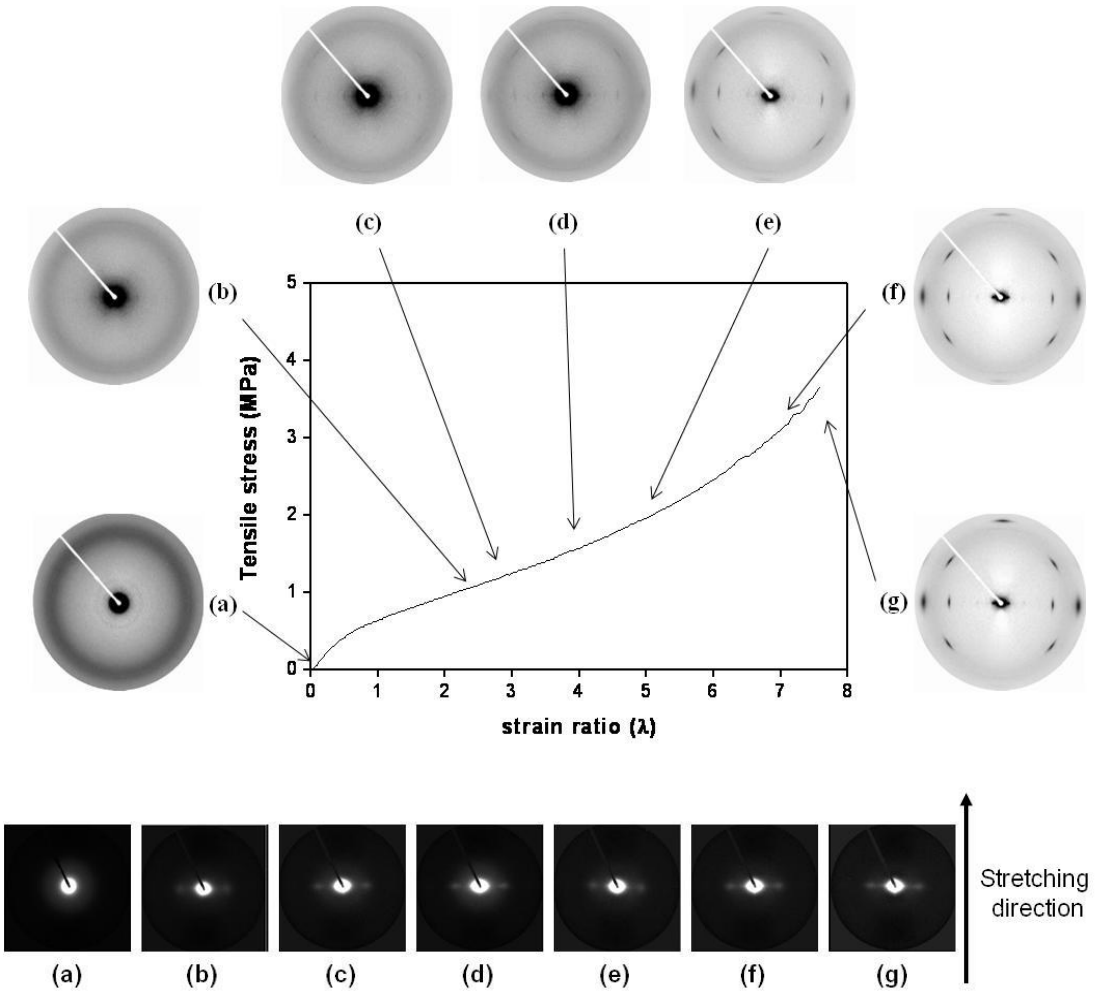

Figure VI.2. Tensile stress-strain curve of the vulcanized NR sample stretched up to λ= 7.5. Insets correspond to WAXS/SAXS patterns of NR upon stretching at room temperature at λ = a) 0, b) 2.5, c) 3.0, d) 4.0, e) 5.0, f) 7.0 and g) 7.5.

In a parallel way, preliminary results on the evolution of the SAXS patterns with the strain ratio are analyzed. It is clearly recognized that the scattering spreads along the equator, indicating the existence of density fluctuation elongated in the

stretching direction. Besides, the degree of intensity localized on the equator increases with increasing the strain ratio, thus confirming that NR crystallizes upon stretching. The average distance between the crystalline lamella and the amorphous domains is obtained from the maximum reflected in the SAXS profiles shown in Figure VI.4 after subtraction of the background using the following equation:

$$L = \frac{2\pi}{q_{max}} \qquad \text{VI.1}$$

The value of the long spacing L estimated from the SAXS patterns is around 3.8-4.0 nm, remaining almost constant during the whole strain ratio range.

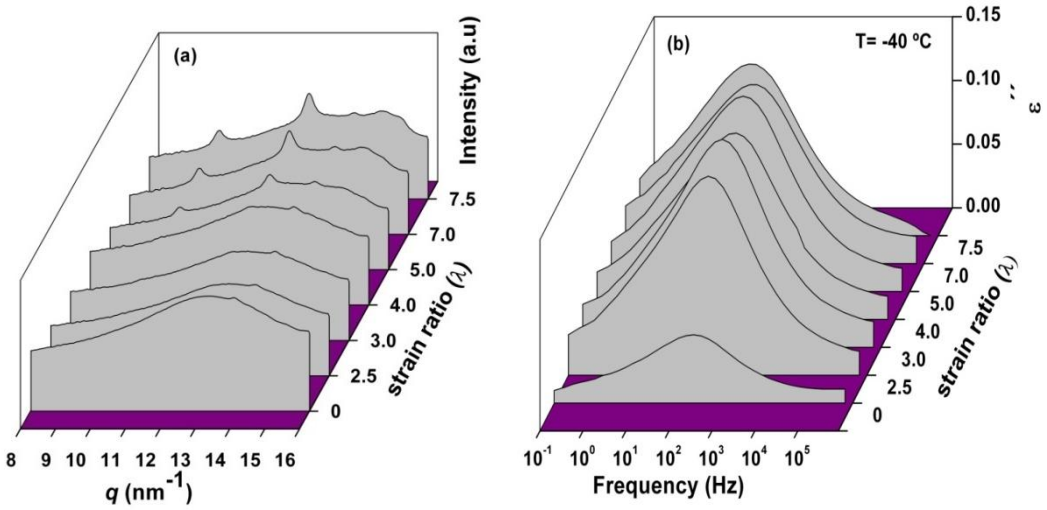

Figure VI.3. (a) Azimuthally integrated intensity of the WAXS patterns as a function of the scattering vector q, and (b) Dielectric loss ε'' as a function of frequency, for vulcanized NR at different strain ratios.

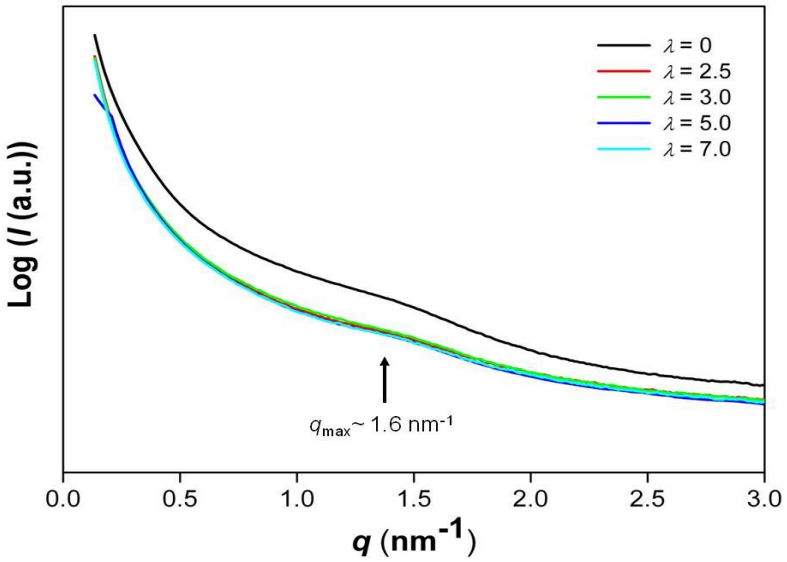

Figure VI.4. Equatorial cake integrated intensity as a function of the scattering vector q taken from the SAXS pattern of stretched NR samples at different strain ratios.

Strain induced crystallization of vulcanized NR is a phenomenon which has been widely reported by several authors elsewhere.[64,199-203] In this case, the WAXS diffraction patterns observed upon strain correspond to that of semi-crystalline vulcanized NR and are consistent with the monoclinic unit cell of polyisoprene.[200,204] Specifically, the patterns present in the equator the reflections corresponding to the (200) and (120) planes. Different procedures have been proposed for the quantitative calculation of the strain-induced crystallinity from WAXS patterns. In this research, the analysis is based on a recent proposal published elsewhere[200] which allows one to estimate a crystallinity index based on the equator diffraction peaks.[132] In this case, the diffraction intensity near the equator was normalized and azimuthally integrated in a cake from 75° to 105° (see inset of Figure VI.5). As an example, Figure VI.5 represents the cake integrated intensity as a function of the scattering vector q for a strain ratio λ=7.5. The resultant profiles were deconvoluted considering the diffraction peaks of the 200 and 120 planes and the amorphous halo using the peakFIT© software. The mass fraction crystallinity index, X_c at room temperature was estimated according to:

$$X_c = \frac{A_c}{A_c + A_a} * 100\% \qquad \text{VI.2}$$

Where A_c is the area below the 200 and 120 crystalline peaks and A_a is the area below the amorphous halo.

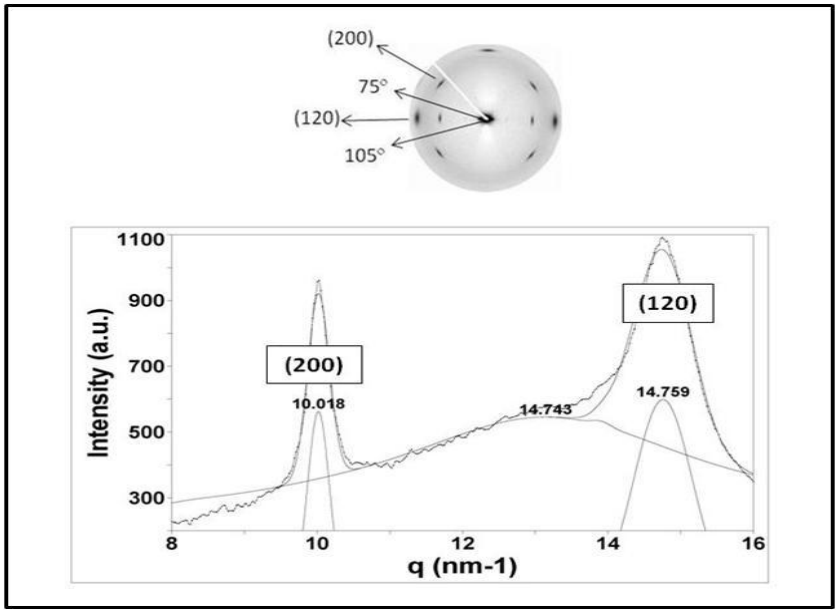

Figure VI.5. Equatorial cake integrated intensity as a function of the scattering vector q taken from the WAXS pattern of stretched vulcanized NR at a strain ratio λ=7.5. Inset shows integration limits from 75° to 105°.

Figure VI.6a shows the calculated crystallinity index, X_c of all specimens as a function of the strain ratio. From these quantitative values, it can be seen that below a strain ratio of 2.5 no significant crystallinity is present. Strain-induced crystallization occurs above a strain ratio λ=2.5 and the crystallinity index increases gradually to reach a maximum value for a strain ratio of 7.5. These results are in accordance with the significant upturn of the strength in the stress-strain measurements (Figure VI.2).

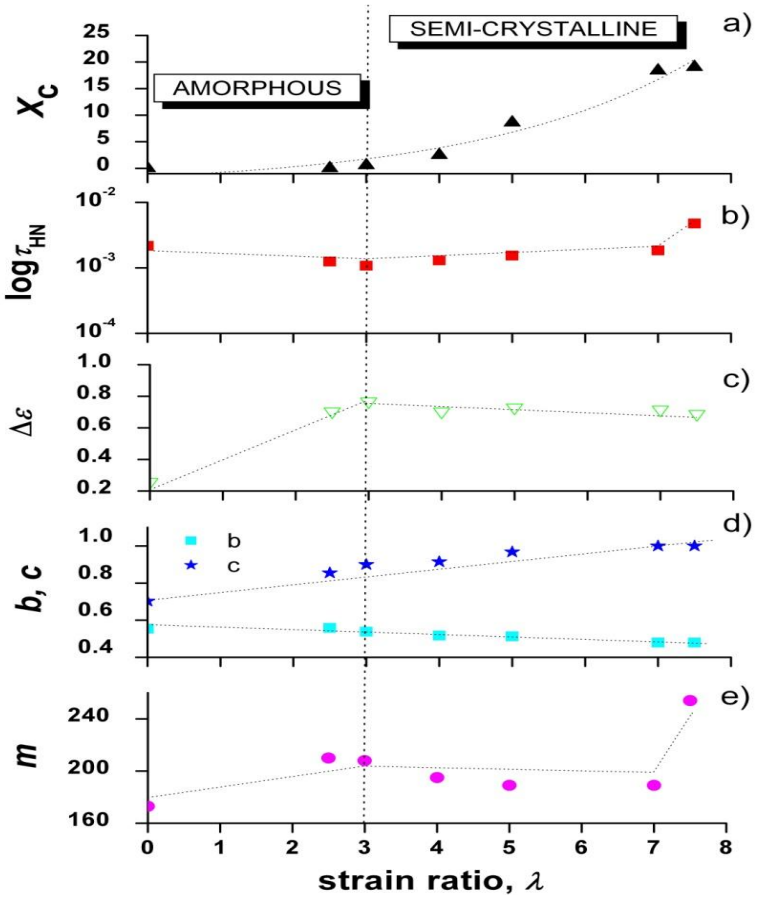

Figure VI.6. From top to bottom: a) Crystallinity index X_c at room temperature, b) segmental relaxation time τ_{HN}, c) dielectric strength $\Delta\varepsilon$, d) dielectric shape parameters (*b, c*), and e) fragility index *m*, as a function of strain ratio for the vulcanized NR samples. The dielectric magnitudes have been extracted from measurements done at T=-40 °C. Dotted lines are guides for the eye.

According to Tosaka *et al.*[204,205] it is conceivable that the real network in vulcanized rubber is composed of molecules with a broad distribution of chain lengths between the network points. Under stretching, only the molecules of small chain length between the densely packed network points can be oriented and form crystallites, whereas the molecules of much longer chain lengths would remain in the random coil state. A schematic representation of this model is displayed in Figure VI.7.

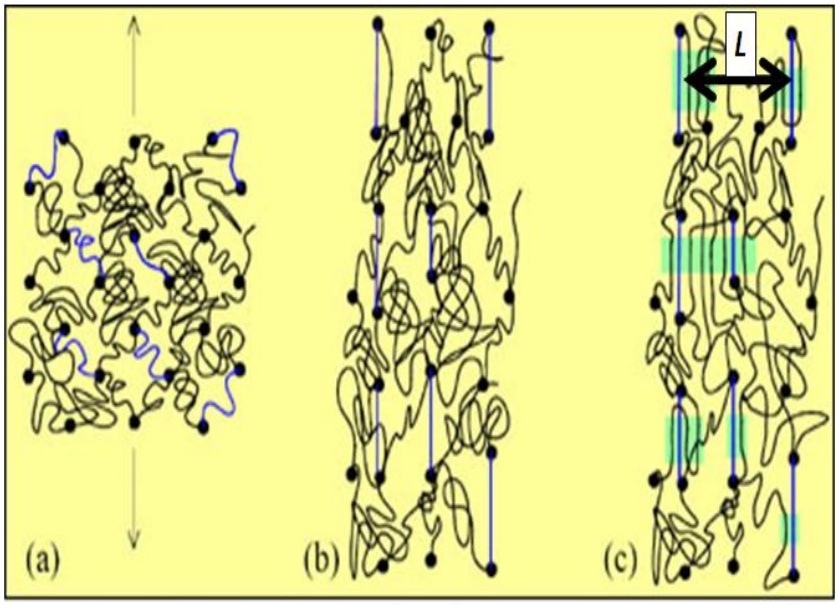

Figure VI.7. Model of nucleation and crystallization in vulcanized NR. Relatively short chains are drawn as blue lines. Filled circles represent cross-links. (a) Before deformation. (b) After deformation: short chains are fully stretched. (c) Crystallites are grown from the stretched chains. The experimental value of the long spacing *L* has been added for illustrative purposes. *Adapted from* [204] *Copyright 2004.*

In this study, the polymer chains, which are initially coiled ($M_w \approx 10^6$ g/mol), are stretched along the drawing direction and partially crystallize once a critical λ =3.0 is reached. Some of the tie molecule chains which have been overflown from fibrillar crystallites between fibrillar and amorphous phases become part of the crystalline regions by the drawing process and hence, the degree of crystallinity increases by subsequent drawing. The effect of such amorphous to semi-crystalline transition on the segmental dynamics of the stretched vulcanized NR samples will be discussed in the next paragraphs.

VI.3.2. *Strain-Induced Changes in the Segmental Dynamics of Natural Rubber*

As previously mentioned in Chapter IV, in vulcanized NR the process associated to chain dynamics, referred to as normal mode,[173] is suppressed as a consequence of the cross-linking. Therefore, vulcanized NR only exhibits above T_g =-64 °C one relaxation process, α-relaxation or segmental mode, which manifests itself by a maximum in ε''(F). The segmental mode is assigned to the segmental motions of

the polymer chains. In order to estimate the effect of stretching on the segmental dynamics of vulcanized NR with different strain ratios, the dielectric loss of every specimen was measured at -40 °C. At this temperature the α-relaxation is well centered within the frequency window. The influence of uniaxial extension on the segmental dynamics of vulcanized NR can be visualized in Figure VI.3b. Here, the dielectric loss spectra for vulcanized NR at the different strain ratios have been represented.

The frequency dependence of ε'' for stretched vulcanized NR at different strain ratios is displayed in Figure VI.8. Dielectric loss data for different stretch ratios can be fitted according to the HN equation (see Chapter I, equation I.12). The fit parameters ($\Delta\varepsilon$, b, c and τ_{HN}) obtained at T=-40 °C can be visualized in Figure VI.6 (b, c, and d). It is worth noting that to the author´s knowledge, the crystalline structure is not expected to change upon cooling since the stretching of the samples was kept by the strained sample-electrode assembly (see Figure VI.1).[206,207] From the analysis of Figure VI.8, the most significant effect is a systematic deviation from the fitting of the experimental results at low frequencies. The contribution of this low frequency tail to the $\Delta\varepsilon$ values shown in Figure VI.6c is less than 3%. This effect has been reported by other authors and attributed to the stearic acid present in the formulation of vulcanized NR.[115] However, the systematic dielectric study presented in Chapter III indicates that ZnO has influence on this excess of dielectric loss.

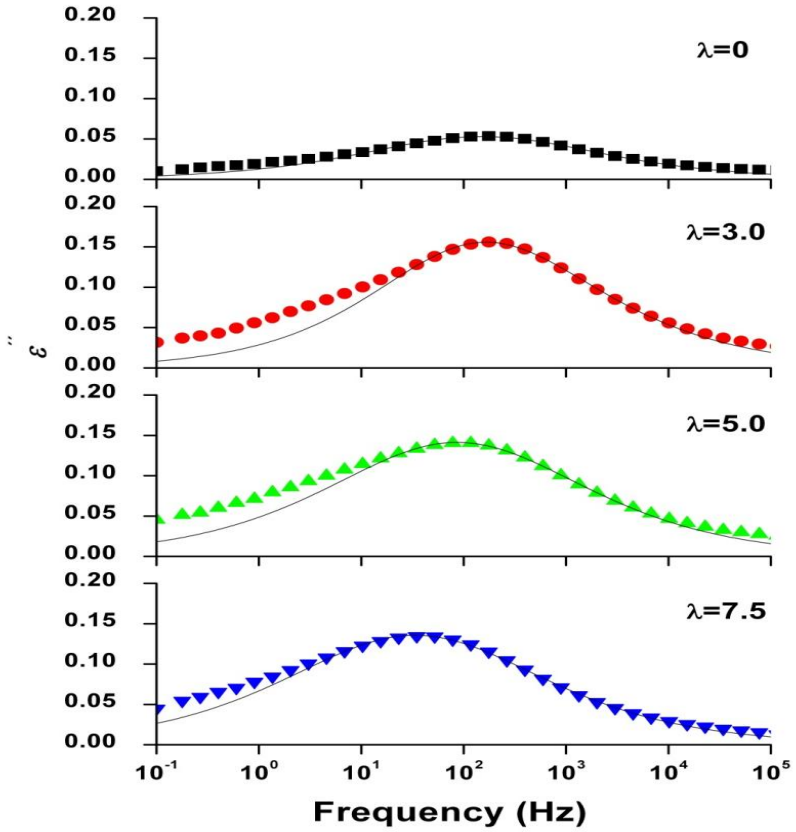

Figure VI.8. Frequency dependence of dielectric loss ε'' of NR samples stretched at different strain ratios as indicated on the plot in the region of the segmental mode (T=-40 °C). Solid lines correspond to best HN fitting.

The dependence of the dielectric magnitudes can be separated into two regimes. In a first regime, for λ <3.0, no crystallization is evidenced. However a dramatic increase of the dielectric strength, $\Delta\varepsilon$, is observed. In the second regime, for λ >3.0, crystallization sets in and the variation of the shape parameters (b decreases and c tends to the unit) with respect to the strain indicates a broadening of the relaxation for the segmental process. In this second regime, a slight decrease in $\Delta\varepsilon$ is observed. This behavior is typical for the crystallization of semi-crystalline polymers where the crystalline domains slow down the segmental dynamics.[160,197] Indeed, in this case the relaxation time, τ_{HN}, tends to increase slightly with the strain once crystallization appears. This effect can be expected since a reduced segmental mobility of the amorphous regions is imposed by the presence of the crystals.

In a first approach, changes in $\Delta\varepsilon$ can be discussed based on the Frölich- Kirkwood (FK) equation[161] which describes the temperature dependence of $\Delta\varepsilon$ as:

$$\Delta\varepsilon \propto \frac{4\pi\rho N_A}{9kTM} g\mu^2 \propto \mu_{eff}^2 \qquad \text{VI.3}$$

Where ρ is the density, μ is the dipole moment, M is the molecular weight of the repeating unit, N_A is Avogadro´s number, k is the Boltzmann constant and g is the correlation factor which contains contributions of both inter and intra chain dipolar correlations and indicates the angular correlation between the dipole groups. The g factor is frequently referred to as a reduction factor since the term $g\mu^2$ corresponds to the effective dipole moment, μ_{eff}^2 , of the material. When no correlation among dipoles is expected, as in the gas state, g approaches to 1. In the first regime, λ <3.0, it is expected an increase of the density by stretching. However, the strong increase in $\Delta\varepsilon$ of about three times cannot be solely explained by this fact. In vulcanized NR the dipole moments contributing to the segmental relaxation are mainly perpendicular to the polymer chain.[108] In the non-deformed state of vulcanized NR, as for most polymers, the variety of conformations partially cancels out some dipolar contribution. However, stretching can counteract this effect through ordering, causing the observed increase of the dielectric strength. The most favourable conformation of *cis*-1,4-polyisoprene is that with alternating CH_3- pendant groups in which dipoles should balance along the chain.[208] However, recent molecular modelling[209] has shown that the molecular asymmetric unit of ordered *cis*-1,4-polyisoprene is a di-isoprene in which the two isoprene residues have distinctive, not symmetrically related conformations. This suggests a possible increase of μ_{eff} upon stretching supporting the increment in $\Delta\varepsilon$ observed. In the second regime, λ >3.0, crystallization induces a decrease of the dielectric strength since dipoles included in the crystalline phase do not contribute to the segmental relaxation. Consequently the effect caused by stretching and that of crystallization producing opposite effects in $\Delta\varepsilon$ induce almost no change with stretching.

A typical Vogel-Fülcher-Tamman (VFT) dependency of τ_{max} against reciprocal temperature is clearly observed in Figure VI.9. The resulting parameters obtained from the best fit of the relaxation map are summarized in Table VI.1.

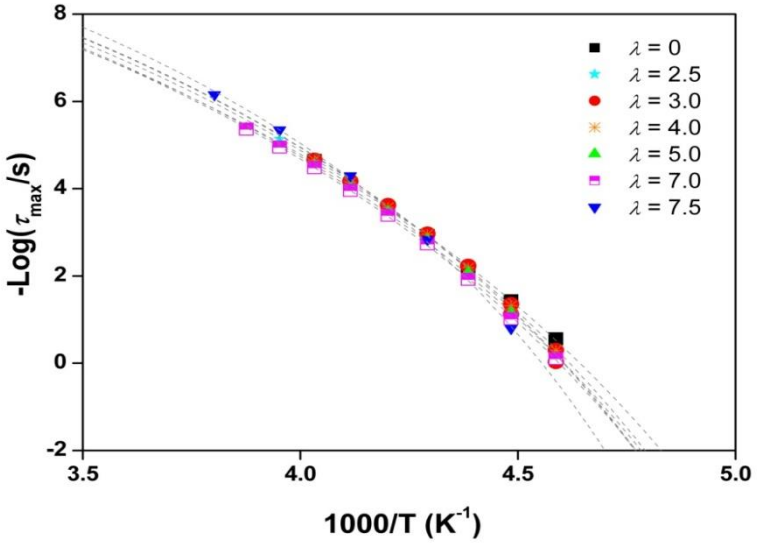

Figure VI.9. Activation plot of the average relaxation time for the segmental mode of NR stretched samples, as a function of strain ratio. The dotted lines represent the fits to the VFT equation.

One can see that the T_0 values for the stretched samples are higher than that of the undeformed vulcanized NR. Again two regimes can be recognized. Before crystallization, λ <3, there is a significant increase of about 10 °C in T_0. This effect contrasts with previous results reported for synthetic polyisoprene cross-linked with dicumyl peroxide in which no variation of the dielectric spectrum was observed upon stretching.[210] However it is worth mentioning that in such study the cross-link density was 6.1×10^{-5} mol/cm^3 while in our case, for vulcanized NR, is of 3.8×10^{-3} mol/cm^3 (see Appendix B). This higher cross-link density of vulcanized NR can explain the different behavior on both cases. For stretched vulcanized NR with λ <3 there is expected a significant reduction on the free volume, as compared with the undeformed sample, causing a significant increase in the glass transition temperature and consequently an increment of T_0. This effect is consistent with the observed increment in the fragility index, *m*, (see Figure VI.6d) since as free

volume reduces by stretching more cooperativity is needed in order to accomplish segmental motions.

For λ>3, as crystals develop, almost no variation in T_0 or in m is observed. In strained vulcanized NR, it is proposed that crystallization starts by nucleation of short stretched chains which act as nuclei. The shorter chains among cross-links become fully stretched while the distribution of cross-links is not uniform keeping many network chains in the random-coil-like state.[204] It is conceivable that during strain induced crystallization the shorter chains are progressively incorporated into the crystals while a significant amount of longer chains remains rather coiled. In this case, during this regime, the segmental dynamics of amorphous phase of vulcanized NR would not experience significant changes. Only for high strains, λ=7.5, the crystallinity is high enough as to provoke a new increment of m and T_0 (see Table VI.1).

Table VI.1. VFT parameters for the segmental mode process of NR stretched at different strain ratios.

Strain ratio (λ)	T_0 (K)	D	m
0	168.7	3.8	173
2.5	177.2	3.0	210
3.0	176.8	3.1	208
4.0	174.8	3.3	195
5.0	175.7	3.4	189
7.0	173.9	3.5	189
7.5	185.3	2.5	255

Finally, it can be partially concluded that the strain-induced crystallization of vulcanized NR exerts a slowdown (τ_{HN} increases) and a broadening (b decreases and c tends to the unit) of the segmental dynamics, with an important increase in $\Delta\varepsilon$ during the orientation stage and no-variation with stretching during the crystallization stage. Correspondingly, the temperature dependency analysis allows concluding that during the orientation stage more cooperativity is needed

in order to accomplish segmental motions (m and T_0 increase), while as crystals develop almost no variation in T_0 or m is observed.

VI.4. Natural Rubber/Layered Silicate Nanocomposites

The phenomenon of strain-induced crystallization (SIC) in NR composites has recently attracted much attention due to the fast development of nanocomposites. Rault *et al*.[211,212] and Poompradub *et al*.[213], for example, investigated the SIC of NR filled with carbon black using techniques such as ^{2}H NMR and synchrotron wide X-ray diffraction (WAXD) measurements. It was shown that the microstructure of the filled NR network changed by stretching, resulting in earlier onset and stronger ability of crystallization. The effect of two-dimensional plate-shaped nanoclay with high aspect ratios on NR microstructure when stretched was also studied by Carretero *et al*.[64,65] and by Huang *et al.*[66,214] More recently, the reinforcement mechanism of NR composites with nano-alumina,[215] carbon nanofiber[216] and with MWCNT[201] has attracted the attention of the scientific community. Despite all the extensive studies on this subject, there is still a lack of information on the relationship between mechanical strain and chain dynamics. Thus, in an attempt to better understand the effect of strain-induced orientation on the segmental dynamics of vulcanized NR/layered silicate nanocomposites, a series of X-ray scattering and broad-band dielectric spectroscopy experiments have been performed and are discussed in the following sections.

VI.4.1. *Stress-Strain Behavior and Development of Crystallites*

It has been recognized that the excellent tensile properties of NR originate from its strain-induced crystallization upon elongation. Since striking improvements in the mechanical properties can be achieved at low loadings of nanoclay, one wonders if these improvements result from an increase in the crystallized fraction. Thus, the evolution of the crystallization behavior of the NR/C15A nanocomposites during stretching was determined. Figure VI.10 shows the stress-strain curve and corresponding WAXS patterns at selected strains for NR filled with 5 phr of

nanoclay C15A. The corresponding stress-strain curve for the unfilled NR is included for comparison. For the nanocomposite, the upturn of stress shifts to lower value compared with that of the vulcanized NR. Incipient contribution of crystalline reflections seem to appear already at a strain λ =2.5. The clear presence of these reflections at λ =3.0 indicates that the nanocomposite has a smaller onset strain (λ^0) of crystallization than that of the matrix. Besides, all patterns exhibit preferred orientation of NR chains, which is evidenced by the alignment of the (200) and (120) reflections of the crystalline phase of the rubber matrix. As expected the intensities of the reflections increase with strain during stretching, while no preferred orientation of the amorphous phase is observed.

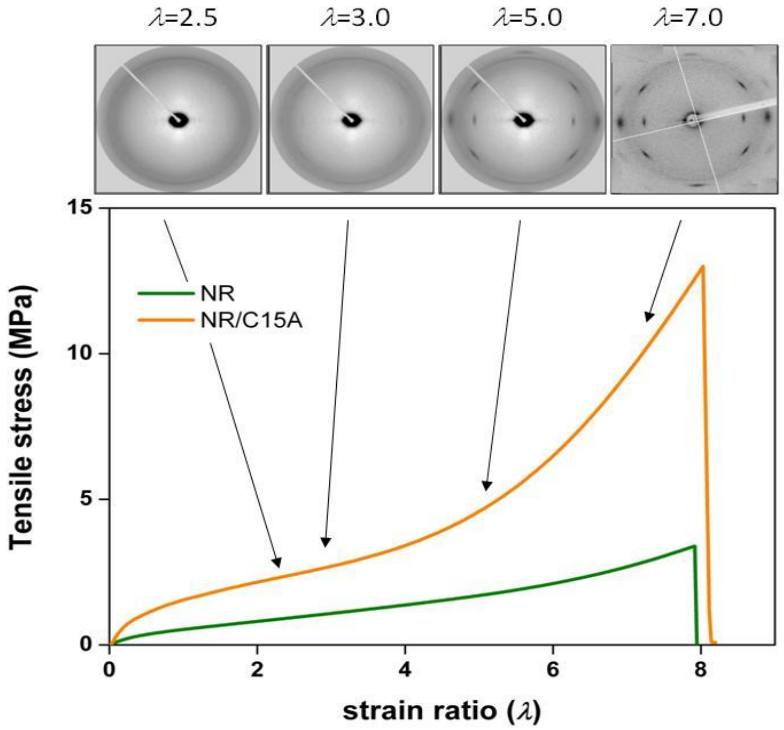

Figure VI.10. Representative stress-strain curves of NR and NR/C15A nanocomposite with corresponding synchrotron WAXS patterns during uniaxial deformation for NR/C15A nanocomposites.

The procedure followed for the estimation of the crystallinity index was based on the equator diffraction peaks, as previously detailed for NR samples in Section VI.3.1. The diffraction intensity near the equator was normalized and azimuthally

integrated in a cake from 75° to 105°, as shown in Figure VI.11. It is also noteworthy that the overall crystallinity index values in NR/C15A nanocomposites are higher than those for the pure rubber (see Figure VI.12). Thus, it is evidenced that the nature of the layered silicate particles plays a key role on the emerging of the first crystallites as well as on the final crystalline content during the deformation of the NR.

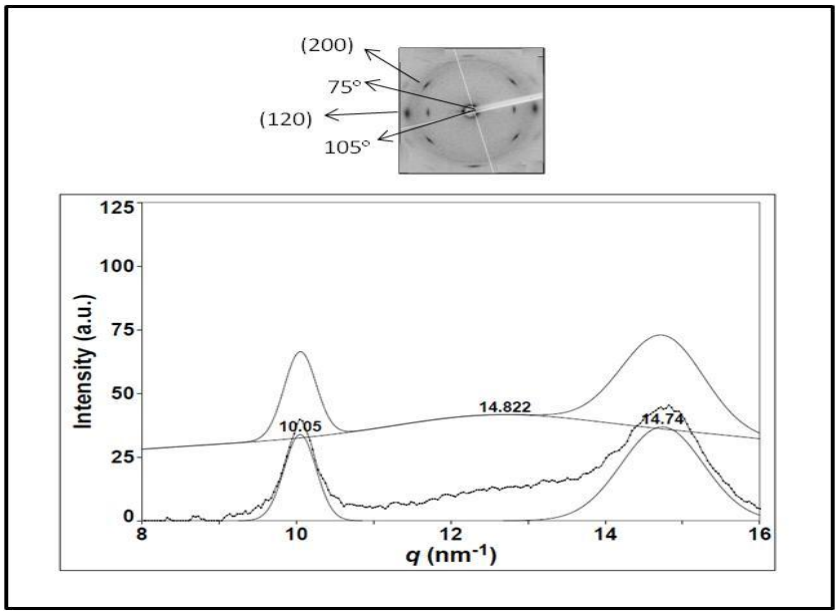

Figure VI.11. Equatorial cake integrated intensity as a function of the scattering vector *q* taken from the WAXS pattern of stretched NR/C15A nanocomposite at λ =7.0. Inset shows integration limits from 75° to 105°.

The onset of crystallization is calculated by interception of the regression line in the plot of crystallinity index against strain ratio,[213,215] obtaining a strain ratio value of λ^0=2.46 for the nanocomposite and a value of λ^0=3.09 for the unfilled rubber (see Figure VI.12). The lower λ^0 of the nanocomposites reveals that an earlier orientation of rubber chains occurs. Upon deformation, exfoliated silicate layers existing within the NR matrix can align along the stretching direction at a very low strain ratio. Because of the high level of interaction between polymer chains and the nanoclay, the alignment of the nanoclay triggers the early orientation of more polymer chains. Furthermore, on the basis of the mechanism proposed by Tosaka *et al.*,[204,205] strain-induced crystals nucleate from the

stretched network chains. Thus, the fact that more polymer chains can be stretched indicates that more nuclei can be formed.[66] It is interesting to say that the values of crystallinity index herein reported for the NR/layered silicate nanocomposite, as well as for the vulcanized NR, are slightly lower than those reported elsewhere. It is noteworthy that the vast literature[65,66,201,204-206,213-215] reports that the experimental conditions in which the WAXS patterns of the stretched samples were collected, correspond to *in situ* experiments followed at very low strain rates (4-10 mm/min) in order to study the real-time structural evolution. In this work, the series of experiments performed do not correspond to simultaneous WAXS and tensile measurements, since the samples are previously stretched at a strain rate of 500 mm/min, as detailed in the experimental section above. Thus, in this case, structural relaxation is expected during holding time previous to measurements rendering to lower crystallinity values than those reported elsewhere.[65,66,214]

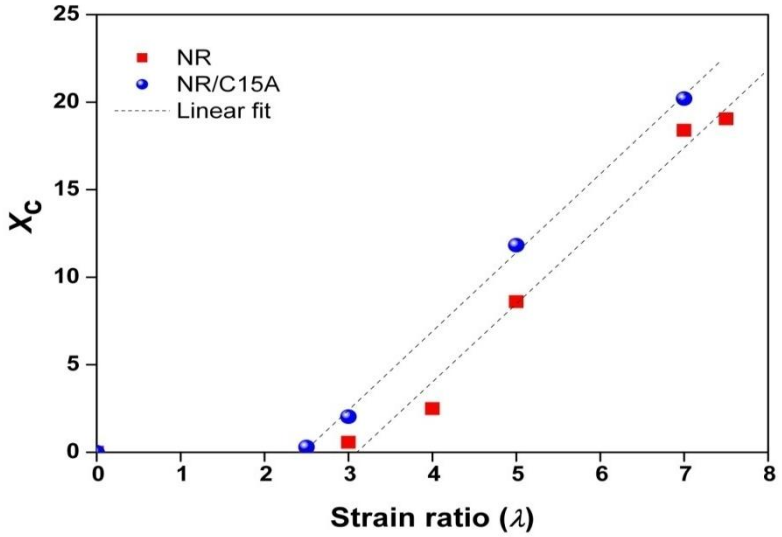

Figure VI.12. Crystallinity index X_c as a function of strain ratio λ for NR and NR/C15A nanocomposite. Dotted lines correspond to a linear fit.

In addition to WAXS patterns, SAXS images provide microstructure information about the distribution of clay particles in the NR matrix. The presence of streaks on the equator is clearly recognized in the SAXS patterns displayed in Figure VI.13. The highly anisotropic SAXS peaks confirm the orientational alignment of exfoliated silicate layers in the NR matrix along the stretching direction. The value

of the long spacing *L* estimated from the SAXS patterns is around 3.7 nm, similar to that obtained for the stretched NR.

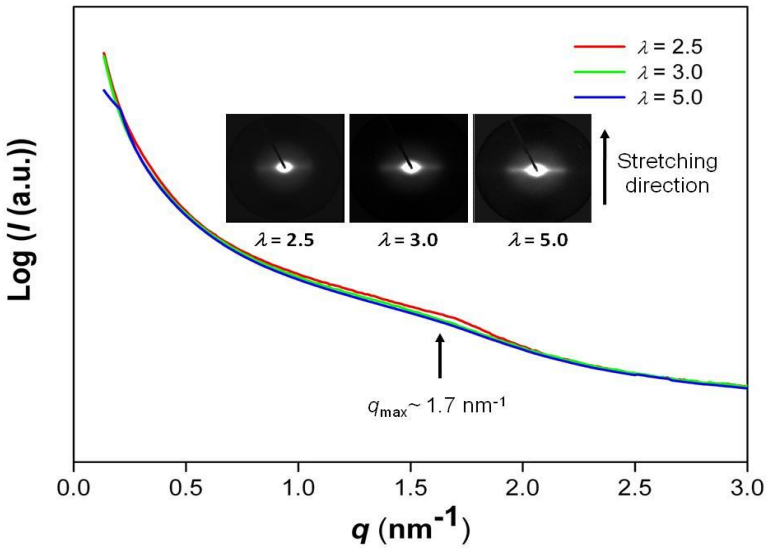

Figure VI.13. Equatorial cake integrated intensity as a function of the scattering vector *q* taken from the SAXS pattern of stretched NR/C15A nanocomposite at different strain ratios.

VI.4.2. *Strain-Induced Changes in the Dynamics of Natural Rubber/Layered Silicate Nanocomposites*

Segmental Mode

Figure VI.14 shows the dielectric loss curves for the segmental mode, as a function of frequency at different strain ratios. In the temperature range studied, the segmental relaxation moves slightly to lower frequencies, broadens and exhibits weaker loss intensity at high strain ratios.

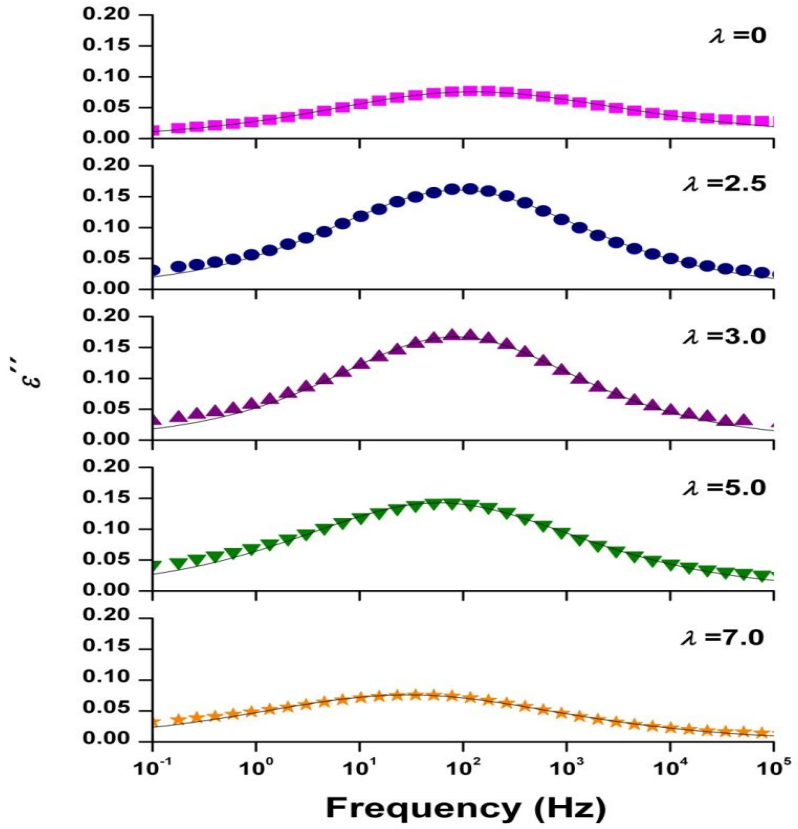

Figure VI.14. Frequency dependence of dielectric loss ε'' of NR/C15A nanocomposite samples stretched at different strain ratios as indicated on the plot in the region of the segmental mode (T=-40 °C). Solid lines correspond to best HN fitting.

The dielectric spectra were fitted to the HN function. The characteristic parameters of this function such as $\Delta\varepsilon$, b, c and τ_{HN} are obtained. Figure VI.15 shows the dependence of these parameters with frequency. The behavior of the crystallinity index with strain ratio is also included in this figure in order to visualize the global effect and to correlate structural magnitudes with dynamic parameters extracted from the dielectric measurements.

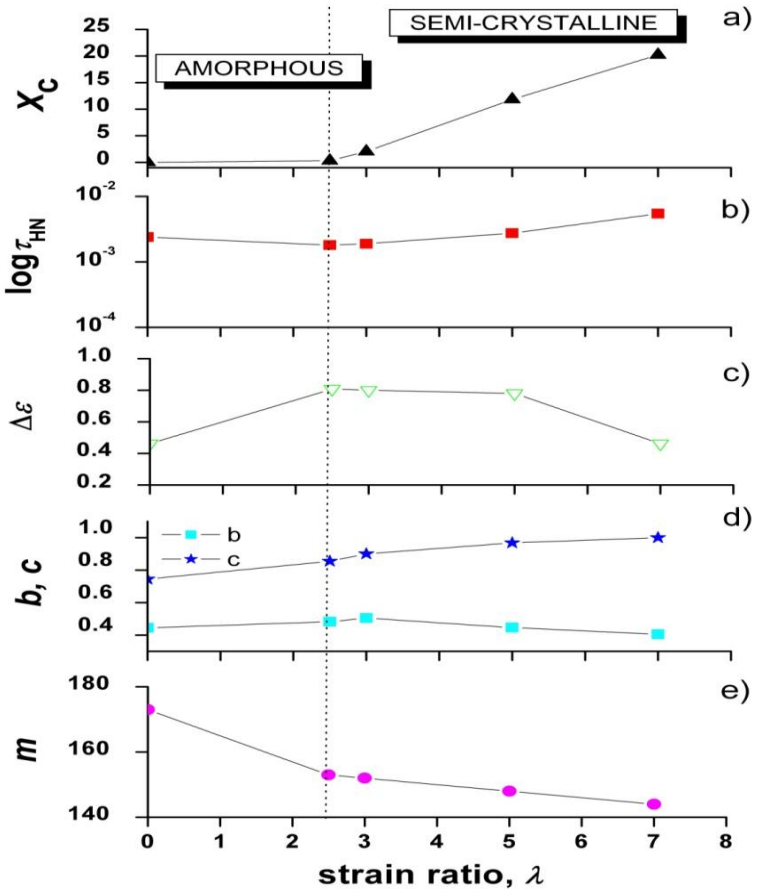

Figure VI.15. From top to bottom: a) Crystallinity index X_c at room temperature, b) segmental relaxation time τ_{HN}, c) dielectric strength $\Delta\varepsilon$, d) dielectric shape parameters (*b, c*), and e) fragility index *m*, as a function of strain ratio for the vulcanized NR/C15A nanocomposite samples. The dielectric magnitudes have been extracted from measurements done at T= -40 °C.

The dependence of the dielectric magnitudes of the NR/C15A nanocomposite can be separated into two regimes, in a similar way to NR. In a first approximation, the transition between the two regimes seems to be located at a strain ratio λ =2.5. The trends in almost all the parameters are in accordance with the ones previously discussed for NR (τ_{HN} increases, *b* decreases and *c* tends to the unit with the strain ratio). Nonetheless, the behavior of $\Delta\varepsilon$ for the nanocomposite seems to differ from the observed behavior for NR. The main driving force to analyze simultaneously structural and dynamic experiments is to have access to information relating both the crystalline and the amorphous phases. In a first approach, the dielectric

strength is related to the amount of mobile amorphous phase while crystallinity relates to the amount of material included in the crystals. In order to further analyze this behavior Figure VI.16a shows the dependence of $\Delta\varepsilon$, normalized to its initial value, as a function of the crystallinity index.

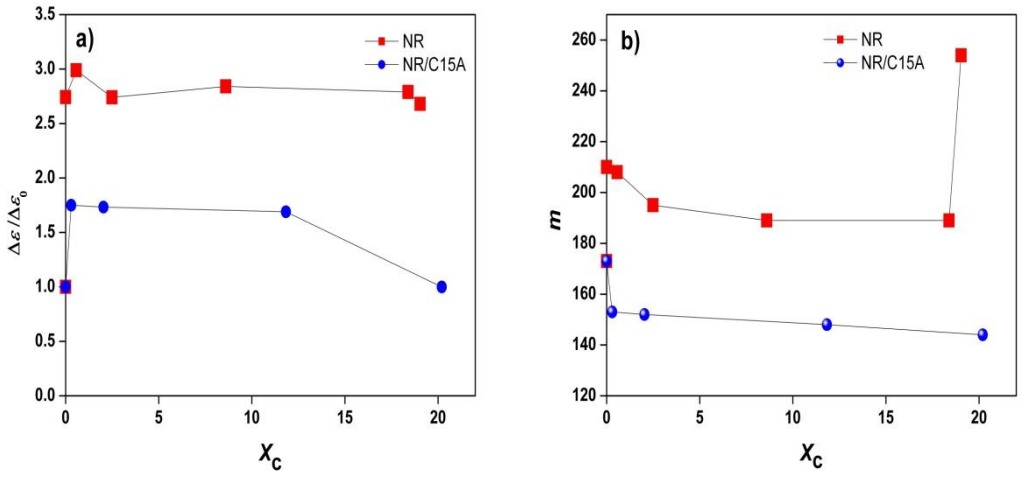

Figure VI.16. a) Normalized dielectric strength to its initial value $\Delta\varepsilon/\Delta\varepsilon_0$ and b) fragility index *m,* as a function of the crystallinity index X_c for vulcanized NR and NR/C15A nanocomposite.

At the initial stages of crystallization (low values of X_c) it is expected an increase of the density by stretching and a possible increase of μ_{eff} upon stretching which support the increment in $\Delta\varepsilon$, as previously discussed. As crystallization proceeds, $\Delta\varepsilon$ decreases with the crystallinity index due to the decrease in the total number of dipole groups that relax through the α-process as more crystalline domains are formed; more tie molecules in the crystalline-amorphous interphase become a part of the crystalline regions. Indeed, the drop off in the nanocomposite values is more abrupt than in the case of the NR and seems to start at earlier stages due to the enhanced orientation of the amorphous phase which is enough to affect the motions of the dipole groups.

Segmental relaxation times, τ_{max}, are plotted against the reciprocal temperature in Figure VI.17. The α-relaxation seems to be unaffected with increasing strain ratio over the entire temperature range. The relaxation times are well described over

the measured range by the Vogel-Fülcher-Tamman (VFT) function. The parameters obtained from the best fit are summarized in Table VI.2., along with the fragility strength *D* and fragility index *m*. Strain ratio has little effect on T_0, but reduces *m*. Besides, the *D* value around 4 indicates that NR is a dynamically fragile system as corresponds in general to polymeric materials.[153]

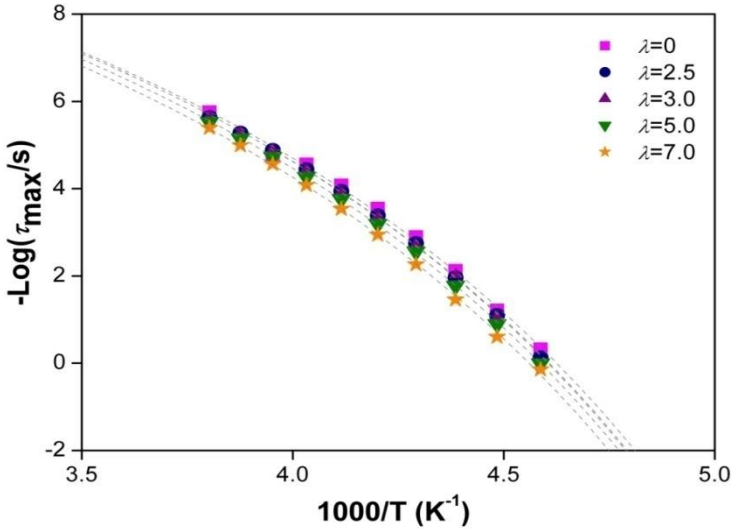

Figure VI.17. Activation plot of the average relaxation time for the segmental mode of NR/C15A nanocomposite stretched samples, as a function of strain ratio. The dotted lines represent the fits to the VFT equation.

Table VI.2. VFT parameters for the segmental mode process of NR/C15A nanocomposite samples stretched at different strain ratios.

Strain ratio (λ)	T_0 (K)	*D*	*m*
0	168.7	3.8	173.3
2.5	170.5	4.3	153.2
3.0	170.1	4.3	152.2
5.0	169.7	4.5	148.3
7.0	169.1	4.6	143.6

With regard to the fragility index (*m*), few ideas have been proposed to explain the fragility in polymers; the free volume modes,[217-219] coupling model,[220-223]

the segmental cooperativity,[153,156] and the generalized entropy theory[224-226] are the most discussed ones. Each approach works well for explaining the results on certain classes of polymers, but fails for other examples. In our case, within this context, the most interesting situation is that in which strain exists but no crystallinity is present. Figure VI.18 shows the α-relaxation dielectric loss at T= -40 °C for NR and NR/C15A nanocomposite at no strain and at λ =2.5. NR/C15A nanocomposite exhibits a slightly broader and slower relaxation than that of NR at λ =2.5. Figure VI.19 shows the activation plot for NR and NR/C15A where again one sees that the differences between the two cases are small.

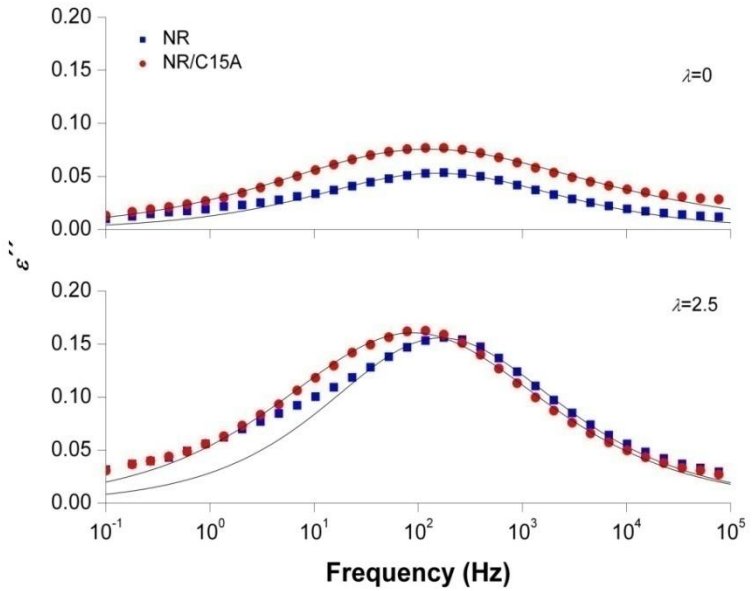

Figure VI.18. Dielectric loss at T= -40 °C for NR and NR/C15A nanocomposite at no strain and at λ =2.5.

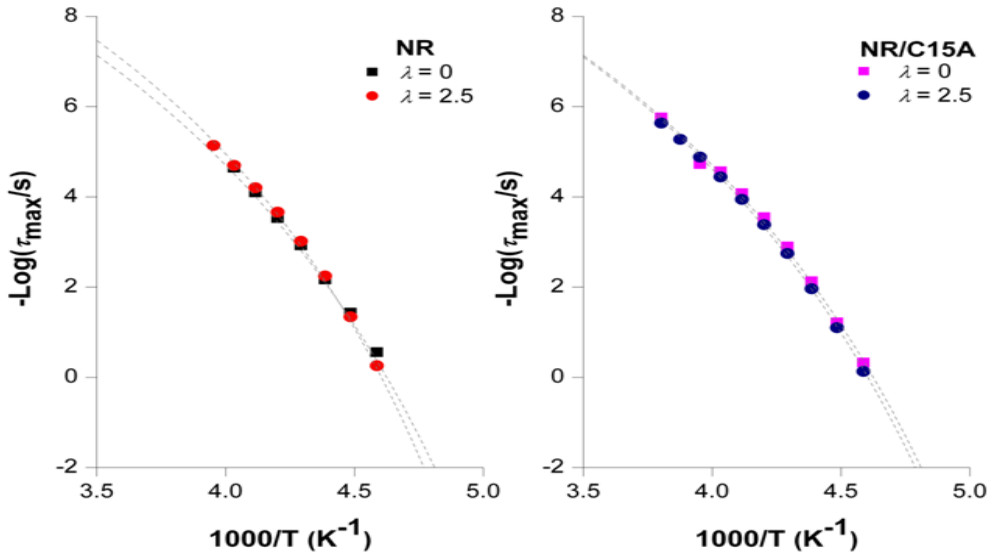

Figure VI.19. Activation plot of the average relaxation time for the segmental mode of NR and NR/C15A nanocomposite stretched samples, at no strain and at λ =2.5. The dotted lines represent the fits to the VFT equation.

The increase in *m* experienced by NR upon stretching (λ =2.5), in absence of crystallization, can be understood considering the reduction in free volume causing a significant increase in the glass transition temperature. This effect is consistent with the observed increment in the fragility index, *m* reported elsewhere.[227] For the NR/C15A nanocomposite the opposite effect for the same strain ratio (λ =2.5) (see Figure VI.16b), also in absence of crystallization, is observed. In this case, it is worth remembering that clay platelets may have a confining effect over the segmental relaxation of NR. As a matter of fact the NR/C15A nanocomposite exhibits a new mode which has been ascribed to as a dynamically restricted NR phase close to the clay surface. Accordingly, it can be imagined that stretching may in one hand, increase the interaction between clay platelets and NR and, on the other hand, exert a physical confining of the segmental relaxation by limiting the available space for the segments to relax. This type of confinement has been shown to decrease the dynamical fragility of the segmental process since the relaxation becomes less cooperative.[172]

New Mode

The dielectric loss measurements of the NR/C15A nanocomposite stretched at different strain ratios were also performed as a function of frequency in the region of the new mode. Figure VI.20 shows the evolution of the dielectric loss as a function of frequency at T=40 °C. This relaxation is manifested by a maximum clearly resolved which exhibits weaker loss intensity at high strain ratios.

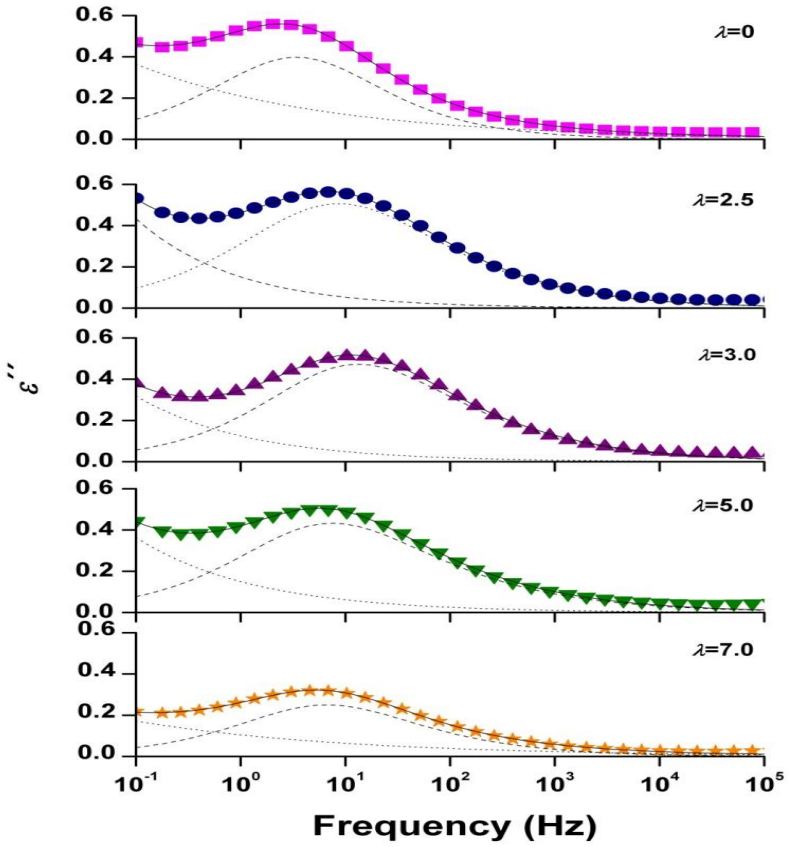

Figure VI.20. Frequency dependence of dielectric loss ε'' of NR/C15A nanocomposite samples stretched at different strain ratios as indicated on the plot in the region of the new mode (T=40 °C). Solid lines correspond to best HN fitting, dashed lines to the individual process and dotted lines to the conductivity contribution.

With regard to the temperature dependence of the new mode, the data shown in Figure VI.21 reveal that this relaxation has a weaker temperature dependence than the segmental relaxation and does not present the curvature characteristic of a

Vogel-Fülcher-Tamman (VFT) behavior, having an almost Arrhenius dependence, as previously discussed in Chapter IV.

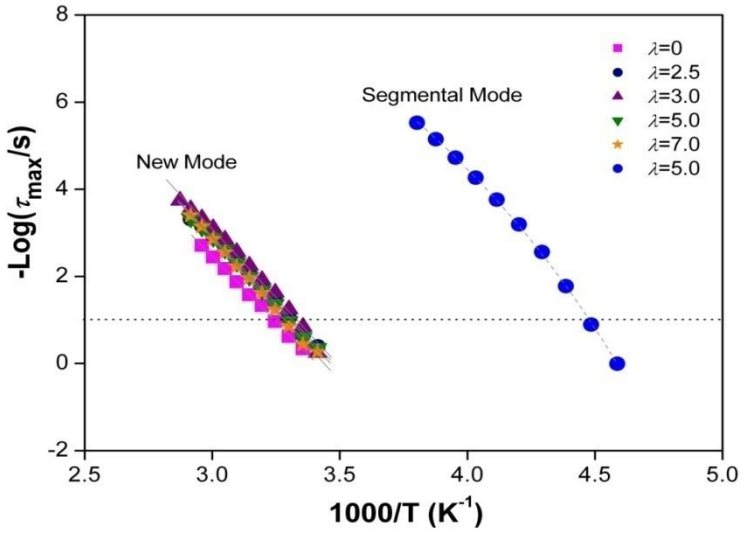

Figure VI.21. Activation plot of the average relaxation time for the new mode of NR/C15A nanocomposite stretched samples, as a function of strain ratio. The curve corresponding to the segmental mode of the NR/C15A nanocomposite at λ =5 has been included for comparative purposes.

In order to further analyze the dependency of this new relaxation with the strain ratio, Figure VI.22 illustrates the temperatures at which the average relaxation time of the new mode reaches a value of 0.1 s. It becomes evident that this dependence can be well separated into two regimes. In the first regime, for λ <2.5, a clear decrease in temperature is observable indicating a fastening of this relaxation upon stretching. As mentioned above, since the new mode of NR/C15A is related to a restricted NR phase associated to the clay interface then, the observed increment in mobility can be associated to a delaminating process tending to separate the restricted NR phase from the clay surface and therefore to decrease the NR-clay interaction. Further extension (λ >2.5) provokes an increment in the reference temperature indicating that the motion capability of the chain segments is reduced. Since in this stretching region crystallization is operative, it is straightforward to associate this effect to the restriction imposed by the anchoring of segment chains into the crystals.

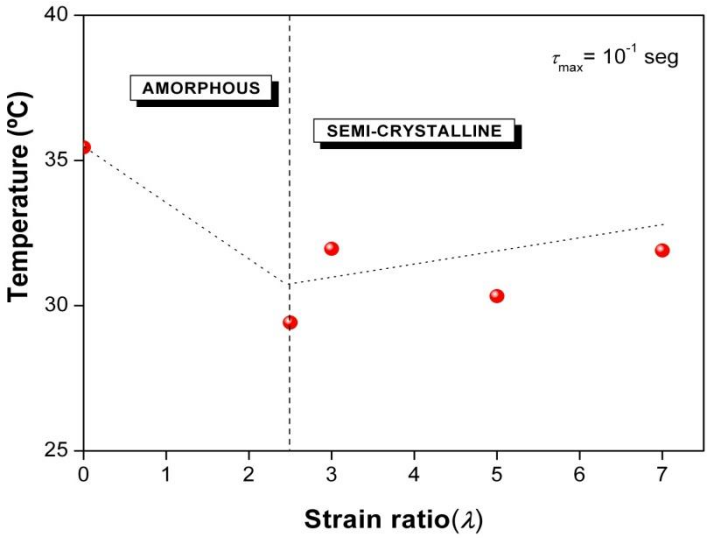

Figure VI.22. Temperature dependence of the new mode at τ_{max}=10^{-1} s for NR/C15A nanocomposite with strain ratio. Dotted lines are guides for the eye.

Finally, Figure VI.23 shows the dependence of $\Delta\varepsilon$ and τ_{HN} with the strain ratio for the segmental and new mode of the NR/C15A nanocomposite. Data corresponding to the segmental mode of NR has been included for comparative purposes. On the basis of these results, it becomes evident that the amorphous to semi-crystalline transition on the segmental dynamics of the stretched NR/C15A nanocomposite samples is also present in the new mode. This transition leads to important changes on the segmental and new mode dynamics of the nanocomposites: 1) an important decrease of the dielectric strength, and 2) a slowing down of both relaxations. These effects further support the similar segmental nature of both relaxations.

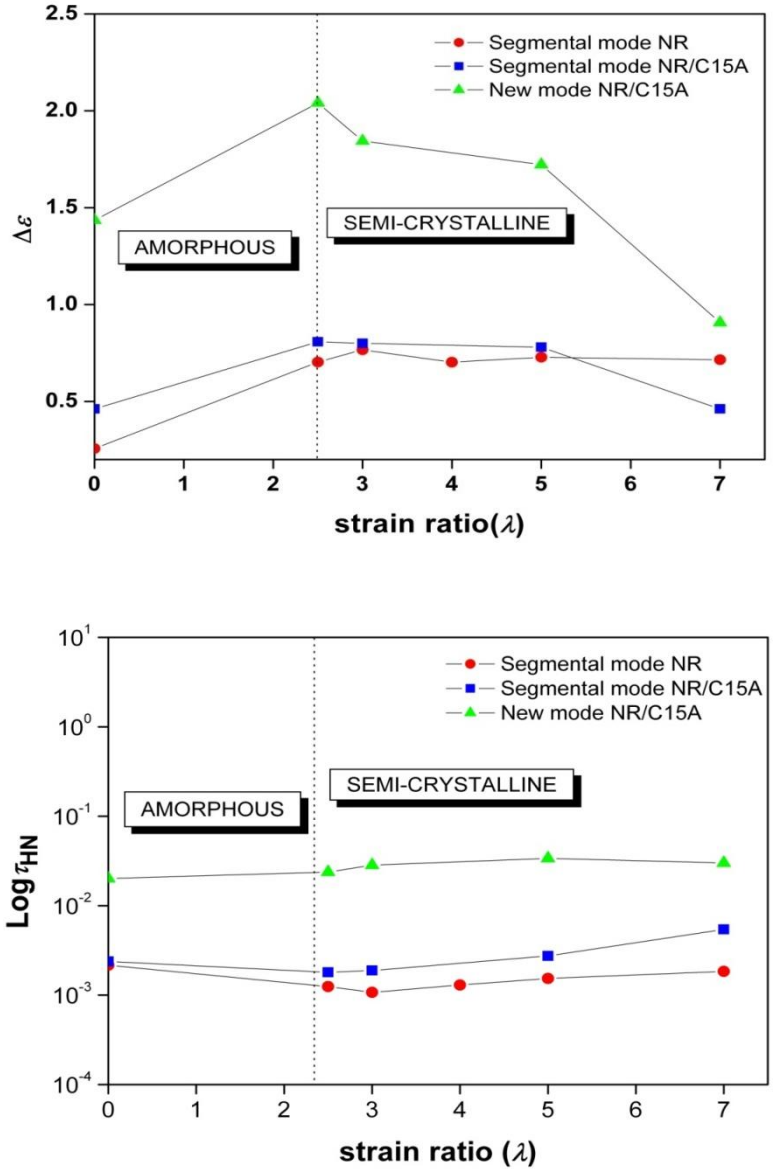

Figure VI.23. Dielectric parameters dependence with the strain ratio for the segmental and new mode of NR and NR/C15A nanocomposites. TOP: dielectric strength, $\Delta\varepsilon$; BOTTOM: HN relaxation time, τ_{HN}.

VI.5. Summary

The effects of strain-induced crystallization on the molecular dynamics of vulcanized NR have been studied by means of broad-band dielectric spectroscopy and X-ray scattering techniques. The segmental dynamics of vulcanized NR is clearly affected by uniaxial stretching. Upon stretching three regimes are detected.

For low strains, λ <3, stretching takes place without crystallization. However a dramatic increase of the dielectric strength, $\Delta\varepsilon$, is observed which cannot be solely explained by an increase in density. It is suggested that an increase of the effective dipole moment upon stretching is responsible for this increment in $\Delta\varepsilon$. Also, the expected reduction of the free volume by stretching causes an increase of the glass transition temperature, with the consequently increment of T_0. This effect is accompanied by an increment in the fragility index, *m*, since as free volume reduces by stretching more cooperativity is needed in order to accomplish segmental motions. In the second regime, 3< λ <7.5, crystals develop and the inclusion of segments into the crystalline phase counteracts the increment in $\Delta\varepsilon$ provoked by stretching. In agreement with previous models, these results indicate that during strain-induced crystallization shorter chains are progressively incorporated into the crystals while a significant amount of longer chains remains rather coiled. In this regime the segmental dynamics of the amorphous phase of vulcanized NR does not experience significant changes. Finally at high strains, λ= 7.5, the crystallinity is high enough as to provoke a new increment of the fragility index *m* and of T_0.

In addition, the presence of interfacial interaction between nanoparticle-polymer matrix is crucial in promoting strain-induced crystallization in NR nanocomposites. Addition of nanoclay leads to enhanced crystallinity and lower onset strain for stretch-induced crystallization compared to unfilled NR. Besides, the new mode present in NR/layered silicate nanocomposites is also affected by the strain-induced crystallization phenomenon, with evidence of an amorphous/semi-crystalline transition around λ= 2.5 which can corroborate its segmental nature.

CHAPTER VII. GENERAL CONCLUSIONS

In this Doctoral Thesis, broad-band dielectric spectroscopy was used to study the molecular dynamics of Natural Rubber (NR) nanocomposites, in order to understand the physical relations between the different phases and interfaces present in the nanocomposite and its implication on the improvement of the final properties of the material. The effects of nanofiller type have been studied for two layered silicates: natural sodium-montmorillonite named Cloisite®Na^+ and its variant organically modified with a quaternary ammonium salt, Cloisite®15A (CNa+, C15A). Additionally two types of carbonaceous nanofillers have been used: carbon nanotubes (multi-walled (MWCNT) and functionalized multi-walled (f-MWCNT)) and functionalized graphene sheets (FGS). Both, nanofiller content and the presence of vulcanizing additives on the dynamics of the elastomeric matrix have been systematically evaluated. In addition, the effect of strain-induced crystallization on the dielectric relaxation of NR nanocomposites was assessed by correlating dielectric spectroscopy results with X-ray scattering.

The following general conclusions can be extracted from this work.

- In NR with layered silicate nanofillers an improved mechanical behavior was achieved when the silicate layers were exfoliated and randomly dispersed throughout the elastomer matrix as monolayers, as in the case of the NR/C15A nanocomposites. Similar situation occurs for the nanocomposite with well exfoliated FGS. In this case, the presence of oxygen containing groups makes FGS to be considered as a suitable nanofiller for a NR matrix. For nanocomposites based on layered silicates and graphenes the strong rubber-filler interactions seem to be the origin of the enhancement of the mechanical properties. The differences in performance between layered silicate and carbon based filler NR nanocomposites can find explanation in terms of the dissimilar filler morphology, namely, particle size or surface area and structure, rather than on the functional groups present on the surface of the nanoparticles.

- It was corroborated that broad-band dielectric spectroscopy is a useful technique in order to study the molecular dynamics of elastomeric

nanocomposites based on a NR matrix. The dielectric spectrum of non-vulcanized NR exhibits two well resolved relaxations, a segmental mode at low temperatures, and a normal mode at high temperatures. The segmental mode was assigned to the segmental motions appearing above the glass transition temperature. The normal mode has been ascribed to the chain dynamics.

- The segmental mode of the non-vulcanized NR matrix was found to be independent of the amount or nature of filler in the nanocomposite. Nonetheless, the segmental mode slows down when vulcanizing additives are added to the rubber matrix. In this case, a second dynamic process appears being slightly slower than the segmental mode of NR. A model has been proposed in order to explain the presence of this slower dynamic process, in which the ionic clusters of ZnO form physical entanglements within the rubber chains, acting as cross-link precursors.

- A “new mode” associated to a restricted segmental relaxation appeared in the dielectric spectrum of NR/C15A nanocomposites. This new mode is absent in the unfilled NR matrix and in all the other NR nanocomposites studied in this research with unmodified clay (CNa+) or with carbon based nanofillers. Such relaxation is believed to be due to the polymeric chains that are in an interface layer around the clay particles. These pioneering results can help to understand why the reinforcing effects in NR/clay nanocomposites are manifested at low filler loadings.

- The normal mode of the nanocomposites exhibited a faster dynamics as compared to that of NR. The present experiments allows to speculate with the possibility that additives in general, both vulcanizing additives and nanofillers, disturb the end chain cross-linking system of NR producing dead ends which could render to faster normal mode.

- The dynamics of vulcanized NR and NR nanocomposites indicates that vulcanizing by sulfur induced a slowing down of the segmental dynamics. Moreover, this segmental process exhibits almost no dependence on the type of

nanofiller added to the rubber matrix. In addition, the process associated to chain dynamics (normal mode) is suppressed as a consequence of the cross-linking.

- The effects of orientation on the molecular dynamics of vulcanized NR were studied for the first time by means of broadband dielectric spectroscopy and X-ray scattering techniques. An amorphous/semi-crystalline transition around a strain ratio λ=3.0 is observed. Below this transition molecular chains show orientation without crystallization. Above this transition, the crystallites formed act as physical cross-links hindering the mobility of the polymer chains. This transition leads to significant changes on the segmental dynamics of vulcanized NR: i) a slowing down of the segmental relaxation, ii) a decrease of the dielectric strength and iii) a broadening of the relaxation process.

- The results on the effect of strain-induced crystallization on the dynamics of the NR/C15A nanocomposites revealed that the addition of nanoclay lead to enhanced crystallinity and lower onset strain for stretch-induced crystallization compared to unfilled NR. Besides, the new mode present in the NR/C15A nanocomposites is also affected by the strain-induced crystallization phenomenon, corroborating its segmental nature and with evidence of an amorphous/semi-crystalline transition around λ=2.5.

The present Doctoral Thesis gathers various studies that have been developed for the scientific understanding of the fundamentals of NR nanocomposites, including structure and dynamics. The promising results reported herein represent a major contribution from the point view of the nanofiller/rubber interactions within elastomer nanocomposites. In spite of the advances made, many challenges still remain to be studied or solved. In particular, the study of the dynamics of the cross-linked networks as a function of the vulcanization system, by means of dielectric spectroscopy and by RMN spectroscopy at low field is a demanding task. Moreover, to extend and complete the work on vulcanized NR, the quasielastic neutron scattering (QENS) technique appears as a powerful tool to characterize

the segmental and rotational dynamics of NR. Finally, it is intended to develop electrically conductive natural rubber latex nanocomposites by the addition of graphene for biomedical applications. The latex consists of aqueous colloidal suspensions, in which a good dispersion of carbon nanoparticles is expected.

CHAPTER VIII. REFERENCES

1. Brydson, J.A., ed. *Rubbery materials and their compounds*. 1988, Elsevier Science Publishers Ltd: Essex. 469.
2. Blow, C.M. and Hepburn, C., eds. *Rubber technology and manufacture*. 2nd ed. 1982, Butterworth Scientific: London. 608.
3. Morton, M., ed. *Rubber technology*. 3rd ed. 1999, Kluwer Academic Publishers: Dordrecht. 639.
4. Brydson, J.A., ed. *Plastics materials*. 4 ed. 1982, Butterworths: London. 800.
5. Verdejo, R.; Hernández, M.; Bitinis, N.; Kenny, J.M. and López-Manchado, M.A., *Vulcanization characteristics and curing kinetics of rubber-organoclay nanocomposites*, in *Rubber-clay nanocomposites*, M. Galimberti, Editor. 2011, John Wiley & Sons: Hoboken. 601.
6. Alexandre, M. and Dubois, P., *Polymer-layered silicate nanocomposites: preparation, properties and uses of a new class of materials.* Materials Science & Engineering R-Reports, 2000. **28**(1-2):1-63.
7. Bhattacharya, S.; Kamal, M.R. and Gupta, R.K., eds. *Polymeric nanocomposites. Theory and practice*. 2008, Carl Hanser Verlag: Munich. 383.
8. Arroyo, M.; Zitzumbo, R.; Avalos, F.; Valentin, J.L. and López-Manchado, M.A., *Elastomer-clay nanocomposites*, in *Encyclopedia of nanoscience and nanotechnology*, H.S. Nalwa, Editor. 2009, American Scientific Publishers.
9. Schmidt, D.; Shah, D. and Giannelis, E.P., *New advances in polymer/layered silicate nanocomposites.* Current Opinion in Solid State & Materials Science, 2002. **6**(3):205-212.
10. Ray, S.S. and Okamoto, M., *Polymer/layered silicate nanocomposites: a review from preparation to processing.* Progress in Polymer Science, 2003. **28**(11):1539-1641.
11. Vaia, R.A. and Wagner, H.D., *Polymer nanocomposites: framework for the future.* Materials Today, 2004. **6**:32- 37.
12. Ray, S. and Easteal, A.J. *Advances in polymer-filler composites: Macro to nano*. in *International Composites Conference*. 2006. Sydney, AUSTRALIA: Taylor & Francis Inc.

13. Maiti, M.; Bhattacharya, M. and Bhowmick, A.K., *Elastomer nanocomposites.* Rubber Chemistry and Technology, 2008. **81**(3):384-469.
14. Mark, J.E., *Ceramic-reinforced polymers and polymer-modified ceramics.* Polymer Engineering and Science, 1996. **36**(24):2905-2920.
15. Reynaud, E.; Gauthier, C. and Perez, J., *Nanophases in polymers.* Revue De Metallurgie-Cahiers D Informations Techniques, 1999. **96**(2):169-176.
16. Ebbesen, T.W., *Carbon nanotubes: preparation and properties*. 1997: CRC Press.
17. Favier, V.; Canova, G.R.; Shrivastava, S.C. and Cavaille, J.Y., *Mechanical percolation in cellulose whisker nanocomposites.* Polymer Engineering and Science, 1997. **37**(10):1732-1739.
18. Giannelis, E.P., *Polymer-layered silicate nanocomposites: Synthesis, properties and applications.* Applied Organometallic Chemistry, 1998. **12**(10-11):675-680.
19. LeBaron, P.C.; Wang, Z. and Pinnavaia, T.J., *Polymer-layered silicate nanocomposites: an overview.* Applied Clay Science, 1999. **15**(1-2):11-29.
20. Ajayan, P.M.; Stephan, O.; Colliex, C. and Trauth, D., *Aligned carbon nanotube arrays formed by cutting a polymer resin-nanotube composite.* Science, 1994. **265**(5176):1212-1214.
21. Yu, M.F.; Files, B.S.; Arepalli, S. and Ruoff, R.S., *Tensile loading of ropes of single wall carbon nanotubes and their mechanical properties.* Physical Review Letters, 2000. **84**(24):5552-5555.
22. Moniruzzaman, M. and Winey, K.I., *Polymer nanocomposites containing carbon nanotubes.* Macromolecules, 2006. **39**(16):5194-5205.
23. Bokobza, L., *Multiwall carbon nanotube elastomeric composites: A review.* Polymer, 2007. **48**(17):4907-4920.
24. Cooper, C.A.; Young, R.J. and Halsall, M., *Investigation into the deformation of carbon nanotubes and their composites through the use of Raman spectroscopy.* Composites Part a-Applied Science and Manufacturing, 2001. **32**(3-4):401-411.
25. de Heer, W.A., *Nanotubes and the pursuit of applications.* Mrs Bulletin, 2004. **29**(4):281-285.

26. Uchida, T. and Kumar, S., *Single wall carbon nanotube dispersion and exfoliation in polymers.* Journal of Applied Polymer Science, 2005. **98**(3):985-989.
27. Gao, G.H.; Cagin, T. and Goddard, W.A., *Energetics, structure, mechanical and vibrational properties of single-walled carbon nanotubes.* Nanotechnology, 1998. **9**(3):184-191.
28. Verdejo, R.; López-Manchado, M.A.; Valentini, L. and Kenny, J.M., *Carbon nanotube reinforced rubber composites*, in *Rubber nanocomposites: preparation, properties and applications*, S. Thomas and R. Stephen, Editors. 2010, John Wiley & Sons, Ltd: Singapore. 147-168.
29. Shaffer, M.S.P. and Sandler, J., *Carbon nanotube/nanofibre polymer composites*, in *Processing and Properties of Nanocomposites*, S.G. Advani, Editor. 2006, World Scientific. 1-59.
30. Hersam, M.C., *Progress towards monodisperse single-walled carbon nanotubes.* Nature Nanotechnology, 2008. **3**(7):387-394.
31. Baughman, R.H.; Zakhidov, A.A. and de Heer, W.A., *Carbon nanotubes - the route toward applications.* Science, 2002. **297**(5582):787-792.
32. Qian, D.; Wagner, G.J. and Liu, W.K., *Mechanics of carbon nanotubes.* Applied Mechanics Reviews, 2002. **55**:39.
33. Harris, P.J.F., ed. *Carbon nanotube science. Synthesis, properties and applications*. 2009, Cambridge University Press: Cambridge. 301.
34. Ramasubramaniam, R.; Chen, J. and Liu, H.Y., *Homogeneous carbon nanotube/polymer composites for electrical applications.* Applied Physics Letters, 2003. **83**(14):2928-2930.
35. Kim, Y.J.; Shin, T.S.; Choi, H.D.; Kwon, J.H.; Chung, Y.C. and Yoon, H.G., *Electrical conductivity of chemically modified multiwalled carbon nanotube/epoxy composites.* Carbon, 2005. **43**(1):23-30.
36. Kim, H.; Abdala, A.A. and Macosko, C.W., *Graphene/polymer nanocomposites.* Macromolecules, 2010. **43**(16):6515-6530.
37. Verdejo, R.; Bernal, M.M.; Romasanta, L.J. and López-Manchado, M.A., *Graphene filled polymer nanocomposites.* Journal of Materials Chemistry, 2011. **21**(10):3301-3310.

38. Ramanathan, T.; Abdala, A.A.; Stankovich, S.; Dikin, D.A.; Herrera-Alonso, M.; Piner, R.D.; Adamson, D.H.; Schniepp, H.C.; Chen, X.; Ruoff, R.S.; Nguyen, S.T.; Aksay, I.A.; Prud'homme, R.K. and Brinson, L.C., *Functionalized graphene sheets for polymer nanocomposites.* Nature Nanotechnology, 2008. **3**(6):327-331.

39. Singh, V.; Joung, D.; Zhai, L.; Das, S.; Khondaker, S.I. and Seal, S., *Graphene based materials: Past, present and future.* Progress in Materials Science, 2011. **56**(8):1178-1271.

40. Somani, P.R.; Somani, S.P. and Umeno, M., *Planer nano-graphenes from camphor by CVD.* Chemical Physics Letters, 2006. **430**(1-3):56-59.

41. Kim, K.S.; Zhao, Y.; Jang, H.; Lee, S.Y.; Kim, J.M.; Kim, K.S.; Ahn, J.-H.; Kim, P.; Choi, J.-Y. and Hong, B.H., *Large-scale pattern growth of graphene films for stretchable transparent electrodes.* Nature, 2009. **457**(7230):706-710.

42. Reina, A.; Jia, X.; Ho, J.; Nezich, D.; Son, H.; Bulovic, V.; Dresselhaus, M.S. and Kong, J., *Large area, few-layer graphene films on arbitrary substrates by chemical vapour deposition.* Nano Letters, 2009. **9**(1):30-35.

43. Stankovich, S.; Dikin, D.A.; Piner, R.D.; Kohlhaas, K.A.; Kleinhammes, A.; Jia, Y.; Wu, Y.; Nguyen, S.T. and Ruoff, R.S., *Synthesis of graphene-based nanosheets via chemical reduction of exfoliated graphite oxide.* Carbon, 2007. **45**(7):1558-1565.

44. Tung, V.C.; Allen, M.J.; Yang, Y. and Kaner, R.B., *High-throughput solution processing of large-scale graphene.* Nature Nanotechnology, 2009. **4**(1):25-29.

45. Lee, J.H.; Shin, D.W.; Makotchenko, V.G.; Nazarov, A.S.; Fedorov, V.E.; Kim, Y.H.; Choi, J.-Y.; Kim, J.M. and Yoo, J.-B., *One-step exfoliation synthesis of easily soluble graphite and transparent conducting graphene sheets.* Advanced Materials, 2009. **21**(43):4383-4387.

46. Potts, J.R.; Dreyer, D.R.; Bielawski, C.W. and Ruoff, R.S., *Graphene-based polymer nanocomposites.* Polymer, 2011. **52**(1):5-25.

47. Gogotsi, Y., ed. *Nanomaterials handbook*. 2006, CRC Press: Boca Raton, Florida USA. 780.

48. Spitalsky, Z.; Tasis, D.; Papagelis, K. and Galiotis, C., *Carbon nanotube-polymer composites: Chemistry, processing, mechanical and electrical properties.* Progress in Polymer Science, 2010. **35**(3):357-401.

49. López-Manchado, M.A.; Herrero, B. and Arroyo, M., *Organoclay-natural rubber nanocomposites synthesized by mechanical and solution mixing method.* Polymer International, 2004. **53**(11):1766-1772.

50. Vaia, R.A.; Ishii, H. and Giannelis, E.P., *Synthesis and properties of 2-dimensional nanostructures by direct intercalation of polymer melts in layered silicates.* Chemistry of Materials, 1993. **5**(12):1694-1696.

51. McWilliams, A., *Nanocomposites, nanoparticles, nanoclays, and nanotubes*. 2006, BCC Research.

52. Bokobza, L., *The reinforcement of elastomeric networks by fillers.* Macromolecular Materials and Engineering, 2004. **289**(7):607-621.

53. Bala, P.; Samantaray, B.K.; Srivastava, S.K. and Nando, G.B., *Effect of alkylammonium intercalated montmorillonite as filler on natural rubber.* Journal of Materials Science Letters, 2001. **20**(6):563-564.

54. Joly, S.; Garnaud, G.; Ollitrault, R.; Bokobza, L. and Mark, J.E., *Organically modified layered silicates as reinforcing fillers for natural rubber.* Chemistry of Materials, 2002. **14**(10):4202-4208.

55. López-Manchado, M.A.; Arroyo, M.; Herrero, B. and Biagiotti, J., *Vulcanization kinetics of natural rubber-organoclay nanocomposites.* Journal of Applied Polymer Science, 2003. **89**(1):1-15.

56. López-Manchado, M.A.; Herrero, B. and Arroyo, M., *Preparation and characterization of organoclay nanocomposites based on natural rubber.* Polymer International, 2003. **52**(7):1070-1077.

57. Arroyo, M.; López-Manchado, M.A. and Herrero, B., *Organo-montmorillonite as substitute of carbon black in natural rubber compounds.* Polymer, 2003. **44**(8):2447-2453.

58. Teh, P.L.; Ishak, Z.A.M.; Hashim, A.S.; Karger-Kocsis, J. and Ishiaku, U.S., *Effects of epoxidized natural rubber as a compatibilizer in melt compounded natural rubber-organoclay nanocomposites.* European Polymer Journal, 2004. **40**(11):2513-2521.

59. Teh, P.L.; Ishak, Z.A.M.; Hashim, A.S.; Karger-Kocsis, J. and Ishiaku, U.S., *Physical properties of natural rubber/organoclay nanocomposites compatibilized with epoxidized natural rubber.* Journal of Applied Polymer Science, 2006. **100**(2):1083-1092.

60. Arroyo, M.; López-Manchado, M.A.; Valentin, J.L. and Carretero, J., *Morphology/behaviour relationship of nanocomposites based on natural rubber/epoxidized natural rubber blends.* Composites Science and Technology, 2007. **67**(7-8):1330-1339.

61. Jurkowska, B.; Jurkowski, B.; Oczkowski, M.; Pesetskii, S.S.; Koval, V. and Olkhov, Y.A., *Properties of montmorillonite-containing natural rubber.* Journal of Applied Polymer Science, 2007. **106**(1):360-371.

62. López-Manchado, M.A.; Valentin, J.L.; Carretero, J.; Barroso, F. and Arroyo, M., *Rubber network in elastomer nanocomposites.* European Polymer Journal, 2007. **43**(10):4143-4150.

63. Edwards, S.F., *Theory of rubber elasticity.* British Polymer Journal, 1977. **9**(2):140-143.

64. Carretero-Gonzalez, J.; Verdejo, R.; Toki, S.; Hsiao, B.S.; Giannelis, E.P. and López-Manchado, M.A., *Real-time crystallization of organoclay nanoparticle filled natural rubber under stretching.* Macromolecules, 2008. **41**(7):2295-2298.

65. Carretero-González, J.; Retsos, H.; Verdejo, R.; Toki, S.; Hsiao, B.S.; Giannelis, E.P. and López-Manchado, M.A., *Effect of nanoclay on natural rubber microstructure.* Macromolecules, 2008. **41**(18):6763-6772.

66. Qu, L.; Huang, G.; Liu, Z.; Zhang, P.; Weng, G. and Nie, Y., *Remarkable reinforcement of natural rubber by deformation-induced crystallization in the presence of organophilic montmorillonite.* Acta Materialia, 2009. **57**(17):5053-5060.

67. López-Manchado, M.A.; Biagiotti, J.; Valentini, L. and Kenny, J.M., *Dynamic mechanical and raman spectroscopy studies on interaction between single-walled carbon nanotubes and natural rubber.* Journal of Applied Polymer Science, 2004. **92**(5):3394-3400.

68. Bokobza, L. and Kolodziej, M., *On the use of carbon nanotubes as reinforcing fillers for elastomeric materials.* Polymer International, 2006. **55**(9):1090-1098.

69. Kolodziej, M.; Bokobza, L. and Bruneel, J.-L., *Investigations on natural rubber filled with multiwall carbon nanotubes.* Composite Interfaces, 2007. **14**(3):215-228.

70. Sui, G.; Zhong, W.; Yang, X. and Zhao, S., *Processing and material characteristics of a carbon-nanotube-reinforced natural rubber.* Macromolecular Materials and Engineering, 2007. **292**(9):1020-1026.

71. Sui, G.; Zhong, W.H.; Yang, X.P. and Yu, Y.H., *Curing kinetics and mechanical behavior of natural rubber reinforced with pretreated carbon nanotubes.* Materials Science and Engineering a-Structural Materials Properties Microstructure and Processing, 2008. **485**(1-2):524-531.

72. Shanmugharaj, A.M.; Bae, J.H.; Lee, K.Y.; Noh, W.H.; Lee, S.H. and Ryu, S.H., *Physical and chemical characteristics of multiwalled carbon nanotubes functionalized with aminosilane and its influence on the properties of natural rubber composites.* Composites Science and Technology, 2007. **67**(9):1813-1822.

73. Bhattacharyya, S.; Sinturel, C.; Bahloul, O.; Saboungi, M.-L.; Thomas, S. and Salvetat, J.-P., *Improving reinforcement of natural rubber by networking of activated carbon nanotubes.* Carbon, 2008. **46**(7):1037-1045.

74. Cataldo, F.; Ursini, O. and Angelini, G., *MWCNTs elastomer nanocomposite, Part 1: the Addition of MWCNTs to a natural rubber-based carbon black-filled rubber compound.* Fullerenes Nanotubes and Carbon Nanostructures, 2009. **17**(1):38-54.

75. Fritzsche, J.; Lorenz, H. and Klüppel, M., *CNT based elastomer-hybrid-nanocomposites with promising mechanical and electrical properties.* Macromolecular Materials and Engineering, 2009. **294**(9):551-560.

76. Lorenz, H.; Fritzsche, J.; Das, A.; Stoeckelhuber, K.W.; Jurk, R.; Heinrich, G. and Klüppel, M., *Advanced elastomer nano-composites based on CNT-hybrid filler systems.* Composites Science and Technology, 2009. **69**(13):2135-2143.

77. Yang, H.; Tian, M.; Jia, Q.-X.; Shi, J.-H.; Zhang, L.-Q.; Lim, S.-H.; Yu, Z.-Z. and Mai, Y.-W., *Improved mechanical and functional properties of elastomer/graphite nanocomposites prepared by latex compounding.* Acta Materialia, 2007. **55**(18):6372-6382.

78. Bai, X.; Wan, C.Y.; Zhang, Y. and Zhai, Y.H., *Reinforcement of hydrogenated carboxylated nitrile-butadiene rubber with exfoliated graphene oxide.* Carbon, 2011. **49**(5):1608-1613.

79. Bhattacharya, M.; Maiti, M. and Bhowmick, A.K., *Tailoring properties of styrene butadiene rubber nanocomposite by various nanofillers and their dispersion.* Polymer Engineering and Science, 2009. **49**(1):81-98.

80. Verdejo, R.; Barroso-Bujans, F.; Rodriguez-Perez, M.A.; de Saja, J.A. and López-Manchado, M.A., *Functionalized graphene sheet filled silicone foam nanocomposites.* Journal of Materials Chemistry, 2008. **18**(19):2221-2226.

81. Liang, J.J.; Xu, Y.F.; Huang, Y.; Zhang, L.; Wang, Y.; Ma, Y.F.; Li, F.F.; Guo, T.Y. and Chen, Y.S., *Infrared-triggered actuators from graphene-based nanocomposites.* Journal of Physical Chemistry C, 2009. **113**(22):9921-9927.

82. Lian, H.Q.; Li, S.X.; Liu, K.L.; Xu, L.R.; Wang, K.S. and Guo, W.L., *Study on modified graphene/butyl rubber nanocomposites. I. Preparation and characterization.* Polymer Engineering and Science, 2011. **51**(11):2254-2260.

83. Prud'homme, R.; Ozbas, B.; Aksay, I.; Register, R. and Adamson, D., *Functional graphene-rubber nanocomposites,* US7745528B2. 2010, US.

84. Zhan, Y.H.; Wu, J.K.; Xia, H.S.; Yan, N.; Fei, G.X. and Yuan, G.P., *Dispersion and exfoliation of graphene in rubber by an ultrasonically-assisted latex mixing and in situ reduction process.* Macromolecular Materials and Engineering, 2011. **296**(7):590-602.

85. Kremer, F. and Schönhals, A., eds. *Broadband dielectric spectroscopy*. 2003, Springer: New York. 721.

86. Blythe, A.R., ed. *Electrical properties of polymers*. Cambridge Solid State Science Series. 1979, Cambridge University Press: Oxford.

87. Runt, J.P. and Fitzgerald, J.J., eds. *Dielectric spectroscopy of polymeric materials. Fundamentals and applications*. 1997, American Chemical Society: Washington, DC. 461.

88. Debye, P., *Polar molecules*. 1945, New York: Dover Publications.

89. Havriliak.S and Negami, S., *A complex plane representation of dielectric and mechanical relaxation processes in some polymers.* Polymer, 1967. **8**(4):161-210.

90. Böttcher, C.J.F. and Bordewijk, P., eds. *Theory of electric polarization*. Vol. II. 1978, Elsevier.

91. Richert, R. and Angell, C.A., *Dynamics of glass-forming liquids. V. On the link between molecular dynamics and configurational entropy.* Journal of Chemical Physics, 1998. **108**(21):9016-9026.

92. Pissis, P.; Fragiadakis, D.; Kanapitsas, A. and Delides, K. *Broadband dielectric relaxation spectroscopy in polymer nanocomposites*. in *17th European Symposium on Polymer Spectroscopy (ESOPS 17)*. 2007. Seggauberg, AUSTRIA: Wiley-V C H Verlag Gmbh.

93. Kalgaonkar, R.A. and Jog, J.P., *Molecular dynamics of copolyester/clay nanocomposites as investigated by viscoelastic and dielectric analysis.* Journal of Polymer Science Part B-Polymer Physics, 2008. **46**(23):2539-2555.

94. Xu, W.; Raychowdhury, S.; Jiang, D.D.; Retsos, H. and Giannelis, E.P., *Dramatic improvements in toughness in poly(lactide-co-glycolide) nanocomposties.* Small, 2008. **4**(5):662-669.

95. Lopez, I.J.; Dolidze, V.; Rivera, M. and Aliev, F., *Relaxation processes and glass transition in polymer filled with nanoparticles.* Macromolecular Symposia, 2008. **267**:63-68.

96. Cheng, L.; Zheng, L.; Li, G.; Zeng, J. and Yin, Q., *Influence of particle surface properties on the dielectric behavior of silica/epoxy nanocomposites.* Physica B-Condensed Matter, 2008. **403**(17):2584-2589.

97. Schönhals, A.; Goering, H.; Costa, F.R.; Wagenknecht, U. and Heinrich, G., *Dielectric properties of nanocomposites based on polyethylene and layered double hydroxide.* Macromolecules, 2009. **42**(12):4165-4174.

98. Fragiadakis, D.; Pissis, P. and Bokobza, L., *Glass transition and molecular dynamics in poly (dimethylsiloxane)/silica nanocomposites.* Polymer, 2005. **46**(16):6001-6008.

99. Fragiadakis, D.; Pissis, P. and Bokobza, L. *Modified chain dynamics in poly(dimethylsiloxane)/silica nanocomposites*. in *5th International Discussion*

Meeting on Relaxations in Complex Systems. 2005. Lille, FRANCE: Elsevier Science Bv.

100. Fragiadakis, D. and Pissis, P., *Glass transition and segmental dynamics in poly(dimethylsiloxane)/silica nanocomposites studied by various techniques.* Journal of Non-Crystalline Solids, 2007. **353**:4344-4352.
101. Fritzsche, J.; Das, A.; Jurk, R.; Stokelhuber, K.W.; Heinrich, G. and Klüppel, M., *Relaxation dynamics of carboxylated nitrile rubber filled with organomodified nanoclay.* Express Polymer Letters, 2008. **2**(5):373-381.
102. Fritzsche, J. and Klüppel, M., *Molecular dynamics of silica and organoclay filled XNBR-nanocomposites.* Kgk-Kautschuk Gummi Kunststoffe, 2009. **62**(1-2):16-22.
103. Fritzsche, J.; Klüppel, M. and Meier, J.G., *Dielectric relaxation spectroscopy of precipitated silica and elastomer-silica composites.* Kgk-Kautschuk Gummi Kunststoffe, 2009. **62**(6):319-325.
104. Adachi, K. and Kotaka, T., *Influence of entanglement on the dielectric normal mode process of cis-polyisoprene.* Macromolecules, 1984. **17**(1):120-122.
105. Adachi, K. and Kotaka, T., *Dielectric normal mode process in undiluted cis-polyisoprene.* Macromolecules, 1985. **18**(3):466-472.
106. Adachi, K. and Kotaka, T., *Dielectric normal mode process in dilute-solutions of cis-polyisoprene.* Macromolecules, 1987. **20**(8):2018-2023.
107. Boese, D.; Kremer, F. and Fetters, L.J., *Molecular dynamics in linear and multiarmed star polymers of cis-polyisoprene as studied by dielectric spectroscopy.* Macromolecules, 1990. **23**(6):1826-1830.
108. Boese, D. and Kremer, F., *Molecular-dynamics in bulk cis-polyisoprene as studied by dielectric spectroscopy.* Macromolecules, 1990. **23**(3):829-835.
109. Serghei, A.; Hartmann, L.; Pouret, P.; Leger, L. and Kremer, F., *Molecular dynamics in thin (grafted) polymer layers.* Colloid and Polymer Science, 2004. **282**(8):946-954.
110. Petychakis, L.; Floudas, G. and Fleischer, G., *Chain dynamics of polyisoprene confined in porous media. A dielectric spectroscopy study.* Europhysics Letters, 1997. **40**(6):685-690.

111. Cerveny, S.; Zinck, P.; Terrier, M.; Arrese-Igor, S.; Alegria, A. and Colmenero, J., *Dynamics of amorphous and semicrystalline 1,4-trans-poly(isoprene) by dielectric spectroscopy.* Macromolecules, 2008. **41**(22):8669-8676.

112. Kowalski, E.L.; de Oliveira, S.M.; de Souza, G.P.; Tomioka, J.; Silva, J.M.M.; Ruvolo, A.; Robert, R. and Ieee, *Dielectric spectroscopy on natural rubber flatted sample with different temperature and time of vulcanization*. Proceedings of the 7th International Conference on Properties and Applications of Dielectric Materials, Vols 1-3. 2003, New York: Ieee. 522-523.

113. Ward, A.A.; El-Sabbagh, S. and El-Aal, N.S.A., *Mechanical, ultrasonic, dielectric and physical properties of natural rubber with different concentrations of zinc stearate.* Kgk-Kautschuk Gummi Kunststoffe, 2008. **61**(9):429-437.

114. Carretero-Gonzalez, J.; Ezquerra, T.A.; Amnuaypornsri, S.; Toki, S.; Verdejo, R.; Sanz, A.; Sakdapipanich, J.; Hsiao, B.S. and López-Manchado, M.A., *Molecular dynamics of natural rubber as revealed by dielectric spectroscopy: The role of natural cross-linking.* Soft Matter, 2010. **6**(15):3636-3642.

115. Ortiz-Serna, P.; Diaz-Calleja, R.; Sanchis, M.J.; Floudas, G.; Nunes, R.C.; Martins, A.F. and Visconte, L.L., *Dynamics of natural rubber as a function of frequency, temperature, and pressure. A dielectric spectroscopy investigation.* Macromolecules, 2010. **43**(11):5094-5102.

116. Page, K.A. and Adachi, K., *Dielectric relaxation in montmorillonite/polymer nanocomposites.* Polymer, 2006. **47**(18):6406-6413.

117. Mijovic, J.; Lee, H.K.; Kenny, J. and Mays, J., *Dynamics in polymer-silicate nanocomposites as studied by dielectric relaxation spectroscopy and dynamic mechanical spectroscopy.* Macromolecules, 2006. **39**(6):2172-2182.

118. Stephen, R.; Thomas, S.; Raju, K.; Varghese, S.; Joseph, K. and Oommen, Z., *Dynamic mechanical and dielectric properties of nanocomposites of natural rubber (NR), carboxylated styrene butadiene rubber (XSBR) latices and their blends.* Rubber Chemistry and Technology, 2007. **80**(4):672-689.

119. Psarras, G.C.; Gatos, K.G.; Karahaliou, P.K.; Georga, S.N.; Krontiras, C.A. and Karger-Kocsis, J., *Relaxation phenomena in rubber/layered silicate nanocomposites.* Express Polymer Letters, 2007. **1**(12):837-845.

120. Psarras, G.C.; Gatos, K.G. and Karger-Kocsis, J., *Dielectric properties of layered silicate-reinforced natural and polyurethane rubber nanocomposites.* Journal of Applied Polymer Science, 2007. **106**(2):1405-1411.

121. Lee, H.K.; Pejanovic, S.; Mondragon, I. and Mijovic, J., *Dynamics of single-walled carbon nanotube (SWNT)/polyisoprene (PI) nanocomposites in electric and mechanical fields.* Polymer, 2007. **48**(25):7345-7355.

122. Ortiz-Serna, P.; Diaz-Calleja, R.; Sanchis, M.J.; Riande, E.; Nunes, R.; Martins, A. and Visconte, L., *Dielectric spectroscopy of natural rubber-cellulose II nanocomposites.* Journal of Non-Crystalline Solids, 2011. **357**(2):598-604.

123. Fragiadakis, D.; Bokobza, L. and Pissis, P., *Dynamics near the filler surface in natural rubber-silica nanocomposites.* Polymer, 2011. **52**(14):3175-3182.

124. www.scprod.com. *Southern Clay Products, Inc.*

125. Harris, P.J.F., *Carbon nanotube science. Synthesis, properties and applications*. 2009: Cambridge University Press.

126. Singh, C.; Shaffer, M.S. and Windle, A.H., *Production of controlled architectures of aligned carbon nanotubes by an injection chemical vapour deposition method.* Carbon, 2003. **41**(2):359-368.

127. Verdejo, R.; Stampfli, R.; Alvarez-Lainez, M.; Mourad, S.; Rodriguez-Perez, M.A.; Bruhwiler, P.A. and Shaffer, M., *Enhanced acoustic damping in flexible polyurethane foams filled with carbon nanotubes.* Composites Science and Technology, 2009. **69**(10):1564-1569.

128. Verdejo, R.; Lamoriniere, S.; Cottam, B.; Bismarck, A. and Shaffer, M., *Removal of oxidation debris from multi-walled carbon nanotubes.* Chemical Communications, 2007(5):513-515.

129. Brodie, B.C., *On the atomic weight of graphite.* Philosophical Transactions of the Royal Society of London, 1859. **149**:249-259.

130. Dreyer, D.R.; Park, S.; Bielawski, C.W. and Ruoff, R.S., *The chemistry of graphene oxide.* Chemical Society Reviews, 2010. **39**(1):228-240.

131. Sics, I.; Ezquerra, T.A.; Nogales, A.; Balta-Calleja, F.J.; Kalnins, M. and Tupureina, V., *On the relationship between crystalline structure and amorphous phase dynamics during isothermal crystallization of bacterial poly(3-hydroxybutyrate-co-3-hydroxyvalerate) copolymers.* Biomacromolecules, 2001. **2**(2):581-587.

132. Rueda, D.R.; Garcia-Gutierrez, M.C.; Nogales, A.; Capitan, M.J.; Ezquerra, T.A.; Labrador, A.; Fraga, E.; Beltran, D.; Juanhuix, J.; Herranz, J.F. and Bordas, J., *Versatile wide angle diffraction setup for simultaneous wide and small angle X-ray scattering measurements with synchrotron radiation.* Review of Scientific Instruments, 2006. **77**(3):5.

133. Hernández, M.; Ezquerra, T.A.; Verdejo, R. and López-Manchado, M.A., *Role of vulcanizing additives on the segmental dynamics of natural rubber.* Macromolecules, 2012. **45**(2):1070-1075.

134. Heideman, G.; Datta, R.N.; Noordermeer, J.W.M. and Van Baarle, B., *Activators in accelerated sulfur vulcanization.* Rubber Chemistry and Technology, 2004. **77**(3):512-541.

135. Steudel, R. and Steudel, Y., *Interaction of zinc oxide clusters with molecules related to the sulfur vulcanization of polyolefins ("rubber").* Chemistry-a European Journal, 2006. **12**(33):8589-8602.

136. Ikeda, Y.; Higashitani, N.; Hijikata, K.; Kokubo, Y.; Morita, Y.; Shibayama, M.; Osaka, N.; Suzuki, T.; Endo, H. and Kohjiya, S., *Vulcanization: new focus on a traditional technology by small-angle neutron scattering.* Macromolecules, 2009. **42**(7):2741-2748.

137. Poh, B.T. and Tang, W.L., *Concentration effect of stearic acid on scorch behavior of epoxidized natural rubber.* Journal of Applied Polymer Science, 1995. **55**(3):537-542.

138. Kim, I.J.; Kim, W.S.; Lee, D.H.; Kim, W. and Bae, J.W., *Effect of nano zinc oxide on the cure characteristics and mechanical properties of the silica-filled natural rubber/butadiene rubber compounds.* Journal of Applied Polymer Science, 2010. **117**(3):1535-1543.

139. Cavdar, S.; Ozdemir, T. and Usanmaz, A., *Comparative study on mechanical, thermal, viscoelastic and rheological properties of vulcanised EPDM rubber.* Plastics Rubber and Composites, 2010. **39**(6):277-282.

140. Kohjiya, S.; Tosaka, M.; Masahiro, F.; Ikeda, Y.; Toki, S. and Hsiao, B.S., *Role of stearic acid in the strain-induced crystallization of crosslinked natural rubber and synthetic cis-1,4-polyisoprene.* Polymer, 2007. **48**:3801-3808.

141. Hofmann, W., *Vulcanization and vulcanizing agents*. 1967: Maclaren. 371.

142. Allan, J.R.; Geddes, W.C.; Hindle, C.S. and Lowe, A.J., *The characterization of zinc-complexes of anthranilic acid and malonic acid as activators for natural rubber.* Plastics Rubber and Composites Processing and Applications, 1991. **16**(2):91-94.

143. Zhao, F.; Zhang, P.; Zhao, S.G.; Yu, J. and Kuhn, W., *Characterization of elastomer networks by NMR parameters - Part III - Influence of activators on the network dynamics of NR vulcanizates.* Kgk-Kautschuk Gummi Kunststoffe, 2008. **61**(5):224-229.

144. Helaly, F.M.; El Sabbagh, S.H.; El Kinawy, O.S. and El Sawy, S.M., *Effect of synthesized zinc stearate on the properties of natural rubber vulcanizates in the absence and presence of some fillers.* Materials & Design, 2011. **32**(5):2835-2843.

145. Soulintzis, A.; Kontos, G.; Karahaliou, P.; Psarras, G.C.; Georga, S.N. and Krontiras, C.A., *Dielectric relaxation processes in epoxy resin-ZnO composites.* Journal of Polymer Science Part B-Polymer Physics, 2009. **47**(4):445-454.

146. Ioannou, G.; Patsidis, A. and Psarras, G.C., *Dielectric and functional properties of polymer matrix/ZnO/BaTiO3 hybrid composites.* Composites Part a-Applied Science and Manufacturing, 2011. **42**(1):104-110.

147. Smaoui, H.; Mir, L.E.L.; Guermazi, H.; Agnel, S. and Toureille, A., *Study of dielectric relaxations in zinc oxide-epoxy resin nanocomposites.* Journal of Alloys and Compounds, 2009. **477**(1-2):316-321.

148. Chapman, A.V., *Safe rubber chemicals: reduction of zinc levels in rubber compounds*. 1997, TARRC/MRPRA: Brickendonbury.

149. Heideman, G.; Datta, R.N.; Noordermeer, J.W.M. and van Baarle, B., *Influence of zinc oxide during different stages of sulfur vulcanization. Elucidated by model compound studies.* Journal of Applied Polymer Science, 2005. **95**(6):1388-1404.

150. Nieuwenhuizen, P.J.; Timal, S.; Van Veen, J.M.; Haasnoot, J.G. and Reedijk, J., *Homogeneous zinc(II) catalysis in accelerated vulcanization I. Reaction-stage modeling and cross-link formation.* Rubber Chemistry and Technology, 1998. **71**(4):750-765.

151. Antony, P.; Bandyopadhyay, S. and De, S.K., *Thermoplastic elastomers based on ionomeric polyblends of zinc salts of maleated polypropylene and maleated EPDM rubber.* Polymer Engineering and Science, 1999. **39**(5):963-974.

152. Hird, B. and Eisenberg, A., *Sizes and stabilities of multiplets and clusters in carboxylated and sulfonated styrene ionomers.* Macromolecules, 1992. **25**(24):6466-6474.

153. Bohmer, R.; Ngai, K.L.; Angell, C.A. and Plazek, D.J., *Nonexponential relaxations in strong and fragile glass formers.* Journal of Chemical Physics, 1993. **99**(5):4201-4209.

154. Kramarenko, V.Y.; Ezquerra, T.A.; Sics, I.; Balta-Calleja, F.J. and Privalko, V.P., *Influence of cross-linking on the segmental dynamics in model polymer networks.* Journal of Chemical Physics, 2000. **113**(1):447-452.

155. Angell, C.A., *Relaxation in liquids, polymers and plastic crystals - Strong fragile patterns and problems.* Journal of Non-Crystalline Solids, 1991. **131**:13-31.

156. Roland, C.M. and Ngai, K.L., *Normalization of the temperature-dependence of segmental relaxation-times.* Macromolecules, 1992. **25**(21):5765-5768.

157. Plazek, D.J. and Ngai, K.L., *Correlation of polymer segmental chain dynamics with temperature-dependent time-scale shifts.* Macromolecules, 1991. **24**(5):1222-1224.

158. Green, J.L.; Ito, K.; Xu, K. and Angell, C.A., *Fragility in liquids and polymers: New, simple quantifications and interpretations.* Journal of Physical Chemistry B, 1999. **103**(20):3991-3996.

159. Angell, C.A., *Why C-1=16-17 in the WLF equation is physical - and the fragility of polymers.* Polymer, 1997. **38**(26):6261-6266.

160. Sanz, A.; Nogales, A. and Ezquerra, T.A., *Influence of fragility on polymer cold crystallization.* Macromolecules, 2010. **43**(1):29-32.

161. Hedvig, P., *Dielectric spectroscopy of polymers*. 1977, Bristol: Adam Hilger Ltd. 340.

162. Hernández, M.; Carretero-Gonzalez, J.; Verdejo, R.; Ezquerra, T.A. and López-Manchado, M.A., *Molecular dynamics of natural rubber/layered silicate nanocomposites as studied by dielectric relaxation spectroscopy.* Macromolecules, 2010. **43**(2):643-651.

163. López-Manchado, M.A.; Valentin, J.L.; Herrero, B. and Arroyo, M., *Novel approach of evaluating polymer nanocomposite structure by measurements of the freezing-point depression.* Macromolecular Rapid Communications, 2004. **25**(14):1309-1313.

164. Ismail, H. and Chia, H.H., *The effects of multifunctional additive and epoxidation in silica filled natural rubber compounds.* Polymer Testing, 1998. **17**(3):199-210.

165. Mousa, A. and Karger-Kocsis, J., *Rheological and thermodynamical behavior of styrene/butadiene rubber-organoclay nanocomposites.* Macromolecular Materials and Engineering, 2001. **286**(4):260-266.

166. Ismail, H. and Chia, H.H., *The effects of multifunctional additive and vulcanization systems on silica filled epoxidized natural rubber compounds.* European Polymer Journal, 1998. **34**(12):1857-1863.

167. Rajeev, R.S. and De, S.K., *Crosslinking of rubbers by fillers.* Rubber Chemistry and Technology, 2002. **75**(3):475-509.

168. Avalos, F.; Ortiz, J.C.; Zitzumbo, R.; López-Manchado, M.A.; Verdejo, R. and Arroyo, M., *Effect of montmorillonite intercalant structure on the cure parameters of natural rubber.* European Polymer Journal, 2008. **44**(10):3108-3115.

169. Reincke, K. and Grellmann, W., *Mechanical and fracture mechanics properties of rubber compositions with reinforcing components*, in *Rubber-clay nanocomposites*, M. Galimberti, Editor. 2011, John Wiley & Sons: Hoboken. 601.

170. Calvet, R., *Dielectric properties of montmorillonites saturated by bivalent cations.* Clays and Clay Minerals, 1975. **23**(4):257-265.

171. Tsangaris, G.M.; Psarras, G.C. and Kouloumbi, N., *Electric modulus and interfacial polarization in composite polymeric systems.* Journal of Materials Science, 1998. **33**(8):2027-2037.

172. Schönhals, A.; Goering, H.; Schick, C.; Frick, B. and Zorn, R., *Glass transition of polymers confined to nanoporous glasses.* Colloid and Polymer Science, 2004. **282**(8):882-891.

173. Boese, D. and Kremer, F., *Molecular dynamics in bulk cis-polyisoprene as studied by dielectric spectroscopy.* Macromolecules, 1990. **23**(3):829-835.

174. George, S.; Varughese, K.T. and Thomas, S., *Dielectric properties of isotactic polypropylene nitrile rubber blends: Effects of blend ratio, filler addition, and dynamic vulcanization.* Journal of Applied Polymer Science, 1999. **73**(2):255-270.

175. Abd-El-Messieh, S.L. and Abd-El-Nour, K.N., *Effect of curing time and sulfur content on the dielectric relaxation of styrene butadiene rubber.* Journal of Applied Polymer Science, 2003. **88**(7):1613-1621.

176. McAllister, M.J.; Li, J.-L.; Adamson, D.H.; Schniepp, H.C.; Abdala, A.A.; Liu, J.; Herrera-Alonso, M.; Milius, D.L.; Car, R.; Prud'homme, R.K. and Aksay, I.A., *Single sheet functionalized graphene by oxidation and thermal expansion of graphite.* Chemistry of Materials, 2007. **19**(18):4396-4404.

177. Dresselhaus, M.S.; Dresselhaus, G.; Saito, R. and Jorio, A., *Raman spectroscopy of carbon nanotubes.* Physics Reports-Review Section of Physics Letters, 2005. **409**(2):47-99.

178. Eklund, P.C.; Holden, J.M. and Jishi, R.A., *Vibrational modes of carbon nanotubes; spectroscopy and theory.* Carbon, 1995. **33**(7):959-972.

179. Ferrari, A.C., *Raman spectroscopy of graphene and graphite: Disorder, electron-phonon coupling, doping and nonadiabatic effects.* Solid State Communications, 2007. **143**(1-2):47-57.

180. Datsyuk, V.; Kalyva, M.; Papagelis, K.; Parthenios, J.; Tasis, D.; Siokou, A.; Kallitsis, I. and Galiotis, C., *Chemical oxidation of multiwalled carbon nanotubes.* Carbon, 2008. **46**(6):833-840.

181. Kudin, K.N.; Ozbas, B.; Schniepp, H.C.; Prud'homme, R.K.; Aksay, I.A. and Car, R., *Raman spectra of graphite oxide and functionalized graphene sheets.* Nano Letters, 2007. **8**(1):36-41.

182. Webb, M.J.; Palmgren, P.; Pal, P.; Karis, O. and Grennberg, H., *A simple method to produce almost perfect graphene on highly oriented pyrolytic graphite.* Carbon, 2011. **49**(10):3242-3249.

183. Ago, H.; Kugler, T.; Cacialli, F.; Salaneck, W.R.; Shaffer, M.S.P.; Windle, A.H. and Friend, R.H., *Work functions and surface functional groups of multiwall carbon nanotubes.* The Journal of Physical Chemistry B, 1999. **103**(38):8116-8121.

184. Okpalugo, T.I.T.; Papakonstantinou, P.; Murphy, H.; McLaughlin, J. and Brown, N.M.D., *High resolution XPS characterization of chemical functionalised MWCNTs and SWCNTs.* Carbon, 2005. **43**(1):153-161.

185. Yang, D.; Velamakanni, A.; Bozoklu, G.; Park, S.; Stoller, M.; Piner, R.D.; Stankovich, S.; Jung, I.; Field, D.A.; Ventrice Jr, C.A. and Ruoff, R.S., *Chemical analysis of graphene oxide films after heat and chemical treatments by X-ray photoelectron and Micro-Raman spectroscopy.* Carbon, 2009. **47**(1):145-152.

186. Wagner, C.D.; Davis, L.E.; Zeller, M.V.; Taylor, J.A.; Raymond, R.H. and Gale, L.H., *Empirical atomic sensitivity factors for quantitative analysis by electron spectroscopy for chemical analysis.* Surface and Interface Analysis, 1981. **3**(5):211-225.

187. Peigney, A.; Laurent, C.; Flahaut, E.; Bacsa, R.R. and Rousset, A., *Specific surface area of carbon nanotubes and bundles of carbon nanotubes.* Carbon, 2001. **39**(4):507-514.

188. Ismail, H.; Ramly, F. and Othman, N., *Multiwall carbon nanotube-filled natural rubber: The effects of filler loading and mixing method.* Polymer-Plastics Technology and Engineering, 2010. **49**(3):260-266.

189. Toki, S.; Sics, I.; Hsiao, B.S.; Murakami, S.; Tosaka, M.; Poompradub, S.; Kohjiya, S. and Ikeda, Y., *Structural developments in synthetic rubbers during uniaxial deformation by in situ synchrotron X-ray diffraction.* Journal of Polymer Science Part B-Polymer Physics, 2004. **42**(6):956-964.

190. Toki, S.; Burger, C.; Hsiao, B.S.; Amnuaypornsri, S.; Sakdapipanich, J. and Tanaka, Y., *Multi-scaled microstructures in natural rubber characterized by synchrotron X-ray scattering and optical microscopy.* Journal of Polymer Science Part B-Polymer Physics, 2008. **46**(22):2456-2464.

191. Connor, M.T.; Roy, S.; Ezquerra, T.A. and Calleja, F.J.B., *Broadband ac conductivity of conductor-polymer composites.* Physical Review B, 1998. **57**(4):2286-2294.

192. Stauffer, D., ed. *Introduction to percolation theory*. 1985, Taylor & Francis: London.

193. Linares, A.; Canalda, J.C.; Cagiao, M.E.; Garcia-Gutierrez, M.C.; Nogales, A.; Martin-Gullom, I.; Vera, J. and Ezquerra, T.A., *Broad-band electrical conductivity of high density polyethylene nanocomposites with carbon*

nanoadditives: multiwall carbon nanotubes and carbon nanofibers. Macromolecules, 2008. **41**(19):7090-7097.

194. Du, F.M.; Fischer, J.E. and Winey, K.I., *Coagulation method for preparing single-walled carbon nanotube/poly(methyl methacrylate) composites and their modulus, electrical conductivity, and thermal stability.* Journal of Polymer Science Part B-Polymer Physics, 2003. **41**(24):3333-3338.
195. Hernández, M.; López-Manchado, M.A.; Sanz, A.; Nogales, A. and Ezquerra, T.A., *Effects of strain-induced crystallization on the segmental dynamics of vulcanized natural rubber.* Macromolecules, 2011. **44**(16):6574-6580.
196. Sanz, A.; Nogales, A.; Ezquerra, T.A.; Soccio, M.; Munari, A. and Lotti, N., *Cold crystallization of poly(trimethylene terephthalate) as revealed by simultaneous WAXS, SAXS, and dielectric spectroscopy.* Macromolecules, 2010. **43**(2):671-679.
197. Nogales, A.; Ezquerra, T.A.; Denchev, Z.; Sics, I.; Calleja, F.J.B. and Hsiao, B.S., *Molecular dynamics and microstructure development during cold crystallization in poly(ether-ether-ketone) as revealed by real time dielectric and x-ray methods.* Journal of Chemical Physics, 2001. **115**(8):3804-3813.
198. Ward, I.M. and Sweeney, J., eds. *An introduction to the mechanical properties of solid polymers*. 2nd ed. 2004, John Wiley & Sons Ltd: West Sussex. 382.
199. Murakami, S.; Senoo, K.; Toki, S. and Kohjiya, S., *Structural development of natural rubber during uniaxial stretching by in situ wide angle X-ray diffraction using a synchrotron radiation.* Polymer, 2002. **43**(7):2117-2120.
200. Toki, S.; Hsiao, B.S.; Amnuaypornsri, S. and Sakdapipanich, J., *New insights into the relationship between network structure and strain-induced crystallization in un-vulcanized and vulcanized natural rubber by synchrotron X-ray diffraction.* Polymer, 2009. **50**(9):2142-2148.
201. Weng, G.S.; Huang, G.S.; Qu, L.L.; Nie, Y.J. and Wu, J.R., *Large-scale orientation in a vulcanized stretched natural rubber network: proved by in situ synchrotron X-ray diffraction characterization.* Journal of Physical Chemistry B, 2010. **114**(21):7179-7188.
202. Tosaka, M.; Kawakami, D.; Senoo, K.; Kohjiya, S.; Ikeda, Y.; Toki, S. and Hsiao, B.S., *Crystallization and stress relaxation in highly stretched samples of*

natural rubber and its synthetic analogue. Macromolecules, 2006. **39**(15):5100-5105.

203. Ikeda, Y.; Yasuda, Y.; Hijikata, K.; Tosaka, M. and Kohjiya, S., *Comparative study on strain-induced crystallization behavior of peroxide cross-linked and sulfur cross-linked natural rubber.* Macromolecules, 2008. **41**(15):5876-5884.
204. Tosaka, M.; Murakami, S.; Poompradub, S.; Kohjiya, S.; Ikeda, Y.; Toki, S.; Sics, I. and Hsiao, B.S., *Orientation and crystallization of natural rubber network as revealed by WAXD using synchrotron radiation.* Macromolecules, 2004. **37**(9):3299-3309.
205. Tosaka, M.; Kohjiya, S.; Murakami, S.; Poompradub, S.; Ikeda, Y.; Toki, S.; Sics, I. and Hsiao, B.S., *Effect of network-chain length on strain-induced crystallization of NR and IR vulcanizates.* Rubber Chemistry and Technology, 2004. **77**(4):711-723.
206. Toki, S.; Sics, I.; Ran, S.F.; Liu, L.Z. and Hsiao, B.S., *Molecular orientation and structural development in vulcanized polyisoprene rubbers during uniaxial deformation by in situ synchrotron X-ray diffraction.* Polymer, 2003. **44**(19):6003-6011.
207. Gent, A.N., *Crystallization in natural rubber. 4. Temperature dependence.* Journal of Polymer Science, 1955. **18**(89):321-334.
208. Benedetti, E.; Corradini, P. and Pedone, C., *Conformational isomorphism in crystalline 1,4-cis-polyisoprene.* European Polymer Journal, 1975. **11**(8):585-587.
209. Rajkumar, G.; Squire, J.M. and Arnott, S., *A new structure for crystalline natural rubber.* Macromolecules, 2006. **39**(20):7004-7014.
210. Lee, H.K.; Fragiadakis, D.; Martin, D.; Milne, A.; Milne, J. and Runt, J., *Dynamics of uniaxially oriented elastomers using broadband dielectric spectroscopy.* Macromolecules, 2010. **43**(7):3125-3127.
211. Trabelsi, S.; Albouy, P.A. and Rault, J., *Effective local deformation in stretched filled rubber.* Macromolecules, 2003. **36**(24):9093-9099.
212. Rault, J.; Marchal, J.; Judeinstein, P. and Albouy, P.A., *Stress-induced crystallization and reinforcement in filled natural rubbers: H-2 NMR study.* Macromolecules, 2006. **39**(24):8356-8368.

213. Poompradub, S.; Tosaka, M.; Kohjiya, S.; Ikeda, Y.; Toki, S.; Sics, I. and Hsiao, B.S., *Mechanism of strain-induced crystallization in filled and unfilled natural rubber vulcanizates.* Journal of Applied Physics, 2005. **97**(10).

214. Nie, Y.J.; Huang, G.S.; Qu, L.L.; Wang, X.A.; Weng, G.S. and Wu, J.R., *New insights into thermodynamic description of strain-induced crystallization of peroxide cross-linked natural rubber filled with clay by tube model.* Polymer, 2011. **52**(14):3234-3242.

215. Nie, Y.; Huang, G.; Qu, L.; Zhang, P.; Weng, G. and Wu, J., *Structural evolution during uniaxial deformation of natural rubber reinforced with nano-alumina.* Polymers for Advanced Technologies, 2011. **22**(12):2001-2008.

216. Jiang, H.-X.; Ni, Q.-Q. and Natsuki, T., *Tensile properties and reinforcement mechanisms of natural rubber/vapor-grown carbon nanofiber composite.* Polymer Composites, 2010. **31**(6):1099-1104.

217. Williams, M.L.; Landel, R.F. and Ferry, J.D., *Temperature dependence of relaxation mechanisms.* Journal of the American Chemical Society, 1955. **77**:7.

218. Fox, T.G. and Flory, P.J., *2nd-order transition temperatures and related properties of polystyrene.1. Influence of molecular weight.* Journal of Applied Physics, 1950. **21**(6):581-591.

219. Simha, R. and Weil, C.E., *Concerning free volume quantities and glass temperature.* Journal of Macromolecular Science-Physics, 1970. **B 4**(1):215-&.

220. Ngai, K.L.; Rajagopal, A.K. and Teitler, S., *Slowing down of relaxation in a complex system by constraint dynamics.* Journal of Chemical Physics, 1988. **88**(8):5086-5094.

221. Ngai, K.L. and Rendell, R.W., *Toward a theory of relaxation in correlated systems - Diffusion in the phase-space of a chaotic hamiltonian.* Journal of Non-Crystalline Solids, 1991. **131**:233-237.

222. Ngai, K.L.; Peng, S.L. and Tsang, K.Y., *Fractal phase-space transport dynamics and relaxations in complex correlated systems.* Physica A, 1992. **191**(1-4):523-531.

223. Ngai, K.L. and Tsang, K.Y., *Similarity of relaxation in supercooled liquids and interacting arrays of oscillators.* Physical Review E, 1999. **60**(4):4511-4517.

224. Dudowicz, J.; Freed, K.F. and Douglas, J.F., *The glass transition temperature of polymer melts.* Journal of Physical Chemistry B, 2005. **109**(45):21285-21292.

225. Dudowicz, J.; Freed, K.F. and Douglas, J.F., *Fragility of glass-forming polymer liquids.* Journal of Physical Chemistry B, 2005. **109**(45):21350-21356.

226. Dudowicz, J.; Freed, K.F. and Douglas, J.F., *Generalized entropy theory of polymer glass formation*, in *Advances in Chemical Physics, Vol 137*, S.A. Rice, Editor. 2008. 125-222.

227. Qin, Q. and McKenna, G.B., *Correlation between dynamic fragility and glass transition temperature for different classes of glass forming liquids.* Journal of Non-Crystalline Solids, 2006. **352**(28-29):2977-2985.

APPENDIX A

A.1. Characterization of Natural Rubber

A.1.1. *Differential Scanning Calorimetry (DSC)*

Figure A.1. shows the DSC curve taken at 10 ºC/min in the temperature range from -90 to 200 ºC, according to the procedure detailed in Section II.3.2.

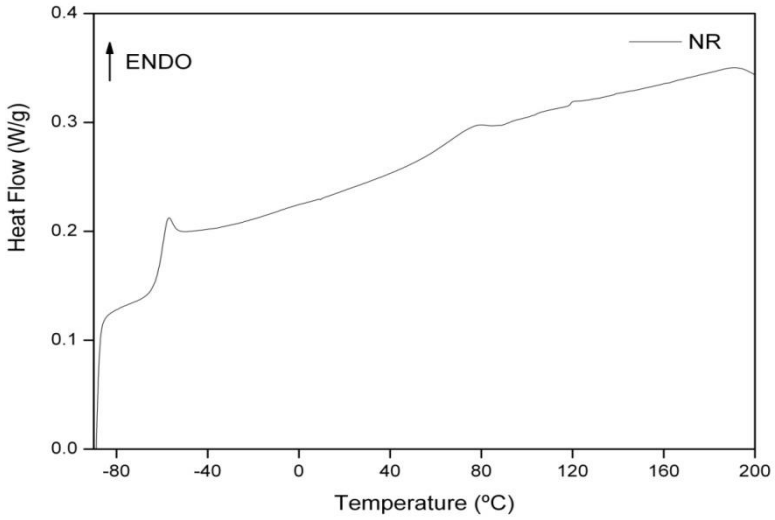

Figure A.1. DSC curve of NR sample taken at 10ºC.

A.1.2. *Thermal Gravimetric Analysis (TGA)*

Thermal degradation measurements were performed using a Mettler Toledo thermogravimetric analyzer (*TGA, model SDTA 851*). The temperature programs were run from 30 ºC to 800 ºC at a heating rate of 10 ºC/min in oxygen atmosphere (20 ml/min).

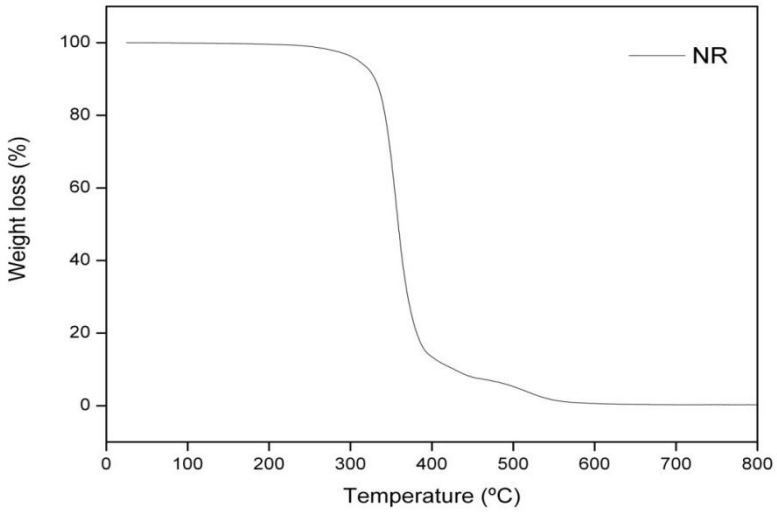

Figure A.2. TGA curve of NR sample.

A.1.3. *Nuclear Magnetic Resonance (NMR)*

Solid-state ^{13}C NMR measurements were performed in a *Bruker Avance 400* spectrometer equipped with a 89 mm wide bore, 9.4 T superconducting magnet (^{1}H and ^{13}C Larmor frequencies at 400.14 and 100.61 MHz, respectively). The data were acquired at room temperature, with a standard Bruker double resonance 4 mm cross-polarization (CP)/magic angle spinning (MAS) NMR probe head using 90º ^{1}H and ^{13}C pulse lengths between 3.1 and 4.5 μs. The MAS spinning rate was 5.0 kHz. The rubber sample was cut in small pieces and packed in a 4 mm zirconia rotor and sealed with Kel-F cap. The ^{13}C CP/MAS NMR spectrum was obtained by averaging 1500 scans, contact time of 1 ms, and repetition rate of 3 s. The free induction decay (FID) was processed using the spectrometer manufacturer's software. The spectrum was externally referenced to adamantane, secondary to TMS.

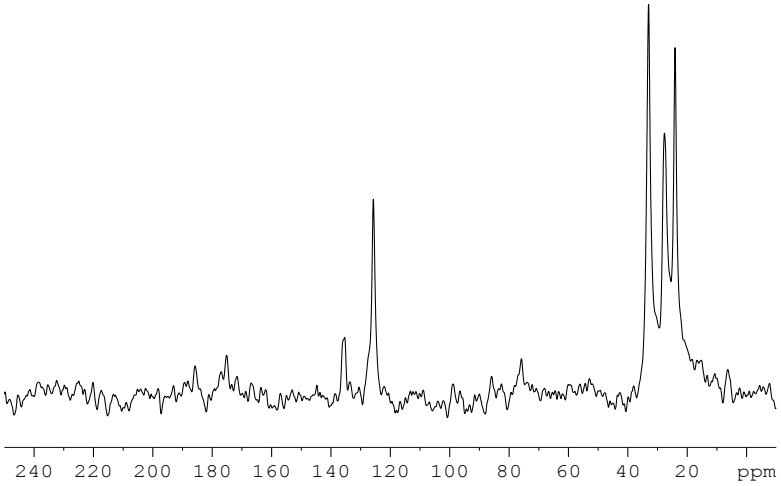

Figure A.3. ^{13}C NMR spectrum for NR sample.

APPENDIX B

B.1. Determination of Cross-linking Density of Natural Rubber

The average mass of network chains between cross-links (cross-linking density) was determined on the basis of solvent-swelling measurements by application of the Flory–Rehner equation (B.1) and assuming the formation of 4-functional cross-links during the vulcanization reaction:

$$\ln(1-\Phi_r)+\Phi_r+\chi\Phi_r^2=-\frac{\rho_r}{M_c}V_s\left(\Phi_r^{1/3}-\frac{2\Phi_r}{f}\right) \qquad \text{B.1}$$

where:

Φ_r= volume fraction of swollen polymer

χ= polymer-solvent interaction parameter (0.8 for NR-toluene)

ρ_r= rubber density

M_c= molecular weight of polymer between two crosslinks

V_s= molar volume of solvent (106.2 mL/mol for toluene)

f= functional cross-links

The volume fraction (Φ_r) of swollen polymer was calculated according to:

$$\Phi_r=\frac{w_i/\rho_r}{w_i/\rho_r+(w_s-w_d)/\rho_s} \qquad \text{B.2}$$

where:

w_i= initial weight of the sample

w_s= swollen weight of the sample

w_d= weight of the dried sample after evaporation of the solvent

ρ_s= solvent density (0.87 g/cm^3 for toluene)

Rubber density (ρ_r) was measured using the hydrostatic weighing method and applying the Archimedes principle:

$$\rho_r = \frac{w_{air}\rho_{water} - w_{water}\rho_{air}}{0.99983(w_{air} - w_{water})} \quad \text{B.3}$$

where w_{air} and w_{water} are the weight of the sample in air and immersed in water, ρ_{water} and ρ_{air} values at 21ºC are 0.9977 g/cm^3 and 0.0012 g/cm^3 respectively, and 0.99983 is a geometric balance correction.

The cross-linking density (ν_r) is then calculated as:

$$\nu_r = \frac{1}{2M_c} \quad \text{B.4}$$

APPENDIX C

C.1 Publications related to this Doctoral Thesis:

- Hernández Marianella, Ezquerra Tiberio A., López-Manchado Miguel A, Effects of Orientation on the Segmental Dynamics of Natural Rubber, *Materials Science Forum* **2012**, 714, 57-61.

- Marianella Hernández, Tiberio A. Ezquerra, Raquel Verdejo, Miguel A. López-Manchado, Role of Vulcanizing Additives on the Segmental Dynamics of Natural Rubber, *Macromolecules* **2012**, 45(2), 1070-1075.

- Raquel Verdejo, Marianella Hernández, Natacha Bitinis, Jose M. Kenny, Miguel A. López Manchado, Vulcanization Characteristics and Curing Kinetics of Rubber-Organoclay Nanocomposites, Chapter 9 in "*Rubber-Clay Nanocomposites*", ed. Maurizio Galimberti, John Wiley & Sons, **2011**, ISBN: 978-0-470-56210-9.

- Natacha Bitinis, Marianella Hernández, Raquel Verdejo, José M. Kenny, Miguel A. López-Manchado, Recent Advances in Clay/Polymer Nanocomposites, *Advanced Materials* **2011**, 23, 5229–5236.

- Marianella Hernández, Miguel A. López-Manchado, Alejandro Sanz, Aurora Nogales, Tiberio A. Ezquerra, Effects of Strain Induced Crystallization on the Segmental Dynamics of Vulcanized Natural Rubber, *Macromolecules* **2011**, 44(16), 6574–6580.

- Marianella Hernández, Javier Carretero-González, Raquel Verdejo, Tiberio A. Ezquerra, Miguel A. López-Manchado, Molecular Dynamics of Natural Rubber/Layered Silicate Nanocomposites as Studied by Dielectric Relaxation Spectroscopy, *Macromolecules* **2010**, 43(2), 643-651.

- Javier Carretero-González, Haris Retsos, Emmanuel P. Giannelis, Tiberio A. Ezquerra, Marianella Hernández, Miguel A. López-Manchado, Miscibility-Dispersion, Interfacial Strength and Nanoclay Mobility Relationships in Polymer Nanocomposites, *Soft Matter* **2009**, 5, 3481-3486.

C.2 Other Publications:

- M. Martín-Gallego, M. Hernández, V. Lorenzo, R. Verdejo, M.A. Lopez-Manchado, M. Sangermano, Cationic Photocured Epoxy Nanocomposites Filled With Different Carbon Fillers, *Polymer* **2012**, 53, 1831-1838.

- Laura J. Romasanta, Marianella Hernández, Miguel A. López-Manchado and Raquel Verdejo, Functionalised Graphene Sheets as Effective High Dielectric Constant Fillers, *Nanoscale Research Letters* **2011**, 6:508.

C.3 Oral Contributions:

- Effects of Orientation on the Segmental Dynamics of Natural Rubber, *Multiphase Polymers and Polymer Composites: From Nanoscale to Macro Composites Conference*. Paris, June **2011**.

- Effects of Strain Induced Crystallization on the Dielectric Behavior of Natural Rubber, *6th International Conference on Broadband Dielectric Spectroscopy and its Applications*. Madrid, September **2010**.

- Estudio de la Dinámica Molecular de Nanocompuestos de Caucho Natural y Organoarcillas Mediante Espectroscopia Dieléctrica, *XI Reunión del Grupo Especializado de Polímeros GEP´ 09*. Valladolid, September **2009**.

Materials Science Forum Vol. 714 (2012) pp 57-61
© (2012) Trans Tech Publications, Switzerland
doi:10.4028/www.scientific.net/MSF.714.57

Effects of Orientation on the Segmental Dynamics of Natural Rubber

HERNANDEZ Marianella[1, a], EZQUERRA Tiberio A.[2,b] and LOPEZ-MANCHADO Miguel A.[1,c]

[1]Instituto de Ciencia y Tecnología de Polímeros (CISC), Juan de la Cierva 3, Madrid 28006, Spain

[2]Instituto de Estructura de la Materia (CSIC), Serrano 121, Madrid 28006, Spain

[a]marherna@ictp.csic.es, [b]imte155@iem.cfmac.csic.es, [c]lmanchado@ictp.csic.es

Keywords: natural rubber, segmental dynamics, strain-induced crystallization, dielectric spectroscopy.

Abstract. The effects of orientation on the segmental dynamics of vulcanized natural rubber have been studied by dielectric relaxation spectroscopy. Morphological changes during the stretching process were also investigated by wide-angle X-ray scattering using a synchrotron radiation. Results reveal that segmental dynamics of NR is affected by uniaxial stretching since a slowing down of the segmental relaxation is achieved. Also, there is evidence of an amorphous/semi-crystalline transition around 300% strain; below this extension, molecular chains show orientation, but no crystallization takes place; while above such strain, the crystalline structure formed limits the segmental dynamics of NR.

Introduction

Natural rubber (NR) is a well studied elastomer. Of particular interest is the ability of NR to crystallize, specifically the strain-induced crystallization that takes place whilst the material is stretched. Moreover, in many elastomer applications, network chain dynamics under external stress/strain are critical for determining ultimate performance. Thus, a study on how the strain-induced crystallization affects the dynamics of a rubbery material is of outmost importance. Lee et al [1] reported their initial findings on the role of uniaxial extension on the relaxation behavior of cross-linked polyisoprene by means of dielectric spectroscopy. Nonetheless, to our best knowledge no in-depth study of the effects of strain induced crystallization on the molecular dynamics of NR has been undertaken, analyzing the relaxation spectra and correlating the molecular motion of chains with its structure. Broadband dielectric spectroscopy (BDS) has been chosen in order to study the dynamic features of segmental dynamics, because it is a comparatively simple technique for the analysis of the relaxation behaviour over a suitable frequency interval. This study is important from a basic and practical point of view, since an elongated crosslinked polymer at equilibrium may be considered as a new anisotropic material whose distribution of relaxation times could be affected by the orientation of the chains.

The present research studies the effect of orientation on the segmental dynamics as a function of the stretching ratio, focusing on the study of the relationship between the network structure and the strain-induced crystallization behavior of vulcanized NR using BDS. Morphological changes during the drawing process are also investigated by X-ray scattering.

Polymer 53 (2012) 1831–1838

Contents lists available at SciVerse ScienceDirect

Polymer

journal homepage: www.elsevier.com/locate/polymer

Cationic photocured epoxy nanocomposites filled with different carbon fillers

M. Martin-Gallego [a,**], M. Hernández [a], V. Lorenzo [b], R. Verdejo [a], M.A. Lopez-Manchado [a], M. Sangermano [c,*]

[a] Instituto de Ciencia y Tecnología de Polímeros, ICTP-CSIC, Juan de la Cierva 3, 28006 Madrid, Spain
[b] Univ Politecnica Madrid, ETS Ingenieros Industriales, Jose Gutierrez Abascal 2, 28006 Madrid, Spain
[c] Politecnico di Torino, Dipartimento di Scienza Applicata e Tecnologia, C.so Duca degli Abruzzi 24, 10129 Torino, Italy

ARTICLE INFO

Article history:
Received 3 January 2012
Received in revised form
17 February 2012
Accepted 27 February 2012
Available online 5 March 2012

Keywords:
Carbon fillers
Nanocomposites
Epoxy resins

ABSTRACT

In this work, the effect of several carbon fillers, exfoliated graphite (EG), functionalized graphene sheets (FGS), multi-walled carbon nanotubes (MWCNTs), and oxidized multi-walled carbon nanotubes (f-MWCNTs), were compared on the curing process and physical properties of a cationically photocurable epoxy resin. The extent of the photopolymerization was monitored by Real-Time FTIR spectroscopy. It was found that all the nanofillers delayed the curing reaction probably due to a shielding effect as well as to an increase of the resin viscosity. All the systems showed an electrical percolation threshold, but with MWCNTs was attained at a lower concentration (<0.1 wt.%). In addition, FGS showed the best response in terms of the dynamic mechanical and microindentation performances. An increase of more than 20 °C in the glass transition temperature was observed with the addition of 1 wt.% of FGS.

1. Introduction

Polymer nanocomposite coatings are attracting great attention in recent decades due to the possibility of adding valuable properties to the matrix. This multifunctionality is essential since polymer coatings should not only meet decorative or protective functions, they should also provide other requirements like electrostatic discharge, high mechanical performance, large operating temperature range and chemical resistance among others [1]. One approach to reach these features is the addition of nanofillers with remarkable mechanical, electrical and thermal properties. In this sense, carbon based nanofiller like carbon nanotubes (CNTs), functionalized graphene sheets (FGS) and expanded graphite (EG) appear as promising candidates for the reinforcement of polymer matrices [2,3].

Numerous reports have already demonstrated the positive effects of CNTs and graphite on epoxy resins [3,4]. Graphene is following the same trend in the last years [5], but just a few of them are related to UV-photocured nanocomposites [6,7]. Nowadays, UV-curing processes are becoming a very reliable alternative to the thermal process due to their particular characteristics [8]: fast transformation of the liquid monomer into a thin solid crosslinked coating with taylored physical and chemical properties without the need of using a solvent, so they are considered as environmental friendly processes. This technique is usually performed at room temperature allowing us to save energy. Furthermore, the use of the cationic photopolymerization provides other advantages compared to the radical one [9].

In this work, we focus on the effect of several carbon based nanofiller on the curing reaction of a photocurable epoxy resin by evaluating the photopolymerization process in real time. We also analyzed the influence of the structural parameters of the carbon nanofillers, such as geometry, structure and chemical composition on the conductivity, dielectric permittivity, percolation threshold and reinforcing effect on epoxy nanocomposites.

2. Experimental section

2.1. Materials

The UV-curable epoxy resin was the bis-cycloaliphatic diepoxy resin 3,4-epoxycyclohexylmethyl-3′,4′-epoxycyclohexyl carboxylate (CE) and the triphenylsulfonium hexafluoroantimonate ($Ph_3S^+SbF_6$) was used as photoinitiator. Both products were purchased from Sigma–Aldrich and used as received without any further purification.

* Corresponding author. Tel.: +39 0110904651.
** Corresponding author. Tel.: +34 912587424.
E-mail addresses: m.martingallego@ictp.csic.es (M. Martin-Gallego), marco.sangermano@polito.it (M. Sangermano).

0032-3861/$ – see front matter © 2012 Elsevier Ltd. All rights reserved.
doi:10.1016/j.polymer.2012.02.054

Macromolecules

Article

pubs.acs.org/Macromolecules

Role of Vulcanizing Additives on the Segmental Dynamics of Natural Rubber

Marianella Hernández,*[,†] Tiberio A. Ezquerra,[§] Raquel Verdejo,[†] and Miguel A. López-Manchado*[,†]

[†]Instituto de Ciencia y Tecnología de Polímeros, ICTP-CSIC, Juan de la Cierva 3, Madrid 28006, Spain

[§]Instituto de Estructura de la Materia, IEM-CSIC, Serrano 119, Madrid 28006, Spain

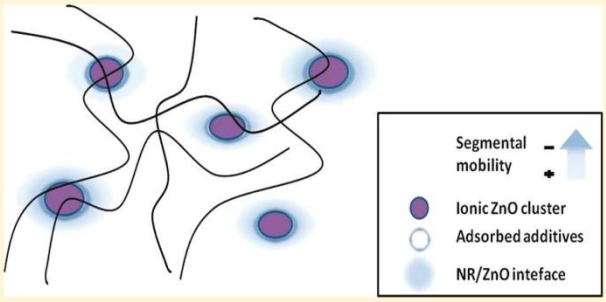

ABSTRACT: The influence of the addition of vulcanizing additives on the molecular dynamics of unvulcanized natural rubber (NR) has been studied by broadband dielectric spectroscopy. Results reveal a slowdown of the segmental dynamics of NR, restricting the motion of the chains tightly bounded to the additive surfaces. In general, when zinc oxide is present a second dynamic process is detected, ascribed to strong interfacial interactions between the zinc ionic clusters and the NR polymer segments. The study of such interactions prior to vulcanization is a very useful strategy to control the vulcanization process, maximizing its benefits and, hence, improving the final products. Here, we demonstrate that broadband dielectric spectroscopy is a good experimental alternative in order to obtain a deeper insight into the vulcanization mechanisms. Furthermore, our results support one previously proposed sulfur vulcanization mechanism, in which molecules of accelerators, sulfur, and fatty acids are adsorbed on the zinc oxide surface.

INTRODUCTION

Natural rubber (NR) holds a unique place in rubber technology due to its outstanding tack and strength in the unvulcanized state; and high tensile strength and crack growth resistance once vulcanized.[1] For most applications, it is necessary to convert the rubbery linear polymer into a three-dimensional network in order to ensure a complete recovery after deformation. Such a network is the result of cross-linking, covalent bonding among some chain segments, by means of temperature and pressure in which an essentially fluid material is transformed into a fully elastic one. This process is commonly known as vulcanization.[1] The sulfur vulcanization is the traditional method for polydiene rubbers, including NR; however, although sulfur vulcanization is a very old large-scale industrial process, and has been considerably studied over the last several decades, a complete fundamental understanding of this complex chemical process remains a significant scientific challenge. A rigorous research effort continues today to unravel the mechanisms of the individual steps in the sulfur vulcanization process.[2,3] The difficulties encountered in this research field must be accredited to a combination of diversity and complexity. This process usually involves several chemicals such as a vulcanizing agent (sulfur (S)), an accelerator, and an activator complex formed by a fatty acid (stearic acid (SA)) and zinc oxide (ZnO). The situation is further complicated by the interaction of the accelerators and activators, each component influencing the reactivity of the other, and the way these interactions affect the vulcanization mechanism.

Plenty of literature[1,4−9] reveals that the addition of these chemicals in small quantities with respect to raw rubber affects the processability and the final properties of the vulcanized compounds. In general, the use of accelerators in combination with zinc activators has a pronounced effect on the speed of vulcanization and on the distribution of cross-links formed. Besides these, the durability of rubber articles as well as the physical properties, in particular the tensile strength, are very much improved by organic accelerators.

Nonetheless, the authors are struck by the fact that despite the enormous practical knowledge developed so far, a detailed description on how these constituents affect the molecular dynamics and related properties of unvulcanized NR is unknown and has not been reported until now. Moreover,

Received: October 17, 2011
Revised: November 29, 2011
Published: December 20, 2011

CHAPTER 9

VULCANIZATION CHARACTERISTICS AND CURING KINETIC OF RUBBER–ORGANOCLAY NANOCOMPOSITES

Q1 R. VERDEJO
M. HERNANDEZ
N. BITINIS
J. M. KENNY
M. A. LOPEZ-MANCHADO

9.1 INTRODUCTION

Unvulcanized raw rubbers are entangled high molecular weight viscoelastic liquids, generally not very strong, sticky, easily deformed when warm, brittle when cold, that do not maintain their shape after a large deformation. They are completely soluble in solvents, have a consistency similar to chewing gum and give rise to inelastic deformation being made of long polymeric chains that can move independently to each other. An uncured rubber cannot be used to make articles with a good level of elasticity.

The transformation to a useful rubber article such as tires and mechanical goods is due to the discovery of the vulcanization process by Goodyear [1]. In this process, physical and chemical cross-links are formed between the polymer chains giving rise to the formation of a three-dimensional network structure. The long rubber chains with molecular weight of the order of 1×10^5 g/mol are cross-linked at many points along their length, producing 10–20 cross-links per primary molecule, so that the chains can no longer move independently. As a result, viscoelastic liquids are converted to viscoelastic solids with a high elasticity. They are prone to suffer considerable deformation under stress but upon release of the stress, the rubber article can go back to its original shape, recovering the energy stored during the

Rubber-Clay Nanocomposites: Science, Technology, and Applications, First Edition.
Edited by Maurizio Galimberti.

Romasanta et al. Nanoscale Research Letters 2011, 6:508
http://www.nanoscalereslett.com/content/6/1/508

Nanoscale Research Letters
a SpringerOpen Journal

NANO EXPRESS Open Access

Functionalised graphene sheets as effective high dielectric constant fillers

Laura J Romasanta, Marianella Hernández, Miguel A López-Manchado and Raquel Verdejo*

Abstract

A new functionalised graphene sheet (FGS) filled poly(dimethyl)siloxane insulator nanocomposite has been developed with high dielectric constant, making it well suited for applications in flexible electronics. The dielectric permittivity increased tenfold at 10 Hz and 2 wt.% FGS, while preserving low dielectric losses and good mechanical properties. The presence of functional groups on the graphene sheet surface improved the compatibility nanofiller/polymer at the interface, reducing the polarisation process. This study demonstrates that functionalised graphene sheets are ideal nanofillers for the development of new polymer composites with high dielectric constant values.
PACS: 78.20.Ci, 72.80.Tm, 62.23.Kn

Keywords: dielectric properties, graphene, interfacial polarisation, nanocomposites, silicones

Introduction

In recent years, elastomeric materials with high dielectric constant have been considered for different functional applications such as artificial muscles, high charge-storage capacitors and high-K gate dielectric for flexible electronics [1,2]. Several methods have been explored in order to increase their dielectric permittivity although the most common approach involves the addition of high dielectric constant ceramics to the elastomeric matrix. This strategy usually requires high loading fractions and, hence, produces an unwanted increase of the system rigidity for the applications already mentioned [3-5]. In some other cases, dielectric constant increments have been met with relatively high loss tangent values (tg (δ)) and frequency dependence which is also undesirable for capacitor applications [6,7]. Obtaining composites with both high dielectric permittivity and low loss tangent values at the same time is specially challenging due the interfacial polarisation or Maxwell-Wagner-Sillars (MWS) process. This mechanism occurs at the interface between materials with different permittivities and/or conductivities and involves rather high ε' and tg (δ) values at low frequencies due to the accumulation of virtual charges at the filler/polymer interface [8]. Altering the interfacial interaction between filler and polymer matrix can regulate the dielectric contrast between matrix and filler and thus, prevent the MWS polarisation [9-11]. Therefore, chemical modification of filler particles has to be taken into account in order to achieve high permittivity composites with low dielectric losses. Nevertheless, filler surface modifications can significantly raise the production costs and thus, make them unfeasible to be produced on large scale.

Thermally expanded graphene sheets are of great interest to overcome the aforementioned problems. The thermal reduction of the graphite oxide has the advantage to produce chemically modified graphene sheets (or so-called functionalised graphene sheets FGS) without the need of further modification steps. Besides, the huge aspect ratio of these carbon-based nanoparticles (experimental value 1850 $m^2 g^{-1}$) [12] reduces considerably the percolation threshold compared to any other type of high dielectric constant filler. Accordingly, very small loading fractions can offer interesting permittivity enhancements without adversely affecting the dielectric losses and mechanical properties of a given polymer matrix.

In this work, as-produced carbon nanotubes (CNTs) and thermally expanded graphene sheets are compared for their possible enhancing effect on an elastomer dielectric response. Results show that FGS are an ideal candidate as high dielectric constant fillers in capacitor applications. The presence of remaining functional

* Correspondence: rverdejo@ictp.csic.es
Instituto de Ciencia y Tecnología de Polímeros, ICTP-CSIC, Juan de la Cierva 3, 28006, Madrid, Spain

Materials Views
www.MaterialsViews.com

ADVANCED MATERIALS
www.advmat.de

Recent Advances in Clay/Polymer Nanocomposites

*N. Bitinis, M. Hernandez, R. Verdejo, J. M. Kenny, and M. A. Lopez-Manchado**

Smectite clays (e.g. montmorillonite), belonging to the structural family called 2:1 phyllosilicates, are the main choice for designing polymer nanocomposites due to their low cost and rich intercalation chemistry allowing them to be chemically modified (organoclays) and to improve the compatibility with the polymer matrix. These hybrid materials, normally called polymeric nanocomposites (PNC), represent a radical alternative to conventional polymer composites and have focused the attention of both academia and industry because of their unexpected properties, and their straightforward synthesis and processing. Such materials on the nanoscale level show significant improvements in mechanical properties, heat distortion temperatures, thermal stability, flame retardancy and enhanced barrier properties. The combination of enhanced properties, weight reduction, and low cost has led to interesting commercial applications such as automotive and packaging, among others. All this justifies the growing interest of both academia and industry in the development of these hybrid materials. In this paper we describe the most significant findings in the clay/polymer nanocomposites field considering three polymer families: elastomers, thermosets and polymers from natural resources or biopolymers.

1. Introduction

Composite materials represent one of the most active fields in the polymer industry. Many different types of fillers, carbon black, calcium carbonate, glass fibres and talc in the micrometer size range have been added to polymers to provide an improvement of the final product properties. However, this improvement is only achieved at high filler concentrations, which lead to an increase in the viscosity of the material and, hence, problems in processing. In recent years, it has been observed that the addition of just a small quantity of nano-sized layered silicates greatly improved the properties of virgin polymers without affecting their processability. Layered silicate clays have been found to be effective reinforcing fillers for polymers due to their lamellar structure and high aspect ratio of about 750 m^2/g. Smectite clays (e.g. montmorillonite), belonging to the structural family called 2:1 phyllosilicates, are the main choice for designing polymer nanocomposites due to their low cost and rich intercalation chemistry allowing them to be chemically modified (organoclays) and to improve the compatibility with the polymer matrix. These hybrid materials, normally called polymeric nanocomposites (PNC), represent a radical alternative to conventional polymer composites and have focused the attention of both academia and industry because of their unexpected properties, and their straightforward synthesis and processing.[1] The ideal design of a nanocomposite involves individual silicate layers (1 nm thick) homogeneously dispersed in a continuous polymer. The uniform dispersion of nanoelements can lead to an ultra-large interfacial area between the constituents per volume of material. Thus, in PNCs with only a low volume percentage of dispersed nanoparticles, the entire polymer matrix may be considered to be a nanoscopically confined interfacial polymer. Such materials on the nanoscale level show significant improvements in mechanical properties, heat distortion temperatures, thermal stability, flame retardance and enhanced barrier properties. The combination of enhanced properties, weight reduction, and low cost has led to interesting commercial applications such as automotive and packaging, among others. All this justifies the growing interest of both academia and industry in the development of these hybrid materials.

We will now describe the most significant findings in the clay/polymer nanocomposites field considering three polymer families: elastomers, thermosets and from natural resources or biopolymers.

2. Elastomer Nanocomposites

Rubbers, or most specifically called elastomers, are one of the most important commercial polymers. They are formed by long chains with molecular weights of the order of 1×10^5 g/mol crosslinked at many points along their length, producing 10–20 crosslinks per primary molecule, giving rise to the formation of a three-dimensional network structure. Their main characteristic is the ability to suffer considerable deformation under stress but upon release of the stress, the rubber article will go back to its original shape, recovering the energy stored during the deformation.

The elastomers are soft and weak materials with a low modulus and strength, so they usually require the inclusion of fillers in order to get a substantial improvement in the physical and mechanical properties of the compound. A wide range of fillers have traditionally been used in the rubber industry, being carbon black and silica the main fillers used in compounding recipes. However, a minimum of 20–30 wt% of conventional fillers is

N. Bitinis, M. Hernandez, Dr. R. Verdejo, Dr. J. M. Kenny, Dr. M. A. Lopez-Manchado
Instituto de Ciencia y Tecnologia de Polimeros
ICTP-CSIC, Juan de la Cierva, 3 28006-Madrid, Spain
E-mail: lmanchado@ictp.csic.es

DOI: 10.1002/adma.201101948

Macromolecules

ARTICLE

pubs.acs.org/Macromolecules

Effects of Strain-Induced Crystallization on the Segmental Dynamics of Vulcanized Natural Rubber

Marianella Hernández,*[,†] Miguel A. López-Manchado,[†] Alejandro Sanz,[‡] Aurora Nogales,[‡] and Tiberio A. Ezquerra*[,‡]

[†]Instituto de Ciencia y Tecnología de Polímeros, ICTP-CSIC, Juan de la Cierva 3, Madrid 28006, Spain

[‡]Instituto de Estructura de la Materia, IEM-CSIC, Serrano 121, Madrid 28006, Spain

Supporting Information

ABSTRACT: The effects of strain-induced crystallization on the segmental dynamics of vulcanized natural rubber (NR) have been studied by combining dielectric relaxation spectroscopy and wide-angle X-ray scattering. Segmental dynamics is clearly affected by uniaxial stretching. For low strains, $\lambda < 3$, stretching takes place without crystallization. However, a dramatic increase of the dielectric strength, $\Delta\varepsilon$, is observed which has been explained by an increase of the effective dipole moment upon stretching. This effect is accompanied by an increment of the fragility parameter, m, since as free volume reduces by stretching more cooperativity is needed in order to accomplish segmental motions. For $3 < \lambda < 7.5$, crystals develop and the inclusion of segments into the crystalline phase counteracts the increment in $\Delta\varepsilon$ provoked by stretching. Our results support a previous morphological model indicating that during strain-induced crystallization shorter chains are progressively incorporated into the crystals while a significant amount of longer chains remains rather coiled.

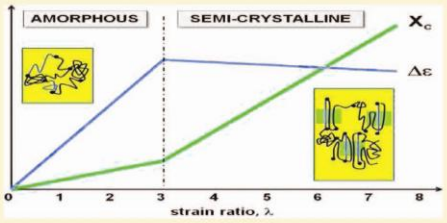

1. INTRODUCTION

Natural rubber (NR) has been recognized as a fascinating industrial material that has both high elasticity and tensile strength. It is one of the most important natural materials which has been widely used in industry as well as in our daily life, e.g., pneumatic tires, tubes, films like surgical gloves, rubber bands, etc. This versatility is derived from its toughness based on the outstanding tensile properties and excellent crack growth resistance.[1−4]

Moreover, the good performance of vulcanized NR products has been thought to originate from the ability to crystallize when subjected to an extensional field. The enhancement of tensile modulus along with the superior stress at break and tear strength under fast deformation should be related to the formation of strain-induced crystals. These crystals, embedded into an amorphous phase, are tens of nanometers in size and may orient themselves in response to macroscopic loading. From the point of view of composite materials, the crystals act like fillers which form in situ upon deformation.[1,5−7] Such strain-induced crystallites form an additional physical cross-linking network, carrying most of the applied load. For this reason strain-induced crystallization of NR still attracts a lot of interest.[2,8−12]

In many elastomeric applications, network chain dynamics under external stress/strain are critical for determining ultimate performance. Thus, a study on how the strain-induced crystallization affects the dynamics of a rubbery material is of outmost importance. Lee et al.[13] reported their initial findings on the role of uniaxial extension on the relaxation behavior of cross-linked polyisoprene (PI) by means of dielectric spectroscopy. They found that the segmental process of lightly cross-linked PI is not affected by uniaxial deformation up to an extension ratio below $\lambda = 4$. Nonetheless, to our best knowledge no in-depth study of the effects of strain induced crystallization on the molecular dynamics of vulcanized NR has been undertaken. In particular, it remains unknown the interrelationship between molecular dynamics and deformation in vulcanized NR. Broadband dielectric spectroscopy (BDS) has been proven to be a powerful technique to investigate both segmental and chain dynamics of natural and synthetic rubbers.[14−16] In addition, the combination of BDS with X-ray scattering techniques has revealed as an efficient approach to deal with order−dynamics relationships.[17,18] The main objective of the present work is to understand the effect of strain-induced orientation on the segmental dynamics of vulcanized NR. We have focused our study in the effect of network structure and the strain-induced crystallization, as investigated by synchrotron X-ray scattering, in the segmental dynamics of NR assessed by BDS.

2. EXPERIMENTAL SECTION

2.1. Materials. Natural rubber (NR) (composed of *cis*-1,4-isoprene units[19]) was kindly supplied by Malaysian Rubber (Berhad, Malaysia)

Received: May 4, 2011
Revised: June 28, 2011
Published: July 28, 2011

Macromolecules
ARTICLE

Macromolecules **2010**, *43*, 643–651 **643**
DOI: 10.1021/ma902379t

Molecular Dynamics of Natural Rubber/Layered Silicate Nanocomposites As Studied by Dielectric Relaxation Spectroscopy

Marianella Hernández,*,†,‡ Javier Carretero-González,‡ Raquel Verdejo,‡ Tiberio A. Ezquerra,§ and Miguel A. López-Manchado*,‡

†*Universidad Simón Bolívar, Departamento de Mecánica, Valle de Sartenejas, Caracas 1081, Venezuela,* ‡*Instituto de Ciencia y Tecnología de Polímeros, CSIC, Madrid 28006, Spain, and* §*Instituto de Estructura de la Materia, CSIC, Madrid 28006, Spain*

Received October 26, 2009; Revised Manuscript Received December 4, 2009

ABSTRACT: The segmental chain dynamics in nonvulcanized and vulcanized natural rubber/layered silicate nanocomposites has been studied by dielectric relaxation spectroscopy. Special consideration has been devoted to the effect of clay type and loading on the time scale of the relaxation processes. Results reveal that the type and concentration of clay do not have an effect on the segmental mode of the NR matrix, while the vulcanization reaction slows down the segmental dynamics. A new mode, slower than the segmental dynamics but faster than the normal mode associated with the chain dynamics, has been observed for both vulcanized and nonvulcanized nanocomposites with fillers having high levels of intercalation. We attribute the new mode to a restricted segmental dynamics of natural rubber chains located at the clay/rubber interfacial regions.

1. Introduction

Nanotechnology is recognized as one of the most promising fields of research of the 21st century. The beginning of nanotechnology and nanoscience research can be traced back over 40 years. However, it was in the past decade that the world witnessed bigger strides of this technology from both academic and industrial points of view.[1−4]

The term "nanocomposite" refers to every type of composite material having fillers in the nanometer size range, at least in one dimension. For such nanocomposites the total interfacial phase becomes the critical parameter, rather than the volume fraction of the filler.[5−7] Because of their nanofillers dispersion, nanocomposites exhibit markedly improved mechanical, thermal, electrical, and gas barrier properties, when compared to pure polymers or their traditional composites. The most common nanosized fillers are inorganic clay minerals consisting of nanolayered silicates. The stacking of the layers of ∼1 nm thickness by weak dipolar forces leads to interlayers or galleries between the layers. These galleries are occupied by cations such as Na^+ and Ca^{2+} which can be replaced by organic cations such as alkylammonium cations via ion exchange reaction rendering to obtain hydrophobic surfaces. This ion exchange produces organophilic clays called organoclays which are more compatible with the polymer.[8,9] The literature search shows that several research groups have prepared nanocomposites based on plastics and rubbers with nanoclays. In particular, rubber/layered silicate nanocomposites are increasingly attracting scientific and technological attention because of the high reinforcing efficiency of the nanosilicate, even at very low loading (< 10 wt %).[10−13] Without the filler, rubber formulations would yield resilient products having elastic properties but very little strength. So, strength properties are introduced by the addition of rigid entities such as nanosilicates, and the inclusion of these nanofillers to rubber formulations results in optimization of properties, especially to meet given application or sets of performance parameters. The high specific surface area is believed to be one of the reasons why the nature of reinforcement is different in composites based on nanofillers. It is expected to provide enhanced interphase effects and tensile strength. Nevertheless, there is yet no satisfactory theoretical explanation for the origin of improvement of the properties of polymer nanocomposites.[14,15] Results obtained by various experimental techniques, as well as by theory and computer simulations, indicate the presence of an interfacial polymer layer around the filler, with structure/morphology and chain dynamics modified with respect to the bulk polymer matrix.[7,15−17]

Broadband dielectric spectroscopy is a powerful tool for the investigation of molecular dynamics of polymers and composites. Dielectric property analysis of filled polymers contributes to a better understanding of the structure−property relationships at the morphological level. More specifically, in order to relate the macroscopic properties of nanocomposites with molecular concepts, one must understand the molecular motions or dynamics of these materials in response to various applied fields.

When placed in an electric field, nanocomposites are subjected to ionic, interfacial, and dipole polarization. These polarization mechanisms have considerable different time and length scales, making dielectric spectroscopy uniquely suited for the study of nanocomposite dynamics.[18] Therefore, motional processes which take place for polymeric systems on extremely different time scales can be investigated in a broad frequency and temperature range. Such motional processes can be localized fluctuations within a backbone segment or local rotational fluctuations of a short side chain. On a larger spatial and longer time scale and for temperatures above the glass transition the so-called segmental motion or α-relaxation becomes relevant. At more extended length scale, for polymers with a component of the dipole moment parallel to the chain, a further process can be observed called normal-mode relaxation, in which the translational motion of the whole chain characterized by the end-to-end vector takes place. In this case, the molecular dipole vectors that are parallel to

*Corresponding authors. E-mail: marherna@ictp.csic.es or marherna@usb.ve (M.H.); lmanchado@ictp.csic.es (M.A.L.-M.).

Published on Web 12/11/2009

PAPER www.rsc.org/softmatter | Soft Matter

Miscibility–dispersion, interfacial strength and nanoclay mobility relationships in polymer nanocomposites†

Javier Carretero-González,*[ab] Haris Retsos,[b] Emmanuel P. Giannelis,[b] Tiberio A. Ezquerra,[c] Marianella Hernández[a] and Miguel A. López-Manchado*[a]

Received 7th January 2009, Accepted 5th June 2009
First published as an Advance Article on the web 8th July 2009
DOI: 10.1039/b900295b

Fully dispersed layered silicate nanoparticles (nanoclay) in a polymer matrix have provided a new class of multi-functional materials exhibiting several performance improvements over conventional composites. Yet the challenges of miscibility and interfacial strength might prevent nanocomposites from realizing their full potential. In this paper we demonstrate the effect of the chemical characteristics of the nanoclay on the miscibility and dispersion in the polymer matrix as well as on the interfacial strength of the bound polymer and the nanoclay mobility, all of which determine the macroscopic properties of the nanocomposite.

Introduction

The effect of nanoscopic platelets of clay in the morphology of homopolymers,[1] block-copolymers[2] and polymer blends,[3] as well as on their dynamic processes[4–6] have been commonly attributed to the high aspect ratio of the rigid nanoclay layers and to the large interfacial contact area between the clay and the polymer matrix.[7] These effects have a profound impact on the mechanical properties of the nanocomposites due to nano-scale reinforcement. Despite these promising results, and continuous efforts by researchers worldwide to control the dispersion of nanoclay in the polymer, other aspects related to controlling the interfacial strength between the clay and the polymer and, thus, the properties of the nanocomposites remain a challenge.

Theoretical[8] and experimental[9] studies provide evidence that polymer and nanoparticle mobility prevents the failure of polymer nanocomposites during deformation by introducing an additional dissipative energy mechanism through the formation of temporary crosslinks between the polymer chains and the inorganic surface of the nanofiller. Although these studies conclude that the introduction of nanoparticles benefits the toughening and strengthening of polymeric matrices, the bound polymer also seems to play a key role in the material's intrinsic properties. This is likely to be a consequence of the large surface area of nanoclay exposed to the polymer molecules, leading to a huge interfacial volume around the nanofillers. Tong *et al.*[10] recently concluded that this model of nanoparticle mobility will only result in toughened plastics if both reduced interparticulate interactions and optima nanofiller/matrix interactions are guaranteed and accompanied by sufficient polymer mobility. Effective physical crosslinking thus requires high mobility and strong interaction between the nanoclay particles and the polymer, allowing them to move with the polymer chains during deformation.

In the present work we report the effect of the alkyl chain length, functionality and the grafting density of organic surfactant molecules, covering the surface of the nanoclay, on both the miscibility and the dispersion of nanoclay in natural rubber (NR) nanocomposites by means of X-ray diffraction (XRD) and transmission electron microscopy (TEM). In an effort to understand the role of the interfacial region and the mobility of the nanoclay in determining the properties of polymer nanocomposites, we have studied the polymer dynamics by means of broadband dielectric spectroscopy (BDS) and the microstructure under dynamic deformation by wide angle X-ray diffraction (WAXD). The anisotropic organoclay nanoparticles are aligned within the rubber matrix by stretching. This allows us to monitor microstructural changes, including crystallization, by *in situ* WAXD. Both the alignment capability and the interaction strength with the polymer matrix are ultimately determined by the chemical characteristics of the nanoclay. These two aspects are crucial in designing new types of high-strength polymer nanocomposites.

Most studies on organoclay/polymer nanocomposites focus on the effect that the extent of exfoliation has on the physical and mechanical properties of the material. However the improvement in polymer/NR matrices is dependent not only on the extent of exfoliation but also in other factors as the spatial distribution and orientation of the clay layers. A small degree of agglomeration results in an inevitable decrease in performance. In the first part of this work, we study which chemical features of the nanoclay can improve the miscibility between the polymer and the nanoclay, and so permit nanoparticle dispersions on different length scales. In the second part of the paper the interplay between interfacial strength and nanoparticle mobility in polymer nanocomposites is discussed.

[a]*Instituto de Ciencia y Tecnología de Polímeros, CSIC, Madrid 28006, Spain. E-mail: jcarretero@ictp.csic.es; lmanchado@ictp.csic.es*
[b]*Department of Material Science and Engineering, Cornell University, Ithaca, New York 14853, USA*
[c]*Instituto de Estructura de la Materia, CSIC, Madrid 28006, Spain*

† Electronic supplementary information (ESI) available: The dielectric loss values for unfilled and vulcanized NR and the unvulcanized NR containing 10 phr of Q-I nanoclay, and dielectric loss *versus* temperature for the nanocomposite containing 15 phr of Q-I nanoclay in the dry state and in the swollen state. See DOI: 10.1039/b900295b

RESUMEN

El siguiente documento es un amplio Resumen en español de la Tesis Doctoral titulada "**ESTUDIO DE LA DINÁMICA MOLECULAR DE NANOCOMPUESTOS DE CAUCHO NATURAL"**, cumpliendo con el art. 4.3 de la normativa de desarrollo del régimen relativo a elaboración, tribunal, defensa y evaluación de la tesis doctoral, del Real Decreto 1393/2007 de la Universidad Complutense de Madrid.

Esta Tesis Doctoral ha sido dividida en 7 capítulos. Como introducción al tema, el Capítulo I abarca una amplia revisión bibliográfica sobre nanocompuestos poliméricos, nanocompuestos de Caucho Natural y sobre el estudio de la dinámica molecular de nanocompuestos elastoméricos. En el Capítulo II se presenta de manera detallada los materiales y las técnicas de caracterización empleadas, así como los procedimientos experimentales seguidos para alcanzar los objetivos planteados.

Los elastómeros son sistemas complejos que consisten de una amplia variedad de aditivos como son los acelerantes, los activadores y los agentes de vulcanización, entre otros. Por lo tanto, el propósito del Capítulo III es obtener una visión detallada de cómo estos constituyentes pueden afectar la dinámica molecular del Caucho Natural. El Capítulo IV, por su parte, considera la dinámica de nanocompuestos de Caucho Natural y silicatos laminares, y el análisis de resultados en términos de cómo el tipo y contenido de carga pueden afectar la dinámica segmental y global de la matriz elastomérica. Adicionalmente, en este capítulo se estudia la influencia del proceso de vulcanización sobre la dinámica molecular de nanocompuestos elastoméricos. De manera análoga, los resultados obtenidos para nanocompuestos de Caucho Natural y nanocargas derivadas de carbono se discuten en el Capítulo V. En el Capítulo VI, se analiza el efecto de la orientación inducida por deformación sobre la dinámica segmental de Caucho Natural vulcanizado y de sus nanocompuestos. El estudio está enfocado en el efecto de la estructura de la red elastomérica y de la cristalización inducida por deformación sobre la dinámica segmental del Caucho Natural, a través de dispersión de rayos X por radiación sincrotrón y de espectroscopia dieléctrica.

Finalmente, el Capítulo VII abarca las conclusiones de la tesis y perspectivas futuras.

A lo largo del período de ejecución de esta Tesis Doctoral, y debido al rápido progreso en este campo de investigación en relación con los conceptos aquí presentados, fue necesario presentar parte de este trabajo para su publicación en revistas científicas internacionales. Las publicaciones son las siguientes:

- Hernández Marianella, Ezquerra Tiberio A., Lopez-Manchado Miguel A, Effects of Orientation on the Segmental Dynamics of Natural Rubber, *Materials Science Forum* **2012**, 714, 57-61.

- Marianella Hernández, Tiberio A. Ezquerra, Raquel Verdejo, Miguel A. López-Manchado; Role of Vulcanizing Additives on the Segmental Dynamics of Natural Rubber, *Macromolecules* **2012**, 45(2), 1070-1075.

- Raquel Verdejo, Marianella Hernández, Natacha Bitinis, Jose M. Kenny, Miguel A. López Manchado, Vulcanization Characteristics and Curing Kinetics of Rubber-Organoclay Nanocomposites, Chapter 9 in "Rubber-Clay Nanocomposites", ed. Maurizio Galimberti, John Wiley & Sons, **2011**, ISBN: 978-0-470-56210-9.

- Natacha Bitinis, Marianella Hernández, Raquel Verdejo, José M. Kenny, Miguel A. López-Manchado, Recent Advances in Clay/Polymer Nanocomposites, *Advanced Materials* **2011**, 23(44), 5229–5236.

- Marianella Hernández, Miguel A. López-Manchado, Alejandro Sanz, Aurora Nogales, Tiberio A. Ezquerra, Effects of Strain Induced Crystallization on the Segmental Dynamics of Vulcanized Natural Rubber, *Macromolecules* **2011**, 44(16), 6574–6580.

- Marianella Hernández, Javier Carretero-González, Raquel Verdejo, Tiberio A. Ezquerra, Miguel A. López-Manchado, Molecular Dynamics of Natural Rubber/Layered Silicate Nanocomposites as Studied by Dielectric Relaxation Spectroscopy, *Macromolecules* **2010**, 43(2),643-651.

- Javier Carretero-González, Haris Retsos, Emmanuel P. Giannelis, Tiberio A. Ezquerra, Marianella Hernández, Miguel A. López-Manchado, Miscibility-Dispersion, Interfacial Strength and Nanoclay Mobility Relationships in Polymer Nanocomposites, *Soft Matter* **2009**, 5(18), 3481-3486.

I. INTRODUCCIÓN

El trabajo de investigación aquí presentado se encuadra en el área de la Nanotecnología. Como su nombre indica, el término "nanotecnología" se aplica a la tecnología relativa a la escala nano, siendo éste el prefijo griego que denota la unidad correspondiente a la milmillonésima (10^{-9}) parte de algo. El comienzo de la investigación en el área de la nanotecnología y la nanociencia se remonta a hace más de 40 años y, hoy por hoy, esta área del conocimiento es reconocida como uno de los campos de la investigación más prometedores del siglo XXI. Específicamente, durante la última década, el mundo ha evidenciado grandes hallazgos desde el punto de vista industrial y académico debido al gran éxito en la síntesis de nanomateriales, así como en la disponibilidad de nuevas herramientas para su caracterización y manipulación.

La esencia de la nanotecnología es la habilidad para trabajar a nivel molecular con miras a crear grandes estructuras con una nueva organización molecular. Estas estructuras a escala nanométrica generalmente poseen propiedades diferentes e incluso superiores a las de sus pares macroscópicos. Un importante ejemplo dentro de los nanomateriales son los nanocompuestos. Un material nanocompuesto se caracteriza por estar constituido principalmente por una fase continua o matriz y, una fase dispersa con al menos una dimensión de tamaño

nanométrico, inmiscibles entre sí y separadas por una interfase.[6-8] Dentro del campo de la nanotecnología, los nanocompuestos de matrices poliméricas han adquirido gran interés en el ámbito científico e industrial. Es ampliamente reconocido que el hecho de introducir nanopartículas de geometrías diferentes como esferas, láminas o tubos en matrices poliméricas mejora significativamente las propiedades mecánicas como rigidez y resistencia tensil (a tracción) y al impacto; más aún, propiedades físicas como barrera ante gases, conductividad eléctrica y térmica, resistencia a la erosión y flamabilidad reducida también pueden ser alcanzadas. Así pues, el desarrollo de una tecnología de nuevos materiales que puedan actuar como compuestos alternativos de bajo costo y altas prestaciones para aplicaciones que van desde el sector de automoción hasta el envasado de alimentos y la biomedicina, se presenta como un hecho irresistible para los investigadores del mundo actual.

Hay ciertas características principales que definen y constituyen la base del comportamiento de los nanocompuestos: i) una matriz polimérica nanoscópicamente confinada, ii) un constituyente orgánico o inorgánico a nanoescala, y iii) un acoplamiento de estos constituyentes a nanoescala. La proliferación de interfases carga/polímero implica que la mayoría de las cadenas poliméricas se encuentran cerca de una superficie de carga. Dicha proximidad afectará al ordenamiento de las cadenas de polímeros y por tanto a su comportamiento de relajación molecular.

La segunda característica fundamental de los nanocompuestos viene determinada por las dimensiones de los nanoelementos incorporados. Al igual que las matrices poliméricas, cuando las dimensiones de los agregados o partículas se aproximan a la escala de longitud fundamental de una propiedad física (efecto de confinamiento), aparecen nuevas propiedades mecánicas, ópticas y eléctricas que no están presentes a nivel macroscópico.

De acuerdo a cuántas dimensiones de la fase dispersa se encuentren en el orden de los nanómetros, se pueden distinguir tres tipos diferentes de nanocompuestos[6]. Si las tres dimensiones de la partícula son nanométricas, la nanopartícula se define

como isodimensional. Ejemplo de este tipo de partículas son las nanopartículas de sílice esféricas.[14,15] Si dos de las dimensiones están en la escala de nanómetros, formando así una estructura alargada, se tienen los llamados nanotubos[16] o nanofibrillas ("whiskers").[17] A modo de ejemplo se pueden citar los nanotubos de carbono, los cuales han sido ampliamente estudiados como nanocargas, ya que permiten una mejora excepcional de las propiedades del material. El tercer tipo de nanocompuesto se caracteriza por tener sólo una dimensión en la escala nanométrica. En este caso la carga está en forma de láminas con espesor de pocos nanómetros mientras que mide cientos a miles de nanómetros en su longitud, por ejemplo los silicatos laminares y las láminas de grafenos.

En particular, los nanocompuestos elastoméricos han captado la atención de los investigadores debido a sus propiedades únicas. Es ampliamente conocido que dentro del campo de los elastómeros, las cargas se utilizan como refuerzos con el fin de lograr productos con propiedades mejoradas para aplicaciones específicas. Sin embargo, muchos aspectos relacionados con la naturaleza del reforzamiento en elastómeros siguen siendo, hoy por hoy, desconocidos. Adicionalmente, cuando el reforzamiento se logra con nanopartículas, resulta más difícil entender la relación entre la microestructura y sus propiedades. El carácter especial de los elastómeros, siendo un sistema multicomponente compuesto básicamente por caucho, agente de vulcanización, acelerantes (entre otros), complica el análisis de los parámetros que afectan la formación del compuesto elastómero/nanopartícula.

Un objetivo importante en el campo de los materiales compuestos es relacionar la dinámica molecular de estos materiales con su estructura, a su vez asociada con las propiedades físicas de éstos. El estudio de la dinámica molecular de materiales poliméricos resulta complejo debido a que, por la gran longitud de sus cadenas moleculares, exhiben una gran variedad de movimientos que pueden ir desde simples movimientos locales, vibracionales o rotacionales de átomos o grupos de átomos, hasta movimientos cooperativos de corto y largo alcance que involucran segmentos de la cadena molecular o incluso a toda ella. Más específicamente, si se trata de nanocompuestos poliméricos, el gran área interfacial y la alta relación superficie-volumen producen cambios inesperados en la dinámica molecular. En

consecuencia, no se puede predecir una simple relación entre la composición del polímero y las propiedades del material, debido a que son muchos los factores que afectan simultáneamente. El análisis de estas relaciones complejas, teniendo en cuenta todas las posibles contribuciones, requiere de técnicas analíticas complementarias a las herramientas tradicionales. Dentro de estas técnicas, se ha mostrado que la espectroscopia mecano dinámica, la resonancia magnética nuclear, y la espectroscopia dieléctrica son adecuadas para estudiar la dinámica de relajación de nanocompuestos poliméricos.

La espectroscopia dieléctrica es una de las técnicas de relajación más útiles para el estudio de la dinámica molecular de sistemas poliméricos debido al amplio intervalo dinámico cubierto que, en principio, puede extenderse desde 10^{-2} Hz hasta 10^{10} Hz. En espectroscopia dieléctrica el agente externo es un campo eléctrico, *E*, que origina la polarización del material produciendo diferentes tipos de respuestas como son: i) la polarización atómica debida a pequeños desplazamientos de átomos o grupos de átomos de la macromolécula, ii) la polarización electrónica que da lugar a dipolos inducidos por la distorsión de la nube electrónica de cada átomo con respecto al núcleo, y iii) la polarización orientacional debida a la reorientación de los dipolos permanentes en la dirección del campo eléctrico. Las polarizaciones atómica y electrónica están caracterizadas por una respuesta instantánea (menor que 10^{-13} s) independientemente de la temperatura. Por tanto, para la ventana de frecuencias empleadas en esta técnica, la polarización orientacional puede ser un instrumento muy útil para comprender el movimiento de las cadenas macromoleculares.

II. OBJETIVOS

En esta investigación se plantea como objetivo principal el estudio de la dinámica molecular de nanocompuestos de Caucho Natural (NR), con el fin de entender las relaciones físicas entre las diferentes fases e interfases presentes en el nanocompuesto y su implicación en la mejora de las propiedades finales del material.

A la vista de este objetivo general se pueden planificar una serie de objetivos específicos como son los siguientes:

- En primer lugar, estudiar el efecto de la presencia de aditivos de vulcanización sobre la dinámica de NR. Una explicación detallada de cómo estos aditivos afectan la dinámica molecular y sus propiedades relacionadas no ha sido reportada en la literatura. Por lo que un mayor conocimiento de la estructura y de la movilidad molecular será de gran utilidad para controlar de manera más precisa el proceso de vulcanización y para mejorar las prestaciones del material final.

- En segundo lugar, evaluar de manera detallada la dinámica molecular de nanocompuestos de NR por medio de la técnica de espectroscopia dieléctrica de banda ancha. A través del estudio de los modos segmental y normal del NR se puede evaluar cómo se ve afectada la dinámica del polímero y cómo se ve influenciado el proceso de vulcanización al variar la concentración y el tipo de nanopartícula (silicatos laminares, nanotubos de carbono y láminas de grafeno funcionalizadas) añadida a la matriz elastomérica.

- Finalmente, se estudia el fenómeno de "cristalización inducida por deformación uniaxial" presente en el NR. Es de sobra conocido que las estructuras cristalinas formadas pueden actuar como cargas reforzantes y ser responsables de las excepcionales propiedades de fatiga y resistencia de este material frente a sus homólogos sintéticos. Es por ello que se hace necesario analizar el efecto de la cristalización inducida por deformación sobre la dinámica segmental del NR y sus nanocompuestos a través de experimentos de espectroscopia dieléctrica y dispersión de rayos X.

III. CONCLUSIONES

Las siguientes conclusiones generales se pueden extraer de esta Tesis Doctoral:

- Los nanocompuestos de NR se caracterizaron de forma general (morfología, reometría y propiedades mecánicas), con el propósito de profundizar en el conocimiento de las propiedades físicas de los materiales aquí desarrollados. Los resultados mostraron que se mejoraron las propiedades mecánicas de los materiales cuando los silicatos laminares se encontraban homogéneamente dispersos en la matriz de caucho alcanzando una morfología exfoliada, en las que las cadenas de caucho se encuentran nanoscópicamente confinadas en las galerías del silicato, como en el caso de los nanocompuestos NR/organoarcilla (C15A). Adicionalmente, se observó que las láminas de grafeno funcionalizadas se comportaban como eficientes refuerzos para matrices elastoméricas. Estas mejoras han sido atribuidas a las fuertes interacciones caucho-carga, mientras que las diferencias en cuanto al desempeño entre los silicatos laminares y las cargas derivadas de carbono pueden explicarse en función a las distintas morfologías de las nanopartículas, fundamentalmente el tamaño de partícula, su área superficial y su estructura.

- Se pudo comprobar que la espectroscopia dieléctrica de banda ancha es una técnica idónea para el estudio de la dinámica molecular de nanocompuestos elastoméricos basados en NR. El espectro dieléctrico de NR no vulcanizado reflejó dos relajaciones, un modo segmental a bajas temperaturas, y un modo normal a altas temperaturas, mientras que en las muestras vulcanizadas únicamente se detectaba la relajación segmental.

- Con respecto al modo segmental de la matriz de NR no vulcanizada, no se evidenciaron cambios, independientemente de la cantidad y naturaleza de la carga en el compuesto. No obstante, el modo segmental se ralentizó en presencia de los aditivos de vulcanización, con la consecuente aparición de un segundo proceso dinámico más lento pero cercano al modo segmental del NR. Se propuso un modelo para explicar la presencia de este segundo proceso más

lento, en el cual los agregados de ZnO forman enmarañamientos físicos con las cadenas elastoméricas, actuando como precursores de la red de entrecruzamientos.

- En el espectro dieléctrico de los nanocompuestos NR/C15A apareció un "nuevo modo" asociado a una relajación segmental restringida. Este nuevo modo está ausente en el NR puro y en todos los otros nanocompuestos estudiados en esta investigación, bien con arcilla no modificada (CNa+) o con nanocargas derivadas de carbono (MWCNT, f-MWCNT y FGS). Tal relajación restringida ha sido atribuida a las cadenas poliméricas que se encuentran parcialmente inmovilizadas como una capa interfacial alrededor de las partículas del silicato. Estos resultados pioneros sirven para entender los efectos de reforzamiento en nanocompuestos de NR y silicatos laminares y por qué se logra tal reforzamiento con bajos contenidos de carga.

- Con respecto al modo normal, el principal efecto observado fue una dinámica acelerada en comparación con la del NR puro. Los resultados de los experimentos aquí desarrollados permitieron especular sobre la posibilidad de que los aditivos en general, tanto aditivos de vulcanización como nanocargas, perturban la red de entrecruzamientos físicos presentes en los extremos de cadena del NR, generando extremos libres que conllevan a movimientos de cadena más rápidos.

- También se evaluó la dinámica de NR y de nanocompuestos de NR vulcanizados. Los resultados indicaron que la vulcanización con azufre conlleva a una ralentización de la dinámica segmental, sin tener ningún tipo de dependencia con el tipo de nanocarga añadida a la matriz de NR. Adicionalmente, el proceso asociado a la dinámica global (modo normal) se ve suprimido como consecuencia de la formación de la red entrecruzada.

- Los efectos de la orientación en la dinámica molecular de NR vulcanizado se estudiaron a través de espectroscopia dieléctrica y dispersión de rayos X por radiación sincrotrón. Se encontró una transición de estado amorfo/semi-

cristalino a bajas deformaciones λ = 3.0. Por debajo de esta transición, las cadenas moleculares mostraron orientación sin llevarse a cabo la cristalización, y el esfuerzo dieléctrico incrementó dramáticamente. Por encima de esta transición, los cristales formados actuaban como entrecruzamientos físicos dificultando la movilidad de las cadenas de NR. Esta transición produce importantes cambios en el modo segmental: i) una ralentización de la dinámica de la relajación; ii) una disminución en el esfuerzo dieléctrico, y iii) un ensanchamiento del proceso de relajación.

- Los resultados del efecto de la cristalización inducida por deformación sobre la dinámica de nanocompuestos NR/C15A revelaron que la incorporación de la nanoarcilla conlleva una mayor cristalinidad y un comienzo más temprano del proceso de cristalización al comparar con el de una matriz de NR no cargada. El "nuevo modo" presente en los nanocompuestos NR/C15A también se ve afectado por el fenómeno de cristalización inducida por deformación, con evidencia de una transición del estado amorfo al estado semi-cristalino alrededor de λ = 2.5, corroborando la naturaleza segmental de esta nueva relajación.

IV. APORTACIONES FUNDAMENTALES

A continuación se presenta un breve resumen de los principales hallazgos obtenidos gracias al desarrollo de esta investigación. En cada una de las siguientes secciones se reflejan las aportaciones fundamentales detalladas en cada uno de los capítulos de Resultados y Discusión de la Tesis Doctoral.

IV.1. Rol de los Aditivos de Vulcanización en la Dinámica Molecular de Caucho Natural

La vulcanización con azufre es considerada como el método tradicional para curar cauchos diénicos, entre los cuales se puede citar el Caucho Natural (NR). Sin embargo, a pesar de que este tipo de vulcanización es un proceso industrial

relativamente antiguo, y que en las últimas décadas han aparecido un considerable número de investigaciones sobre el mismo, actualmente sigue siendo un reto científico la total comprensión de este proceso químico complejo. Hoy por hoy, continúan los esfuerzos por descifrar los mecanismos de cada paso individual dentro del proceso de vulcanización con azufre.[134,135] Las dificultades encontradas en este campo de investigación se pueden atribuir a la combinación de factores como diversidad y complejidad. La reacción de vulcanización generalmente involucra el uso de diversos ingredientes químicos, tales como un agente de vulcanización (azufre), un acelerante, y un complejo activador formado por un ácido graso (ácido esteárico) y un óxido metálico (óxido de zinc, ZnO). Esta situación se complica aún más por dos factores: a) la interacción entre los acelerantes y activadores, cada componente influye sobre la reactividad del otro, y b) la forma en cómo estas interacciones afectan al mecanismo de vulcanización.

La existencia de numerosas investigaciones[1,113,136-140] revela que la adición de estos componentes químicos en pequeñas cantidades con respecto al caucho puro afecta la procesabilidad y las propiedades finales de los compuestos vulcanizados. En general, el uso de acelerantes en combinación con activadores de zinc tiene un efecto importante sobre la velocidad de vulcanización y sobre la distribución de los entrecruzamientos formados. Adicionalmente, la durabilidad de los artículos elastoméricos, así como sus propiedades físicas (resistencia tensil) se mejoran ampliamente por los acelerantes orgánicos.

No obstante, resulta extraño que a pesar de todo el conocimiento práctico desarrollado hasta ahora, no exista aún una descripción detallada de cómo estos constituyentes afectan la dinámica molecular y propiedades del NR sin vulcanizar. La mayoría de los sistemas de vulcanización han sido desarrollados basados en el método del ensayo y error.[141] Una discusión detallada sobre la relación entre la dinámica molecular y el efecto de cada uno de los aditivos del sistema de vulcanización, previo al proceso de curado, resulta de gran interés no solo desde el punto de vista tecnológico, sino también con miras a lograr una mejor comprensión de las propiedades del NR.

En esta sección, se presentan evidencias experimentales, mediante el uso de espectroscopia dieléctrica de banda ancha, de los cambios en la dinámica segmental y global de NR no vulcanizado al introducir cada uno de los aditivos de vulcanización. Se muestra cómo una descripción detallada de cómo las interacciones entre estos aditivos y las cadenas de caucho puede contribuir a elucidar las reacciones involucradas en el mecanismo de vulcanización con azufre.

Los resultados obtenidos revelan una ralentización de la dinámica segmental del NR, restringiendo los movimientos de las cadenas de caucho enlazadas a la superficie de los aditivos. En general, se puede detectar un segundo proceso dinámico cuando el ZnO está presente. La eliminación sistemática de los diferentes aditivos de vulcanización conlleva relacionar este proceso con una fuerte interacción interfacial en las interfaces entre los agregados iónicos del ZnO y los segmentos de caucho, formando enredos físicos iniciales entre ambos componentes, que pueden actuar como precursores del entrecruzamiento. Estos resultados sirven para comprender aspectos básicos relacionados con la estructura de la red entrecruzada y con la movilidad molecular del NR, factores esenciales para la optimización del proceso de vulcanización, del rol de cada uno de los aditivos y de sus interacciones con la matriz elastomérica. La mejor comprensión del papel que juega el ZnO en la reacción de vulcanización es un factor clave para los esfuerzos actuales en tratar de reducir el contenido de zinc en las formulaciones de caucho sin detrimento de la calidad final de los productos.

Por otro lado, la dinámica global del NR también se ve afectada por la presencia de los aditivos de vulcanización; con un efecto contrario al encontrado en los movimientos segmentales. Se puede apreciar una disminución en la escala de tiempo del modo normal como consecuencia del efecto de confinamiento que tienen las cadenas de NR en los dominios de aditivos.

V.2. Dinámica Molecular de Nanocompuestos de Caucho Natural y Silicatos Laminares

El propósito de esta sección es estudiar las propiedades dieléctricas de nanocompuestos de NR y silicatos laminares, analizando sus espectros de relajación y correlacionando los movimientos locales y globales de las cadenas elastoméricas con su estructura. Inicialmente se describen resultados de la caracterización global de los nanocompuestos por medio de dispersión de rayos X, microscopía electrónica de transmisión, reometría y propiedades mecánicas. A continuación, se detallan los resultados de espectroscopia dieléctrica, examinando cómo los modos segmental y normal de la matriz de NR se ven afectados por la presencia de partículas de silicatos. También se estudia el efecto de la concentración de arcilla sobre la escala de tiempo de los procesos de relajación, además de una comparación entre tipos de nanosilicatos. Finalmente, se discute la influencia de la vulcanización y cómo el proceso de entrecruzamiento afecta el espectro dieléctrico de los nanocompuestos.

En este estudio se ha probado que la espectroscopia dieléctrica es una técnica eficaz para investigar la dinámica molecular de nanocompuestos formados por una matriz de NR y por silicatos laminares. Los resultados obtenidos indican que ni el contenido de nanosilicato ni la naturaleza del mismo tienen un efecto importante sobre el modo segmental de la matriz elastomérica. Adicionalmente, el efecto conocido como Maxwell-Wagner-Sillars (MWS) está presente en todos los nanocompuestos y es atribuible a la polarización interfacial en la interface polímero/nanoarcilla.

El resultado más relevante es la aparición de una relajación segmental restringida en los nanocompuestos de NR y arcilla orgánicamente modificada. Este nuevo modo ha sido atribuido a la dinámica segmental de cadenas poliméricas en las regiones interfaciales polímero-nanopartícula. Parte de las cadenas poliméricas se presentan parcialmente inmovilizadas como una capa interfacial alrededor de las partículas de arcilla, por lo que los efectos interfaciales dominan sobre las propiedades del material.

V.3. Dinámica Molecular de Nanocompuestos de Caucho Natural y Cargas Derivadas de Carbono

La presente sección está enfocada en el estudio de la dinámica de compuestos de NR preparados con diferentes nanopartículas derivadas de carbono, como lo son los nanotubos de carbono multicapa (MWCNT), nanotubos de carbono multicapa funcionalizados (f-MWCNT) y láminas de grafeno funcionalizadas (FGS). Se detalla fundamentalmente los resultados del comportamiento dieléctrico, pero también las características de curado, propiedades mecánicas y estructura de los nanocompuestos preparados. De igual manera, se presentan las relaciones entre estas propiedades y la naturaleza de las nanopartículas, siendo el objetivo principal el estudio de la influencia de las nanocargas y de los aditivos de vulcanización sobre la dinámica molecular de los nanocompuestos de NR.

Los resultados de este estudio indican que la dinámica segmental del NR no se ve afectada, independientemente del tipo y cantidad de nanocarga añadida a la matriz polimérica. Sin embargo, la presencia de aditivos de vulcanización sí tiene influencia sobre la dinámica de los nanocompuestos de NR y cargas derivadas de carbono, siendo evidencia de esta influencia la ralentización del modo segmental y la ligera disminución en la escala de tiempo del modo normal. El primer efecto se ha atribuido a las fuertes interacciones interfaciales presentes en las interfases entre los agregados de aditivos y los segmentos de NR, formando una red de entrecruzamientos físicos incipientes. Mientras que el segundo efecto se visualiza como consecuencia de la longitud más corta de las cadenas dentro de los dominios de aditivos, lo cual acelera la dinámica global de la matriz de NR.

Adicionalmente, las fuertes interacciones interfaciales entre las FGS y la matriz elastomérica aceleran la reacción de vulcanización y producen una importante mejora en el comportamiento mecánico de los nanocompuestos de NR.

V.4. Dinámica Molecular de Nanocompuestos de Caucho Natural bajo Deformación Uniaxial

La dinámica de la red entrecruzada sometida a esfuerzos y deformaciones externas es un factor crítico para determinar el desempeño final de muchas aplicaciones elastoméricas. Así pues, un estudio de cómo la cristalización inducida por deformación puede afectar la dinámica de un material elastomérico posee en la actualidad una importancia elevada. No se ha encontrado hasta el momento un estudio en profundidad de los efectos de la cristalización inducida por deformación en la dinámica molecular de NR. En particular, sigue siendo desconocida la interrelación entre la dinámica molecular y la deformación en NR vulcanizado. Adicionalmente, en esta investigación se encontraron mejoras significativas en el comportamiento mecánico de nanocompuestos de NR y silicatos laminares, por lo que el estudio del comportamiento de cristalización inducida por deformación en este tipo de nanocompuestos serviría para lograr una mayor comprensión del mecanismo de reforzamiento de las nanoarcillas.

Por su parte, se ha destacado que la espectroscopia dieléctrica de banda ancha es una técnica poderosa para investigar tanto la dinámica segmental como la global de cauchos sintéticos y naturales.[114,173] La combinación de la espectroscopia dieléctrica con técnicas de dispersión de rayos X ha demostrado ser un método eficiente para estudiar las relaciones dinámicas.[196,197]

De ahí que se plantea como objetivo de esta sección estudiar el efecto de la cristalización inducida por deformación sobre la dinámica segmental de NR y de nanocompuestos de NR y silicatos laminares. El estudio se enfoca en el efecto de la estructura de la red y de la cristalización, analizada a través de dispersión de rayos X, sobre la dinámica del NR estudiada mediante espectroscopia dieléctrica.

Los resultados obtenidos indican que la dinámica segmental de NR vulcanizado se ve claramente afectada al someter el caucho a estiramiento uniaxial. Durante el proceso de estiramiento se pueden detectar claramente tres regímenes. Para bajas deformaciones, $\lambda < 3$, se presenta orientación sin cristalización. Esta orientación se

ve acompañada de un incremento importante en la resistencia dieléctrica, $\Delta\varepsilon$, el cual no se puede explicar solamente como consecuencia de un incremento en la densidad del material. Se sugiere que un incremento en el momento dipolar efectivo con el estiramiento es el responsable de este aumento. Además, la reducción esperada en el volumen libre por el estiramiento genera un incremento en la temperatura de transición libre, con el consecuente aumento en la temperatura ideal o Vogel, T_0. Este efecto se ve acompañado por un incremento en el índice de fragilidad, m, ya que a medida que el volumen libre se va reduciendo como consecuencia del estiramiento, se hace necesaria mayor cooperatividad para alcanzar movimientos segmentales. En el segundo régimen, $3 < \lambda < 7.5$, los cristales comienzan a formarse y la inclusión de segmentos de caucho en la fase cristalina contrarresta el incremento en $\Delta\varepsilon$ provocado por el estiramiento. De acuerdo al modelo propuesto por Tosaka y colaboradores,[204,205] estos resultados indican que durante la cristalización inducida por deformación, las cadenas cortas de caucho son progresivamente incorporadas a la fase cristalina, mientras que un importante número de cadenas largas permanecen desorientadas. En este régimen, la dinámica segmental del NR no evidencia cambios significativos. Finalmente, a altas deformaciones, $\lambda = 7.5$, la cristalinidad es suficientemente alta como para provocar un nuevo incremento en el índice de fragilidad, m y en la temperatura Vogel, T_0.

Adicionalmente, la presencia de interacciones interfaciales entre la matriz polimérica y las nanopartículas es crucial en la promoción de la cristalización inducida por deformación en nanocompuestos de NR. La adición de silicatos laminares conlleva una mayor cristalinidad y un comienzo más temprano del proceso de cristalización al comparar con el de una matriz de NR no cargada. El "nuevo modo" presente en los nanocompuestos de NR y silicatos laminares, tal como se expuso en la sección *V.2*, también se ve afectado por el fenómeno de cristalización inducida por deformación, con evidencia de una transición del estado amorfo al estado semi-cristalino alrededor de $\lambda = 2.5$, corroborando la naturaleza segmental de esta nueva relajación.